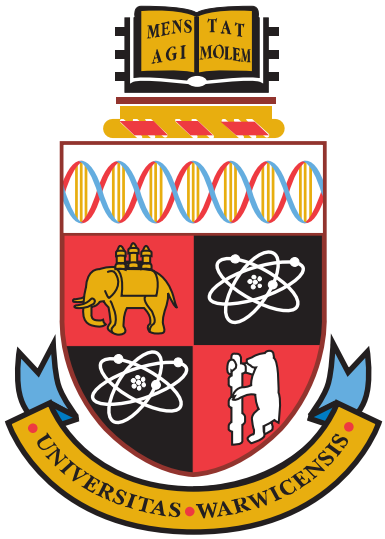

Performance Analyses and Design for Cognitive Radios

By

Liang Tang

A thesis submitted in partial fulfillment of the requirements for the degree of

Doctor of Philosophy

School of Engineering

October 2012

For my beloved family.

Table of Contents

Acknowledgments

I would like to thank all of those who have helped and supported me along this long but fulfilling journey.

First and foremost, I would like to express my heartfelt gratitude to my supervisor, Dr. Yunfei Chen. This work would not have been possible without his warm support, patient guidance, constructive suggestions and valuable time. I have been extremely lucky, as one simply could not wish for a better or friendlier supervisor. It has been a privilege to be his student, and I will always be grateful for the opportunities he has given me. I am also extremely indebted for his help in obtaining me the funding for my study at Warwick.

I would also like to sincerely acknowledge my second supervisor, Prof. Evor Hines, and the Director of Graduate Studies, Dr. Mark Leeson, for providing me the lab spaces and resources for my research.

My sincere thanks also goes to my examiners Dr. Tardi Tjahjadi and Prof. Lie-Liang Yang, for their constructive feedback.

Most importantly, I would like to thanks my beloved parents for being proud of me and having faith in me. Their constant encouragement, unconditional sacrifices, and continuous support both financially and emotionally throughout my life were the bedrock and my driving force in achieving goals in life. Without their unwavering

love, I would not have had the courage to embark on this journey.

It is my fortune to thank my husband, for his companionship along the way. He was always beside me during the happy and hard moments to push me and motivate me. A journey is easier when you travel together. Interdependence is certainly more valuable than independence. Thank you does not seem sufficient but it is said with appreciation.

I would also like to take this opportunity to show my deep appreciation to my parents-in-law, for their understanding, patience and everyday interest into my life.

Last but not the least, I would also like to dedicate this thesis to the memory of my grandfather, Shucheng (1918-1991), who is a constant source of inspiration. I hope he would have been proud.

Declaration

This thesis is submitted in partial fulfillment for the degree of Doctor of Philosophy under the regulations set out by the Graduate School at the University of Warwick. This thesis is solely composed of research completed by Liang Tang, except where stated, under the supervision of Dr. Yunfei Chen and Prof. Evor Hines between the dates of July 2009 and September 2012. No part of this work has been previously submitted to any institution for admission to a higher degree.

Liang Tang

October 2012

List of Figures

List of Abbreviations

ACR	Adaptive Continuous Rate
AM	Adaptive Modulation
AWGN	Additive White Gaussian Noise
BER	Bit Error Rate
CDF	Cumulative Distribution Function
CLT	Central Limit Theorem
COVA	Covariance-based detection
CPE	Consumer Premises Equipment
CR	Cognitive Radio
CSA	Concurrent Spectrum Access
DARPA	Defence Advanced Research Projects Agency
DSA	Dynamic Spectrum Access
DySPAN	Dynamic Spectrum Access Networks
E2R	End-to-End Reconfigurability
ED	Energy Detection
FCC	Federal Communications Commission
iid	independent and identically distributed
INR	Interference-to-noise ratio

ITU	International Telecommunication Union
ITU-R	International Telecommunication Union Radiocommunication Section
MAC	Media Access Layer
ME	Maximum-eigenvalue detection
NSF	National Science Foundation
OFCOM	The Office of Communications
OSA	Opportunistic Spectrum Access
P2MP	Point to Multipoint
PDF	Probability Density Function
PMF	Probability Mass Function
PHY	Physical Layer
QoS	Quality of Service
RKRL	Radio Knowledge Representation Language
ROC	Receiver Operation Characteristic
SE	Spectral Efficiency
SPTF	Spectrum Policy Task Force
SNR	Signal-to-noise ratio
UHF	Ultra High Frequency
VHF	Very High Frequency
WRAN	Wireless Regional Area Networks
XG	NeXt Generation

List of Important Symbols

$C_{(\cdot)}$	Channel capacity for different hypothesis
f_c	Carrier frequency
f_s	Sampling frequency
f_α	Probability mass function of idle channel holding time
f_β	Probability mass function of busy channel holding time
f_γ	Probability density function of the channel SNR in Nakagami-m fading channel
f_Y	Probability density function of Y
$f_{X\alpha}$	Probability mass function of idle channel holding time in novel structure
$f_{X\beta}$	Probability mass function of busy channel holding time in novel structure
$F_\alpha(t)$	Cumulative distribution function of idle channel holding time
$F_\beta(t)$	Cumulative distribution function of busy channel holding time
$\Gamma(\cdot)$	Gamma function, $\Gamma(x) = \int_0^\infty t^{x-1}e^{-t}dt$.
$\Gamma(\cdot,\cdot)$	Incomplete gamma function, $\Gamma(x,z) = \int_0^z t^{x-1}e^{-t}dt$.
$h_{(\cdot)}$	Fading coefficient for different channels
$H_{(\cdot)}$	Different hypothesis

i	Sample index
I	Number of samples in the spectrum sensing slot
$I_z(\cdot)$	z-th order modified Bessel function of the first kind, $\mathcal{I}_z(x) = \left(\frac{x}{2}\right)^z \sum_{j=0}^{\infty} \frac{(x^2/4)^j}{j!\Gamma(z+j+1)}$.
j	Sample index
J	Number of samples in the secondary frame
k	Index of possible different regions of the SDR
$k_{(\cdot)}$	Shape parameters of different distributions
$K_{0H_{(\cdot)}}$	The total number of samples during the sensing period that contain only noise for different hypothesis
$K_{1H_{(\cdot)}}$	The total number of samples during the sensing period that contain signal and noise for different hypothesis
m	m parameter of Nakagami-m fading channel
M	Constellation size
N	Maximum number of primary user occupancy status changes
p_b	Instant probability of busy channel
p_e	Instant probability of idle channel
$P_{d(\cdot)}$	Probability of detection for different hypothesis
$P_{fa(\cdot)}$	Probability of false alarm for different hypothesis
$P_{ber_{(\cdot)}}$	BER for different cases
$P_{ser_{(\cdot)}}$	Symbol error rate for different cases
P_{mo}	Probability of missed opportunity
P_{md}	Probability of mis-detection
$P_{(\cdot)}$	Probability of different hypothesis occurring
$\hat{P}_d$	Target probability of detection

$Q(\cdot)$	Q-function, $Q(t) = \frac{1}{\sqrt{2\pi}} \int_t^\infty e^{-u^2/2} du$.
$Q_m(\cdot)$	Marcum Q-function, $Q_m(x, z) = \int_z^\infty \frac{t^m}{x^{m-1}} e^{-\frac{t^2+x^2}{2}} \mathcal{I}_{m-1}(xt)\, dt$.
$R_{(\cdot)}$	Achievable throughput for different cases
$s(t)$	Primary user signal received at the secondary user
$s_{s,j}$	Secondary user signal samples
S_p	Primary user signal power
S_s	Secondary user signal power
t_s	Symbol duration
t_ζ	Secondary user signal symbol duration
T	Frame duration
U	Total number of secondary frames
w_0	Noise power
$w(t)$	Additive white Gaussian noise
W	Bandwidth
X	Frame index
$y(t)$	Received signal at the secondary user
$Y_{(\cdot)}$	Test statistics for spectrum sensing in different hypothesis
α	Symbol at which primary user arrival occurs
β	Symbol at which primary user departure occurs
γ	SNR
$\Delta_{(\cdot)}$	Minimum number of samples required
θ_{max}	Maximum eigenvalue of the covariance matrix of the received signal
θ_{min}	Minimum eigenvalue of the covariance matrix of the received signal

$\mu_{(\cdot)}$	Mean
$\sigma^2_{(\cdot)}$	Variance
τ	Spectrum sensing slot duration
$\tilde{\tau}$	Optimal spectrum sensing time
$\Psi_{(\cdot)}$	Decision threshold for different cases
Ω	Number of primary user status changes

Abstract

Cognitive radio has been proposed as a promising solution to the conflict between the spectrum scarcity and spectrum under-utilization. As the demand increases for wireless communication services, cognitive radio technology attracts huge attention from both commercial industries and academic researches. The purpose of this thesis is to provide an analytical evaluation of the cognitive radio system performance while taking into consideration of some realistic conditions. Several problems are investigated in this thesis. First, by adopting a dynamic primary user traffic model with one primary user occupancy status change and exponentially distributed channel holding times, its effect on the cognitive radio system performance is evaluated. In the evaluation, the sensing-throughput tradeoff of the cognitive radio is used as the examination criteria, while energy detection is applied during the spectrum sensing. The thesis then takes the investigation further by establishing a primary user multiple changes traffic model which considers multiple primary user occupancy status changes and any reasonable channel holding time distributions. The effect of the primary user multiple changes traffic on the spectrum sensing performance is investigated while the channel holding times are assumed to be exponential, Gamma, Erlang and log-normal distributed. The analytical evaluation of cognitive radio is also carried out from the secondary user transmission perspective, where the per-

formance of the adaptive modulation in cognitive radio system is investigated. The effect of the cognitive radio distinctive features on the performance of both the adaptive continuous rate scheme and the adaptive discrete rate scheme of the adaptive modulation are examined. The BER performance and the link spectral efficiency performance are derived for both schemes.

A novel frame structure where the spectrum sensing is performed by using the recovered received secondary frames is also evaluated in this thesis. A realistic scenario which considers the secondary user signal decoding errors is examined for the novel structure, while an ideal upper bound performance is given when the decoding process is assumed perfect. By extending the system to include multiple consecutive secondary frames, the performance of the novel structure is compared to the performance of the traditional frame structure proposed by the IEEE 802.22 WRAN standard. The effect of the primary user multiple changes traffic is also examined for the novel structure.

Several major findings are made from the analytical evaluations presented in this thesis. Through numerical examinations, it was shown that, first, the dynamic primary user traffic degrades the performance of cognitive radio systems. Second, the degree of the performance degradation of the cognitive radio systems is related to the number of primary user status changes and the primary user traffic intensity. Different primary user channel holding times distributions also lead to different sensitivities of the system performance to the primary user traffic. Third, cognitive radio distinctive features degrades the performance of the adaptive modulation. When the novel structure is applied for cognitive radio, a higher secondary achievable throughput can be obtained with a limited saturation threshold.

List of Publications

Journal Papers

1. L. Tang, Y. Chen, A. Nallanathan and E. L. Hines, "Performance evaluation of spectrum sensing using recovered secondary frames with decoding errors," *IEEE Transactions on Wireless Communications*, vol. 11, no. 8, pp. 2934 -2945, August 2012.

2. L. Tang, Y. Chen, E. L. Hines and M. -S. Alouini, "Performance analysis of spectrum sensing with multiple status changes in primary user traffic," *IEEE Communications Letters*, vol. 16, no. 6, pp. 874 -877, June 2012.

3. Y. Chen, M. -S. Alouini, L. Tang and F. Khan, "Analytical evaluation of adaptive-modulation-based opportunistic cognitive radio in Nakagami-m fading channels," *IEEE Transactions on Vehicular Technology*, vol. 61, no. 7, pp. 3294 -3300, September 2012.

4. L. Tang, Y. Chen, E. L. Hines and M. -S. Alouini, "Effect of primary user traffic on sensing-throughput tradeoff for cognitive radios", *IEEE Transactions on Wireless Communications*, vol. 10, no. 4, pp. 1063 -1068, April 2011.

5. Y. Chen and L. Tang, "Performance evaluation of collaborative spectrum sens-

ing without dedicated sensing period for cognitive radios", *Wireless Communications and Mobile Computing*, submitted.

Conference Papers

1. L. Tang, Y. Chen, A. Nallanathan and E. L. Hines, "Spectrum sensing based on recovered secondary frame in the presence of realistic decoding error", *IEEE International Conference on Communications (ICC 2012)*, pp. 1 -5, June 2012.

2. Y. Chen, M.-S. Alouini and L. Tang, "Performance analysis of adaptive modulation for cognitive radios with opportunistic access", *IEEE International Conference on Communications (ICC 2011)*, pp. 1 -5, June 2011.

Chapter 1

Introduction

1.1 Introduction to Cognitive Radios

In the past two decades, the desire for high data rate wireless communications has increased extensively, as a consequence of the transition from voice-only communication to multimedia type applications [1]. Since the emergence of the new wireless devices and applications, consumers' interests in the wireless services has seen an unprecedented rise. According to the prediction study conducted by the International Telecommunication Union Radiocommunication Section (ITU-R), there will be further strong growth in the market demand of the wireless communication for the years to come [2].

Radio frequency spectrum is a fundamental component that enables wireless communications [3]. The development of new wireless devices and the enhancement of the existing ones both place enormous demand for the frequency spectrum, which is a naturally limited resource.

1.1.1 Frequency Spectrum Management

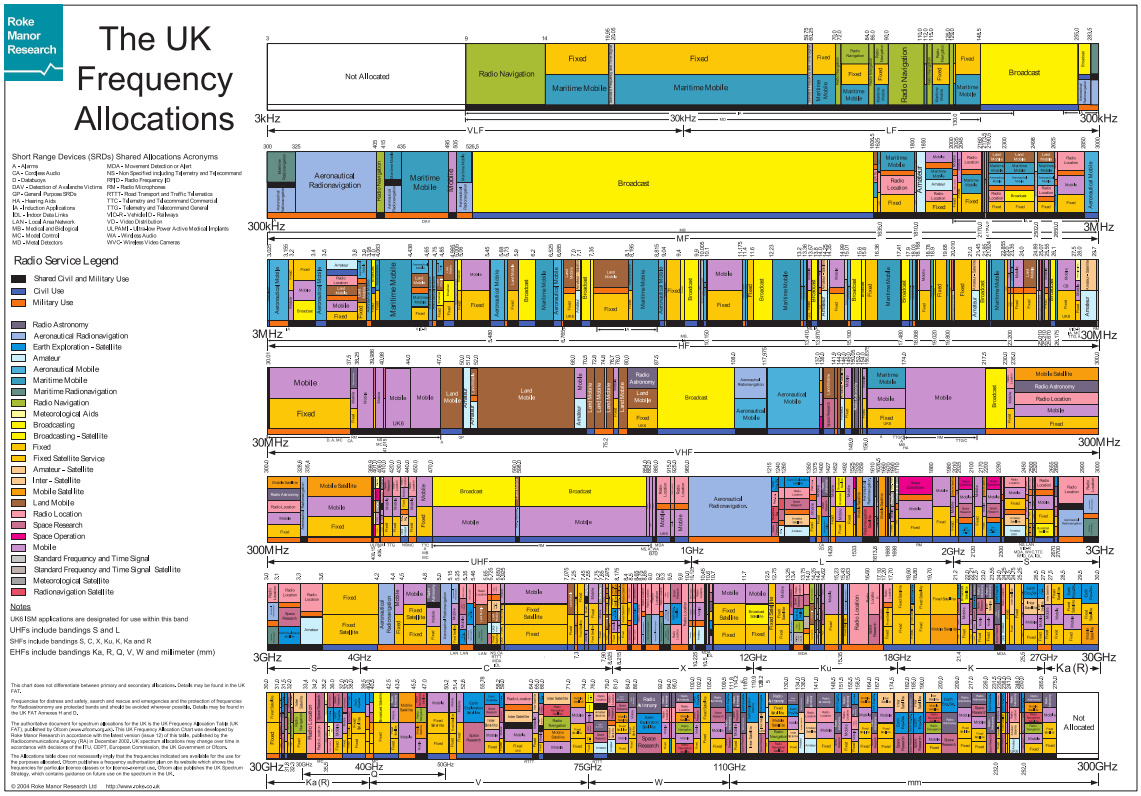

Figure 1.1: Spectrum allocations in the UK [4].

Currently, the frequency spectrum is regulated by the International Telecommunication Union (ITU) internationally, and by the governmental agencies and regulatory bodies nationally, such as The Office of Communications (Ofcom) in the UK and the Federal Communications Commission (FCC) in the USA [6]. With them regulating the communication industry, the vast majority of the frequency spectrum is restricted to licensed-only access. The wireless service providers can purchase the license to exclusively utilize a band of certain frequency within a large geographic region. The purchases are generally for a finite and long period of time with renewal expectations, while the allowable operating parameters are specified [7]. Under this

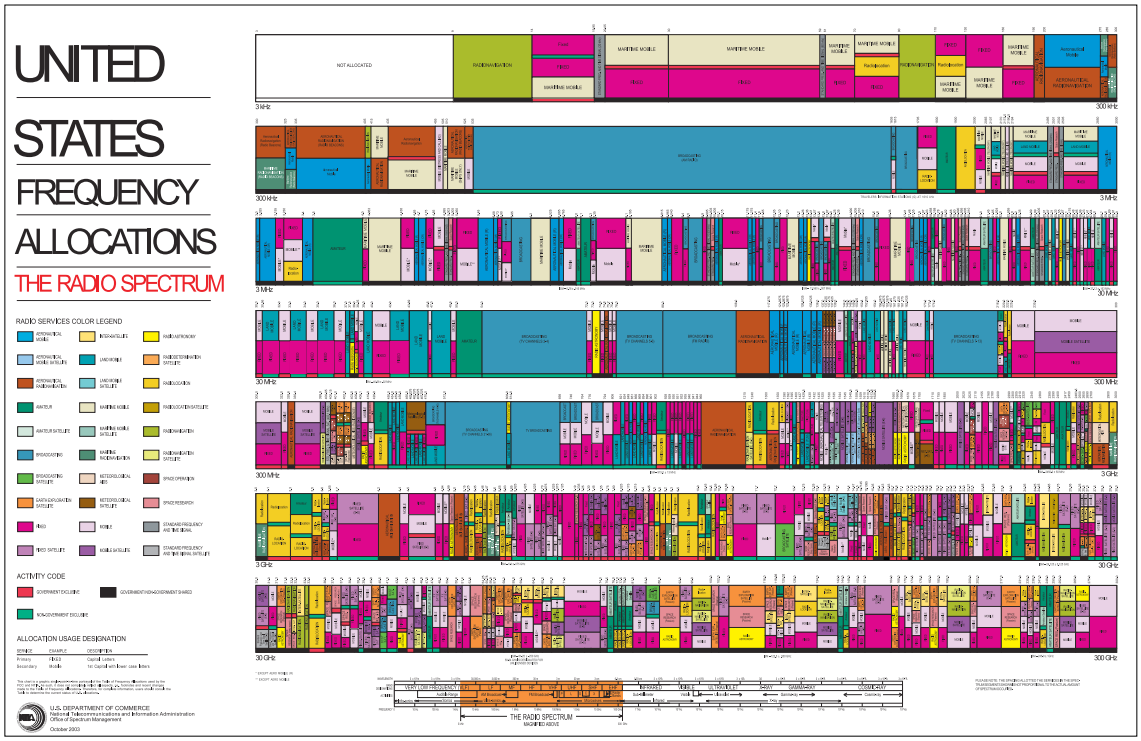

Figure 1.2: Spectrum allocations in the USA [5].

regulation, only the dedicated license holders have the rights to exploit the allocated spectrum, and the service providers without the legal license are forbidden from utilizing the spectrum regardless of its current occupancy status. Hence, protections against the unlicensed user interference can be guaranteed for the licensed user under this regulation.

Fig. 1.1 and Fig. 1.2 present the frequency spectrum allocations for the UK and the USA, respectively, where each colour indicates a different type of service. As shown, since the spectrum allocation is performed locally according to the geographic locations, the detailed allocations in the two charts varies. However in both cases, most frequency spectrum bands of up to 300 GHz has been allocated for various purposes, despite the multi-billion pounds purchasing price [4, 5, 8]. In

related literatures, words such as "congested", "over crowded" start to frequently appear. Due to the naturally limiting availability of the frequency spectrum, spectrum scarcity is becoming an exceeding significant problem, and it is a common belief that the economically usable frequencies are running out [9].

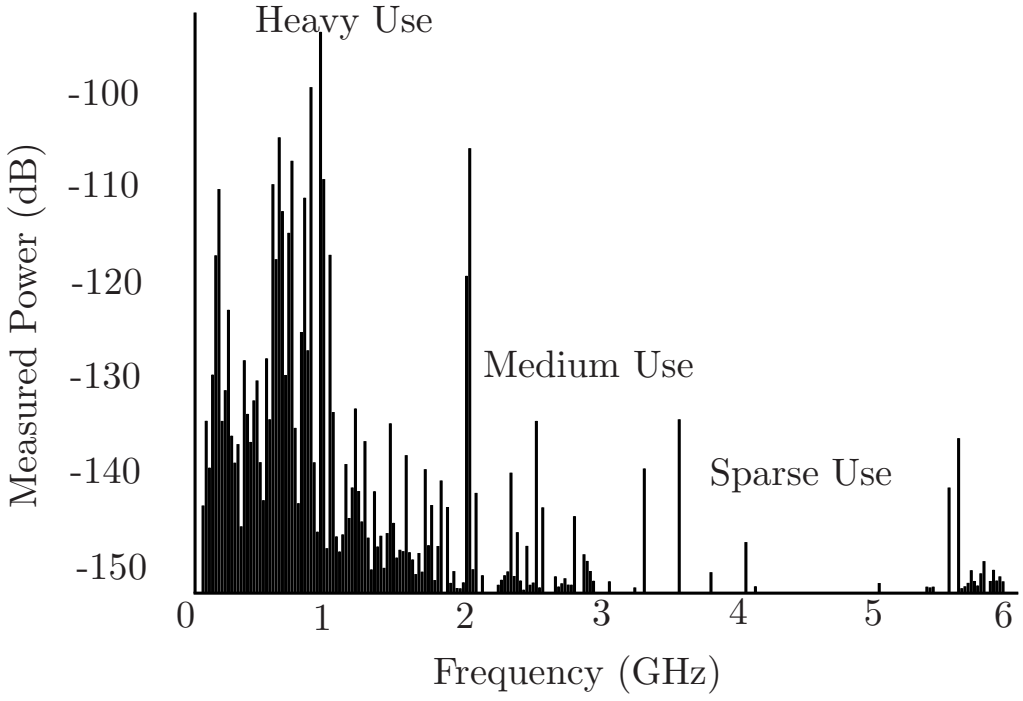

Figure 1.3: Measurements of spectrum utilization in downtown Berkeley in the USA. Adapted from [10].

However, after many researches being conducted on the spectrum utilizations in diverse locations, it has been shown that the utilizations of many allocated spectrum bands are very inefficient [7, 12–18]. According to the FCC, the occupancy of the allocated spectrum is sporadic with a high time and spatial variation ranging from 15% - 85% [7]. Fig. 1.3 illustrates the results of a utilization measurement performed in downtown Berkeley in the USA. As can be seen, there were portions of the spectrum being heavily utilized whilst certain portions of the spectrum were

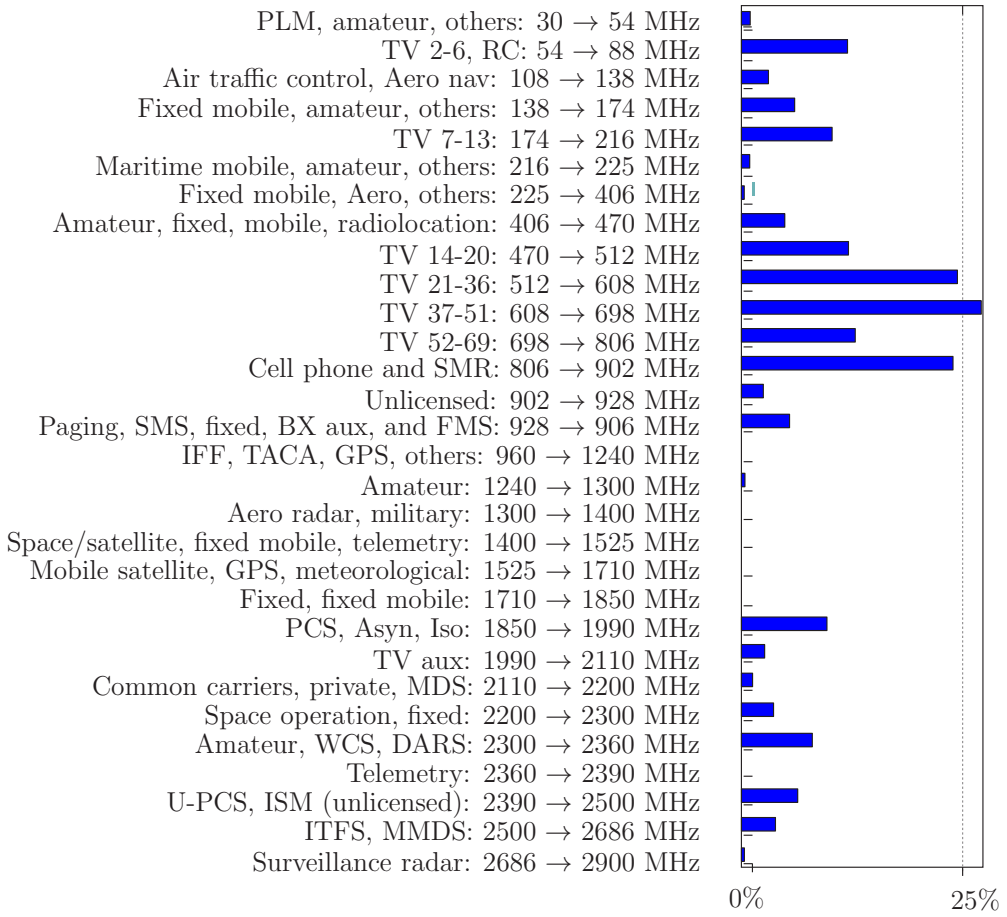

Figure 1.4: Measurements of average spectrum utilization over six different locations in the USA in 2004. Adapted from [11].

significantly under-utilized. To be more specific, the actual utilization of the $3-4$ GHz frequency band in Berkeley was only 0.5 % and became even less in the $4-5$ GHz band [10].

Another example is the study of the frequency spectrum utilization between 30 MHz and 3 GHz in [13]. By measuring and averaging the spectrum utilization over six different locations in the USA in 2004, it was found that the average utilization of the allocated spectrum was only 5.2 %, as shown in Fig. 1.4.

Similar findings have also been observed in the UK. For example, around 30 %

of the spectrum below 15 GHz is allocated to defence purpose, which was accessed by the Ministry of Defence for virtually free until the late 1990s [19]. However, a spectrum demand study by the PA Consulting together with the Prof. Cave's audit report have identified that additional spectrum utilization opportunities in this frequency band may exist [19, 20]. Measurements in other countries have also shown similar results, such as Singapore [14], New Zealand [16], China [17] and Germany [18].

As the list goes on, all these measurement results seem to be contradictory to the concern of spectrum scarcity. It is obvious that the spectrum scarcity faced by the governmental agencies and regulatory bodies today, is essentially an artificial result caused by the traditional static spectrum allocation policies and the inefficient utilization by the license holders, rather than any physical shortage of the spectrum resource itself. Therefore, in order to solve the conflict between the spectrum scarcity and the under-utilization, and maintaining the sustainable development of the wireless communication industry, a new flexible, efficient and reliable communication paradigm is needed to achieve a more intensive and comprehensive utilization of the frequency spectrum. Prompted by this observation, cognitive radio is proposed as a promising solution.

1.1.2 Historical Development of Cognitive Radio

Cognitive radio is an intelligent radio technology built on the software-defined radio platform [21]. It removes the licensing barriers and facilitates the development of the secondary markets in the spectrum utilization through the concept of dynamic spectrum access (DSA) [22]. In cognitive radio terminology, DSA means two types of entities operating in the same licensed spectrum band: the primary user and the

secondary user. The primary user is the license holder who has higher priority and legacy rights to utilize the specific spectrum band. The secondary user is the cognitive user who has lower priority to the spectrum band and operates on a dynamic basis under strict conditions. The secondary user should be equipped with the ability to obtain awareness of its surrounding radio environment such that the intelligent secondary exploitation of the licensed spectrum can be achieved. At all time, the secondary user should not cause any harmful interference to the primary user, so that the operation of the primary user is protected even if it is not exclusively utilizing the licensed spectrum [1].

By using the cognitive radio techniques, more flexible exploitation and efficient utilization of the allocated frequency spectrum can be achieved. This state-of-art technology, is consequently widely expected to be the next Big Bang in the wireless communications [23, 24].

Unlike the conventional radio technology which has a history that dates back to the 1901 [25], despite the rapid development in cognitive radio, it is a relatively new technology. The concept of cognitive radio was first proposed by Dr. Mitola in [26] in 1999, where he described the term as the radio knowledge representation language (RKRL) that could enhance the flexibility of personal wireless services. The following year, in his doctoral thesis at the Royal Institute of Technology, Sweden [27], Dr. Mitola further explained the idea of RKRL and presented a conceptual overview of cognitive radio as an exciting multidisciplinary subject. At the same time, the Defense Advanced Research Projects Agency (DARPA) in the USA conducted a series of measurements that indicated the allocated spectrum was not utilized very efficiently in the USA. Two years later in 2002, the NeXt Generation (XG) project was initiated by the DARPA to investigate the enabling technologies and system

concepts for the time domain and spatial domain sharing of the spectrum with multiple devices for military communications [22]. In the same year, the FCC Spectrum Policy Task Force (SPTF) also conducted measurements on the spectrum utilization and concluded that the spectrum under-utilization is a bigger problem than the spectrum scarcity [12]. For this reason, the SPTF recommended the development of new regulations that allow more intensive spectrum usage. In 2003, the National Science Foundation (NSF) in the USA joined the research on DSA and started their research projects in the spectrum measurements. Also proposed by the SPTF, the first cognitive radio workshop was held in Washington DC, USA, in 2003 [28]. The workshop was followed by a cognitive radio conference in 2004, held in Las Vegas, USA [28].

The year before the conference, cognitive radio has also started to draw attentions in the Europe. The DSA technologies are included by the European Union (EU) Information Society Technologies as part of the Sixth Framework Program. Research projects in DSA and spectrum measurements have also been started. In 2004, the EU initiated the End-to-End Reconfigurability (E^2R) Project in the Information Society Technologies. In the same year, the FCC issued the Notice of Proposed Rulemaking on Facilitating Opportunities for Flexible, Efficient, and Reliable Spectrum Use Employing Cognitive Radio Technologies [29]. In 2005, the DARPA XG and NSF projects started in 2002 and 2003 have completed their spectrum measurements. It was found that only less than 10 % of the spectrum under 3 GHz was utilized in time-space [25]. At the same time, the IEEE began to hold annual conference on Dynamic Spectrum Access Networks (DySPAN). In 2007, the FCC started the testing of prototype devices for un-licensed usage of the un-utilized TV broadcasting spectrum. In the same year, new opportunities for cognitive radio

usage of the un-occupied spectrum without causing interference was created by an Ofcom Consultation. In 2008, the End-to-End Efficiency (E^3) project was initiated in the Europe with 21 industry and academia partners [22]. Around the same time, several research projects were also stated, such as the Wireless World New Radio Initiated+ (WINNER+), the Self-Optimisation and Self-configuRATion in wirelEss networkS (SOCRATES), and the Reconfigurable OFDMA-based cooperative NetworKs Enabled by Agile SpecTrum Use (ROCKET). Also in 2008, opportunistic spectrum access was successfully demonstrated by the DARPA XG project. In 2010, the first phone call over a cognitive radio network was made in the center for wireless communications at the University of Oulu, Finland.

Until today, the development of cognitive radio technology is still continuing. As well as the regulatory researches, there are now also significant industrial involvements of many big name companies from different industries, such as Philips and Samsung from the consumer electronics industry, Alcatel-Lucent, Ericsson and Motorola from the mobile equipment industry, BT and Orange from the network operates, Microsoft and Google from the Internet and softwares industry, and HP and Dell from the computer industry [30].

While the definitions of cognitive radio are still being perfected by industry and academia [31], the definition made by the FCC has been widely adopted [29]

> *"A radio or system that senses its operational electromagnetic environment and can dynamically and autonomously adjust its radio operating parameters to modify system operation, such as maximize throughput, mitigate interference, facilitate interoperability, and access secondary markets."*

1.1.3 Spectrum Access Techniques

A keyword can be recognized from the above definition for cognitive radio: *dynamic*. Accessing the licensed spectrum in a dynamic manner is essentially the key of cognitive radio. This requires the secondary user to be equipped with cognitive capability and reconfigurability [32]. Cognitive capability refers to the ability to obtain awareness of the surrounding radio environment through means of sensing and capturing information. With the cognitive capability, the secondary user can gather information and identify the best available spectrum bands for operation. Reconfigurability refers to the secondary user's ability of dynamically programming its operational parameters such as the transmission frequency, bandwidth, power, modulation scheme, etc., according to the gathered radio environment information. With the reconfigurability, the secondary user can achieve optimal performance in its chosen spectrum bands [32].

Depending on the cognitive capability, the secondary user can achieve DSA using different approaches. The accessing approaches are generally divided into two categories: the spectrum underlay approach [9] and the spectrum overlay approach [33].

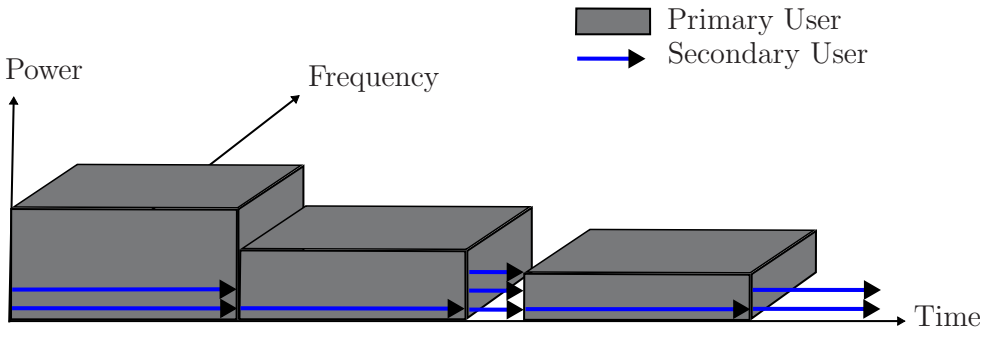

Figure 1.5: The concept of spectrum underlay.

The spectrum underlay is also referred to as the concurrent spectrum access (CSA) [34]. As illustrated by Fig. 1.5, in CSA, the secondary user coexists with the active primary user, and is permitted to transmit simultaneously with the primary user. Since the primary user has the priority in the licensed channel, the secondary user transmitter must ensure that its transmission power is restrained at all time. By doing so, the secondary user is always operating below the noise floor of the primary user and the interference caused to the primary user is limited to within the tolerable level [35]. However, this approach imposes some fundamental constraints on the secondary user resulting in major disadvantages. First, due to the restrained transmission power, the secondary user can only operate with extremely low power and thus within a very short range [36]. In most cases, spread spectrum techniques have to be adopted by the secondary user to achieve short-range high data rate communication. Second, the secondary user is also required to predict the interference temperature limit of the primary user and the interference power level that is received at a particular primary user receiver [37, 38]. Achieving an accurate prediction of these parameters can be complicated. Hence, the secondary user implemented spectrum underlay tends to be complex in terms of hardware design. Moreover, in case of estimation errors occurring at the secondary user, this approach also imposes potential threats to the quality of service (QoS) of the primary user.

The spectrum overlay is also referred to as opportunistic spectrum access (OSA) [39]. As the name states, in OSA, the secondary user accesses the licensed spectrum in an opportunistic manner. Through capturing its surrounding radio environment information, the secondary user identifies un-utilized frequency spectrum bands. These un-utilized bands are licensed spectrum that are not being occupied by the primary user at the particular fragments of time in the particular given spatial lo-

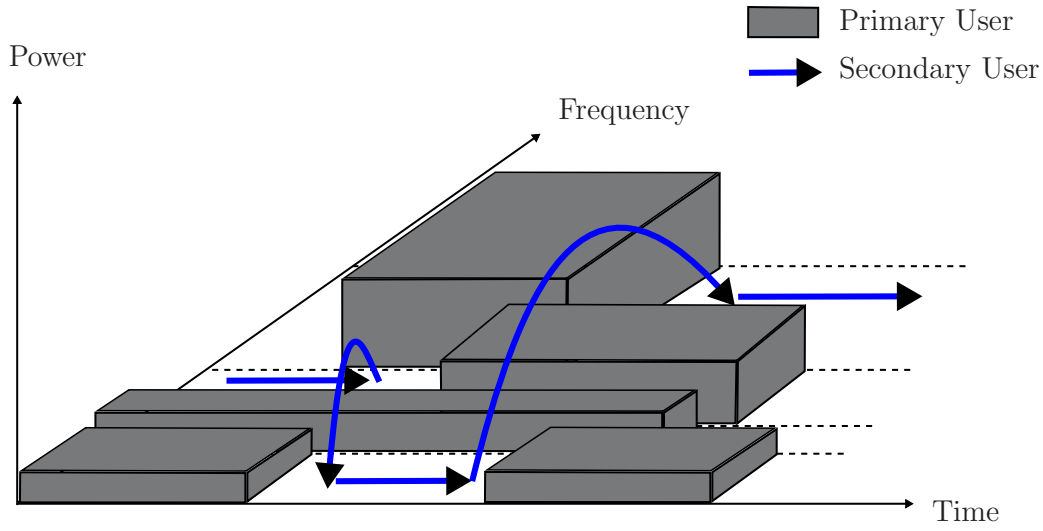

Figure 1.6: The concept of spectrum overlay. Adapted from [7].

cation. They are also named as spectrum holes or white space. Upon finding these spectrum holes, the secondary user reconfigures its operating parameters to achieve optimal performance in the chosen spectrum band. In some literatures, this is also referred to as the "listen-before-talk" etiquette [40]. In OSA, the secondary user is only permitted to utilize the spectrum when the primary user is inactive, as illustrated by Fig. 1.6. In this case, the secondary user transmission power is not refrained as the primary user interference tolerance level is no longer an operation condition [7]. Hence, most transmission techniques can be applied. Instead, as the primary user has the right to reclaim the licensed channel at any time, the secondary user has to be constantly aware of the channel occupancy status. This requires the secondary user to frequently monitor the channel status through database knowledge, spectrum sensing or other methods, which will be discussed in more detail in later chapters. Upon acknowledging the primary user's arrival, the secondary user must vacate the channel.

Owing to the aforementioned limitations of the spectrum underlay approach, the spectrum overlay is a much more widely adopted approach in many researches. For this reason, in this thesis, the research will be focused on cognitive radio systems implementing the spectrum overlay approach.

1.2 IEEE 802.22 Standard Overview

The introduction to cognitive radio will not be complete without mentioning the IEEE 802.22 standard, which is the first world wide standard based on the cognitive radio technologies [41].

Broadcasting TV operates in the licensed channel in both the very high frequency (VHF) band and the ultra high frequency (UHF) band. In most developed countries, such as the US and UK, most of the EU and many other countries in the world, the switchover from analogue TV to digital TV is either completed or in progress. As a result of the switchover, large portions of the VHF and UHF analogue TV spectrum are or will become available due to the higher spectrum efficiency of the digital TV. Some of these vacated channels are being reallocated through auctions, for instance, the proposed auctions of 800 MHz and 2.6 GHz frequency bands for the 4G network in the UK. Furthermore, due to the interference planning issues among the co-channel or adjacent channel stations, there are typically a few digital TV channels not being utilized in a given geographic location. Thus, the capacity of un-utilized TV spectrum is significant. According to the research conducted by the Ofcom, around 100 MHz of un-utilized spectrum is available at 90% of the UK, whereas around 150 MHz of un-utillized spectrum is available at 50 % of the UK locations.

In as early as 2004, the FCC proposed to enable the secondary usage of the

un-utilized TV channels in the VHF and UHF bands [29]. Following the proposal, the IEEE 802.22 working group on Wireless Regional Area Networks (WRANs) was formed in October 2004. From then on, there has been overwhelming interests to develop a WRAN system operating on the TV white space using the cognitive radio techniques. In 2008, prototypes were put forward to the FCC by Adaptrum , I^2R, Microsoft, Motorola and Phillips [42]. In the November of the same year, the FCC released a Second Report and Order that issued permission for the opportunistic utilization of the TV white space.

1.2.1 The IEEE 802.22 WRAN Standard

The IEEE 802.22 standard also known as the IEEE 802.22 WRAN standard is the first standard developed for the WRANs defining both the Physical Layer (PHY) and the Media Access Layer (MAC) functionalities [43]. It was expected to be finalized in 2010, but was published in July 2011 in the end [44]. While the initial geographical focus was in the North America, the standard enables the secondary utilization of the VHF and UHF TV bands between $54-862$ MHz in the USA, with a debating extension to $41-910$ MHz [45]. This corresponds to the TV channels $5-13$ in the VHF band and $14-51$ in the UHF band [46]. Each channel has a bandwidth of 6, 7 or 8 MHz. The application of the IEEE 802.22 WRAN standard is the broadband access to the rural areas in the USA where are normally hard to reach and the population density is typically very low. The broadband access service is restricted to a non-interfering basis, such that no harmful interference can be caused to the TV broadcasting and other licensed low-power devices operating in the channel, such as the wireless microphones.

As has been specified by the IEEE 802.22 WRAN standard, the network operates

in a point to multipoint basis (P2MP), consisting of a base station and multiple customer-premises equipments (CPEs) [47]. The base station controls the spectrum access for all the CPEs attached to it. The broadband access achieved through implementing the standard will cover rural areas of up to 100 km from each base station and serving up to 255 fixed CPEs with outdoor directional antennas located at 10 m above ground level [45].

1.2.2 Superframe and Frame Structure

The IEEE 802.22 WRAN standard enables flexible and efficient utilization of the TV white space through cognitive capability, while reliably protecting both the TV broadcasting and the wireless microphone signals. One of the IEEE 802.22 WRAN standard features that is particularly worth noticing, is the proposed superframe structure, as this structure is widely used in cognitive radio researches and will hence be adopted in this thesis.

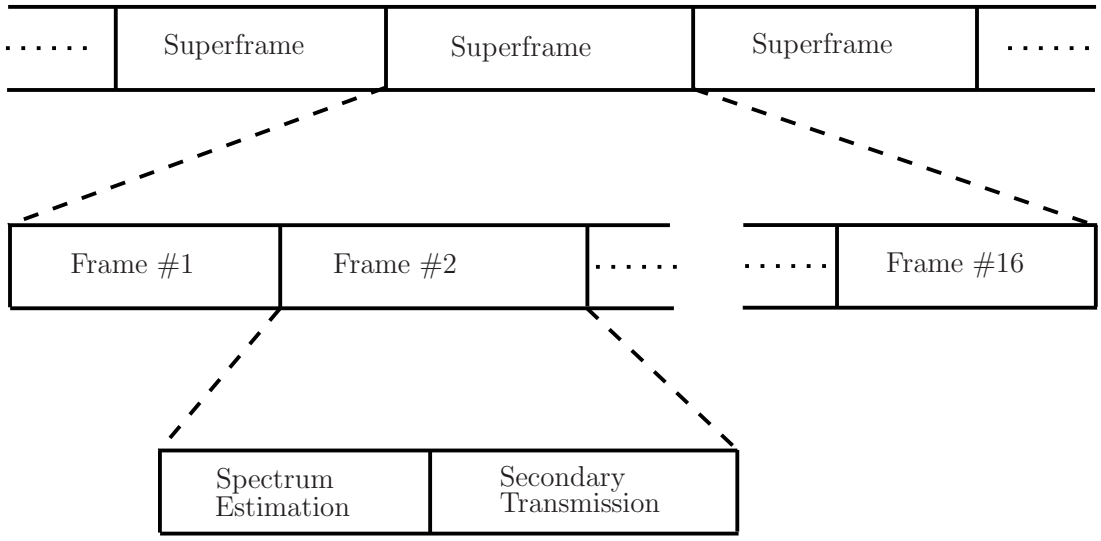

Figure 1.7: IEEE 802.22 WRAN standard superframe structure. Adapted from [48].

In order to fulfill the no harmful interference regulation of the standard, the secondary user is required to be aware of any existing primary user signals with a signal to noise ratio (SNR) of as low as -21 dB [1]. This means it is crucial for the secondary user to constantly monitor the channel occupancy status. For this reason, the IEEE 802.22 MAC employs a superframe structure, such that the primary user protection and the secondary data transmission can be efficiently managed. As illustrated by Fig. 1.7, the operation of the secondary user is divided into multiple consecutive superframes in the time domain, whilst each superframe is then subdivided into multiple consecutive MAC frames. In the IEEE 802.22 WRAN standard, there are 16 MAC frames each with a duration of 10 ms in one superframe [48]. The MAC frames are then further subdivided, where each MAC frame consists of two slots. In the sense of cognitive radio with OSA approach, the MAC frame is divided into a spectrum estimation slot and a secondary data transmission slot. By employing this structure, the spectrum estimation and secondary data transmission is performed chronologically and periodically, such that constant awareness of the channel status can be achieved. Here, spectrum estimation refers to obtaining information of the channel occupancy status by using cognitive capability. A more comprehensive discussion on the spectrum estimation is presented in Chapter 2.

1.3 Thesis Outline

1.3.1 Research Motivation

In this thesis, the research is focused on cognitive radio systems implementing the spectrum overlay approach for the reasons given above. As previously mentioned, the primary user has the priority to operate in the licensed channel, it can therefore

claim the spectrum band at anytime regardless of the secondary user's occupancy status. As required by the regulation, the secondary user is obliged to ensure its high level of awareness of the primary user's arrival at the licensed channel and vacate the channel immediately, in order to prevent causing harmful interference to the primary user. In most literatures [49–54], by adopting the superframe structure, this is achieved through the periodic spectrum estimation. However, in these literatures, the cognitive radio system models are established based on an assumption that the primary user's channel holding time is always longer than the secondary MAC frame duration. This implies that the primary user always has a constant occupancy status within an entire secondary MAC frame. In other words, they have assumed that the primary user is either always active or always inactive during both the spectrum estimation slot and the secondary data transmission slot. However, in reality, this might not always be the case, especially when the primary user network has a high traffic rate or when a long MAC frame duration is chosen by the secondary user. Thus, part of the secondary MAC frame may see an occupied licensed channel while part of the frame may see an idle licensed channel. In these cases, the conventional performance evaluations for cognitive radios are no longer accurate. Therefore, it is worth reformulating some of the performance evaluations for cognitive radio while taking the realistic dynamic primary user traffic scenarios into account. By incorporating a dynamic primary user traffic model, the examination of its effect on various system performances can provide a valuable contribution to future system designs for cognitive radios.

On the other hand, to achieve the secondary utilization of the licensed spectrum through carrying out the secondary data transmission is the ultimate goal of cognitive radios. Therefore, it is a natural choice to apply traditional trans-

mission enhancing techniques, such as adaptive modulation, to the cognitive radio systems. However, due to the un-licensed utilization nature of the cognitive radio, its transmission performance exhibits unique characteristics. Therefore, some special considerations must be included when evaluating the performances of these techniques in cognitive radio system. Hence, it will be of great interest to investigate the performance of transmission enhancing techniques in cognitive radio systems with consideration of the distinctive cognitive radio features. Such investigation will provide significant enhancement to the performance prediction capabilities for future applications of transmission enhancing techniques in cognitive radio systems.

The maximization of the achievable throughput is not limited to the means of transmission techniques, but also the transmission time itself. In the aforementioned MAC frame structure, the chronological coexistence of the spectrum estimation slot and the secondary data transmission slot in the same MAC frame potentially imposes one of the major design challenges for cognitive radio systems. As will be discussed in more details later in Chapter 3, the choice of the duration for each slot is a popular research topic in cognitive radio. Nevertheless, this problem can also be explored from a different perspective, where the choice of the optimal durations are not required. To maximize the secondary transmission time and hence the achievable throughput, the entire secondary MAC frame could be used to perform spectrum estimation and data transmission simultaneously. By presenting and evaluating the performance of cognitive radio system with such structure, the investigation would have important contributions for the future direction of cognitive radio research, as the traditional secondary MAC frame structure would no longer be the only option.

1.3.2 Chapter Outlines

Motivated by the above reasons, the performance of the cognitive radio system is analytically evaluated in this thesis, while taking into consideration of realistic conditions. Several practical issues of cognitive radio system are examined. Mathematical derivations are provided for the discussion and in most cases, closed-form equations are derived. Numerical results are also provided to verify the derivations.

In Chapter 2, a comprehensive overview of the cognitive radio technology is presented. The details of the two main aspects of cognitive radio is introduced: the spectrum estimation and the secondary data transmission. A review of different spectrum estimation technologies are provided, where their performance merit and limitations are discussed. Different spectrum sensing algorithms are also presented with their advantages and disadvantages analyzed. A review of the secondary data transmission in a conventional cognitive radio system is also provided. Some fundamental theoretical details are also given, such that it can be used as a reference for comparison purpose for the performance evaluations presented in the later chapters.

In Chapter 3, the effect of the dynamic primary user traffic on the tradeoff between the spectrum sensing quality and the achievable throughput is analyzed. The analysis adopts a dynamic primary user traffic model that takes into consideration of one primary user occupancy status changes, while assuming exponentially distributed channel holding times. By implementing energy detection for the spectrum sensing, the performance of the new system model with dynamic primary user traffic is derived and thereafter compared to the performance of the conventional model.

Chapter 4 further develops the dynamic primary user traffic model presented in the Chapter 3 to include multiple primary user occupancy status changes and any reasonable channel holding time distributions. Through establishing the primary

user multiple changes traffic model, its effect on the energy detection performance is investigated. Closed-form expressions for the spectrum sensing qualities are derived. By comparing the performances of the cognitive radio system with different numbers of primary user status changes, a lower boundary of the spectrum sensing performance is predicted. The effect of different primary user channel holding distributions are also examined.

In Chapter 5, the performance of the adaptive modulation in cognitive radio are investigated. Different to the existing literatures on adaptive modulation, in this investigation, the distinctive characteristics of the cognitive radio are taken into consideration, such as the spectrum sensing errors, the secondary transmission interference caused by the active primary user, and the dynamic primary user traffic. Both the adaptive continuous rate (ACR) scheme and the adaptive discrete rate (ADR) scheme for the adaptive modulation are examined. Theoretical derivations are presented for both the bit error rate (BER) performance and the link spectral efficiency (SE) performance. The performance of the adaptive modulation in cognitive radio is then compared to the performance the conventional adaptive modulation.

Chapter 6 evaluates the performance of a novel structure for cognitive radio where the spectrum sensing is performed by using the recovered received secondary frames. Unlike previous work, in this evaluation, the practical secondary user decoding errors are taken into consideration. The performance of the novel structure applying different spectrum sensing algorithms are examined. By presenting the analysis for a realistic case of the novel structure, the chapter presented a comprehensive comparison between the novel structure and the traditional model that adopts the IEEE 802.22 MAC frame structure. Moreover, the analysis has also been expended to include multiple consecutive secondary frames and established a real-

istic scenario where the secondary transmission achievable throughput is affected by the accumulated decoding errors, which has also not been previously considered. Both the receiver operating characteristics (ROC) curves for the spectrum sensing and the achievable throughput for the secondary data transmission are derived. Effects of fading channel and error control codes (ECC) are also investigated.

Finally in Chapter 7, the executive conclusion of this thesis is given. The research results and findings are summarized with their potential impact analyzed. Possible future work directions are also discussed.

Chapter 2

Cognitive Radio Overview

2.1 Introduction

A comprehensive overview of the cognitive radio technology is provided in this chapter to form a theoretical foundation for the rest of this thesis.

Defined by the fundamental concept and objectives of cognitive radio, the two main aspects of cognitive radio technology are to identify the unoccupied spectrum holes through necessary observations of the surrounding radio environment, and to achieve the secondary utilization of the licensed spectrum on an opportunistic basis. To accomplish these, two major functions of the cognitive radio system can be concluded: the spectrum estimation and the secondary data transmission. This can also be recognized from the defined superframe and MAC frame structure of the IEEE 802.22 WRAN. In this chapter, a detailed overview is provided for both of these functions.

First, in Section 2.2, an overview of the spectrum estimation techniques are presented, while their performance merits and limitations are introduced. At the end of the Section 2.2, one category of spectrum estimation technique is chosen

as the focus for the rest of the thesis with reasons provided. In Section 2.3, the chosen spectrum estimation technology is elaborated. Different types of algorithms belonging in this category are introduced. The advantages and disadvantages of each algorithm are also discussed. In Section 2.4, an overview of the secondary data transmission in cognitive radio system is presented. Finally, in Section 2.5, a brief summary is given for the discussions in this chapter.

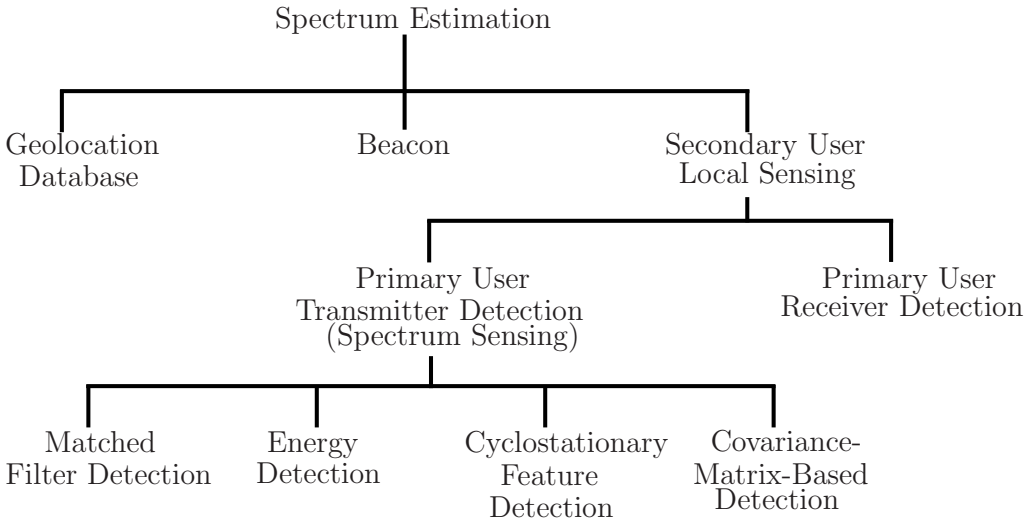

Figure 2.1: Comparison of different spectrum estimation methods.

2.2 Spectrum Estimation Overview

As the fundamental concept of the cognitive radio implementing OSA indicates, the secondary user can only utilize the licensed channel if it is considered as a spectrum hole. Thus, accurate identification of the spectrum holes is the first crucial step toward the realization of cognitive radio systems. Spectrum estimation enables the secondary user to perceive the presence of the primary user and the appearance of the spectrum holes. It is therefore the key enabling technology for spectrum hole

identification. As illustrated by Fig. 2.1, there are several techniques that can be used by the secondary user to achieve spectrum estimation: geolocation database, beacon and secondary user local spectrum sensing.

2.2.1 Geolocation Database

For some wireless communication services, such as the TV broadcasting, the primary user spectrum utilization patterns including the transmission power, the frequency bands and the operating durations, etc., are predetermined for specific geographic locations. In this case, a geolocation database of the spectrum utilization pattern can be established [55–62]. By equipping the secondary user with a Global Positioning System (GPS) or other similar technologies, the geolocation database can acquire its position information and feedback the channel occupancy information in return [11,34]. However, this method has several practical problems. First, to establish the geolocation database, the primary user is required to register its operating information. This forces the primary user to adjust its existing system. Secondly, after the establishment of the geolocation database, the associated maintaining and operating issues create further challenges which may be complicated and expensive. Thirdly, an alternative band is also needed so that the channel occupancy information held by the database can be transmitted to the secondary user. Finally, while the GPS can provide the secondary user position information with enough accuracy in outdoor environments, its performance significantly degrades deep inside buildings, leading to inaccurate feedbacks.

2.2.2 Beacon

There are two different ways for the secondary user to achieve spectrum estimation by using beacon. First, an instruction beacon can be sent out by the primary user to indicate the availability of the licensed channel [63]. The secondary user can consider the channel to be occupied by the primary user upon receiving of the instruction beacon, whereas the channel can be considered as idle if the instruction beacon is not received by the secondary user within a certain amount of time. However, to achieve this, necessary beacon transmitting structure is required, leading to the operating and maintaining issues associated with it. In the case of the beacon transmitting structure being operated by the primary user, modifications to the existing primary user infrastructure also becomes compulsory. Moreover, unreliable spectrum estimation performance can also occur when the transmitted beacon is lost due to fading and shadowing, causing potential threats to the primary user QoS.

On the other hand, sensing beacon can also be sent out by the secondary user [64]. Upon receiving of its own beacon, the secondary user can determine the licensed channel occupancy status by comparing it to the original beacon signal. However, sensing beacon transmitted by the secondary user can create significant interference to the primary user if proper precautions have not been taken into consideration.

2.2.3 Secondary User Local Spectrum Sensing

The spectrum estimation can also be achieved through secondary user local spectrum sensing. Performed by the secondary user transmitter, it estimates the channel occupancy status through collecting and analyzing the local measurements of the spectrum parameters. With a small increase in the secondary user transceiver com-

plexity, this method depends solely on the secondary user and requires no further modifications to the exiting primary user infrastructure.

Following the MAC frame structure, the secondary user transmitter perform local spectrum sensing during the spectrum estimation slot of the frame. The local spectrum sensing can be further divided into two sub-categorizes: primary user receiver detection and primary user transmitter detection.

- Primary user receiver detection

  The secondary user local spectrum sensing can be performed through detecting the active primary user receiver [65–67]. It is the most obvious and efficient way of avoiding causing interference to the primary user, since it is the primary user receiver that requires protection from the harmful interference.

  Generally, when the primary user receiver is receiving data from the active primary user transmitter, the received signal needs to be converted from the carrier frequency to intermediate frequency to prepare for further processing. While performing the conversion, the RF front-end of the receiver emits local oscillator leakage power. By exploring this power, the secondary user can determine the occupancy status of the primary user [65]. However, while this detection is possible in theory, it is almost impractical in reality. As the local oscillator leakage signal power is typically extremely low and the accurate detection of such power would be extremely difficult. Currently, this is only achievable in the detection of the TV receivers, used by British Broadcast to find fee evaders [66]. For this reason, most recent work focuses on the detection of the primary user transmitter [7].

- Primary user transmitter detection

Since it is difficult for the secondary user to have a direct measurement of the primary user receiver, the active primary user transmitter can be detected instead. By doing so, the secondary user can determine if a signal is being transmitted in the licensed channel, which indicates an occupied spectrum band. There are four algorithms generally used for the primary user transmitter detection: matched filter detection, energy detection, cyclostationary feature detection and covariance-matrix-based detection. Depending on the system model and the sensing quality requirement, different sensing algorithms can be applied in different circumstances. In the following section, these will be investigated in details.

As a conclusion for the spectrum estimation techniques discussed so far, both the geolocation database and beacon techniques have complex infrastructure and requires modification to the primary user network, whereas the secondary user local spectrum sensing has much lower infrastructure requirements and broader application areas. Due to the aforementioned merits and limitations of the implementation and performance, the secondary user local sensing of the primary user transmitter is adopted by the vast majority of researches [1]. Consequently, the research in this thesis is also focused on this method. In most literatures and for the rest of this thesis, the secondary user local sensing of the primary user transmitter is simply referred to as spectrum sensing. For this reason, the aforementioned spectrum estimation slot in the IEEE 802.22 MAC frame structure, will be referred to as the spectrum sensing slot hereafter.

2.3 Spectrum Sensing Algorithms

The goal of spectrum sensing is to distinguish between the absence and the presence of the primary user. Denote these two scenarios as H_0 and H_1, respectively. The spectrum sensing can then be regarded as a binary hypothesis testing problem between the hypotheses H_0 and H_1. The received signal at the secondary user can by presented as [68]

$$y(t) = \begin{cases} w(t), & H_0, \\ s(t) + w(t), & H_1, \end{cases} \tag{2.1}$$

where $y(t)$ denotes the received signal at the secondary user, $w(t)$ represents the additive white Gaussian noise (AWGN) and $s(t)$ represents the primary user signal received at the secondary user.

When performing the spectrum sensing, there are two parameters that are used as criteria for evaluating the sensing quality: the probability of false alarm and the probability of detection. The probability of false alarm P_{fa} is defined as the probability that the secondary user mistakenly consider the primary user to be present in the licensed channel while it is actually absent. It can be represented as $Pr\{H_1|H_0\}$. The probability of detection P_d is defined as the probability that the secondary user correctly detects the existence of the primary user in the licensed channel. It can be represented as $Pr\{H_1|H_1\}$. In some literatures, the probability of missed opportunity $P_{mo} = Pr\{H_1|H_0\} = P_{fa}$ and the probability of mis-detection $P_{md} = Pr\{H_0|H_1\} = 1 - P_d$ are also used.

The spectrum sensing performance is characterized through its ROC curves, such as the example in Fig. 2.2. In a good spectrum sensing performance, P_d should be

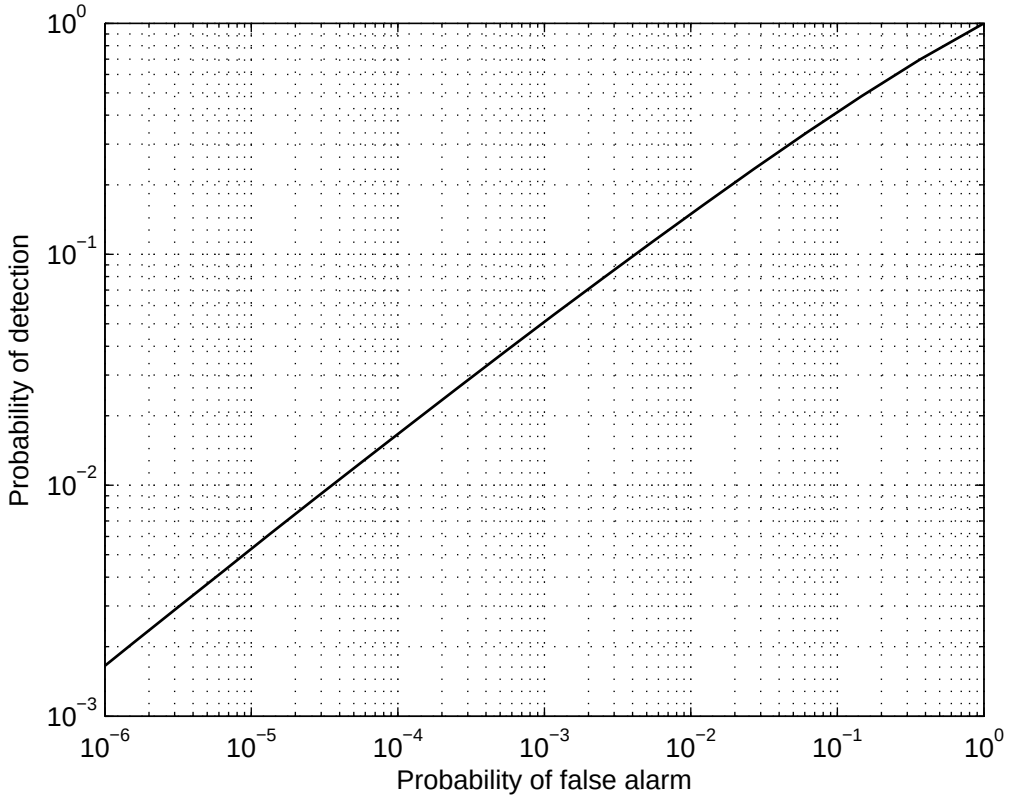

Figure 2.2: Example of ROC curve of the spectrum sensing performance.

high enough to guarantee the protection of the primary user while P_{fa} is minimized to a certain level to optimize the secondary utilization efficiency. The decision threshold of the spectrum sensing is determined by setting a target probability for the spectrum sensing performance. In practice, the target is normally set for the probability of detection so that the protection towards the primary user can be ensured. If a 100% protection is required by the primary user, no secondary utilization of the spectrum will be permitted. Therefore, the target probability of detection $\widehat{P_d}$ is normally chosen to be close to but less than 1. Depending on the system model and the sensing quality requirement, different sensing algorithms can

be applied in different circumstances.

2.3.1 Matched Filter

Matched filter detection [69–73] is the optimal detection scheme for AWGN channel when the precise primary user signal information is known by the secondary user, such as the modulation type and order, the pulse shape, the packet format, and the transmission channel [69, 70]. As a coherent detection algorithm, matched filter detection can achieve good sensing performance with short sensing time [73]. However, although the knowledge of the primary user signal can be estimated at the secondary user using the primary user's pilot, preamble or training sequence, when spectrum sensing is required for a wide spectrum band with different types of primary user signals, the estimation process becomes impractically complex and extremely difficult to implement [70]. Moreover, when the primary user SNR is low, the estimation can have large error and consequently leads to poor sensing results.

2.3.2 Energy Detection

Energy detection [74–76] is a non-coherent detection method which can be used for spectrum sensing when the primary user signal is unknown to the secondary user [70,77] . It is performed by measuring the energy of the received signal samples and is the optimal detection method for detecting independent and identically distributed (iid) signal.

Suppose that the interested licensed channel has a carrier frequency f_c and the received signal from the licensed channel is pre-filtered by a band-pass filter of bandwidth W. The total number of received signal samples during the sensing slot duration τ is $I = \tau f_s$, where f_s is the sampling frequency. For simplicity, assume

that I is an integer and $I = 2\tau W$.

At the energy detector, the output of the band-pass filter is squared and integrated over τ. The output of the integrator Y, is used as the test statistic for the energy detection and can be derived as, [1]

$$Y(I) = \begin{cases} \sum_{i=1}^{I} w_i^2, & H_0, \\ \sum_{i=1}^{I} (s_i + w_i)^2, & H_1, \end{cases} \tag{2.2}$$

where $i = 1, 2, \ldots, I$ is the sample index.

$Y(I)$ is then compared to the decision threshold to determine whether the primary user is present. The decision threshold, Ψ, is selected to meet the sensing performance requirement. A well chosen decision threshold can minimize the spectrum sensing errors and finding an optimum balance between the P_d and P_{fa}.

The hypothesis testing problem using energy detection can therefore be formulated as

$$Y(I) \underset{H_1}{\overset{H_0}{\lessgtr}} \Psi. \tag{2.3}$$

Thus, the probability of false alarm and the probability of detection can be expressed as

$$P_{fa} = Pr\{H_1|H_0\} = Pr\{Y > \Psi|H_0\}, \tag{2.4}$$

and

$$P_d = Pr\{H_1|H_1\} = Pr\{Y > \Psi|H_1\}, \tag{2.5}$$

respectively.

Although the energy detection can be performed without any knowledge of the primary user signal, it has several practical defects. First, since the energy of the received signal is used to perform the detection, it can not differentiate between the primary user signal and the noise, or distinguish different types of primary user signal. This makes the energy detection vulnerable to high noise power, and leading to poor sensing results in the low SNR regimes. Secondly, a small noise power estimation error could lead to SNR wall and significant performance loss of the energy detection, as the chosen of the decision threshold depends on the noise variance. However, due to its low computational and implementation complexity and no requirement on *a priori* knowledge of the primary user signals, energy detection is the most popular and commonly used detection algorithm [69].

2.3.3 Cyclostationary Feature Detection

Cyclostationary feature detection [78–81] was first introduced in [82], which exploits the cyclostationary feature of the received signal statistics for spectrum sensing.

In wireless communications, transmitted signals are generally modulated signals with certain carriers, pulse trains, repeating spreading, hopping sequences or cyclic prefixes, with inherent periodicities. Therefore, the statistics of the primary user signal emerges cyclostationary features while the noise is a stationary process with no such feature. Consequently, cyclostationary feature detection can be applied to differentiate between the primary user signals and noise, or even different primary users with different cyclic frequencies [32].

Since the cyclostationary feature of the primary user signal is not affected by the SNR of the received signal, this detection method is robust to noise uncertainties and can achieve good sensing performance even in very low SNR regimes. However, in

order to perform the cyclostationary feature detection, the knowledge of the primary user cyclic frequency is required, which may not be realistic for many cognitive radio applications. Moreover, it generally involves much higher computational complexity than the aforementioned energy detection algorithm and hence much longer sensing time.

2.3.4 Covariance-Matrix-Based Detection

Covariance-matrix-based detection operates based on the statistical covariances or auto-correlations of the received signal. Since the statistical covariance matrix or autocorrelations of signal and noise are generally different, this difference can be used for spectrum sensing when there is no priori knowledge of the primary user. It is an optimal detection algorithm when a correlated signal is used by the primary user in iid noise channel, as the covariance matrix of the received signal catches the correlations among signal samples.

In this method, based on the received signal samples at the secondary user, the sample covariance matrix of the received signal is first computed. Different test statistics are then calculated from the sample covariance matrix. Depending on the test statistic choices, the covariance matrix based detection has several algorithm options, including: maximum-eigenvalue detection [83], maximum-minimum-eigenvalue detection [84, 85], energy with minimum eigenvalue detection [85] and covariance-based detection [86, 87]. Finally, the test statistics are compared to the decision threshold which is chosen according to the random matrix theory, to determine the channel occupancy status. For different algorithm options, the comparison criteria and selected decision threshold are different.

- Maximum-eigenvalue detection

In the maximum-eigenvalue detection, the maximum eigenvalue of the sample covariance matrix is used as the test statistic, and compared to the selected decision threshold. The primary user is considered to be present in the licensed channel if the maximum eigenvalue is greater than the threshold. Otherwise, the licensed channel can be considered as idle. This can be represented as

$$\theta_{max} \underset{H_1}{\overset{H_0}{\lessgtr}} \Psi_{ME}, \tag{2.6}$$

where θ_{max} is the maximum eigenvalue of the covariance matrix of the received signal and Ψ_{ME} is the chosen decision threshold.

- Maximum-minimum-eigenvalue detection

  In the maximum-minimum-eigenvalue detection, both the maximum eigenvalue and the minimum eigenvalue of the sample covariance matrix are used as the test statistics. It uses the ratio of the maximum and minimum eigenvalues to determine the occupancy status of the licensed channel. The primary user is considered to be present in the licensed channel if the maximum eigenvalue is greater than the product of the decision threshold and the minimum eigenvalue of the sample covariance matrix. Otherwise, the licensed channel is considered idle. It can be represented as

$$\theta_{max} \underset{H_1}{\overset{H_0}{\lessgtr}} \theta_{min}\Psi_{MME}, \tag{2.7}$$

where θ_{min} is the minimum eigenvalue of the covariance matrix of the received signal and Ψ_{MME} is the chosen decision threshold.

- Covariance-based detection

  The elements of the covariance matrix can also be used to perform the spectrum sensing. It utilizes the fact that the covariance matrices of the correlated primary user signal is not diagonal. Hence, when the correlated primary user is present in the licensed channel, the off-diagonal elements of the covariance matrix are not all zeros, whereas when the licensed channel is idle and contains only noise, the off-diagonal elements should be zeros.

- Energy with minimum eigenvalue detection

  The covariance matrix based detection can also be implemented while the energy detection functions are incorporated. By computing the average power of the received signal and the minimum eigenvalue of the covariance matrix as the test statistics, the primary user can be considered as present in the licensed channel if the ratio of the test statistics are greater than the decision threshold. Otherwise, the primary user can be considered as absent, represented as

$$\frac{Y}{\theta_{min}} = \begin{array}{c} H_0 \\ \lessgtr \\ H_1 \end{array} \Psi_{EME}, \tag{2.8}$$

  where Ψ_{EME} is the chosen decision threshold.

When a narrow-band filter is used at the secondary user, the noise samples in the received signal will sometimes no longer be iid. In this case, as the covariance matrix of the noise is determined by the filter, its structure is known. Based on this

structure, a new covariance matrix can be formed for the received signal, which can then be used to perform covariance-matrix-based spectrum sensing in the same way as above discussed.

The covariance-matrix-based detection has better performance than the energy detection when the primary user signal is correlated, whereas its performance approaches the energy detection when the primary user is iid signal. Therefore, the covariance matrix based detection algorithm is more generalized than the energy detection, as it includes the energy detection as a special case. Moreover, the covariance-matrix-based detection does not require knowledge of noise variance. However, due to the calculations involved in the covariance matrix based detection algorithm, it is more computational complexed than the energy detection.

2.4 Secondary Transmission Overview

Ultimately, the goal of the cognitive radio is to achieve the secondary utilization of the licensed channel through performing secondary data transmission. Therefore, the secondary transmission is the other important aspect of cognitive radio. After the completion of the spectrum sensing, if the primary user is considered to be present in the licensed channel by the secondary user, no secondary utilization of the channel can be carried out. In this case, the secondary user will wait until the beginning of the next MAC frame to perform spectrum sensing again for opportunities of secondary utilization. Otherwise, the secondary user starts its transmission in the following transmission slot of the MAC frame. The secondary transmission can be characterized by the secondary channel capacity.

The secondary user will consider the licensed channel to be idle in two scenarios. First, when the primary user is actually absent from the licensed channel and a

detection of its absence is made by the spectrum sensing without mistakes with probability of $1 - P_{fa}$. In this case, only the secondary user is operating in the licensed channel during the secondary transmission slot. According to the Shannon-Hartley theorem, the normalized secondary channel capacity can be expressed as [88]

$$\begin{aligned} C_{H_0} &= \log_2\left(1 + \frac{S_s}{w_0}\right) \\ &= \log_2\left(1 + \gamma_s\right), \qquad (Bits/Sec/Hz), \end{aligned} \tag{2.9}$$

where S_s is the average received secondary signal power at the secondary user receiver, w_0 is the noise power of the AWGN $w(t)$ in (2.1), γ_s is the secondary transmission SNR and $\log_2(\cdot)$ is the logarithm to the base 2.

Second, when the primary user is actually present in the licensed channel, however, its presence is not correctly recognized by the spectrum sensing, with probability of $1 - P_d$. In this case, the secondary user starts its secondary transmission even through the primary user is presenting in the licensed channel. From the secondary user's perspective, the existing primary user signal becomes interference to its transmission. The normalized channel capacity can therefore be expressed while taking this interference into account,

$$\begin{aligned} C_{H_1} &= \log_2\left(1 + \frac{S_s}{w_0 + S_p}\right) \\ &= \log_2\left(1 + \frac{\gamma_s}{1 + \gamma_p}\right), \qquad (Bits/Sec/Hz), \end{aligned} \tag{2.10}$$

where S_p is the average primary user signal power and γ_p is the primary user SNR received at the secondary user. From the secondary user's perspective, γ_p is also the interference-to-noise ratio (INR).

Note that in practice, the secondary user has no knowledge of the primary user

SNR γ_p. As the primary user is mistakenly considered to be absent in H_1, the secondary user will therefore carry out secondary transmission with datarate equals to C_{H_0}. In this case, the actual datarate is larger than the channel capacity ($C_{H_0} > C_{H_1}$), resulting in large errors in the received secondary signal.

2.5 Summary

In this chapter, a comprehensive overview of the cognitive radio technology was provided for both the spectrum estimation aspect and the secondary data transmission aspect. In the overview of spectrum estimation, with the details of different spectrum estimation technologies and algorithms discussed, the secondary user local detection of the primary user transmitter was chosen as the main sensing technique used in the rest of this thesis. In the overview of the secondary transmission, some fundamental calculations of the achievable throughput were introduced. With the theoretical foundation of cognitive radio established, the analytical evaluation of the cognitive radio performance can begin.

Chapter 3

Sensing-Throughput Tradeoff with Primary User Traffic

3.1 Introduction

As was previously introduced in the Chapter 1, the MAC frame structure proposed by the IEEE 802.22 WRAN standard is widely adopted in researches of the cognitive radios. In this structure, while consisting of a spectrum sensing slot and a secondary transmission slot, the MAC frame duration is fixed. During the spectrum sensing process, for a target probability of false alarm, the probability of detection increases when the sensing period increases. From the primary user's perspective, the higher the probability of detection is, the better protection it will obtain from the secondary user. At the same time, for a target probability of detection, the probability of false alarm decreases when the sensing duration increases. From the secondary user's perspective, the lower the probability of false alarm is, the higher secondary transmission opportunities it will have. Therefore, a better sensing quality can be

achieved by having a spectrum sensing slot with longer duration. However, the increase in the sensing duration results in a decrease in the transmission duration as the overall length of the frame is fixed. This direct decrease of the secondary transmission time leads to a reduction in the conditional achievable throughput of the secondary network. Thus, there exists a tradeoff between the spectrum sensing quality and the achievable secondary throughput [88–90].

This sensing-throughput tradeoff problem has been investigated in [88] and [89]. The authors showed that for a target probability of detection, there exists an optimal sensing time at which the achievable throughput can be maximized. However, in [88] and [89], the problem was formulated based on an assumption that the primary user has a constant occupancy status during the entire frame. In other words, they have assumed that the primary user is either always present or always absent for the whole secondary MAC frame period.

In reality, as the primary user has the higher priority to the licensed channel, it may randomly arrive or depart from the channel at anytime, especially when the primary user network has a high traffic rate or when a long secondary frame duration is used. In these cases, part of the secondary frame may see a busy licensed channel while part of the secondary frame may see an idle licensed channel. Therefore, it is worth reformulating the problem while taking into consideration of the random arrival and departure of the primary user, and investigate the effect of this dynamic primary user traffic on the sensing-throughput tradeoff performance.

In this chapter, the constant primary user occupancy status assumption for the sensing-throughput tradeoff problem discussed in [88] and [89] is taken away by considering a more realistic case where a primary user random arrival or departure from the licensed channel during the secondary frame duration is included. The

rest of this chapter is organized as follows. In Section 3.2, the conventional sensing-throughput tradeoff of the cognitive radio system where the primary user is assumed to be static, is briefly described for comparison purpose. The dynamic primary user traffic model that considers a random arrival and departure of the primary user is then presented in Section 3.2. In Section 3.3, the effect of the dynamic primary user traffic on the sensing-throughput tradeoff is analyzed. In Section 3.4, the derivations from Section 3.3 are examined by presenting some numerical results. Finally, the findings of this chapter are concluded in Section 3.5.

3.2 Conventional Sensing-Throughput Tradeoff

Consider the cognitive radio system introduced in the Chapter 2, where the primary user and the secondary user are operating in the same licensed channel employing OSA. The MAC frame structure of IEEE 802.22 WRAN standard is adopted with the sensing slot duration τ and frame duration T. During the sensing slot, spectrum sensing is carried out using energy detection.

Conventionally, the primary user is assumed to be either always present or always absent during the entire frame duration. Thus, the energy detection is a binary hypothesis testing problem given by (2.1), with test statistic Y given by (2.2).

Under hypothesis H_0, Y can be viewed as the sum of squares of I standard real Gaussian variables with zero means and unit variances. Therefore, Y follows a central chi-square distribution with I degrees of freedom. Under hypothesis H_1, Y follows a non-central chi-square distribution with I degrees of freedom and a non-centrality parameter of $I\gamma_p$. Therefore, the probability density function (PDF) of

Y can be expressed as [77]

$$f_Y(Y) = \begin{cases} \frac{1}{2^{\frac{I}{2}}\Gamma\left(\frac{I}{2}\right)} Y^{\frac{I}{2}-1} e^{-\frac{Y}{2}}, & H_0, \\ \frac{1}{2} e^{-\frac{I}{2}\gamma_p - \frac{Y}{2}} \left(\frac{Y}{I\gamma_p}\right)^{\frac{I-2}{4}} \mathcal{I}_{\frac{I}{2}-1}\left(\sqrt{I\gamma_p Y}\right), & H_1, \end{cases} \tag{3.1}$$

where $\mathcal{I}_z(\cdot)$ is the z-th order modified Bessel function of the first kind given by $\mathcal{I}_z(x) = \left(\frac{x}{2}\right)^z \sum_{j=0}^{\infty} \frac{(x^2/4)^j}{j!\Gamma(z+j+1)}$ [91] and $\Gamma(\cdot)$ is the Gamma function given by $\Gamma(x) = \int_0^\infty t^{x-1}e^{-t}dt$ [91].

By using (3.1), the probability of false alarm of the energy detection in the conventional model can be derived as

$$\begin{aligned} P_{fa\chi^2}\left(\Psi_{\chi^2}, I\right) &= \int_{\Psi_{\chi^2}}^{\infty} f_Y(Y, H_0) \cdot dY \\ &= 1 - \frac{\Gamma\left(\frac{I}{2}, \frac{\Psi_{\chi^2}}{2}\right)}{\Gamma\left(\frac{I}{2}\right)}, \end{aligned} \tag{3.2}$$

where Ψ_{χ^2} is the decision threshold in this case and $\Gamma(\cdot,\cdot)$ is the incomplete Gamma function given by $\Gamma(x,z) = \int_0^z t^{x-1}e^{-t}dt$. The probability of detection can be derived as

$$\begin{aligned} P_{d\chi^2}\left(\Psi_{\chi^2}, I\right) &= \int_{\Psi_{\chi^2}}^{\infty} f_Y(Y, H_1) \cdot dY \\ &= Q_m\left(\sqrt{I\gamma_p}, \sqrt{\Psi_{\chi^2}}\right), \end{aligned} \tag{3.3}$$

where symbols are defined as before and $Q_m(\cdot,\cdot)$ is the generalized Marcum Q-function, give by $Q_m(x,z) = \int_z^\infty \frac{t^m}{x^{m-1}} e^{-\frac{t^2+x^2}{2}} \mathcal{I}_{m-1}(xt)\, dt$.

When the number of samples in spectrum sensing is relatively large, the central limit theorem (CLT) can be applied to approximate the distribution of Y [75, 89, 92]. The PDF of Y under both hypothesis can be approximated by a Gaussian

distribution [75,89]. The mean μ and variance σ^2 of Y in hypothesis H_0 and H_1 are given by [68]

$$\begin{cases} \mu_{H_0} = I, & \sigma^2_{H_0} = 2I, & H_0, \\ \mu_{H_1} = I + I\gamma_p, & \sigma^2_{H_1} = 4I\gamma_p + 2I, & H_1. \end{cases} \tag{3.4}$$

Hence, the probability of false alarm can be re-derived as [75]

$$P_{faG}\left(\Psi_G, I\right) = \frac{1}{2}\text{erfc}\left(\frac{\Psi_G - I}{2\sqrt{I}}\right), \tag{3.5}$$

where Ψ_G is the decision threshold and erfc$(\cdot)$ is the complementary error function. The probability of detection can be derived as,

$$P_{dG}\left(\Psi_G, I\right) = \frac{1}{2}\text{erfc}\left(\frac{\Psi_G - I - I\gamma_p}{2\sqrt{I + 2I\gamma_p}}\right). \tag{3.6}$$

Denoting P_{H_0} and P_{H_1} as the *a priori* probabilities of the primary user being absent and present at the licensed channel, respectively. Then, there is $P_{H_0} + P_{H_1} = 1$. When the spectrum sensing is completed, the secondary transmission starts in the transmission slot if the licensed channel is considered to be idle, as has been discussed in Chapter 2. Therefore, the total average achievable throughput of the secondary transmission in the conventional model is

$$\begin{aligned} R_G\left(\Psi_G, I\right) =& R_{H_0}\left(\Psi_G, I\right) + R_{H_1}\left(\Psi_G, I\right) \\ =& \frac{T-\tau}{T} P_{H_0}\Big(1 - P_{faG}\left(\Psi_G, I\right)\Big) C_{H_0} \\ &+ \frac{T-\tau}{T} P_{H_1}\Big(1 - P_{dG}\left(\Psi_G, I\right)\Big) C_{H_1}, \qquad (Bits/Sec/Hz). \end{aligned} \tag{3.7}$$

When chi-square distribution of Y is used, the total achievable throughput can

be obtained using (3.2) and (3.3) instead of (3.5) and (3.6) in (3.7).

Note that the achievable throughput presented in (3.7) is an averaged value based on the probability of each hypothesis. In practice, this value cannot always be achieved, as only limited number of frames are included in the coding block design. The actual throughput value of the secondary transmission depends on the primary user occupancy status in each frame as well as the number of frames included in the coding implementation.

3.3 Dynamic Primary User Traffic Model

In the analysis of the conventional model above, the primary user is assumed to have a constant occupancy status. It is assumed to be either always active or always inactive for the entire frame duration. In reality, the primary user may not always abide by the conventional model. Define the duration for which the primary user being present in the licensed channel as the primary user busy channel holding time, and define the duration for which the primary user is absent from the channel as the primary user idle channel holding time. In some applications, such as TV broadcasting, the primary user has relatively long channel holding times, and the occupancy status of the licensed channel changes relatively slow. In this case, the conventional model is a good approximation to the actual scenario. In some cases, however, the primary user may have short channel holding times and the channel status therefore changes frequently. The primary user may arrive at the originally idle channel or depart from the originally busy licensed channel during the frame. In this case, the conventional model discussed above is no longer a good approximation to the real situation.

Let '1' represent a busy licensed channel occupied by the primary user and '0'

represent an idle channel, the dynamic primary user traffic can be modelled as a Markov 1-0 random process. Many work has been done on the channel holding time distributions among which, exponential distribution is a widely used model [93, 94]. In this chapter, it is assumed that both the busy channel holding time and the idle channel holding time are exponentially distributed, with rate parameters λ_b and λ_e, respectively. At any time instant, the channel is busy with probability $p_b = \frac{\lambda_b}{\lambda_b+\lambda_e}$, and idle with probability $p_e = 1 - p_b$. Denote the duration of each sample as t_s. The transition probability for when the channel is in state 'z' $\in \{0, 1\}$ given that t_s seconds ago it was in state 'x'$\in \{0, 1\}$ is given by [92]

$$\begin{aligned} p_{xz}\left(t_s; \lambda_b, \lambda_e\right) &= \begin{pmatrix} p_{00}\left(t_s\right) & p_{01}\left(t_s\right) \\ p_{10}\left(t_s\right) & p_{11}\left(t_s\right) \end{pmatrix} \\ &= \frac{1}{\lambda_b + \lambda_e} \begin{pmatrix} \lambda_b + \lambda_e e^{-(\lambda_b+\lambda_e)t_s} & \lambda_e - \lambda_e e^{-(\lambda_b+\lambda_e)t_s} \\ \lambda_b - \lambda_b e^{-(\lambda_b+\lambda_e)t_s} & \lambda_e + \lambda_b e^{-(\lambda_b+\lambda_e)t_s} \end{pmatrix}. \end{aligned} \tag{3.8}$$

It is assumed that the primary user occupancy status transition occurs only once within each frame or that the frame duration of the primary user is longer than the frame duration of the secondary user. This is the case when the primary user and secondary user are providing similar services such that their frame sizes are comparable. It is further assumed that the primary user status transition can be completed within one sample. Let the total number of samples in the frame duration be J. Denote β and α as the sample at which the primary user departs and arrives at the licensed channel, respectively. As illustrated by Fig. 3.1, there are six possible scenarios:

- $H_{0,0(0)}$: In this scenario, the primary user is absent from the licensed channel for the entire frame duration. This is the same as the hypothesis H_0 of the

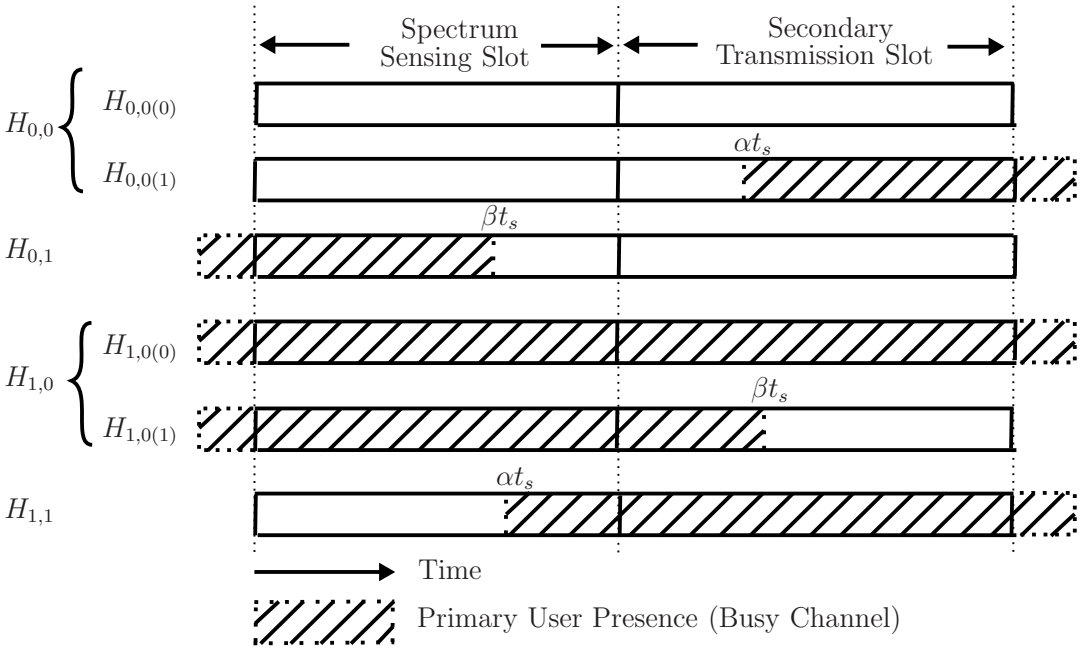

Figure 3.1: Scenarios for the dynamic primary user traffic model with one primary user occupancy status change.

conventional model.

- $H_{0,0(1)}$: The primary user is absent during the sensing slot. It then arrives at the licensed channel during the secondary data transmission slot.

- $H_{0,1}$: The primary user is present at the beginning of the sensing slot. It then departs from the licensed channel during the sensing slot and remains absent for the rest of the secondary frame.

- $H_{1,0(0)}$: The primary user is present at the licensed channel for the entire frame duration. This is the same as the hypothesis H_1 of the conventional model.

- $H_{1,0(1)}$: The primary user is present during the sensing slot and then departs from the licensed channel during the transmission slot.

- $H_{1,1}$: The primary user is absent at the beginning of the sensing slot and then arrives during the sensing slot. It remains present for the rest of the frame.

In Fig. 3.1 and the above descriptions, the subscripts to the notations $H_{a,b}$ or $H_{a,b,(c)}$ indicate different scenarios. To be more specific, the first subscript 'a' indicates the channel status at the end of the sensing period, where '1' represents a busy channel and '0' represents an idle channel. the second subscript 'b' indicates the number of primary user status changes during the sensing period, where '1' and '0' represent one change or no change at all, respectively. The third subscript '(c)' represents the number of changes during the transmission period when no change occurred during the sensing period, where '1' and '0' represent one change or no change at all during the transmission period, respectively.

By using the transition probabilities in (3.8), the probabilities of each of the above scenario occurring can be derived as

$$\begin{aligned}
P_{H_{0,0(0)}}(\lambda_b,\lambda_e) &= p_e p_{00}^{J}(t_s), \\
P_{H_{0,0(1)}}(\lambda_b,\lambda_e) &= \sum_{\alpha=I+1}^{J-1}\Big(p_e p_{00}^{\alpha}(t_s)\, p_{01}(t_s)\, p_{11}^{J-\alpha-1}(t_s)\Big), \\
P_{H_{0,1}}(\lambda_b,\lambda_e) &= \sum_{\beta=1}^{I}\Big(p_b p_{11}^{\beta}(t_s)\, p_{10}(t_s)\, p_{00}^{J-\beta-1}(t_s)\Big), \\
P_{H_{1,0(0)}}(\lambda_b,\lambda_e) &= p_b p_{11}^{J}(t_s), \\
P_{H_{1,0(1)}}(\lambda_b,\lambda_e) &= \sum_{\beta=I+1}^{J-1}\Big(p_b p_{11}^{\beta}(t_s)\, p_{10}(t_s)\, p_{00}^{J-\beta-1}(t_s)\Big), \\
P_{H_{1,1}}(\lambda_b,\lambda_e) &= \sum_{\alpha=1}^{I}\Big(p_e p_{00}^{\alpha}(t_s)\, p_{01}(t_s)\, p_{11}^{J-\alpha-1}(t_s)\Big).
\end{aligned} \tag{3.9}$$

In the next section, by using the dynamic traffic model presented in (3.9), its effect on the sensing-throughput tradeoff will be analyzed.

3.4 Sensing-Throughput Tradeoff with Primary User Traffic

3.4.1 Spectrum Sensing Performance

As shown in Fig. 3.1, from the spectrum sensing hypothesis test point of view, the six scenarios presented is categorized into four hypothesis: $H_{0,0}$, $H_{0,1}$, $H_{1,0}$ and $H_{1,1}$, representing the absence, departure, arrival and presence of the primary user during the spectrum sensing slot, respectively. The new spectrum sensing is therefore a quarternary hypotheses testing problem given by

$$Y_H = \begin{cases} \sum_{i=1}^{I} w_i^2, & H_{0,0}, \\ \sum_{i=1}^{\beta} (s_i + w_i)^2 + \sum_{i=\beta+1}^{I} w_i^2, & H_{0,1}, \\ \sum_{i=1}^{I} (s_i + w_i)^2, & H_{1,0}, \\ \sum_{i=1}^{\alpha} w_i^2 + \sum_{i=\alpha+1}^{I} (s_i + w_i)^2, & H_{1,1}. \end{cases} \tag{3.10}$$

By using (3.10) and conditioned on the values of α and β, the conditional probabilities of false alarm and the conditional probabilities of detection for the spectrum sensing can be obtained. In hypothesis $H_{0,0}$, the primary user is always absent during the sensing slot, it is therefore the same as that of H_0 of the conventional model from the spectrum sensing point of view. The conditional probability of false alarm

for $H_{0,0}$ hence equals to that of H_0, given by

$$\begin{aligned} P_{faH_{0,0}\chi^2}\left(\Psi_{H\chi^2}, I\right) &= P_{fa\chi^2}\left(\Psi_{\chi^2}, I\right) \\ &= 1 - \frac{\Gamma\left(\frac{I}{2}, \Psi_{H\chi^2}/2\right)}{\Gamma\left(\frac{I}{2}\right)}, \end{aligned} \tag{3.11}$$

where $\Psi_{H\chi^2}$ is the decision threshold for spectrum sensing with consideration of the primary user traffic.

In the hypothesis $H_{0,1}$, as the licensed channel is only idle after the β^{th} sample for part of the sensing slot, Y_H follows a non-central chi-square distribution with I degrees of freedom and a non-centrality parameter of $\beta\gamma_p$. Conditioned on the value of β, the conditional probabilities of false alarm can be derived as

$$P_{faH_{0,1}\chi^2}\left(\Psi_{H\chi^2}, I, \beta\right) = Q_m\left(\sqrt{\beta\gamma_p}, \sqrt{\Psi_{H\chi^2}}\right). \tag{3.12}$$

In the hypothesis $H_{1,0}$ the primary user is always present during the sensing slot which is equivalent to H_1 of the conventional model. The conditional probability of detection for $H_{1,0}$ is therefore given by

$$\begin{aligned} P_{dH_{1,0}\chi^2}\left(\Psi_{H\chi^2}, I\right) &= P_{d\chi^2}\left(\Psi_{\chi^2}, I\right) \\ &= Q_m\left(\sqrt{I\gamma_p}, \sqrt{\Psi_{H\chi^2}}\right). \end{aligned} \tag{3.13}$$

In the hypothesis $H_{1,1}$, as the licensed channel is only busy after the α^{th} sample for part of the sensing slot, Y_H follows a non-central chi-square distribution with I degrees of freedom and non-centrality parameter $I\gamma_p - \alpha\gamma_p$. Conditioned on the value of α, the conditional probabilities of detection can be derived as

$$P_{dH_{1,1}\chi^2}\left(\Psi_{H\chi^2}, I, \alpha\right) = Q_m\left(\sqrt{I\gamma_p - \alpha\gamma_p}, \sqrt{\Psi_{H\chi^2}}\right). \tag{3.14}$$

It can be noted that for the special cases when $\beta = 0$ and $\alpha = 0$ indicating the primary user occupancy status change is not occurring during the sensing slot, (3.12) and (3.14) degenerate to (3.11) and (3.13), respectively. The system is then the same as the conventional model where the primary user traffic is assumed to be static.

Similarly, the distribution of Y_H can also be approximated as Gaussian distribution when the value of I is large, with mean and variance of each hypothesis given by

$$\begin{cases} \mu_{H_{0,0}} = I, & \sigma^2_{H_{0,0}} = 2I, & H_{0,0}, \\ \mu_{H_{0,1}} = I + \beta\gamma_p, & \sigma^2_{H_{0,1}} = 2I + 4\beta\gamma_p, & H_{0,1}, \\ \mu_{H_{1,0}} = I + I\gamma_p, & \sigma^2_{H_{1,0}} = 4I\gamma_p + 2I, & H_{1,0}, \\ \mu_{H_{1,1}} = I + I\gamma_p - \alpha\gamma_p, & \sigma^2_{H_{1,1}} = 4I\gamma_p + 2I - 4\alpha\gamma_p, & H_{1,1}. \end{cases} \tag{3.15}$$

The conditional probabilities of false alarm for hypothesis $H_{0,0}$ and $H_{0,1}$ can then be derived as

$$P_{faH_{0,0}}(\Psi_H, I) = \frac{1}{2}\text{erfc}\left(\frac{\Psi_H - I}{2\sqrt{I}}\right), \tag{3.16}$$

and

$$P_{faH_{0,1}}(\Psi_H, I, \beta) = \frac{1}{2}\text{erfc}\left(\frac{\Psi_H - I - \beta\gamma_p}{2\sqrt{I + 2\beta\gamma_p}}\right), \tag{3.17}$$

respectively, where Ψ_H is the decision threshold for the spectrum sensing in this case. The conditional probability of detection for hypothesis $H_{1,0}$ and $H_{1,1}$ can then be derived as

$$P_{dH_{1,0}}(\Psi_H, I) = \frac{1}{2}\text{erfc}\left(\frac{\Psi_H - I - I\gamma_p}{2\sqrt{I + 2I\gamma_p}}\right), \tag{3.18}$$

and

$$P_{dH_{1,1}}\left(\Psi_H, I, \alpha\right) = \frac{1}{2}\mathrm{erfc}\left(\frac{\Psi_H - I - \left(I-\alpha\right)\gamma_p}{2\sqrt{\left(I + 2\left(I-\alpha\right)\gamma_p\right)}}\right), \tag{3.19}$$

respectively.

By using (3.11) and (3.12) for the chi-square distribution, or (3.16) and (3.17) for the Gaussian approximation of Y_H, the unconditional probability of false alarm for the spectrum sensing with primary user traffic, can be found by averaging the conditional probabilities of false alarm over the probabilities of occurring for different values of β. It can be derived as

$$\begin{aligned}\overline{P_{faH}}\left(\Psi_H, I\right) =& \frac{\left(P_{H_{0,0(0)}}(\lambda_b,\lambda_e) + P_{H_{0,0(1)}}(\lambda_b,\lambda_e)\right)\cdot P_{faH_{0,0}}\left(\Psi_H, I\right)}{P_{H_{0,0(0)}}(\lambda_b,\lambda_e) + P_{H_{0,0(1)}}(\lambda_b,\lambda_e) + P_{H_{0,1}}(\lambda_b,\lambda_e)} \\ &+ \frac{\sum_{\beta=1}^{I}\left(p_b p_{11}^{\beta}\left(t_s\right) p_{10}\left(t_s\right) p_{00}^{J-\beta-1}\left(t_s\right)\cdot P_{faH_{0,1}}\left(\Psi_H, I, \beta\right)\right)}{P_{H_{0,0(0)}}(\lambda_b,\lambda_e) + P_{H_{0,0(1)}}(\lambda_b,\lambda_e) + P_{H_{0,1}}(\lambda_b,\lambda_e)},\end{aligned} \tag{3.20}$$

By using (3.13) and (3.14), or (3.18) and (3.19), the unconditional probability of detection can be derived by averaging the conditional probabilities of detection over the probabilities of occurring for each value of α, expressed as

$$\begin{aligned}\overline{P_{dH}}\left(\Psi_H, I\right) =& \frac{\left(P_{H_{1,0(0)}}(\lambda_b,\lambda_e) + P_{H_{1,0(1)}}(\lambda_b,\lambda_e)\right)\cdot P_{dH_{1,0}}\left(\Psi_H, I\right)}{P_{H_{1,0(0)}}(\lambda_b,\lambda_e) + P_{H_{1,0(1)}}(\lambda_b,\lambda_e) + P_{H_{1,1}}(\lambda_b,\lambda_e)} \\ &+ \frac{\sum_{\alpha=1}^{I}\left(p_e p_{00}^{\alpha}\left(t_s\right) p_{01}\left(t_s\right) p_{11}^{J-\alpha-1}\left(t_s\right)\cdot P_{dH_{0,1}}\left(\Psi_H, I, \alpha\right)\right)}{P_{H_{1,0(0)}}(\lambda_b,\lambda_e) + P_{H_{1,0(1)}}(\lambda_b,\lambda_e) + P_{H_{1,1}}(\lambda_b,\lambda_e)},\end{aligned} \tag{3.21}$$

3.4.2 Secondary User Transmission

Once the spectrum sensing is completed, the secondary transmission starts if the secondary user decides that the primary user is absent from the licensed channel. According to the definition of $H_{0,0(0)}$ and $H_{0,1}$, the primary user is always absent during the secondary transmission slot in these two scenarios, as shown in Fig. 3.1. Thus for both scenarios, the conditional channel capacity is effectively the same as that of H_0 in the conventional model. One has

$$\begin{aligned} C_{H_{0,0(0)}} &= C_{H_{0,1}} \\ &= C_{H_0} = \log_2(1+\gamma_s), \qquad (Bits/Sec/Hz). \end{aligned} \tag{3.22}$$

On the other hand, in $H_{0,0(1)}$, the primary user arrives at the licensed channel during the secondary transmission slot, as illustrated by Fig. 3.1. The conditional channel capacity is affected by the arrival of the primary user which acts as interference to the secondary transmission. Conditioned on the value of α, it can be derived as

$$C_{H_{0,0(1)}}(\alpha) = \log_2\left(1+\frac{\gamma_s}{1+\frac{J-\alpha}{J-I}\gamma_p}\right), \quad I+1 \le \alpha < J, \qquad (Bits/Sec/Hz). \tag{3.23}$$

where $I+1 \le \alpha < J$ indicates the primary user arrives during the transmission slot. Note that when $\alpha = J$, (3.23) becomes the same as (3.22) where the primary user is always absent during the transmission slot.

When mis-detection occurs in the spectrum sensing, the secondary transmission starts even though the primary user is present. In these cases, the primary user signal acts as interference to the secondary transmission.

In both $H_{1,0(0)}$ and $H_{1,1}$, the primary user is present during the whole secondary

transmission slot. The channel capacity is therefore effectively the same as C_{H_1} in the conventional model. One has,

$$\begin{aligned} C_{H_{1,0(0)}} &= C_{H_{1,1}} \\ &= C_{H_1} = \log_2\left(1+\frac{\gamma_s}{1+\gamma_p}\right), \qquad (Bits/Sec/Hz)\,. \end{aligned} \tag{3.24}$$

In $H_{1,0(1)}$, while the primary user is present for the whole sensing slot and the first part of the transmission slot, it then departs from the channel during the transmission slot at the β^{th} sample. Thus, the conditional channel capacity is affected by primary user traffic, and conditioned on the value of β, it becomes,

$$C_{H_{1,0(1)}}(\beta) = \log_2\left(1+\frac{\gamma_s}{1+\frac{\beta-I}{J-I}\gamma_p}\right), \quad I+1 \leq \beta < J, \qquad (Bits/Sec/Hz)\,. \tag{3.25}$$

where $I+1 \leq \beta < J$ indicates the primary user arrives during the transmission slot. When $\beta = J$, (3.25) becomes the same as (3.24) where the primary user is always present during the sensing slot.

Finally, taking into consideration the probabilities of occurring and the conditional channel capacity in (3.22) to (3.25), the average total achievable throughput

for the secondary user transmission can be derived as

$$\begin{aligned}
R_H(\Psi_H, I) &= R_{H_{0,0(0)}}(\Psi_H, I) + R_{H_{0,0(1)}}(\Psi_H, I) + R_{H_{0,1}}(\Psi_H, I) \\
&\quad + R_{H_{1,0(0)}}(\Psi_H, I) + R_{H_{1,0(1)}}(\Psi_H, I) + R_{H_{1,1}}(\Psi_H, I) \\
&= \frac{T-\tau}{T}\left(1 - \overline{P_{faH}}(\Psi_H, I)\right) P_{H_{0,0(0)}}(\lambda_b, \lambda_e)\, C_{H_{0,0(0)}} \\
&\quad + \frac{T-\tau}{T}\left(1 - \overline{P_{faH}}(\Psi_H, I)\right) \sum_{\alpha=I+1}^{J-1} \left(p_e p_{00}^{\alpha}(t_s) p_{01}(t_s) p_{11}^{J-\alpha-1}(t_s) C_{H_{0,1}}(\alpha)\right) \\
&\quad + \frac{T-\tau}{T}\left(1 - \overline{P_{faH}}(\Psi_H, I)\right) P_{H_{0,1}}(\lambda_b, \lambda_e)\, C_{H_{0,1}} \\
&\quad + \frac{T-\tau}{T}\left(1 - \overline{P_{dH}}(\Psi_H, I)\right) P_{H_{1,0(0)}}(\lambda_b, \lambda_e)\, C_{H_{1,0(0)}} \\
&\quad + \frac{T-\tau}{T}\left(1 - \overline{P_{dH}}(\Psi_H, I)\right) \sum_{\beta=I+1}^{J-1} \left(p_b p_{11}^{\beta}(t_s) p_{10}(t_s) p_{00}^{J-\beta-1}(t_s) C_{H_{1,1}}(\beta)\right) \\
&\quad + \frac{T-\tau}{T}\left(1 - \overline{P_{dH}}(\Psi_H, I)\right) P_{H_{1,1}}(\lambda_b, \lambda_e)\, C_{H_{1,1}}, \qquad (Bits/Sec/Hz).
\end{aligned} \tag{3.26}$$

Comparing the derived average achievable throughput in (3.26) to that of the conventional model in (3.7), it can be seen that both the sensing quality and the secondary achievable throughput are affected by the random arrival and departure of the primary user. The conventional model can therefore be treated as a special case where the primary user's random arrival and departure occurs outside of the frame of interests. Similar to (3.7), the throughput in (3.26) is also a averaged value based on the probability of each scenarios. Depending on the code implementation and design, the actual throughput value in practice may be different, depending on the number of frames included and primary user occupancy status in each frame.

3.5 Numerical Results and Discussions

In this section, the effect of the dynamic primary user traffic on the sensing-throughput tradeoff is examined by presenting some numerical results. For all the results, the sample duration is set to $t_s = 0.02\ ms$ and the SNR of the secondary transmission γ_s is set to 10 dB. The Neyman-Pearson rule is used to determine the detection threshold by minimizing the probability of false alarm at $\widehat{P_d} = 0.9$. Other rules can be examined in a similar way.

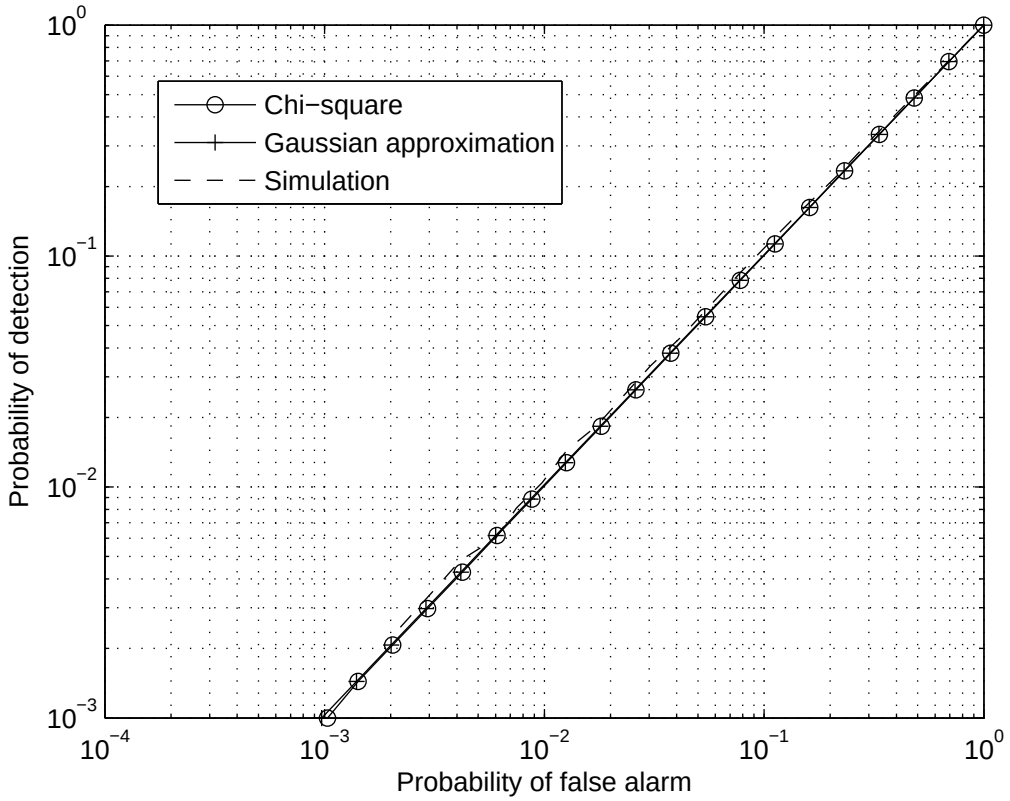

Figure 3.2: The ROC curves of the spectrum sensing performance for the chi-square distribution, Gaussian approximation and the simulation results.

Fig. 3.2 compares the ROC curves of the spectrum sensing performance for

both the chi-square distribution and the Gaussian approximation of Y_H. In this comparison, $m = 50$, giving a sensing duration of 2 ms. The received primary user SNR is set at $\gamma_p = -20$ dB. Without loss of generality, the channel holding times $\lambda_b^{-1} = \lambda_e^{-1} = 1\ ms$ are assumed. As can be observed, the ROC curves of the Gaussian distribution match well with the results obtained using chi-square distribution. The Gaussian distribution therefore provides a good approximation to the actual distribution of Y_H. This is also verified by computer simulation, where 10^6 iterations were used. Due to its computational simplicity, Gaussian approximation will thus be used for the rest of this thesis, while the chi-square distribution method can always be examined in a similar way.

Fig. 3.3 examines the effect of the primary user traffic on the spectrum sensing performance. The comparison of the ROC curves of the spectrum sensing for the conventional model and the model with primary user traffic are presented for different traffic intensities. In the figure, $\gamma_p = -10$ dB and the primary user busy channel holding time λ_b^{-1} and idle channel holding time λ_e^{-1} are set at $1/5\tau$, $1/2\tau$, τ, 2τ and 5τ, respectively. As can be observed, comparing with the conventional model, the spectrum sensing performance is degraded when the primary user traffic is taken into consideration. Moreover, the sensing performance further degrades with the decrease of the channel holding times, due to the increase in the probability of occurring for primary user status changes.

Fig. 3.4 compares the average achievable secondary throughput for different sensing time of the conventional model to the new model when the dynamic primary user traffic exists. In this figure, $\gamma_p = 0$ dB. Similar to the conventional model in [88] and [89], there is an optimal sensing time for the new model with the primary user traffic, at which the maximum throughput is achieved, as expected. However,

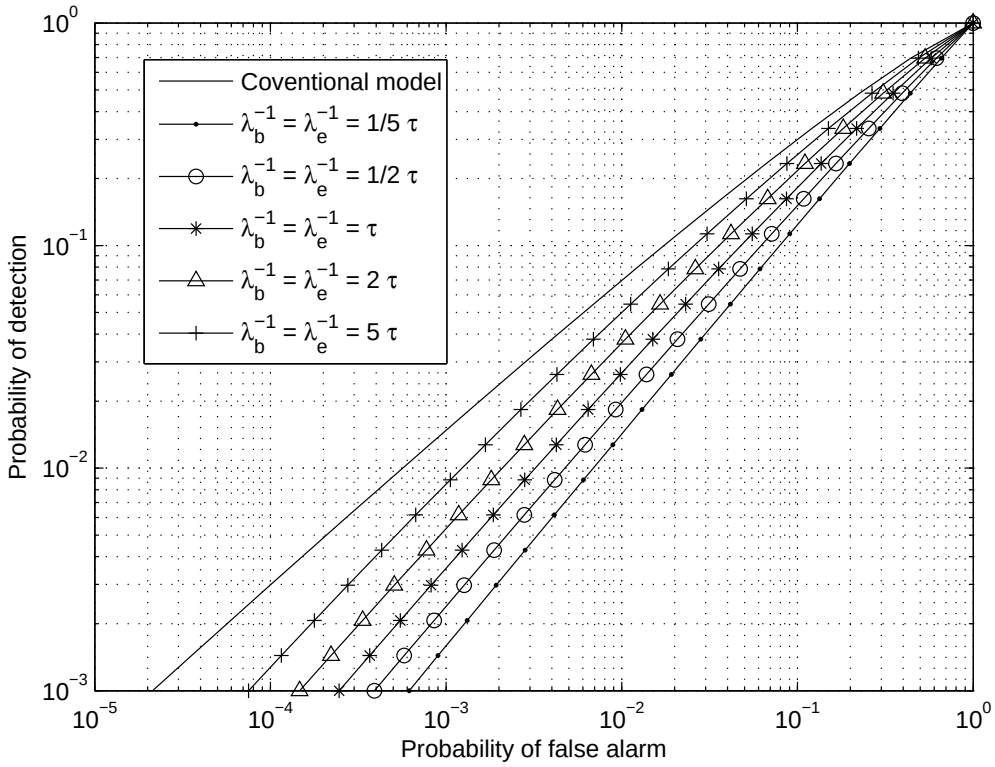

Figure 3.3: The ROC curves of the sensing performance for the conventional model and the new model with dynamic primary user traffic for different primary user traffic intensities.

it can be seen that the achievable throughput of the secondary use is reduced when the random departure and arrival of the primary user exists. There are two possible causes for this phenomenon. Firstly, as shown in Fig. 3.3, the spectrum sensing performance degrades when the primary user traffic is taken into consideration. For the same $\widehat{P_d}$, the resultant probability of false alarm is increased comparing to the conventional model. Hence, the secondary transmission opportunity is reduced. Secondly, when the primary user arrives at the licensed channel during the secondary transmission slot, it acts as an interference and reduces the conditional channel capacity, hence the achievable throughput. It is also shown that, in oder

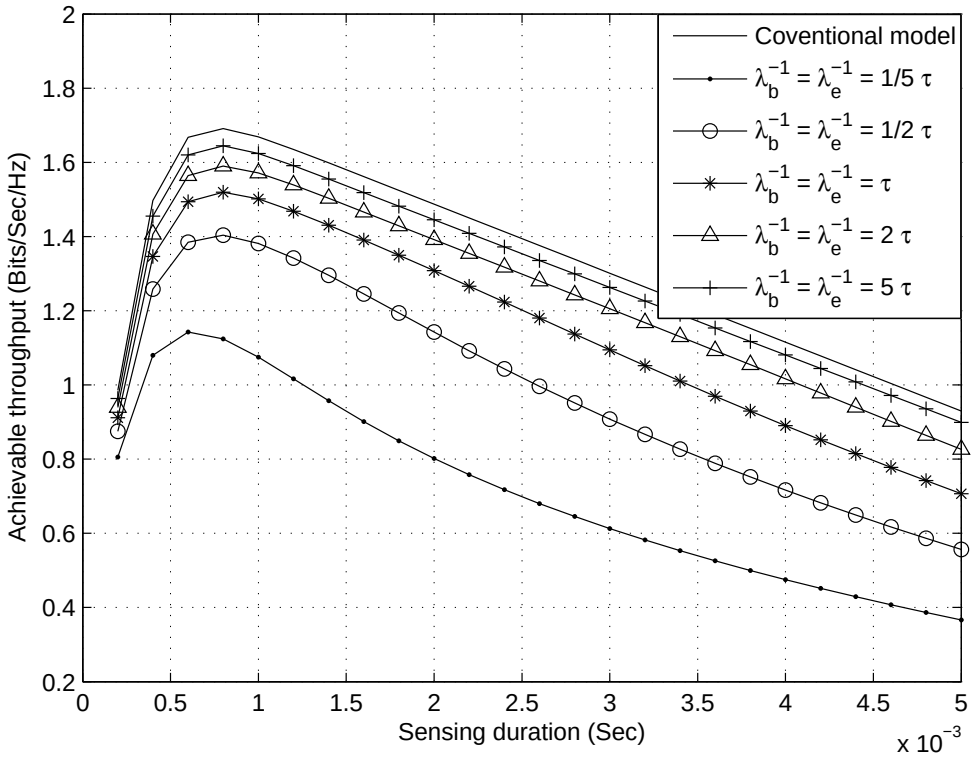

Figure 3.4: Comparison of the average achievable throughput of the conventional model and the new model with dynamic primary user traffic, with $\gamma_p = 0$ dB.

to compensate for the loss of the secondary transmission opportunities, the optimal sensing time is reduced when the primary user traffic is considered comparing with that of the conventional model, so that a longer transmission slot can be obtained.

Fig. 3.5 has the same settings as Fig. 3.4 with γ_p decreased from 0 dB to -10 dB. Similar to Fig. 3.4, as the decrease of λ_b^{-1} and λ_e^{-1}, the achievable throughput and the optimal sensing time reduces comparing with that of the conventional model. In contrast with Fig. 3.4, it can be observed that the maximum achievable throughput is reduced when the received primary user SNR decreases. This is explained as follows. A lower γ_p affects the sensing-throughput tradeoff in two

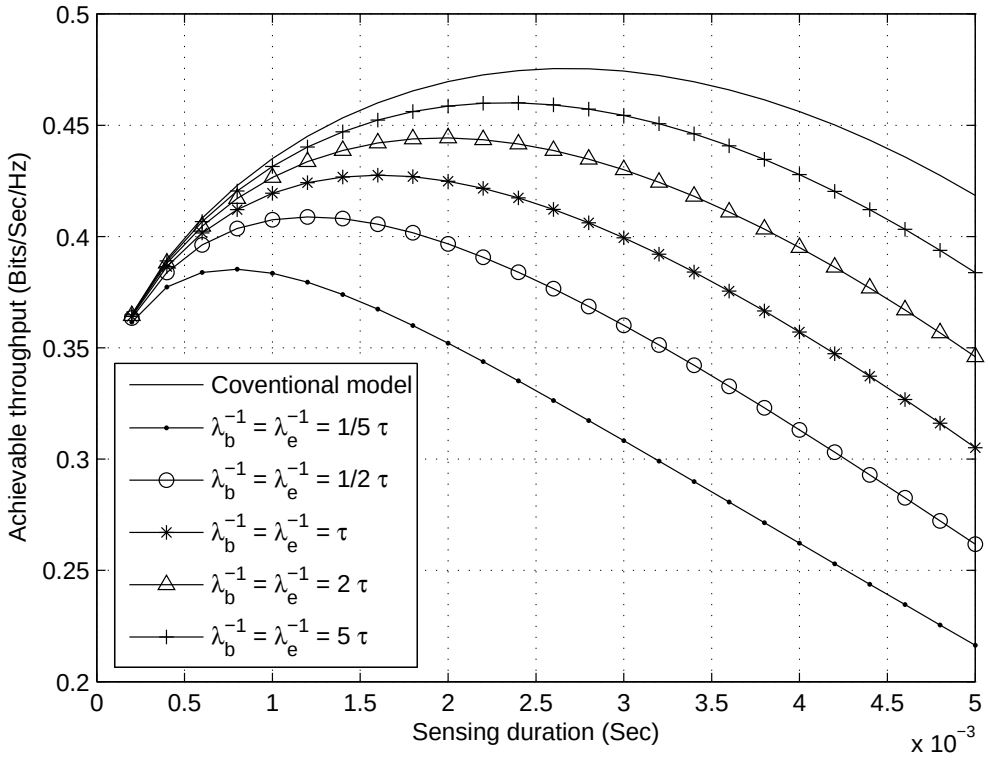

Figure 3.5: Comparison of the average achievable throughput between the conventional model and the model with dynamic primary user traffic, with $\gamma_p = -10$ dB.

ways. First, the sensing performance will be degraded, resulting in a larger unconditional probability of false alarm, $\overline{P_{faH\chi^2}}(\Psi_{H\chi^2}, I)$ in the chi-square distribution or $\overline{P_{faH}}(\Psi_H, I)$ in the Gaussian approximation. The increased unconditional probability of false alarm leads to reduction in the secondary transmission opportunities, and hence the achievable throughput. Second, since the secondary transmission is carried out while the primary user is present in the channel in the case of misdetection occurs or when the primary user arrives during the transmission slot, the conditional achievable throughput will increase when the received primary user SNR decreases. However, since in a practical system, the unconditional probability of de-

tection should be much greater than the unconditional probability of false alarm and the conditional channel capacity is much greater when the primary user interference is absent, the total achievable throughput is hence dominated by the conditional achievable throughput in the case when the primary user is absent from the channel during the transmission slot. Therefore, the overall maximum achievable throughput is reduced from the decrease of the transmission opportunity $(1-\overline{P_{faH}}(\Psi_H, I))$. Moreover, the optimal sensing time has to be increased in order to compensate for this degradation at lower received primary user SNR, which explains why the optimal sensing time increases when γ_p decreases.

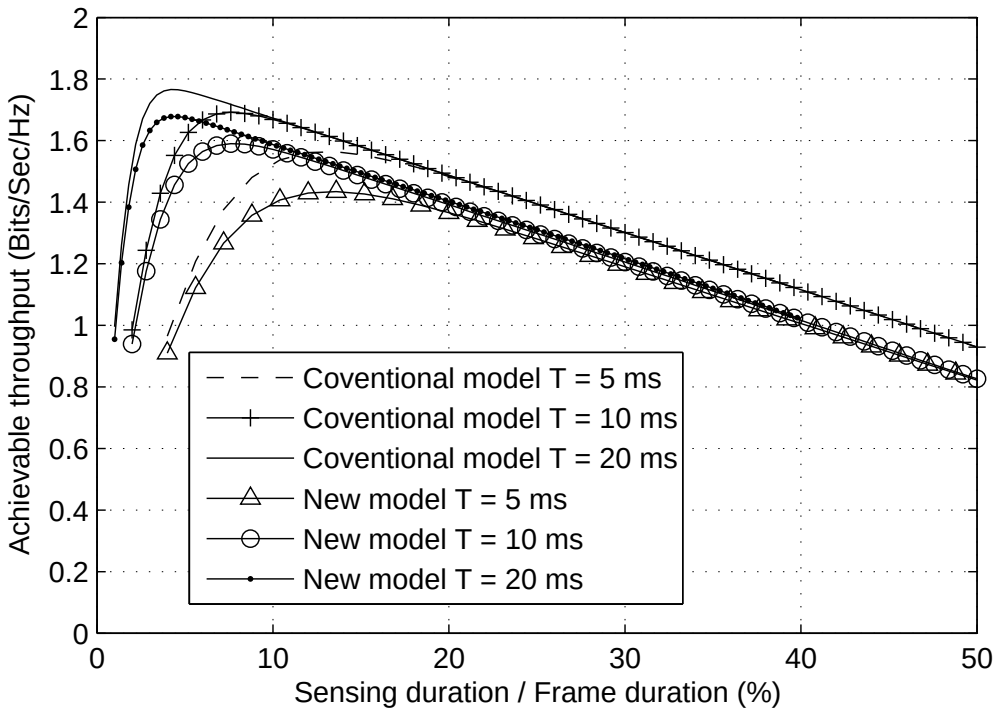

Figure 3.6: The average achievable throughput verses the sensing-duration-frame-duration ratio.

Fig. 3.6 examines the effect of the dynamic primary user traffic on the sensing-

throughput tradeoff for different secondary frame durations. It can be observed that the optimal ratio of the sensing time to the frame duration is reduced when the frame duration increases. That is to say, the longer the frame duration is, the smaller portion of the frame is required to perform the spectrum sensing. Moreover, when the primary user traffic is taken into consideration, the achievable throughput is always reduced compared to that of the conventional model used in [88] and [89]. This agrees with the findings from the previous figures.

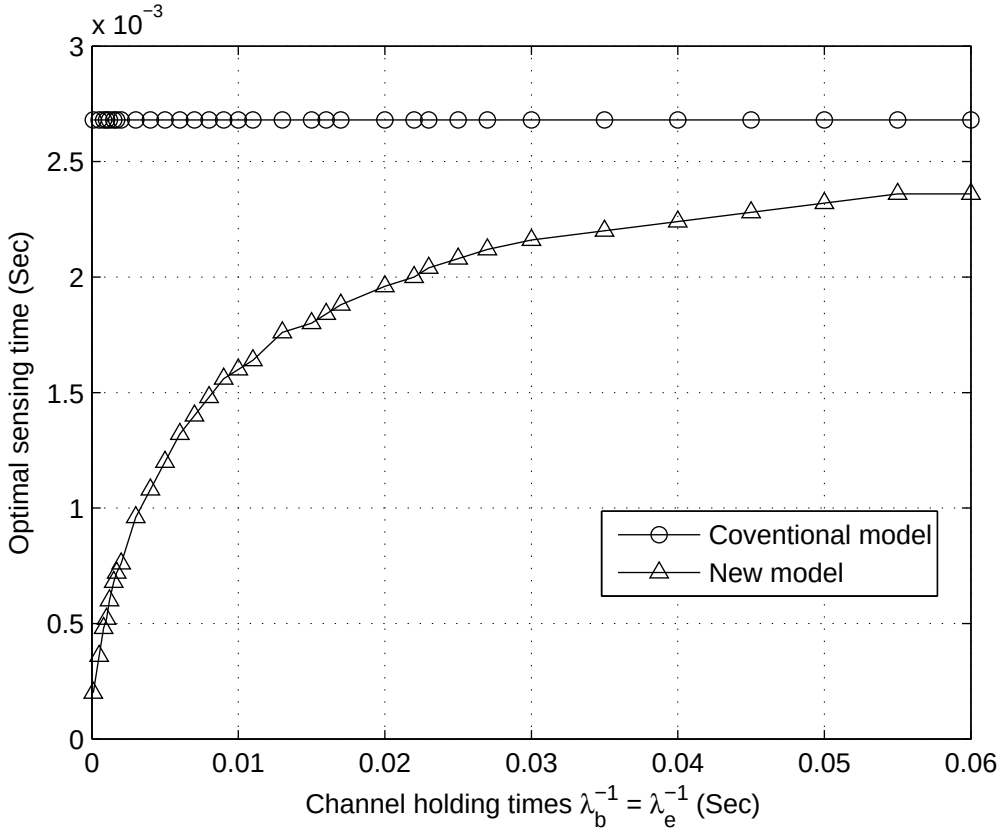

Figure 3.7: The optimal sensing time for different busy and idle channel holding time, λ_b^{-1} and λ_e^{-1}.

Fig. 3.7 provides the relationship between the optimal sensing time $\tilde{\tau}$ and the channel holding times λ_b^{-1} and λ_e^{-1} where $\lambda_b^{-1} = \lambda_e^{-1}$ is assumed. When λ_b^{-1} and

λ_e^{-1} decreases, the optimal sensing time decreases. This is explained as follows. The decrease of λ_b^{-1} and λ_e^{-1} means shorter channel holding times, which result in a decrease in the achievable throughput. In order to compensate for this reduction in the throughput, either the sensing time has to be increased to reduce the probability of false alarm and increase the secondary transmission opportunity, or the transmission time has to be increased to achieve a higher conditional throughput. In this case when the total frame duration is fixed, the increase of one period will lead to a decrease in the other. As the improvement in the probability of false alarm with the increase of the sensing time is insignificant compared with the loss in the conditional throughput caused by the reduced transmission time, the sensing time need to be decreased in order for the achievable throughput to be maximized. Furthermore, as can be seen from Fig. 3.7, as the channel holding times λ_b^{-1} and λ_e^{-1} increase to a certain value, the increase of the optimal sensing time slows down and approaches to the conventional model where primary user traffic is assumed to be static, as in this case the probability of primary user status changes occurs becomes very small.

3.6 Conclusions

In this chapter, the effect of the primary user traffic on the sensing-throughput tradeoff of the cognitive radio has been examined. Both the chi-square distribution and the Gaussian approximation have been considered for the test statistic of the energy detection. By adopting a primary user traffic model which takes into consideration of one primary user status change and exponential channel holding time, performance degradation has been observed in both the spectrum sensing performance and the secondary transmission. Numerical results showed that this degradation

is related to the primary user traffic intensity, as well as the received primary user SNR at the secondary user. It was also shown that the optimal sensing time for the sensing-throughput tradeoff may also be changed when the primary user traffic is taken into account. Moreover, the ratio of the optimal sensing time and the frame duration is also affected by the actual length of the frame.

Chapter 4

Spectrum Sensing with Multiple Status Changes in Primary User Traffic

4.1 Introduction

One of the main research challenges of the cognitive radio is the possibility of the primary user changing its occupancy status while the secondary user is operating. In the last chapter, a dynamic primary user traffic model where the primary user randomly departs or arrives at the licensed channel for at most once during the secondary frame was discussed, while the focus of the analysis was its effect on the sensing-throughput tradeoff performance.

In this chapter, the dynamic primary user traffic problem is generalized by considering a more general case, where the primary user has multiple occupancy status changes in the licensed channel during the secondary frame. In practice, this is the

case when the primary user traffic is bursty and the primary user frame is very short. In this case, one primary user comes and leaves frequently due to the relatively short frame interval. For example, due to severe fading or shadowing, the acknowledge or Request to Send messages in the initialization may be lost so that these short control messages have to be sent over and over again by the primary user. This is also the case when the primary traffic is high such that one primary user arrives shortly after the other primary user leaves and so on in the frame duration. The number of status changes is determined by the burstiness, the traffic of the primary network as well as the length of the sensing slot to achieve certain accuracy. Therefore, the effect of primary user multiple occupancy status changes on the cognitive radio performance is a topic worth investigating. The analysis in this chapter is general enough to take all these cases into account.

Different from Chapter 3, in this chapter, the analysis is focused on the effect of multiple status changes on the performance of the spectrum sensing. Many works have been conducted on spectrum sensing [53, 68, 95–97]. In [95] and [53], spectrum sensing was studied without considering the primary user status changes. In [68, 96, 97], the authors considered the primary user status changes in spectrum sensing but assumed that the primary user only arrives at the licensed channel before the spectrum sensing starts and remains unchanged thereafter. Therefore, the spectrum sensing performance with primary user multiple status changes is evaluated in this chapter.

To extend the investigation further, different channel holding time distributions for the primary user traffic with multiple status changes are also investigated, including exponential distribution [93, 98], log-normal distribution [99, 100], Gamma distribution [101, 102] and Erlang distribution [103].

The rest of this chapter is organized as follows. In Section 4.2, the realistic primary user traffic model with multiple status changes is established. In Section 4.3, the effect of the established traffic model on the spectrum sensing performance is analyzed. In Section 4.4, numerical results and discussions are presented, while the findings are concluded in Section 4.5.

4.2 Primary User Multiple Changes Traffic Model

Consider the cognitive radio system model similar to that used in the last chapter. In this chapter, the primary user is assumed to depart or arrive at the licensed channel several times such that its status changes frequently during the sensing period. Assume that each primary user status change takes one sample to complete. The number of status changes during the sensing period is an integer $\Omega \in [0, N]$, where N is the maximum number of changes with values from 1 to I, and $I \in [1, \infty)$. This takes an arbitrary number of status changes into account. The primary user traffic is modelled as a Markov 1-0 random process. Define the samples at which the primary user arrives and departs from the licensed channel as α_j and β_j, respectively, where j represents the j^{th} arrival or departure.

Denote the cumulative distribution functions (CDFs) of the busy channel holding time and idle channel holding time of the licensed channel as $F_\alpha(t)$ and $F_\beta(t)$, respectively, which are determined by the primary user traffic. Since the primary user and the secondary user are not synchronized and both of their traffics are functions of time, there is always a primary user status change that has happened immediately before the current secondary user frame starts if one goes back in time from the instant when the secondary frame starts, so that the same CDF applies to all the idle and busy durations in the secondary frame regardless of when this status

change occurs. This does not contradict with the exponential holding time and its memoryless property examined and used later.

In this chapter, the traffic model is generalized so that it follows any reasonable distributions. In the case of exponentially distributed primary user channel holding times, there is [104]

$$F_{\alpha}(t) = 1 - e^{-\lambda_b t}, \tag{4.1}$$

and

$$F_{\beta}(t) = 1 - e^{-\lambda_e t}, \tag{4.2}$$

for the busy and idle channel holding times, respectively, where λ_b and λ_e are the exponentially distributed channel holding time rate parameters defined as before.

Similarly, in the case of Gamma distributed channel holding times, there is [104]

$$F_{\alpha}(t) = \frac{\gamma\left(k_{gam,\alpha}, \frac{t}{\theta_{gam,\alpha}}\right)}{\Gamma\left(k_{gam,\alpha}\right)}, \tag{4.3}$$

and

$$F_{\beta}(t) = \frac{\gamma\left(k_{gam,\beta}, \frac{t}{\theta_{gam,\beta}}\right)}{\Gamma\left(k_{gam,\beta}\right)}, \tag{4.4}$$

where $k_{gam,\alpha}$ and $k_{gam,\beta}$ are the shape parameters of the Gamma distribution for the busy and idle channel holding times, respectively, $\theta_{gam,\alpha}$ and $\theta_{gam,\beta}$ are the scale parameters.

In the case of Erlang distribution, the CDF follows [104]

$$F_{\alpha}(t) = \frac{\gamma\left(k_{er,\alpha}, \lambda_{er,\alpha} t\right)}{\left(k_{er,\alpha} - 1\right)!}, \tag{4.5}$$

and

$$F_{\beta}(t) = \frac{\gamma(k_{er,\beta}, \lambda_{er,\beta} t)}{(k_{er,\beta} - 1)!}, \tag{4.6}$$

where $k_{er,\alpha}$ and $k_{er,\beta}$ are shape parameters of the Erlang distribution for the busy and idle channel holding times, respectively, $\lambda_{er,\alpha}$ and $\lambda_{er,\beta}$ are the rate parameters of the distribution.

In the case of log-normal distributed channel holding times, there is [104]

$$F_{\alpha}(t) = \frac{1}{2} + \frac{1}{2} erfc\left(\frac{\ln t - \mu_{log,\alpha}}{\sqrt{2\sigma_{log,\alpha}^2}}\right), \tag{4.7}$$

and

$$F_{\beta}(t) = \frac{1}{2} + \frac{1}{2} erfc\left(\frac{\ln t - \mu_{log,\beta}}{\sqrt{2\sigma_{log,\beta}^2}}\right), \tag{4.8}$$

where $\mu_{log,\alpha}$ and $\mu_{log,\beta}$ are the means of $\ln t$ for busy and idle channel holding times, respectively, $\sigma_{log,\alpha}$ and $\sigma_{log,\beta}$ are the standard deviations of $\ln t$.

Assume that for all considered primary user traffic models, each time interval can be modelled independently. This is the case when the primary user follows Poison process, or not Poison process but the time intervals are weakly related. The probability that a primary user status change occurs is therefore equal to the probability mass function (PMF) of the channel holding times. Consequently, in the case when the primary user arrives at the channel at the sample α_j during the sensing period, the PMF of α_j, $f_{\alpha}(\alpha_j)$ can be obtained from the CDF as [105]

$$f_{\alpha}(\alpha_j) = F_{\alpha}(\alpha_j t_s) - F_{\alpha}\Big((\alpha_j - 1) t_s\Big). \tag{4.9}$$

Similarly, in the case when the primary user departs from the channel during

the sensing period at the sample β_j, the PMF of β_j, $f_\beta(\beta_j)$ is derived as

$$f_\beta(\beta_j) = F_\beta(\beta_j t_s) - F_\beta\Big((\beta_j - 1)\, t_s\Big). \tag{4.10}$$

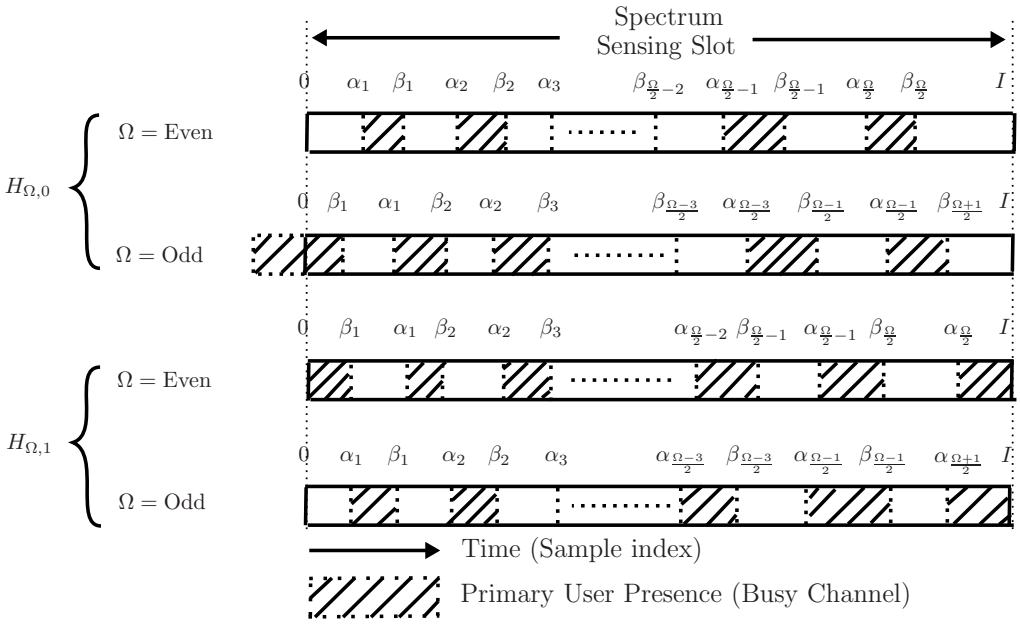

Figure 4.1: Scenarios for the primary user traffic with multiple occupancy status changes.

Inherently, as illustrated by Fig. 4.1, the arrivals and departures of the primary user occur one after the other. Denote the idle hypothesis as $H_{\Omega,0}$ where after Ω status changes, the primary user is absent at the end of the sensing slot. Denote the busy hypothesis as $H_{\Omega,1}$ indicating that the primary user is present at the end of the sensing slot after Ω status changes.

According to the definition of an idle licensed channel, the primary user need to be absent at the end of the sensing slot. Hence, in $H_{\Omega,0}$, when Ω is an even number, the primary user must be absent at the beginning of the sensing period, and after Ω arrivals and departures, it is eventually still absent and does not return again

during the sensing slot. The probability for this event to occur is the product of the probabilities for all arrivals and departures, conditioned on their respective previous departures or arrivals. Therefore, the occurring probability of this scenario can be derived as

$$\begin{aligned} P_{H_{\Omega,0}}(\Omega = even) =& p_e \cdot f_\alpha(\alpha_1) \cdot f_\beta(\beta_1) \cdot f_\alpha(\alpha_2) \cdot f_\beta(\beta_2) \quad \cdots\cdots \quad f_\alpha(\alpha_{\frac{\Omega}{2}-1}) \\ & \cdot f_\beta(\beta_{\frac{\Omega}{2}-1}) \cdot f_\alpha(\alpha_{\frac{\Omega}{2}}) \cdot f_\beta(\beta_{\frac{\Omega}{2}}) \cdot \left(1 - \left(F_\alpha\left(It_s\right) - F_\alpha\left(\beta_{\frac{\Omega}{2}} t_s\right)\right)\right) \\ =& p_e \prod_{j=1}^{\frac{\Omega}{2}} f_\alpha\left(\alpha_j\right) \prod_{j=1}^{\frac{\Omega}{2}} f_\beta\left(\beta_j\right) \left(1 - \left(F_\alpha\left(It_s\right) - F_\alpha\left(\beta_{\frac{\Omega}{2}} t_s\right)\right)\right) \end{aligned} \tag{4.11}$$

In the above equation, $\prod_{j=1}^{\frac{\Omega}{2}} f_\alpha\left(\alpha_j\right) \prod_{j=1}^{\frac{\Omega}{2}} f_\beta\left(\beta_j\right)$ is the probability that the arrival and departure of the primary user happens one after another for a total of Ω (Ω = even) times, and $\left(1 - \left(F_\alpha\left(It_s\right) - F_\alpha\left(\beta_{\frac{\Omega}{2}} t_s\right)\right)\right)$ is the probability that the primary user does not return again after the last departure until the end of the sensing slot.

Similarly, the case when Ω is odd for $H_{\Omega,0}$ can be derived in a similar way. The conditional probability of occurring for $H_{\Omega,0}$ can therefore be represented as

$$P_{H_{\Omega,0}} = \begin{cases} p_e \prod_{j=1}^{\frac{\Omega}{2}} f_\alpha\left(j\right) \prod_{j=1}^{\frac{\Omega}{2}} f_\beta\left(j\right) \left(1 - \left(F_\alpha\left(It_s\right) - F_\alpha\left(\beta_{\frac{\Omega}{2}} t_s\right)\right)\right), & \Omega = even, \\ p_b \prod_{j=1}^{\frac{\Omega-1}{2}} f_\alpha\left(j\right) \prod_{j=1}^{\frac{\Omega+1}{2}} f_\beta\left(j\right) \left(1 - \left(F_\alpha\left(It_s\right) - F_\alpha\left(\beta_{\frac{\Omega+1}{2}} t_s\right)\right)\right), & \Omega = odd. \end{cases} \tag{4.12}$$

Note that when $\Omega = 0$, the primary user does not change its occupancy status during the spectrum sensing so that it is absent during the whole sensing slot, hence $H_{\Omega,0}$ becomes the same as the hypothesis H_0 in the conventional spectrum sensing. In this case, the conditional probability $P_{H_{\Omega,0}}$ becomes $P_{H_0} = p_e\Big(I - F_\alpha\left(It_s\right)\Big)$.

By using similar methodology, the conditional probability of occurring for $H_{\Omega,1}$

can also be derived as

$$P_{H_{\Omega,1}} = \begin{cases} p_b \prod_{j=1}^{\frac{\Omega}{2}} f_\beta(j) \prod_{j=1}^{\frac{\Omega}{2}} f_\alpha(j) \left(1 - \left(F_\beta(It_s) - F_\beta\left(\alpha_{\frac{\Omega}{2}} t_s\right)\right)\right), & \Omega = even, \\ p_e \prod_{j=1}^{\frac{\Omega+1}{2}} f_\alpha(j) \prod_{j=1}^{\frac{\Omega-1}{2}} f_\beta(j) \left(1 - \left(F_\beta(It_s) - F_\beta\left(\alpha_{\frac{\Omega+1}{2}} t_s\right)\right)\right), & \Omega = odd. \end{cases} \tag{4.13}$$

Similarly, when $\Omega = 0$ under hypothesis $H_{\Omega,1}$, the primary user is always present during the whole sensing slot, similar to the hypothesis H_1 in the conventional model, and the conditional probability $P_{H_{\Omega,1}}$ becomes $P_{H_1} = p_b\Big(1 - F_\beta(It_s)\Big)$.

4.3 Spectrum Sensing with Primary User Multiple Changes Traffic

As can be seen from Fig. 4.1, the considered received samples contain only noise (w_i) when the primary user is absent in the licensed channel, and contain both signal and noise ($s_i + w_i$) when the primary user is present in the channel. Using the energy detection for the spectrum sensing, the test statistic can be expressed as the sum of energy of all samples used for spectrum sensing. Therefore, the test

statistic for $H_{\Omega,0}$ with $\Omega = even$ can be derived based on the considered samples as

$$\begin{aligned} Y_{H_{\Omega,0}}(\Omega = even) = &\sum_{i=1}^{\alpha_1} w_i^2 + \sum_{i=\alpha+1}^{\beta_1} (s_i + w_i)^2 + \sum_{i=\beta_1+1}^{\alpha_2} w_i^2 + \sum_{i=\alpha_2+1}^{\beta_2} (s_i + w_i)^2 \\ &+ \sum_{i=\beta_2+1}^{\alpha_3} w_i^2 + \sum_{i=\alpha_3+1}^{\beta_3} (s_i + w_i)^2 \quad \cdots\cdots \quad + \sum_{i=\beta_{\frac{\Omega}{2}-2}+1}^{\alpha_{\frac{\Omega}{2}-1}} w_i^2 \\ &+ \sum_{i=\alpha_{\frac{\Omega}{2}-1}+1}^{\beta_{\frac{\Omega}{2}-1}} w_i^2 + \sum_{i=\beta_{\frac{\Omega}{2}-1}+1}^{\alpha_{\frac{\Omega}{2}}} w_i^2 + \sum_{i=\alpha_{\frac{\Omega}{2}}}^{\beta_{\frac{\Omega}{2}}} (s_i + w_i)^2 + \sum_{i=\beta_{\frac{\Omega}{2}}}^{I} w_i^2. \end{aligned} \tag{4.14}$$

where $Y_{H_{\Omega,0}}$ is the output of the integrator under hypothesis $H_{\Omega,0}$.

Similarly, when Ω is an odd number, the primary user must be present at the beginning of the sensing slot, it is then absent from the licensed channel at the end of the sensing period after Ω departures and arrivals. The test statistics for the energy detection for $\Omega = odd$ in $H_{\Omega,0}$ can therefore be derived as

$$\begin{aligned} Y_{H_{\Omega,0}}(\Omega = odd) = &\sum_{i=1}^{\beta_1} (s_i + w_i)^2 + \sum_{i=\beta_1+1}^{\alpha_1} w_i^2 + \sum_{i=\alpha_1+1}^{\beta_2} (s_i + w_i)^2 + \sum_{i=\beta_2+1}^{\alpha_2} w_i^2 \\ &+ \sum_{i=\alpha_2+1}^{\beta_3} (s_i + w_i)^2 \quad \cdots\cdots \quad + \sum_{i=\beta_{\frac{\Omega-3}{2}}+1}^{\alpha_{\frac{\Omega-3}{2}}} w_i^2 + \sum_{i=\alpha_{\frac{\Omega-3}{2}}+1}^{\beta_{\frac{\Omega-1}{2}}} (s_i + w_i)^2 \\ &+ \sum_{i=\beta_{\frac{\Omega-1}{2}}+1}^{\alpha_{\frac{\Omega-1}{2}}} w_i^2 \sum_{i=\alpha_{\frac{\Omega-1}{2}}+1}^{\beta_{\frac{\Omega+1}{2}}} (s_i + w_i)^2 + \sum_{i=\beta_{\frac{\Omega+1}{2}}+1}^{I} w_i^2. \end{aligned} \tag{4.15}$$

This can be simplified as

$$Y_{H_{\Omega,0}} = \begin{cases} \sum_{j=1}^{\frac{\Omega}{2}} \sum_{i=\alpha_j+1}^{\beta_j} (s_i + w_i)^2 + \sum_{i=1}^{\alpha_1} w_i^2 \\ \quad + \sum_{j=1}^{\frac{\Omega}{2}-1} \sum_{i=\beta_j+1}^{\alpha_{j+1}} w_i^2 + \sum_{i=\beta_{\frac{\Omega}{2}}+1}^{I} w_i^2, & \Omega = even, \\ \sum_{j=1}^{\frac{\Omega-1}{2}} \sum_{i=\alpha_j+1}^{\beta_{j+1}} (s_i + w_i)^2 + \sum_{i=1}^{\beta_1} (s_i + w_i)^2 \\ \quad + \sum_{j=1}^{\frac{\Omega-1}{2}} \sum_{i=\beta_j+1}^{\alpha_j} w_i^2 + \sum_{i=\beta_{\frac{\Omega+1}{2}}+1}^{I} w_i^2, & \Omega = odd. \end{cases} \tag{4.16}$$

By using the same methodology, according to the definition of an unavailable channel, the primary user is present at the end of the sensing slot. Hence, in $H_{\Omega,1}$, when Ω is even, the primary user must be present at the beginning of the sensing slot, and is eventually still present at the end of the sensing slot after even number of departures and arrivals. Similarly, when Ω is odd, the primary user must be absent at the beginning of the sensing slot. The test statistics for the energy detection in $H_{\Omega,1}$ can therefore be derived as

$$Y_{H_{\Omega,1}} = \begin{cases} \sum_{i=1}^{\beta_1} (s_i + w_i)^2 + \sum_{j=1}^{\frac{\Omega}{2}-1} \sum_{i=\alpha_j+1}^{\beta_{j+1}} (s_i + w_i)^2 + \\ \quad \sum_{i=\alpha_{\frac{\Omega}{2}}+1}^{I} (s_i + w_i)^2 + \sum_{j=1}^{\frac{\Omega}{2}} \sum_{i=\beta_j+1}^{\alpha_j} w_i^2, & \Omega = even, \\ \sum_{j=1}^{\frac{\Omega-1}{2}} \sum_{i=\alpha_j+1}^{\beta_j} (s_i + w_i)^2 + \sum_{i=\alpha_{\frac{\Omega+1}{2}}+1}^{I} (s_i + w_i)^2 \\ \quad + \sum_{i=1}^{\alpha_1} n_i^2 + \sum_{j=1}^{\frac{\Omega-1}{2}} \sum_{i=\beta_j+1}^{\alpha_{j+1}} n_i^2, & \Omega = odd. \end{cases} \tag{4.17}$$

By performing energy detection using the test statistics derived in (4.16) and (4.17), the conditional probabilities of false alarm and the conditional probability of detection, conditioned on the value of α and β can be derived.

4.3.1 Conditional Probability of False Alarm

To derive the conditional probability of false alarm, Let $g_{0_i} = w_i$ and $d_{0_i} = g_{0_i}^2$. The expectation and variance of d_{0_i} can be derived as

$$\begin{aligned} E\left[d_{0_i}\right] &= Var\left[g_{0_i}\right] + \left(E\left[g_{0_i}\right]\right)^2 \\ &= \sigma_{g_0}^2 + \mu_{g_0}^2, \end{aligned} \tag{4.18}$$

and

$$\begin{aligned} Var\left[d_{0_i}\right] &= E\left[d_{0_i}^2\right] - \left(E\left[d_{0_i}\right]\right)^2 \\ &= 4\mu_{g_0}^2\sigma_{g_0}^2 + 2\sigma_{g_0}^2, \end{aligned} \tag{4.19}$$

respectively, where $E\left[\cdot\right]$ denotes the expectation, $Var\left[\cdot\right]$ denotes the variance, μ_{g_0} is the mean of g_{0_i}, and $\sigma_{g_0}^2$ is the variance of g_{0_i}.

Let $D_0 = \sum d_{0_i}$ and define $\mathcal{Z}_{0_j}$ as

$$\mathcal{Z}_{0_j} = \frac{D_0 - K_{0H_{\Omega,0}} E\left[d_{0_i}\right]}{\sqrt{K_{0H_{\Omega,0}} Var\left[d_{0_i}\right]}}, \tag{4.20}$$

where $K_{0H_{\Omega,0}}$ is the total number of samples during the sensing period that contain only noise in $H_{\Omega,0}$. Thus, according to the CLT, $\mathcal{Z}_{0_j}$ has approximately zero mean and unit variance, and there is

$$D_0 = \mathcal{Z}_{0_j}\sqrt{K_{0H_{\Omega,0}} Var\left[d_{0_i}\right]} + K_{0H_{\Omega,0}} E\left[d_{0_i}\right]. \tag{4.21}$$

Hence, as g_{0_i} has zero mean and unit variance, the expectation and variance of D_0 can be obtained as

$$\begin{aligned} E[D_0] &= K_{0H_{\Omega,0}}\left(\sigma_{g_0}^2 + \mu_{g_0}^2\right) \\ &= K_{0H_{\Omega,0}}, \end{aligned} \tag{4.22}$$

and

$$\begin{aligned} Var[D_0] &= K_{0H_{\Omega,0}}\left(2\sigma_{g_0}^4 + 4\sigma_{g_0}^2\mu_{g_0}^2\right) \\ &= 2K_{0H_{\Omega,0}}, \end{aligned} \tag{4.23}$$

Similarly, let $g_{1_i} = s_i + w_i$, and $d_{1_i} = g_{1_i}^2$. The expectation and variance of d_{1_i} can be derived as

$$\begin{aligned} E[d_{1_i}] &= Var[g_{1_i}] + (E[g_{1_i}])^2 \\ &= \sigma_{g_1}^2 + \mu_{g_1}^2. \end{aligned} \tag{4.24}$$

and

$$\begin{aligned} Var[d_{1_i}] &= E\left[d_{1_i}^2\right] - (E[d_{1_i}])^2 \\ &= E\left[g_{1_i}^4\right] - (E[d_{1_i}])^2 \\ &= 2\sigma_{g_1}^4 + 4\sigma_{g_1}^2\mu_{g_1}^2, \end{aligned} \tag{4.25}$$

where $\sigma_{g_1}^2$ is the variance of g_{1_i} and μ_{g_1} is the mean of g_{1_i}. Let $D_1 = \sum d_{1_i}$ and define $\mathcal{Z}_{1_j}$ as

$$\mathcal{Z}_{1_j} = \frac{D_1 - K_{1H_{\Omega,0}}E[d_{1_i}]}{\sqrt{K_{1H_{\Omega,0}}Var[d_{1_i}]}}, \tag{4.26}$$

where $K_{1H_{\Omega,0}}$ as the total number of samples that contain the primary user signal and noise during the sensing slot in $H_{\Omega,0}$. According to the CLT, $\mathcal{Z}_{1_j}$ has approximately zero mean and unit variance. As d_{1_i} has mean of $\sqrt{\gamma_p}$ and unit variance, the expectation and variance of D_1 can be derived according to the CLT as

$$\begin{aligned} E[D_1] &= K_{1H_{\Omega,0}}\left(\sigma_{g_1}^2 + \mu_{g_1}^2\right) \\ &= K_{1H_{\Omega,0}} + K_{1H_{\Omega,0}}\gamma_p, \end{aligned} \tag{4.27}$$

$$\begin{aligned} Var\left[D_1\right] &= K_{1H_{\Omega,0}}\left(2\sigma_{g_1}^4 + 4\sigma_{g_1}^2\mu_{g_1}^2\right) \\ &= 2K_{1H_{\Omega,0}} + 4K_{1H_{\Omega,0}}\gamma_p. \end{aligned} \tag{4.28}$$

Hence, by using (4.22) and (4.27), the expectation $Y_{H_{\Omega,0}}$ can be obtained as

$$\begin{aligned} E\left[Y_{H_{\Omega,0}}\right] &= E\left[D_0\right] + E\left[D_1\right] \\ &= K_{0H_{\Omega,0}} + K_{1H_{\Omega,0}} + K_{1H_{\Omega,0}}\gamma_p \\ &= I + K_{1H_{\Omega,0}}\gamma_p, \end{aligned} \tag{4.29}$$

and by using (4.23) and (4.28), the variance of $Y_{H_{\Omega,0}}$ can be derived as

$$\begin{aligned} Var\left[Y_{H_{\Omega,0}}\right] &= Var\left[D_0\right] + Var\left[D_1\right] \\ &= 2K_{0H_{\Omega,0}} + 2K_{1H_{\Omega,0}} + 4K_{1H_{\Omega,0}}\gamma_p \\ &= 2I + 4K_{1H_{\Omega,0}}\gamma_p, \end{aligned} \tag{4.30}$$

.

From (4.16), $K_{0H_{\Omega,0}}$ and $K_{1H_{\Omega,0}}$ under hypothesis $H_{\Omega,0}$ can be derived as

$$K_{0H_{\Omega,0}} = \begin{cases} I - \sum_{j=1}^{\frac{\Omega}{2}} \beta_j + \sum_{j=1}^{\frac{\Omega}{2}} \alpha_j, & \Omega = even, \\ I - \sum_{j=1}^{\frac{\Omega+1}{2}} \beta_j + \sum_{j=1}^{\frac{\Omega-1}{2}} \alpha_j, & \Omega = odd, \end{cases} \tag{4.31}$$

and

$$K_{1H_{\Omega,0}} = \begin{cases} \sum_{j=1}^{\frac{\Omega}{2}} \beta_j - \sum_{j=1}^{\frac{\Omega}{2}} \alpha_j, & \Omega = even, \\ \sum_{j=1}^{\frac{\Omega+1}{2}} \beta_j - \sum_{j=1}^{\frac{\Omega-1}{2}} \alpha_j, & \Omega = odd. \end{cases} \tag{4.32}$$

respectively.

In [75], the conditional probability of false alarm is defined as

$$P_{fa}(\Psi) = \frac{1}{2} erfc\left(\frac{\Psi - E\left[Y_{H_0}\right]}{\sqrt{2Var\left[Y_{H_0}\right]}}\right), \tag{4.33}$$

where $E\left[Y_{H_0}\right]$ and $Var\left[Y_{H_0}\right]$ is the expectation and variance of the energy detection test statistic for idle channel hypothesis.

Hence, by substituting (4.29) and (4.30) into (4.33), one has the conditional probabilities of false alarm as

$$P_{faH_{\Omega,0}}(\Psi_m, I) = \frac{1}{2} erfc\left(\frac{\Psi_m - \left(I + K_{1H_{\Omega,0}}\gamma_p\right)}{2\sqrt{I + 2K_{1H_{\Omega,0}}\gamma_p}}\right), \tag{4.34}$$

where Ψ_m is the decision threshold for the energy detection where multiple primary user status changes is considered. By applying the Neyman-Pearson rule, for a target probability of false alarm $\widehat{P_{faH_{\Omega,0}}}$, the detection threshold Ψ_m can be found as

$$\Psi_m = erfc^{-1}\left(2\widehat{P_{faH_{\Omega,0}}}\right)\sqrt{2I + 8K_{1H_{\Omega,0}}\gamma_p} + I + K_{1H_{\Omega,0}}\gamma_p. \tag{4.35}$$

4.3.2 Conditional Probability of Detection

By using similar method, the conditional probability of detection can also be derived. In hypothesis $H_{\Omega,1}$, the total number of samples during the sensing period that contain only noise can be derived as

$$K_{0H_{\Omega,1}} = \begin{cases} \sum_{j=1}^{\frac{\Omega}{2}} \alpha_j - \sum_{j=1}^{\frac{\Omega}{2}} \beta_j, & \Omega = even, \\ \sum_{j=1}^{\frac{\Omega+1}{2}} \alpha_j - \sum_{j=1}^{\frac{\Omega-1}{2}} \beta_j, & \Omega = odd. \end{cases} \tag{4.36}$$

The total number of samples during the sensing period that contain signal and noise can be derived as

$$K_{1H_{\Omega,1}} = \begin{cases} I - \sum_{j=1}^{\frac{\Omega}{2}} \alpha_j + \sum_{j=1}^{\frac{\Omega}{2}} \beta_j, & \Omega = even, \\ I - \sum_{j=1}^{\frac{\Omega+1}{2}} \alpha_j + \sum_{j=1}^{\frac{\Omega-1}{2}} \beta_j, & \Omega = odd. \end{cases} \tag{4.37}$$

In [75], the conditional probability of detection is defined as

$$P_d(\Psi) = \frac{1}{2} erfc\left(\frac{\Psi - E\left[Y_1\right]}{\sqrt{2Var\left[Y_1\right]}}\right), \tag{4.38}$$

where $E\left[Y_1\right]$ and $Var\left[Y_1\right]$ are the expectation and variance of the energy detection test statistic for busy channel hypothesis.

In $H_{\Omega,1}$, the expectation and variance of $Y_{H_{\Omega,1}}$ can be derived as

$$E[Y_{H_{\Omega,1}}] = I + K_{1H_{\Omega,1}}, \tag{4.39}$$

and

$$Var[Y_{H_{\Omega,1}}] = 2I + 4K_{1H_{\Omega,1}}\gamma_p, \tag{4.40}$$

respectively. By substituting (4.39) and (4.40) into (4.38), the conditional probability of detection in this case can be derived as

$$P_{dH_{\Omega,1}}(\Psi_m, I) = \frac{1}{2} erfc\left(\frac{\Psi_m - \left(I + K_{1H_{\Omega,1}}\gamma_p\right)}{2\sqrt{I + 2K_{1H_{\Omega,1}}\gamma_p}}\right). \tag{4.41}$$

4.3.3 Unconditional Probability of False Alarm and Detection

By using the conditional probabilities of occurring for $H_{\Omega,0}$ in (4.12) and the conditional probabilities of false alarm in (4.34), the unconditional probability of false alarm can be obtained as

$$\overline{P_{faH\Omega,0}}(\Psi_m, I) = \frac{\sum_{\Omega=0}^{N} \left(P_{faH_{\Omega,1}}(\Psi_m, I) P_{H_{\Omega,0}} \right)}{\sum_{\Omega=0}^{N} P_{H_{\Omega,0}}}. \tag{4.42}$$

Similarly, by using the conditional probabilities of occurring for $H_{\Omega,1}$ in (4.13) and the conditional probabilities of detection in (4.41), the unconditional probability of detection can be obtained as

$$\overline{P_{dH_{\Omega,1}}}(\Psi_m, I) = \frac{\sum_{\Omega=0}^{N} \left(P_{dH_{\Omega,1}}(\Psi_m, I) P_{H_{\Omega,1}} \right)}{\sum_{\Omega=0}^{N} P_{H_{\Omega,1}}}. \tag{4.43}$$

Note that in (4.34) and (4.41), the conditional probabilities $P_{faH_{\Omega,0}}$ and $P_{dH_{\Omega,1}}$ of different cases may be the same even if the value of Ω is different, depending on the cumulative number of samples occupied by the primary user. However, the unconditional probabilities of false alarm and detection in (4.42) and (4.43) are different for different values of N, as it is obtained by averaging the conditional probabilities over the occurring probability of each case, which is determined by the primary user traffic.

4.4 Numerical Results and Discussions

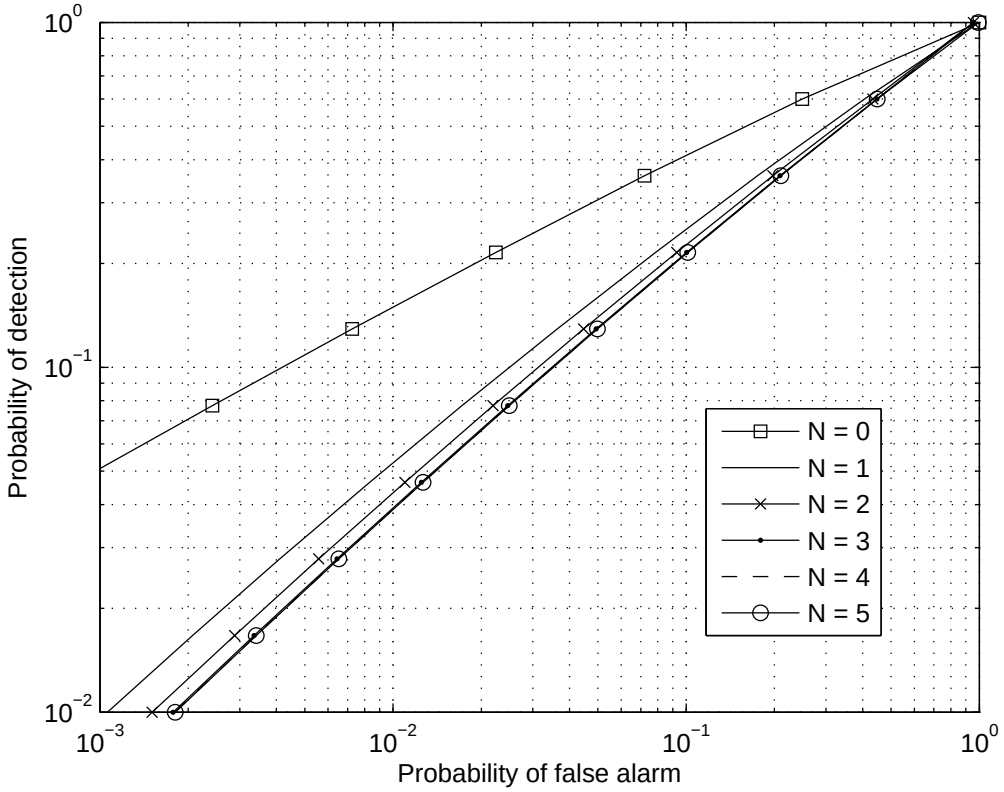

Figure 4.2: The ROC curves of the spectrum sensing performance with primary user multiple changes traffic for exponentially distributed channel holding times, with $\lambda_b^{-1} = \lambda_e^{-1} = 1/5\tau$.

In this section, the effect of the primary user traffic with multiple status changes during the sensing slot is investigated by presenting some numerical examples. In all the examples, the Neyman-Pearson is applied to obtain the decision threshold. In this case, the decision threshold is determined by letting $\overline{P_{dH_{\Omega,1}}}$ equal to the target probability of 0.9. The probability of false alarm $\overline{P_{faH_{\Omega,0}}}$ is hence obtained by using the determined decision threshold. N is the maximum number of changes while $\Omega \in [0, N]$. In all the comparisons, $N = 0$ indicates the case when there is no

primary user status change occurring during the spectrum sensing slot, the system performance becomes the same as that of the conventional model in this case.

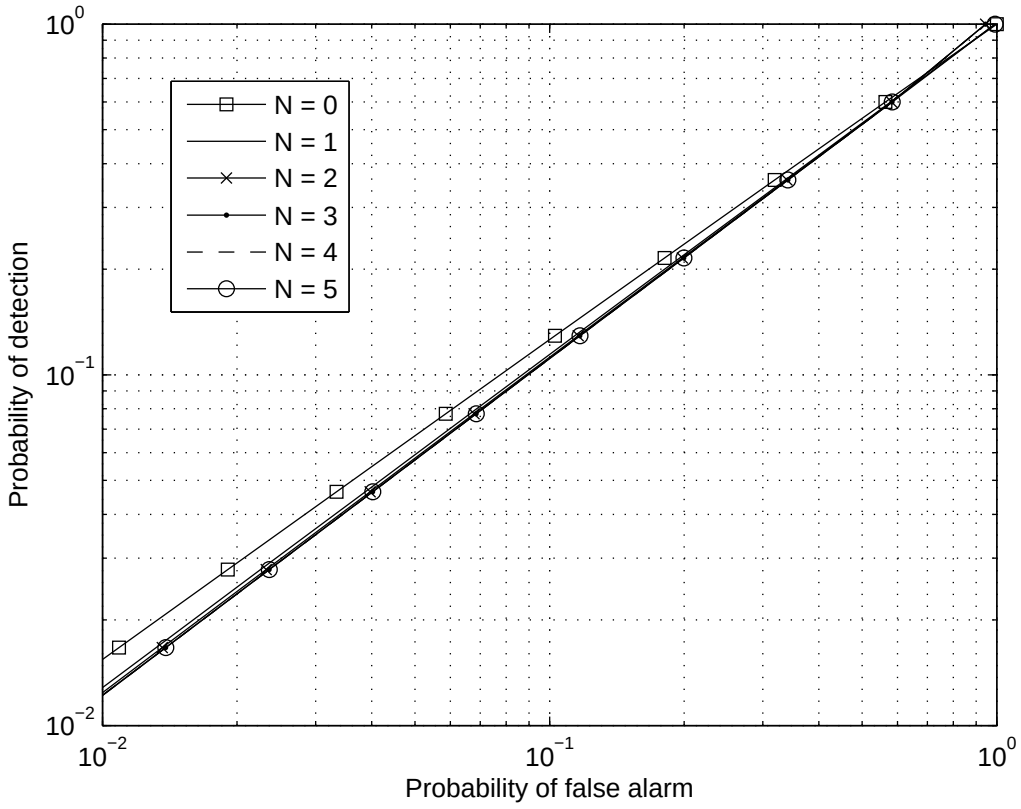

Figure 4.3: The ROC curves of spectrum sensing performance with primary user multiple changes traffic for exponentially distributed channel holding times, with $\lambda_b^{-1} = \lambda_e^{-1} = \tau$.

Fig. 4.2 examines the effect of the primary user traffic with multiple status changes on the sensing performance. In this figure, the sensing period τ is 20 ms and $\gamma_p = -5$ dB. The exponentially distributed traffic model is applied with both the busy and idle channel holding time set at $\frac{1}{5}\tau$. As can be observed, when the number of the primary occupancy status changes increases, the spectrum sensing performance degrades. However, the amount of degradation decreases as the number

of status changes increases, and the spectrum sensing performance become almost identical for $N > 3$ in this case. This is because for the given values of τ, λ_b and λ_e in this case, the probability that more than five status changes occur becomes very small. This suggests lower bound of the sensing performance and converges to a minimum performance due to the limited sensing slot duration and the primary user traffic intensities.

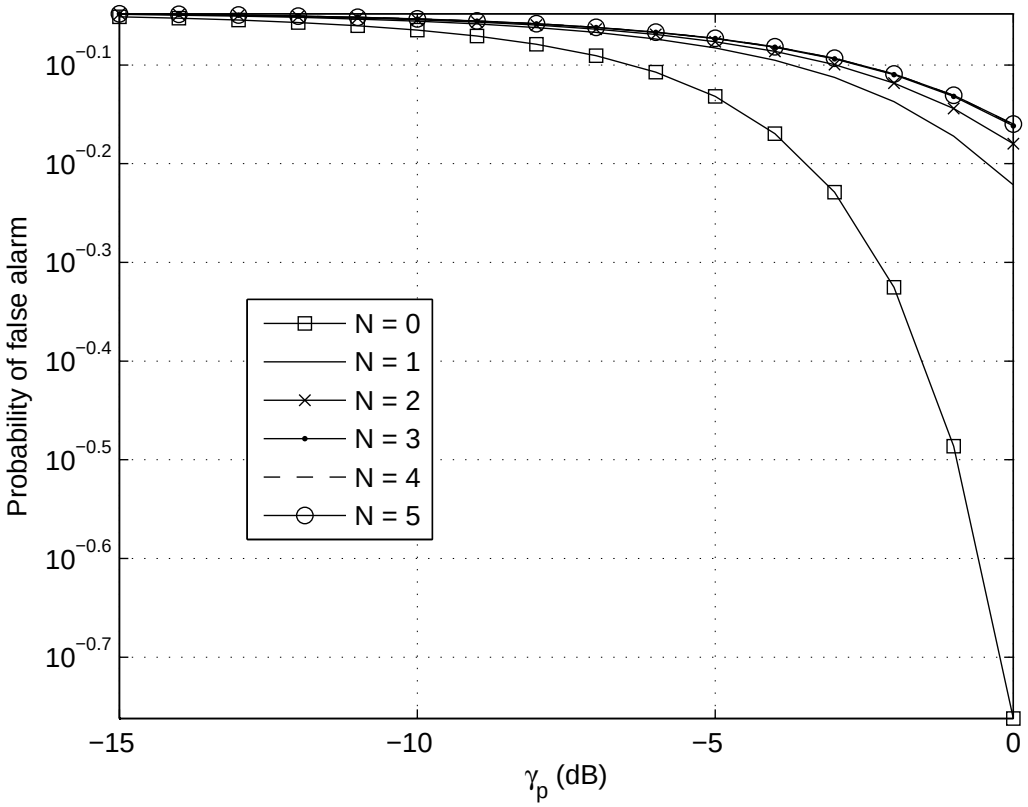

Figure 4.4: The spectrum sensing performance for different received primary user SNR.

Fig. 4.3 examines the effect of the primary user traffic intensity on the spectrum sensing performance. In this figure, the channel holding times are increased to be comparable with the sensing slot duration at $\lambda_b^{-1} = \lambda_e^{-1} = 20\ ms$. As can be

seen from the figure, in contrast with Fig. 4.2, the sensing performance degradation caused by the primary user traffic becomes less significant and is almost identical for different values of N. This is because when the busy and idle channel holding times are increased to be comparable with the spectrum sensing duration, the probability for the primary user multiple status changes during the sensing slot becomes very small. The sensing performance therefore becomes closer to that of the conventional model where $N = 0$, as it is less affected by the primary user traffic.

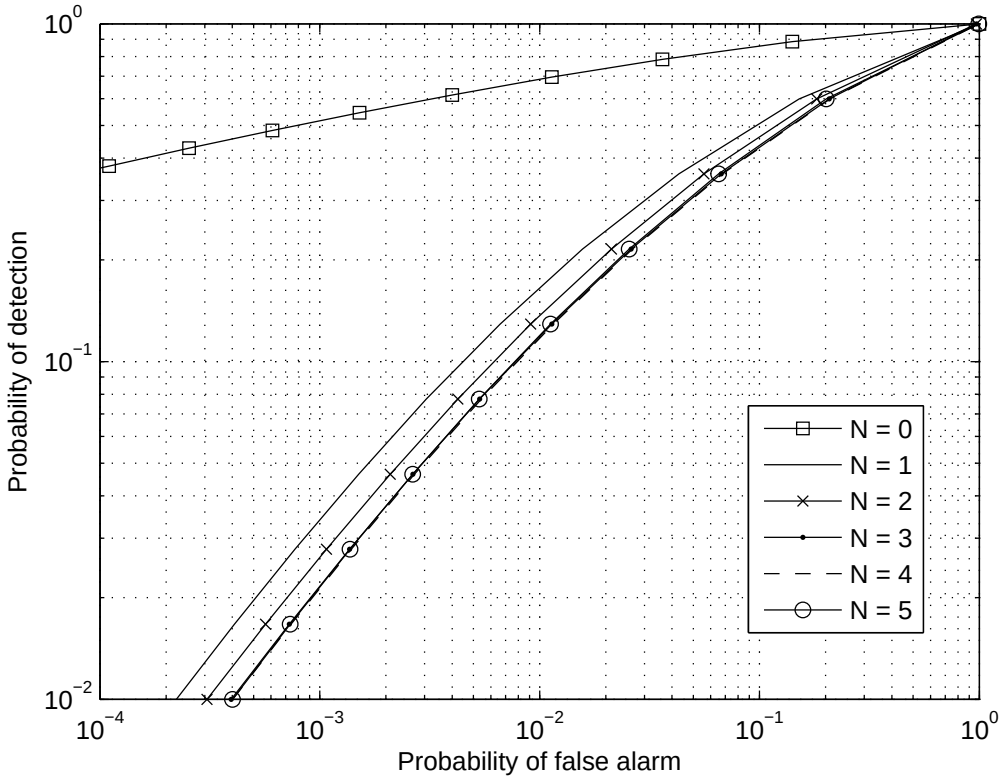

Figure 4.5: The ROC curves of spectrum sensing performance with the primary user multiple changes traffic for Gamma distributed channel holding times.

Fig. 4.4 examines the effect of the received primary user SNR on the spectrum sensing performance with primary user multiple status changes. The exponential

distribution model is applied for the primary user traffic channel holding times. As can be seen, the probability of false alarm increases as the value of N increases, indicating a degradation in the spectrum sensing performance when the primary user traffic with multiple status changes is considered. Moreover, although the spectrum sensing performance improves with the increase of the received primary user SNR γ_p for all values of N, this improvement becomes much smaller and slower when the multiple status change of the primary user traffic is taken into consideration.

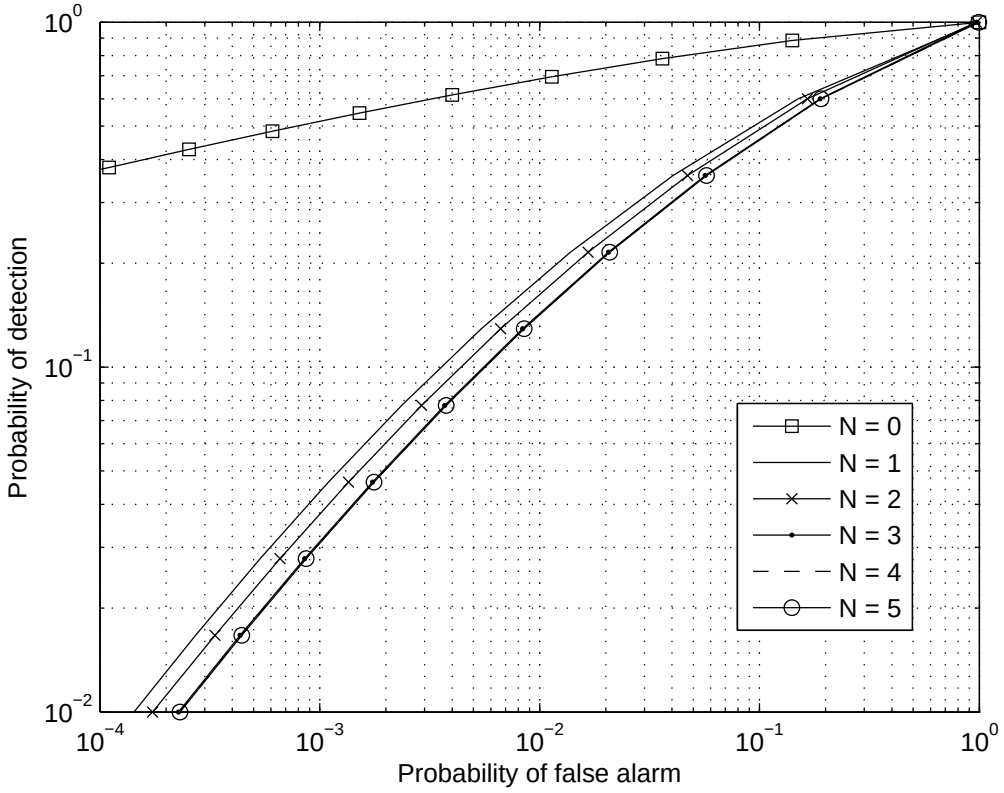

Figure 4.6: The ROC curves of spectrum sensing performance with the primary user multiple changes traffic for Erlang distributed channel holding times.

Fig. 4.5 to Fig. 4.7 investigate the effect of the primary user multiple changes traffic on the sensing performance for different distributions of the channel holding

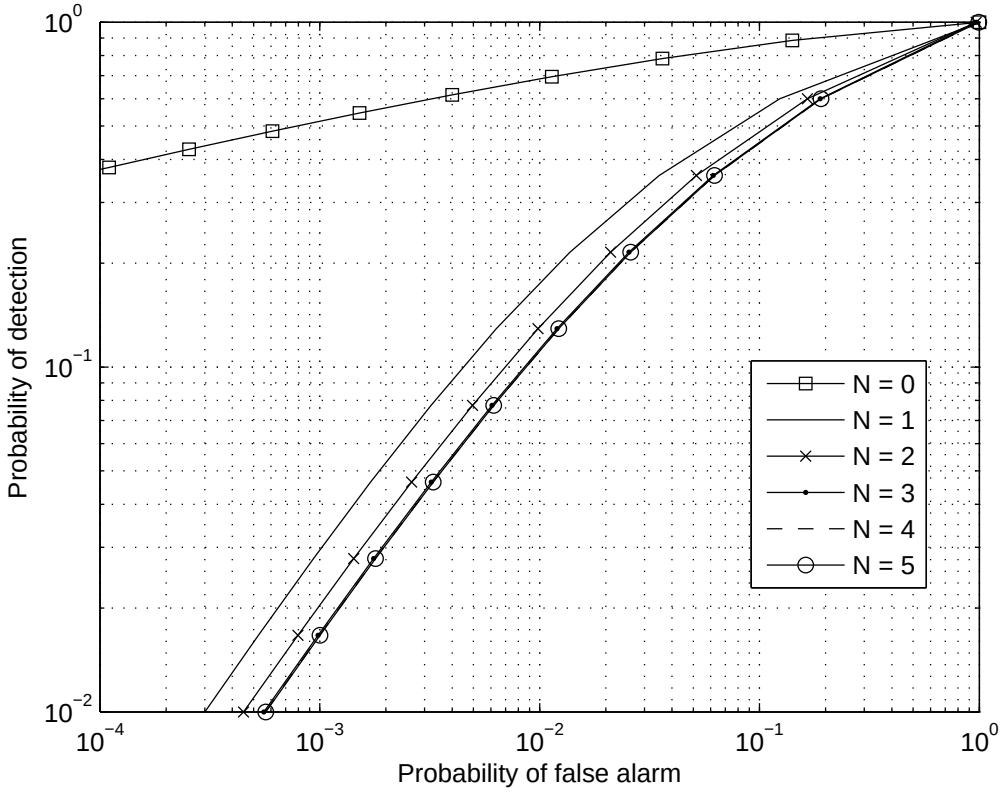

Figure 4.7: The ROC curves of spectrum sensing performance with the primary user multiple changes traffic for log-normal distributed channel holding times.

times. For all distributions, $\gamma_p = 0$ dB, and the mean channel holding time is set at $\frac{1}{5}\tau$. Fig. 4.5 presents the ROC curves of the spectrum sensing with the primary user multiple status changes for Gamma distributed channel holding times. In this figure, the shape parameters are set at $k_{gam,\alpha} = k_{gam,\beta} = 10$, and the scale parameters are $\theta_{gam,\alpha} = \theta_{gam,\beta} = \frac{1}{2500}$. As can be seen, similar findings can be observed as earlier figures. The spectrum sensing performance degrades when the multiple status changes of the primary user is taken into account. Fig. 4.6 presents the ROC curves of spectrum sensing for Erlang distributed busy and idle channel holding times. The shape parameters of the distribution are set at $k_{er,\alpha} = k_{er,\beta} = 20$,

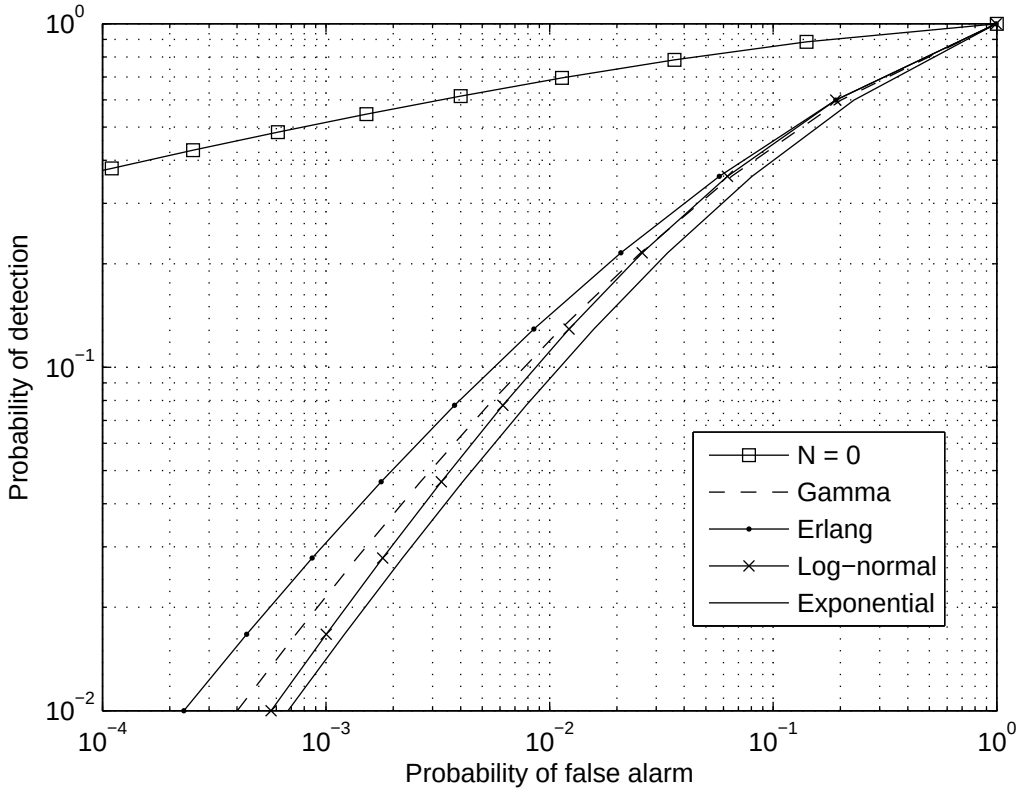

Figure 4.8: Comparison of the ROC curves of spectrum sensing performance for differently distributed channel holding times, with $N = 5$.

and the rate parameters are $\lambda_{er,\alpha} = \lambda_{er,\beta} = 5000$. Fig. 4.7 shows the ROC curves of spectrum sensing for log-normal distributed busy and idle channel holding times. In this case, the standard deviations are set at $\sigma_{log,\alpha} = \sigma_{log,\beta} = 1$, and the means are $\mu_{log,\alpha} = ln(\frac{1}{250}) - \frac{\sigma^2_{log,\alpha}}{2}$ and $\mu_{log,\beta} = ln(\frac{1}{250}) - \frac{\sigma^2_{log,\beta}}{2}$. Comparing Fig. 4.5, Fig. 4.6 and Fig. 4.7, the primary user with multiple status changes has different degree of impacts on the sensing performance, due to the difference in the primary user traffic distribution model. However, it has been shown that the sensing performance always degrades as the increase of N and reaches to a lower bound performance regardless of the distribution models.

Fig. 4.8 compares the spectrum sensing performance for differently distributed channel holding times while $N = 5$. As can be observed, the sensing performance degradation caused by the primary user traffic with multiple changes, has different level of sensitivity to different channel holding time distribution models. In this case, the sensing performance is least sensitive to the Erlang model while it is most sensitive to the exponential model. Similar patterns can also be found from the results of $N = 1$ to $N = 4$. This suggests that the same sensing scheme may have different performances when operating with different primary systems.

4.5 Conclusions

The impact of the primary user traffic with multiple status changes on the spectrum sensing performance is analyzed. Closed-form expressions for the probabilities of false alarm and detection are derived. Numerical results show that the multiple status changes of the primary user cause considerable degradation in the sensing performance. This degradation depends on the number of changes, the primary user traffic model, the primary user traffic intensity and the SNR ratio of the received signal. Numerical results also show that the amount of degradation decreases when the number of changes increases, and converges to a minimum sensing performance due to the limited sensing period and primary holding time.

Chapter 5

Adaptive-Modulation-Based Cognitive Radio

5.1 Introduction

Cognitive radio has enabled the efficient utilization of the frequency spectrum. By adopting the superframe structure, the secondary data transmission starts once the spectrum sensing identifies the idle channel status. In the last chapter, the focus of the research was on the spectrum sensing performance of the cognitive radio. In this chapter, the focus is moved on to research related to the other main aspect of the cognitive radio, the secondary data transmission.

In conventional data transmission, a fixed constellation size is generally adopted by the modulation. The transmission is hence carried out at the same data rate regardless of the changes in the channel conditions. However, most practical wireless channels suffer from multipath fading, leading to dramatic changes in the channel condition over time. This results in two major disadvantages of the conventional

modulation method. First, the conventional modulation transmits data at the same data rate even when the channel condition is harsh where the higher reliability becomes more important than the higher data rate. Second, the conventional modulation still transmits data at the same data rate when the channel condition is good, wasting the capacity of achieving a higher data rate [106].

An existing solution for this problem is the adaptive modulation. It adapts the constellation size of the modulation according to the channel condition, such that a larger constellation size for higher data rate can be used when the channel condition is good or the SNR in the channel is high, whereas a smaller constellation size can be chosen for lower data rate and higher reliability when the channel condition is harsh or the SNR in the channel is low. By adapting the constellation size of the modulation according to the channel conditions, the average link spectral efficiency (link SE) can be significantly increased [107].

Aiming at flexibility and efficiency itself, the secondary transmission of the cognitive radio would definitely benefits greatly from the adaptive modulation. Consequently, the marriage of the cognitive radio and the adaptive modulation is a natural choice which provides additional flexibility. When adaptive modulation is applied, the cognitive radios can adjust the constellation size of the modulation used in the secondary data transmission of each frame.

However, in a cognitive radio system, there is a possibility that mis-detection occurs during the spectrum sensing, such that the licensed channel is considered as idle whist the primary user is actually present. In this case, the active primary user signal acts as interference to the adaptive modulation of the secondary user. The performance of the adaptive modulation is hence affected by the spectrum sensing results. Moreover, as was introduced in the previous chapters, the dynamic primary

user traffic is a practical issue that affects the performance of the cognitive radio system. In this case, when the primary user randomly departs or arrives at the licensed channel, it creates a mismatch between the channel condition based on which the constellation size is chosen and the channel condition the actual data transmission experiences. This will also affect the performance of the adaptive modulation. Thus, it is of great interest to analyze the performance of the adaptive modulation in the cognitive radios while taking into consideration of all these conditions.

In this chapter, the rate adaptive modulation which is the key to achieve high link SE is considered. The effect of the spectrum sensing and the dynamic primary user traffic on the performance of the adaptive modulation in cognitive radio system is analyzed. The rest of this chapter is organized as follows. First, in Section 5.2, a brief description of the conventional adaptive modulation is given, which will be used as a comparison reference for the performance of the adaptive modulation in cognitive radio system. In Section 5.3, the system model of the adaptive modulation in cognitive radio used in this chapter is presented. Section 5.4 and Section 5.5 provide the analysis of the ACR scheme and the ADR scheme, respectively, where both the BER performance and the link SE performance are derived. Numerical results are also presented for both sections to examine the mathematical derivations. Finally, the findings of this chapter will be summarized in Section 5.6.

5.2 Conventional Adaptive Modulation

Consider an adaptive modulation system for the conventional case, with multi-level quadrature amplitude modulation (M-QAM) scheme. The BER of the coherent M-QAM with two-dimensional Gray coding over an AWGN channel can be approx-

imated as [106]

$$P_{ber}\left(M,\gamma\right) \approx \frac{1}{5}e^{-\frac{3\gamma}{2(M-1)}}, \tag{5.1}$$

where M is the constellation size and γ is the signal-to-disturbance radio (SDR) in the channel which includes the noise and interference, if any. It has been a common method to replace the SNR with the SDR in the calculation of error rate [108] [109]. In (5.1), the value of P_{ber} is often predetermined in practice at a target value $\widehat{P_{ber}}$ and is available at the transmitter. The value of γ can be estimated using estimators in [110] by the receiver and then fed back to the transmitter. As it is not the main focus of the work in this chapter, it is assumed that perfect knowledge of γ is available. The constellation size M is then determined from γ using (5.1) before the transmission starts.

5.2.1 Adaptive Continuous Rate Scheme

Conventionally, when the ACR scheme is used for the adaptive modulation, the constellation size can be obtained by using (5.1) before the transmission starts as

$$M_{_{ACR}} \approx 1 - \frac{3\gamma}{2ln\left(5\widehat{P_{ber}}\right)}. \tag{5.2}$$

After the transmission, the actual BER of the ACR scheme can be derived by using (5.2) in (5.1), giving

$$\begin{aligned} P_{ber_{ACR}} &\approx \frac{1}{5}e^{-\frac{3\gamma}{2\left(M_{ACR}-1\right)}} \\ &= \widehat{P_{ber}}, \end{aligned} \tag{5.3}$$

which is equivalent to the fixed target value.

In a Nakagami-m fading channel, γ is a random variable and the probability

density function of γ is given by [111]

$$f_\gamma(\gamma) = \left(\frac{m}{\gamma_a}\right)^m \frac{\gamma^{m-1}}{\Gamma(m)} e^{-m\frac{\gamma}{\gamma_a}}, \qquad \gamma \geq 0, \tag{5.4}$$

where m is the parameter reflecting the channel, γ_a represents the fading power and $\Gamma(\cdot)$ is the Gamma function defined before. Using (5.3) and (5.4), the average BER of the ACR scheme in a Nakagami-m fading channel can be derived as

$$\begin{aligned} < P_{ber_{ACR}} > &= \int_0^\infty P_{ber_{ACR}} f_\gamma(x) \cdot dx \\ &= \widehat{P_{ber}}, \end{aligned} \tag{5.5}$$

which is the same as the instantaneous BER in (5.3), as (5.3) is independent of γ.

The link SE of the channel is given by [106]

$$\begin{aligned} \frac{R}{W}_{ACR} &= log_2\left(M_{ACR}\right) \\ &= log_2\left(1 - \frac{3\gamma}{2ln\left(5\widehat{P_{ber}}\right)}\right). \end{aligned} \tag{5.6}$$

The average link SE in the Nakagami-m fading channel can therefore be derived as

$$\begin{aligned} < \frac{R}{W} >_{ACR} = & \frac{e^{-\frac{2m\cdot ln(5\widehat{P_{ber}})}{3\gamma_a}}}{ln2} \sum_{q=0}^{m-1} \left(-\frac{2m\cdot ln(5\widehat{P_{ber}})}{3\gamma_a}\right)^q \\ & \cdot \Gamma\left(-q, -\frac{2m\cdot ln(5\widehat{P_{ber}})}{3\gamma_a}\right). \end{aligned} \tag{5.7}$$

5.2.2 Adaptive Discrete Rate Scheme

When the ADR scheme is used in the conventional adaptive modulation, the value of M has to be an integer that is a power of 2. Instead of (5.2), the constellation

size is chosen before the transmission according to [106]

$$M_{_{ADR}} = 2^k, \qquad \gamma_k < \gamma \leq \gamma_{k+1}, \tag{5.8}$$

where $k = 1, 2, \cdots, K$ is the index of possible different regions of the SDR in the channel, $\gamma_k = \left(erfc^{-1}\left(2\widehat{P_{ber}}\right)\right)^2$ when $k = 1$, $\gamma_k = +\infty$ when $k = K+1$ and $\gamma_k = -\frac{2}{3}ln(5\widehat{P_{ber}})(2^k - 1)$ when $k = 2, 3, \cdots, K$. Effectively, the SDR has been quantized to different regions with each region corresponding to an integer value of the constellation size.

After the transmission, the actual instant BER for the ADR scheme in the conventional adaptive modulation can be derived using (5.8) as

$$\begin{aligned} P_{ber_{ADR}}(M_{_{ADR}}, \gamma) &\approx \frac{1}{5} e^{\frac{3\gamma}{2\left(1 - M_{_{ADR}}\right)}} \\ &= \frac{1}{5} e^{\frac{3\gamma}{2(1-2^k)}}, \qquad \gamma_k < \gamma \leq \gamma_{k+1}. \end{aligned} \tag{5.9}$$

Thus, in a Nakagami-m fading channel, the average BER for the ADR scheme in the conventional adaptive modulation is derived as

$$\begin{aligned} < P_{ber_{ADR}} > = & \frac{\left(\frac{m}{\gamma_a}\right)^m}{5\Gamma(m) \sum_{k=1}^{K} kA_k} \cdot \sum_{k=1}^{K} \left(\frac{k\Gamma\left(m, \frac{m\gamma_k}{\gamma_a} + \frac{3\gamma_k}{2\left(2^k-1\right)}\right)}{\left(\frac{m}{\gamma_a} + \frac{3}{2\left(2^k-1\right)}\right)^m} \right. \\ & \left. - \frac{k\Gamma\left(m, \frac{m\gamma_{k+1}}{\gamma_a} + \frac{3\gamma_{k+1}}{2\left(2^k-1\right)}\right)}{\left(\frac{m}{\gamma_a} + \frac{3}{2\left(2^k-1\right)}\right)^m} \right), \end{aligned} \tag{5.10}$$

where

$$A_k = \int_{\gamma_k}^{\gamma_{k+1}} f_\gamma(\gamma) \cdot d_\gamma = \frac{\Gamma\left(m, \frac{m\gamma_k}{\gamma_a}\right) - \Gamma\left(m, \frac{m\gamma_{k+1}}{\gamma_a}\right)}{\Gamma(m)} \tag{5.11}$$

The link SE of the ADR scheme in the conventional adaptive modulation is given by

$$\frac{R}{W}_{ADR} = log_2\left(M_{ADR}\right) = k, \qquad \gamma_k < \gamma \leq \gamma_{k+1}. \tag{5.12}$$

The average link SE in a Nakagami-m fading channel is therefore

$$< \frac{R}{W} >_{ADR} = \sum_{k=1}^{K} kA_k. \tag{5.13}$$

5.3 Adaptive Modulation in Cognitive Radio

When the adaptive modulation is applied in the cognitive radio system, the secondary user adjusts the constellation size of the modulation used in the secondary data transmission slot of each frame. The main difference between adaptive modulation in the cognitive radio and the conventional adaptive modulation is that the performance of the adaptive modulation in cognitive radio is also affected by the distinctive features of the cognitive radio system. Spectrum sensing errors, decided by the spectrum sensing quality of the cognitive radio system, can cause interference to the adaptive modulation in cognitive radio. The dynamic primary user traffic, determined by the primary user traffic intensity, can result in a mismatch between the channel condition based on which the constellation size is chosen and the actual channel condition at which the secondary data transmission takes place.

Consider the cognitive radio system discussed in the Chapter 3, where the dynamic primary user traffic is taken into consideration. For the adaptive modulation applied in cognitive radio system in this chapter, it is assumed that the constellation size of the modulation is chosen before the secondary data transmission starts in the transmission slot of the secondary frame. Once the constellation size is chosen,

it is fixed until the end of the frame and will not be chosen again regardless of the changes in the channel condition during the transmission process. The dynamic primary user traffic probability model presented in (3.9) is also assumed in this chapter.

As can been seen from Fig. 3.1, while assuming the primary user only changes its occupancy status once during each frame, there are six possible scenarios with their probability of occurring given by (3.9). The spectrum sensing is therefore given by the hypothesis test in (3.10) when energy detection is applied. The unconditional probability of false alarm and the unconditional probability of detection are given by (3.20) and (3.21), respectively. Once the spectrum sensing is complete, the secondary transmission starts if the licensed channel is considered to be idle. The average BER and the average link SE for the adaptive modulation in cognitive radio are derived for both the ACR and ADR schemes in the following sections. Note that in the derivations, different symbols are used to denote BERs and link SEs in different conditions, where $< \cdot >$ indicates averaged values in a Nakagami-m fading channel, $\overline{\cdot}$ indicates unconditional values that have been averaged over the probability of occurring, and $\overline{< \cdot >}$ indicates averaged unconditional values for a Nakagami-m fading channel.

5.4 Adaptive Continuous Rate Scheme in Cognitive Radio

5.4.1 BER Performance

- Idle hypotheses - idle licensed channel at the end of the sensing slot.

When the licensed channel is actually idle at the end of the sensing slot and this idle status is correctly detected by the secondary user with a probability of $1 - \overline{P_{faH}}(\Psi_H, I)$, the secondary transmission starts in the transmission slot of the secondary frame. By applying the ACR scheme for the adaptive modulation in the cognitive radio system, the choice of the constellation size is made before the secondary transmission starts according to

$$M_{ACR0cr} = 1 - \frac{3\gamma_s}{2ln\left(5\widehat{P_{ber}}\right)}, \tag{5.14}$$

where $\gamma = \gamma_s$ is used as the primary user is absent from the licensed channel hence there is no interference when the choice of constellation size is made, and γ_s is the secondary user SNR defined as before.

Once the constellation size is chosen, the secondary user starts the transmission using the chosen constellation size. As can be seen from Fig. 3.1, in $H_{0,0(0)}$ and $H_{0,1}$, the primary user remains absent from the licensed channel for the entire transmission slot. In this case, the channel condition based on which the constellation size is chosen is the same as that the actual transmission experienced. The BERs for the ACR scheme are therefore derived as

$$\begin{aligned} P_{ber_{ACR0cr}1} &= \frac{1}{5}e^{-\frac{3\gamma_s}{2\left(M_{ACR0cr}-1\right)}} \\ &= \widehat{P_{ber}}, \end{aligned} \tag{5.15}$$

which is the same as that of the conventional adaptive modulation. The average BER in the Nakagami-m fading channel is therefore represented as

$$< P_{ber_{ACR0cr}1} >= \widehat{P_{ber}}, \tag{5.16}$$

which is also the same as that of the conventional adaptive modulation in (5.5).

On the other hand, in the hypothesis $H_{0,0(1)}$, the primary user is absent when the secondary transmission starts, as illustrated by Fig. 3.1. It then arrives at the licensed channel during the transmission slot at the α^{th} sample. This implies that $I+1 \leq \alpha < J$, and the first $\alpha - I$ samples of the transmission slot experience an idle channel whilst the last $J-\alpha$ samples suffers from the primary user interference. This means that the first $\alpha - I$ samples of the transmission slot do not experience any channel condition changes such that the actual average BERs are the same as (5.15) and (5.16). After the arrival of the primary user at the α^{th} sample, the last $J-\alpha$ samples of the transmission slot suffers from a mismatch between the actual channel SDR and the SDR according to which the constellation size is chosen, caused by the primary user interference. Their actual BERs are therefore become different and can be derived as,

$$\begin{aligned} P_{ber_{ACR0cr}2}\left(M_{_{ACR0cr}}, \frac{\gamma_s}{1+\gamma_p}\right) &= \frac{1}{5} e^{-\frac{3}{2\left(M_{ACR0cr}-1\right)}\frac{\gamma_s}{(1+\gamma_p)}} \\ &= \frac{1}{5}\left(5\widehat{P_{ber}}\right)^{\frac{1}{1+\gamma_p}}, \end{aligned} \tag{5.17}$$

where $\gamma = \dfrac{\gamma_s}{1+\gamma_p}$ is used for the actual channel SDR when the primary user is present and γ_p is the primary user SNR defined as before. From the secondary user's perspective, γ_p is the INR.

In a Nakamgami-m fading channel, (5.17) is averaged over (5.4). Since (5.17) is independent of γ_s, the average BERs $< P_{ber_{ACR0cr}2} >$ is therefore the same as (5.17). Thus, for hypothesis $H_{0,0(1)}$, the average BER can be derived as

$$< P_{ber_{ACR0cr}3} > (\alpha) = \frac{1}{J-I}\left((\alpha - I)\,\widehat{P_{ber}} + (J-\alpha)\,\frac{1}{5}\left(5\widehat{P_{ber}}\right)^{\frac{1}{1+\gamma_p}}\right). \tag{5.18}$$

Note that when $\alpha = J$, it indicates that the primary user does not arrive during the secondary transmission slot, and the model becomes the same as the conventional adaptive modulation. (5.18) degenerates to be $\widehat{P_{ber}}$ which is the same as (5.5).

- Busy hypotheses - busy licensed channel at the end of the sensing slot.

Similarly, when the licensed channel is actually busy at the end of the sensing slot but is mistakenly considered as idle by the secondary user with a probability of $1 - \overline{P_{dH}}(\Psi_H, I)$, the secondary transmission starts in the transmission slot. In this case, the selection of the constellation size is made before the secondary transmission according to the actual channel SDR, as

$$M_{ACR1cr} = 1 - \frac{3}{2ln\left(5\widehat{P_{ber}}\right)} \frac{\gamma_s}{(1+\gamma_p)}. \tag{5.19}$$

In the above equation, the value of $\frac{\gamma_s}{1+\gamma_p}$ can be estimated by using estimators in [110], where the signal amplitude can be estimated using the sample mean of the received signal and the disturbance power can be estimated using the sample variance of the received signal. In the estimation, only the disturbance power is known but not the individual primary user interference power and the noise power. Therefore, in reality, the secondary user does not require the exact knowledge of the primary user interference power.

Once the constellation size is chosen, the secondary user start the transmission. In $H_{1,0(0)}$ and $H_{1,1}$, as illustrated in Fig. 3.1, the primary user remains present in the licensed channel for the entire transmission slot. Hence, the channel condition is consistent for the whole transmission duration, and there is no mismatch between the actual channel condition and the channel condition based on which the constellation

size was chosen. Their BERs for the ACR scheme are therefore,

$$\begin{aligned} P_{ber_{ACR1cr}1} &\approx \frac{1}{5} e^{-\frac{3}{2\left(M_{ACR1cr}-1\right)}\frac{\gamma_s}{(1+\gamma_p)}} \\ &= \widehat{P_{ber}}, \end{aligned} \tag{5.20}$$

which is independent of γ_s. Thus, the average BER in the Nakagami-m fading channel, $< P_{ber_{ACR1cr}1} >$, averaged over the distribution of γ_s is the same as (5.20).

On the other hand, in $H_{1,0(1)}$, the primary user is present during the sensing slot and the first $\beta - I$ samples of the secondary transmission period, it then departs from the licensed channel at the β^{th} sample and remains absent for the rest of the transmission slot. This implies that $I + 1 \leq \beta < J$, and the actual channel SDR that the first $\beta - I$ samples experiences is the same as the SDR based on which the constellation size is chosen. Thus, there is no mismatch in the channel conditions, even though the secondary transmission suffers from the interference caused by the primary user signal. The BERs and the average BERs in the Nakagami-m fading channel hence both equal to the target BER.

After the departure of the primary user at the β^{th} sample, the last $J - \beta$ samples of the transmission period no longer suffer from the interference caused by the primary user. However, as the constellation size is chosen according to (5.19) and the channel effective SDR is changed, the actual BERs therefore no longer equal to the target BER, and become

$$\begin{aligned} P_{ber_{ACR1cr}2}\left(M_{ACR1cr}, \gamma_s\right) &\approx \frac{1}{5} e^{-\frac{3\gamma_s}{2\left(M_{ACR1cr}-1\right)}} \\ &= \frac{1}{5}\left(5\widehat{P_{ber}}\right)^{(1+\gamma_p)}. \end{aligned} \tag{5.21}$$

As (5.21) is independent of γ_s, and the average BERs in a Nakagami-m fading

channel $< P_{ber_{ACR1cr2}} >$ is therefore the same as (5.21).

Thus, for hypothesis $H_{1,0(1)}$, the average BER in Nakagami-m fading channel can be derived as

$$< P_{ber_{ACR1cr3}} > (\beta) = \frac{1}{J-I}\left((\beta - I)\,\widehat{P_{ber}} + (J-\beta)\,\frac{1}{5}\left(5\widehat{P_{ber}}\right)^{1+\gamma_p}\right). \tag{5.22}$$

When $\beta = J$, it indicates the primary user does not depart from the licensed channel during the transmission slot, which is the same as the conventional adaptive modulation. In that case, (5.22) simplifies to $\widehat{P_{ber}}$, same as (5.5).

By taking into consideration the probability of occurring in (3.9) and the spectrum sensing performance in (3.20) and (3.21), the unconditional average BER for the adaptive modulation with ACR scheme in cognitive radio with dynamic primary user traffic in Nakagami-m fading channel, can be derived as

$$\begin{aligned}
\overline{< P_{berACRcr} >} =& \frac{1}{P_{H_{sum}0} + P_{H_{sum}1}}\Big(P_{H_{0,0(0)}}(\lambda_b,\lambda_e)\left(1-\overline{P_{faH}}(\Psi_H,I)\right)\widehat{P_{ber}} \\
&+ P_{H_{0,1}}(\lambda_b,\lambda_e)\left(1-\overline{P_{faH}}(\Psi_H,I)\right)\widehat{P_{ber}} \\
&+ \sum_{\alpha=I+1}^{J-1}\left(p_e p_{00}^{\alpha} p_{01} p_{11}^{J-\alpha-1} < P_{ber_{ACR0cr3}} > (\alpha)\right)\left(1-\overline{P_{faH}}(\Psi_H,I)\right) \\
&+ P_{H_{1,0(0)}}(\lambda_b,\lambda_e)\left(1-\overline{P_{dH}}(\Psi_H,I)\right)\widehat{P_{ber}} \\
&+ P_{H_{1,1}}(\lambda_b,\lambda_e)\left(1-\overline{P_{dH}}(\Psi_H,I)\right)\widehat{P_{ber}} \\
&+ \sum_{\beta=I+1}^{J-1}\Big(p_b p_{11}^{\beta} p_{10} p_{00}^{J-\beta-1} < P_{ber_{ACR1cr3}} > (\beta)\Big)\left(1-\overline{P_{dH}}(\Psi_H,I)\right)\Big)
\end{aligned} \tag{5.23}$$

where

$$P_{H_{sum}0} = P_{H_{0,0(0)}}(\lambda_b,\lambda_e) + P_{H_{0,0(1)}}(\lambda_b,\lambda_e) + P_{H_{0,1}}(\lambda_b,\lambda_e), \tag{5.24}$$

and

$$P_{H_{sum}1} = P_{H_{1,0(0)}}(\lambda_b, \lambda_e) + P_{H_{1,0(1)}}(\lambda_b, \lambda_e) + P_{H_{1,1}}(\lambda_b, \lambda_e). \tag{5.25}$$

From (5.23), it can be seen that the unconditional averaged BER of the ACR scheme is affected by the spectrum sensing quality as well as the dynamic primary user traffic.

5.4.2 Link Spectrum Efficiency Performance

Next, the link SE for the ACR scheme is derived. Unlike the BER derived in the above section, the link SE is determined before the secondary transmission starts. Therefore the average link SE is not affected by the changes of channel condition during the data transmission slot caused by the dynamic primary user traffic. However, it is still affected by the spectrum sensing performance and the dynamic primary user traffic during the sensing slot.

When the primary user is actually absent from the channel at the end of the sensing slot, the decision of the constellation size is made according to (5.14), in this case, the instantaneous link SE can be derived as

$$\begin{aligned} \frac{R}{W}_{ACR0cr}(\gamma_s) &= log_2 M_{ACR0cr} \\ &= log_2\left(1 - \frac{3\gamma_s}{2ln\left(5\widehat{P_{ber}}\right)}\right). \end{aligned} \tag{5.26}$$

The average link SE in a Nakagami-m fading channel in this case is therefore

obtained by averaging (5.26) over (5.4) as

$$< \frac{R}{W} >_{ACR0cr} = \frac{e^{-\frac{2m \cdot ln(5\widehat{P_{ber}})}{3\gamma_a}}}{ln2} \sum_{q=0}^{m-1} \left(-\frac{2m \cdot ln(5\widehat{P_{ber}})}{3\gamma_a} \right)^q \cdot \Gamma\left(-q, -\frac{2m \cdot ln(5\widehat{P_{ber}})}{3\gamma_a} \right). \tag{5.27}$$

On the other hand, when the primary user is present at the end of the sensing slot, the decision of the constellation size is made according to (5.19), the instantaneous link SE in this case is derived as

$$\begin{aligned} \frac{R}{W}_{ACR1cr} \left(\frac{\gamma_s}{1+\gamma_p} \right) &= log_2 M_{_{ACR1cr}} \\ &= log_2 \left(1 - \frac{3\gamma_s}{2ln\left(5\widehat{P_{ber}}\right)(1+\gamma_p)} \right), \end{aligned} \tag{5.28}$$

and the average link SE in a Nakagami-m fading channel can be derived by averaging (5.28) over (5.4) as

$$< \frac{R}{W} >_{ACR1cr} = \frac{e^{-\frac{2m \cdot ln(5\widehat{P_{ber}})(1+\gamma_p)}{3\gamma_a}}}{ln2} \sum_{q=0}^{m-1} \left(-\frac{2m \cdot ln(5\widehat{P_{ber}})\,(1+\gamma_p)}{3\gamma_a} \right)^q \cdot \Gamma\left(-q, -\frac{2m \cdot ln(5\widehat{P_{ber}})\,(1+\gamma_p)}{3\gamma_a} \right). \tag{5.29}$$

By taking into consideration the probability of occurring in (3.9) and the spectrum sensing performance in (3.20) and (3.21), the average link SE for the ACR scheme in a Nakagami-m fading channel for cognitive radio systems with dynamic

primary user traffic can be derived as

$$\begin{aligned} \overline{< \frac{R}{W} >_{ACRcr}} = P_{H_{sum}0} \left(1 - \overline{P_{faH}} \left(\Psi_H, I\right)\right) < \frac{R}{W} >_{ACR0cr} \\ + P_{H_{sum}1} \left(1 - \overline{P_{dH}} \left(\Psi_H, I\right)\right) < \frac{R}{W} >_{ACR1cr} . \end{aligned} \tag{5.30}$$

In practical design of cognitive radio systems applying adaptive modulation, as the feedback channel between the secondary receiver and the secondary transmitter for the purpose of adaptive modulation already exists, it may be used to improve the sensing efficiency. The secondary user transmitter and receiver can in fact perform spectrum sensing simultaneously and exchange sensing results with each other through the feedback channel. By doing so, cooperative sensing can be achieved and consequently improves the sensing performance due to the diversity gain.

5.4.3 Numerical Results and Discussions

In this section, numerical examples are presented to examine the effect of the cognitive radio features, including the spectrum sensing performance and the dynamic primary user traffic, on the adaptive modulation performance applying ACR scheme. In this examination, the frame duration is set at $T = 10$ ms, with $J = 42$. This gives $t_s = 0.24$ ms. Assume $I = 10$ and the target probability of detection for the spectrum sensing is set at $\widehat{P_d} = 0.9$. The target BER is set at $\widehat{P_{ber}} = 10^{-5}$. In all the figures, AM denotes adaptive modulation, whilst CR denotes cognitive radio.

Fig. 5.1 compares the BER performance of the conventional adaptive modulation applying the ACR scheme with that of the adaptive modulation in cognitive radio in a Nakagami-m fading channel. First, as can be observed, the BER performance of the adaptive modulation is degraded when its applied in the cognitive radio system. For example, the BER of the conventional adaptive modulation is at the target BER

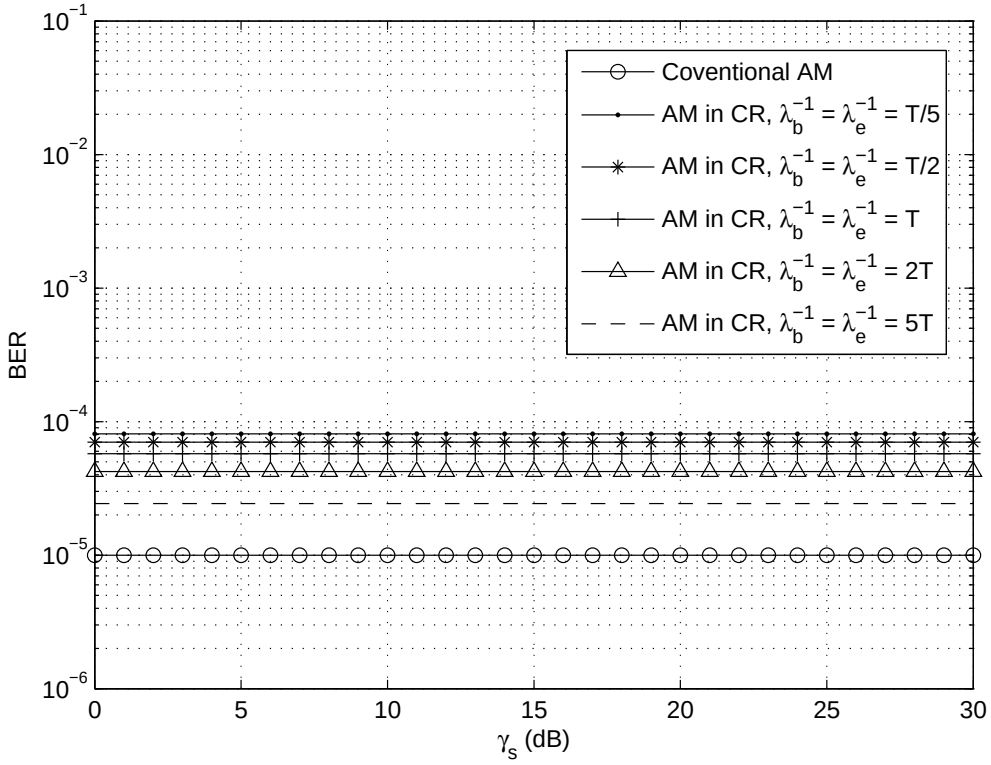

Figure 5.1: Comparison of the BER performance for the conventional adaptive modulation with the BER performance for the adaptive modulation in cognitive radio with ACR scheme and different channel holding times, with $\gamma_p = 0$ dB.

10^{-5}, whereas the BER of the adaptive modulation in cognitive radio is increased to around 10^{-4} which are much higher values. The increment might be considered as very significant in some applications. Second, as the λ_b^{-1} and λ_e^{-1} increase, the gap between the conventional adaptive modulation and the adaptive modulation in cognitive radio is decreased. This is because as the value of λ_b^{-1} and λ_e^{-1} increase, the primary user traffic intensity decreases, such that the probability of a primary user status change occurs decreases. However, even when the channel holding time is large, the gap between the conventional adaptive modulation and the adaptive modulation in cognitive radio is still significant, as a result of being degraded by

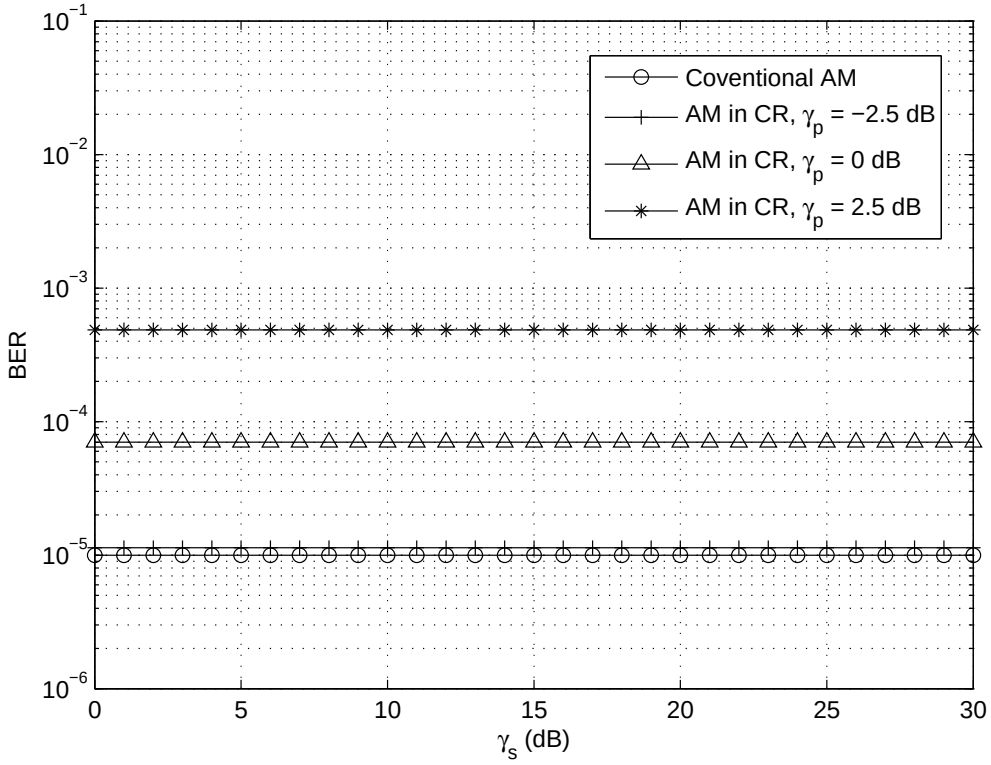

Figure 5.2: Comparison of the BER performance for the conventional adaptive modulation with the BER performance for the adaptive modulation in cognitive radio with ACR scheme and different values of γ_p, with $\lambda_b^{-1} = \lambda_e^{-1} = T$.

the spectrum sensing errors. Thirdly, it can also be seen that although the BER performance is degraded by the spectrum sensing performance and the dynamic primary user traffic of the cognitive radio, the BER values still remain the same as the increase of γ_s. This is the same as the conventional adaptive modulation where the BER performance is independent of γ_s.

Fig. 5.2 compares the BER performance for the conventional adaptive modulation applying the ACR scheme and the adaptive modulation in cognitive radio for different values of γ_p. In this comparison, $\lambda_b^{-1} = \lambda_e^{-1} = T$. As can be seen, when the value of γ_p increases, the gap between the BER performance of the conventional

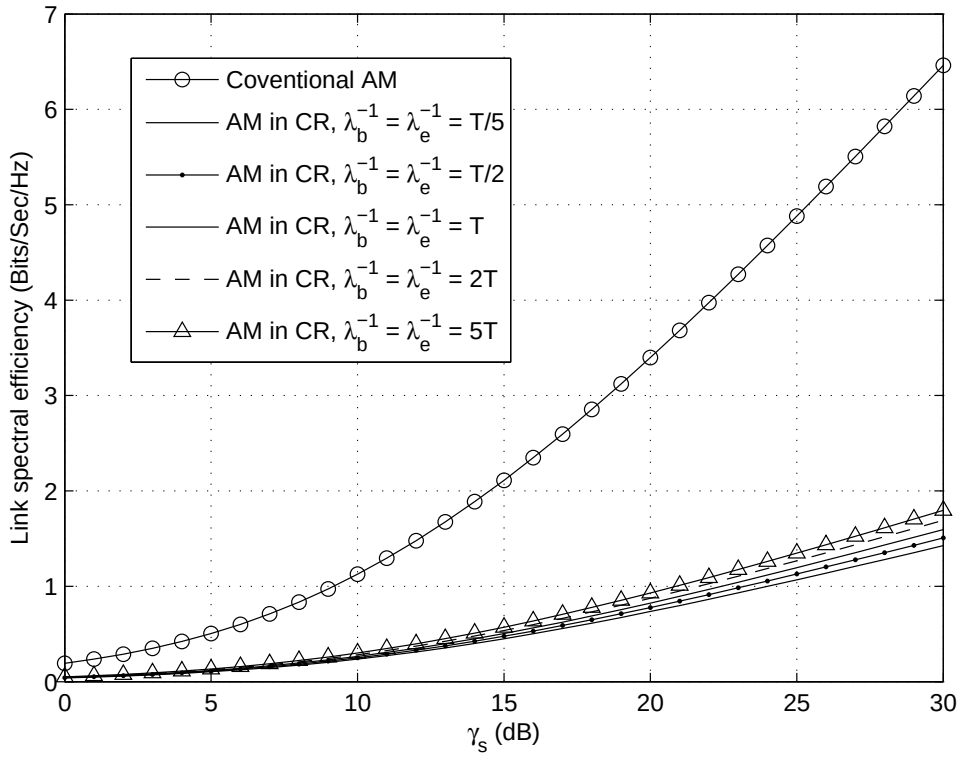

Figure 5.3: Comparison of the link SE performance for the conventional adaptive modulation with the link SE performance for the adaptive modulation in cognitive radio with ACR scheme and different values of $\lambda_b^{-1} = \lambda_e^{-1}$, with $\gamma_p = 0$ dB.

ACR scheme and the ACR scheme in cognitive radio also increases. This is explained as follows. As the received primary user SNR γ_p increases, the spectrum sensing performance improves. However, as shown in Fig. 4.4 in the last chapter, this improvement becomes much less significant when the primary user traffic is taken into consideration. On the other hand, as the increases of γ_p, the INR of the secondary transmission increases, which consequently degrades the secondary transmission performance. Moreover, as was discussed in the Chapter 3, the secondary transmission performance degrades further when the primary user traffic is taken into consideration. Hence overall, the BER performance of the adaptive modulation

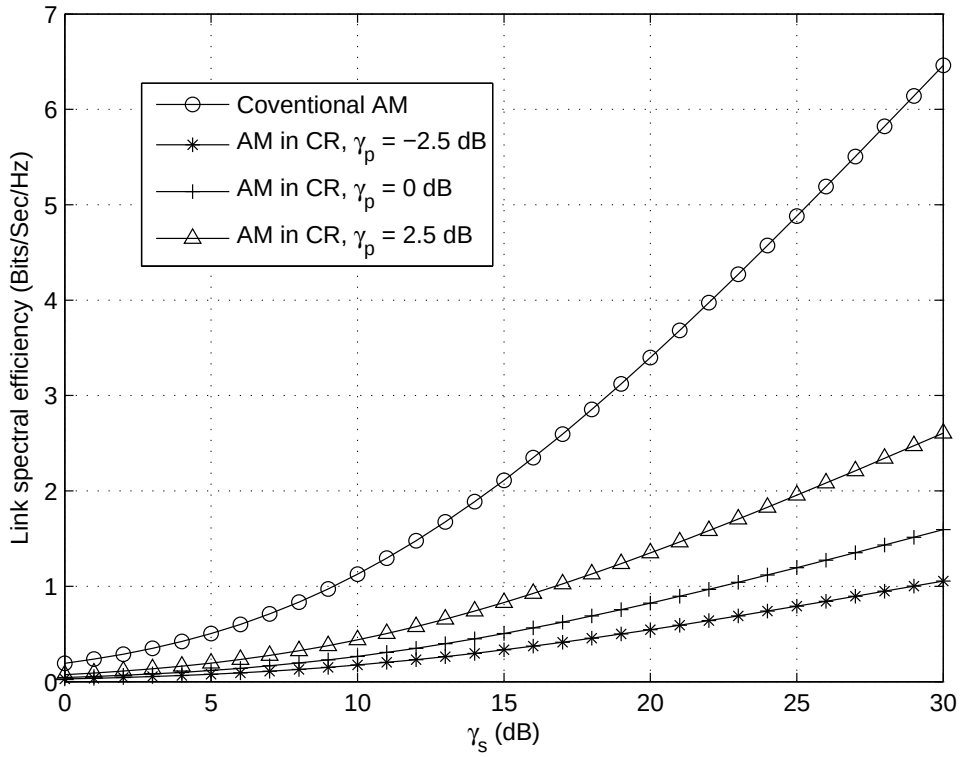

Figure 5.4: Comparison of the link SE performance for the conventional adaptive modulation with the link SE performance for the adaptive modulation in cognitive radio with ACR scheme and different values of γ_p, with $\lambda_b^{-1} = \lambda_e^{-1} = T$.

in cognitive radio degrades as the increase of γ_p.

Fig. 5.3 compares the link SE performance of the conventional ACR scheme and the ACR scheme in cognitive radio for different primary user traffic intensity. As can be seen, first, the link SE performance is degraded when adaptive modulation is applied in cognitive radio, as expected. Although the link SE performance is not affected by the primary user traffic during the secondary transmission, it is still affected by the sensing performance and the primary user traffic during the sensing slot. Therefore, when the busy and idle channel holding times λ_b^{-1} and λ_e^{-1} increase, the spectrum sensing performance improves as a result of the decreased primary

user traffic intensity. Hence, the link SE performance improves.

Fig. 5.4 examines the link SE performance for the conventional adaptive modulation applying the ACR scheme and the adaptive modulation in cognitive radio for different values of γ_p. As can be seen, unlike the BER performance of the ACR scheme in cognitive radio which degrades as the increase of γ_p, the link SE performance improves as the increase of γ_p. This is explained as follow. Since the link SE is determined before the secondary user transmission starts, it is therefore not affected by the primary user interference during the secondary transmission, it is however, still affected by the spectrum sensing performance. As the increase of γ_p, the spectrum sensing performance increases, hence the link SE performance improves.

5.5 Adaptive Discrete Rate Scheme in Cognitive Radio

5.5.1 BER Performance

By using the same method, the performance of the ADR scheme in cognitive radio can also be analyzed.

When the licensed channel is actually idle at the end of the sensing slot and is correctly detected by the secondary user, the selection of the constellation size is made before the secondary user transmission starts according to

$$M_{ADR0cr} = 2^k, \quad \gamma_k < \gamma_s < \gamma_{k+1}, \tag{5.31}$$

which is the same as that of the conventional ADR scheme.

In $H_{0,0(0)}$ and $H_{0,1}$, the primary user remains absent from the licensed channel for the entire transmission slot, retaining the same channel conditions. The BERs for the ADR scheme are therefore

$$P_{ber_{ADR0cr}1}(M_{_{ADR0cr}}, \gamma_s) \approx \frac{1}{5} e^{\frac{3\gamma_s}{2(1-2^k)}}, \qquad \gamma_k < \gamma_s \leq \gamma_{k+1}, \tag{5.32}$$

and the average BER for the ADR scheme in cognitive radio in a Nakagami-m fading channel is given by

$$\begin{aligned} < P_{ber_{ADR0cr}1} > = & \frac{\left(\frac{m}{\gamma_a}\right)^m}{5\Gamma(m)\sum_{k=1}^{K} kA_k} \cdot \sum_{k=1}^{K} \left(\frac{k\Gamma\left(m, \frac{m\gamma_k}{\gamma_a} + \frac{3\gamma_k}{2\left(2^k-1\right)}\right)}{\left(\frac{m}{\gamma_a} + \frac{3}{2\left(2^k-1\right)}\right)^m} \right. \\ & \left. - \frac{k\Gamma\left(m, \frac{m\gamma_{k+1}}{\gamma_a} + \frac{3\gamma_{k+1}}{2\left(2^k-1\right)}\right)}{\left(\frac{m}{\gamma_a} + \frac{3}{2\left(2^k-1\right)}\right)^m} \right), \end{aligned} \tag{5.33}$$

where symbols are defined as before.

In $H_{0,0(1)}$, the actual channel condition of the secondary transmission for the first $\alpha - I$ samples of the transmission slot remains the same as that based on which the constellation size is chosen. The BERs are hence the same as (5.32) and (5.33).

After the arrival of the primary user at the α^{th} sample, the actual channel condition of the secondary transmission in the last $J - \alpha$ samples of the transmission slot is changed. Their actual BERs are therefore become different and can be derived as

$$P_{ber_{ADR0cr}2}\left(M_{_{ADR0cr}}, \frac{\gamma_s}{1+\gamma_p}\right) \approx \frac{1}{5} e^{\frac{3\gamma_s}{2(1-2^k)(1+\gamma_p)}}, \qquad \gamma_k < \gamma_s < \gamma_{k+1}. \tag{5.34}$$

The average BER in a Nakagami-m fading channel can be derived as,

$$< P_{ber_{ADR0cr}2} >= \frac{\left(\frac{m}{\gamma_a}\right)^m}{5\Gamma(m)\sum_{k=1}^{K} kA_k} \cdot \sum_{k=1}^{K} \left(\frac{k\Gamma\left(m, \frac{m\gamma_k}{\gamma_a} + \frac{3\gamma_k}{2\left(2^k-1\right)(1+\gamma_p)}\right)}{\left(\frac{m}{\gamma_a} + \frac{3}{2\left(2^k-1\right)(1+\gamma_p)}\right)^m} - \frac{k\Gamma\left(m, \frac{m\gamma_{k+1}}{\gamma_a} + \frac{3\gamma_{k+1}}{2\left(2^k-1\right)(1+\gamma_p)}\right)}{\left(\frac{m}{\gamma_a} + \frac{3}{2\left(2^k-1\right)(1+\gamma_p)}\right)^m} \right). \tag{5.35}$$

Thus, the average BER for ADR scheme in hypothesis $H_{0,0(1)}$ can be derived as

$$< P_{ber_{ADR0cr}3} > (\alpha) = \frac{1}{J-I}\left((\alpha - I) < P_{ber_{ADR0cr}1} > + (J-\alpha) < P_{ber_{ADR0cr}2} >\right) \tag{5.36}$$

Similarly, when the licensed channel is actually busy at the end of the sensing slot. The constellation size is selected before the secondary transmission according to the actual channel SDR, as

$$M_{_{ADR1cr}} = 2^k, \qquad \gamma_k < \frac{\gamma_s}{1+\gamma_p} \leq \gamma_{k+1} \tag{5.37}$$

The primary user occupying status remains unchanged during the secondary transmission slot in hypothesis $H_{1,0(0)}$ and $H_{1,1}$, the BERs for the ADR scheme in cognitive radio in this case can be derived as

$$P_{ber_{ADR1cr}1}\left(M_{_{ADR1cr}}, \frac{\gamma_s}{1+\gamma_p}\right) = \frac{1}{5} e^{\frac{3}{2(1-2^k)}\frac{\gamma_s}{(1+\gamma_p)}}, \tag{5.38}$$

and the average BER in a Nakagami-m fading channel can be derived as

$$< P_{ber_{ADR1cr}1} >= \frac{\left(\frac{m}{\gamma_a}\right)^m}{5\Gamma(m)\sum_{k=1}^{K} kB_k} \sum_{k=1}^{K} \left(\frac{k\Gamma\left(m, \frac{m\gamma_k(1+\gamma_p)}{\gamma_a} + \frac{3\gamma_k}{2\left(2^k-1\right)}\right)}{\left(\frac{m}{\gamma_a} + \frac{3}{2\left(2^k-1\right)(1+\gamma_p)}\right)^m} - \frac{k\Gamma\left(m, \frac{m\gamma_{k+1}(1+\gamma_p)}{\gamma_a} + \frac{3\gamma_{k+1}}{2\left(2^k-1\right)}\right)}{\left(\frac{m}{\gamma_a} + \frac{3}{2\left(2^k-1\right)(1+\gamma_p)}\right)^m} \right), \tag{5.39}$$

where

$$B_k = \frac{\Gamma\left(m, \frac{m\gamma_k(1+\gamma_p)}{\gamma_a}\right) - \Gamma\left(m, \frac{m\gamma_{k+1}(1+\gamma_p)}{\gamma_a}\right)}{\Gamma\left(m\right)}. \tag{5.40}$$

In $H_{1,(0),1}$, the channel status of the first $\beta - I$ samples of the transmission slot remains the same, the BERs and the average BER are therefore the same as (5.38) and (5.39). After the departure of the primary user at the β^{th} sample, the actual channel SDR is no longer the same as the SDR based on which the constellation size is chosen. The BERs hence become

$$P_{ber_{ADR1cr}2}\left(M_{_{ADR1cr}}, \gamma_s\right) = \frac{1}{5} e^{\frac{3\gamma_s}{2(1-2^k)}}, \tag{5.41}$$

and the average BER in a Nakagami-m fading channel becomes

$$< P_{ber_{ADR1cr}2} >= \frac{\left(\frac{m}{\gamma_a}\right)^m}{5\Gamma(m)\sum_{k=1}^{K} kB_k} \sum_{k=1}^{K} \left(\frac{k\Gamma\left(m, \frac{m\gamma_k(1+\gamma_p)}{\gamma_a} + \frac{3\gamma_k(1+\gamma_p)}{2\left(2^k-1\right)}\right)}{\left(\frac{m}{\gamma_a} + \frac{3}{2\left(2^k-1\right)}\right)^m} - \frac{k\Gamma\left(m, \frac{m\gamma_{k+1}(1+\gamma_p)}{\gamma_a} + \frac{3\gamma_{k+1}(1+\gamma_p)}{2\left(2^k-1\right)}\right)}{\left(\frac{m}{\gamma_a} + \frac{3}{2\left(2^k-1\right)}\right)^m} \right). \tag{5.42}$$

Therefore, the average BER for ADR scheme in hypothesis $H_{1,0(1)}$ can be derived as

$$< P_{ber_{ADR1cr}3} > (\beta) = \frac{1}{J-I}\left((\beta - I) < P_{ber_{ADR1cr}1} > + (J-\beta) < P_{ber_{ADR1cr}2} >\right) \tag{5.43}$$

By taking into consideration the probability of occurring for each hypothesis in (3.9) and the spectrum sensing performance in (3.20) and (3.20), the average BER for the ADR scheme in a Nakagami-m fading channel for cognitive radio systems with dynamic primary user traffic can be derived as

$$\begin{aligned}
\overline{< P_{berADRcr} >} =& \frac{1}{P_{H_{sum}0} + P_{H_{sum}1}}\Big(P_{H_{0,0(0)}}(\lambda_b, \lambda_e)\left(1 - \overline{P_{faH}}(\Psi_H, I)\right) < P_{ber_{ADR0cr}1} > \\
&+ P_{H_{0,1}}(\lambda_b, \lambda_e)\left(1 - \overline{P_{faH}}(\Psi_H, I)\right) < P_{ber_{ADR0cr}1} > \\
&+ \sum_{\alpha=I+1}^{J-1}\left(p_e p_{00}^{\alpha} p_{01} p_{11}^{J-\alpha-1} < P_{ber_{ADR0cr}3} > (\alpha)\right)\left(1 - \overline{P_{faH}}(\Psi_H, I)\right) \\
&+ P_{H_{1,0(0)}}(\lambda_b, \lambda_e)\left(1 - \overline{P_{dH}}(\Psi_H, I)\right) < P_{ber_{ADR1cr}1} > \\
&+ P_{H_{1,1}}(\lambda_b, \lambda_e)\left(1 - \overline{P_{dH}}(\Psi_H, I)\right) < P_{ber_{ADR1cr}1} > \\
&+ \sum_{\beta=I+1}^{J-1}\Big(p_b p_{11}^{\beta} p_{10} p_{00}^{J-\beta-1} < P_{ber_{ADR1cr}3} > (\beta)\Big)\left(1 - \overline{P_{dH}}(\Psi_H, I)\right)\Big)
\end{aligned} \tag{5.44}$$

5.5.2 Link Spectral Efficiency Performance

In this section, the link SE for ADR scheme in cognitive radio system with the dynamic primary user traffic is derived. As has been mentioned earlier, the average link SE is determined before the secondary transmission period starts, therefore it is affected by the sensing performance but not the primary user status change in the data transmission slot.

When the primary user is actually absent from the channel at the end of the sensing slot, the average link SE in a Nakagami-m fading channel can be derived as

$$< \frac{R}{W} >_{ADR0cr} = \sum_{k=1}^{K} kA_k. \tag{5.45}$$

When the primary user is actually present at the channel at the end of the sensing slot, the average link SE in a Nakagami-m fading channel can be derived as

$$< \frac{R}{W} >_{ADR1cr} = \sum_{k=1}^{K} kB_k. \tag{5.46}$$

By taking into consideration of the probability of occurring and the sensing performance, the average link SE for the ADR scheme in a Nakagami-m fading channel for cognitive radio system with dynamic primary user traffic can be derived as

$$\begin{aligned} < \frac{R}{W} >_{ADRcr} = P_{H_{sum}0} \left(1 - \overline{P_{faH}}\left(\Psi_H, I\right)\right) < \frac{R}{W} >_{ADR0cr} \\ + P_{H_{sum}1} \left(1 - \overline{P_{dH}}\left(\Psi_H, I\right)\right) < \frac{R}{W} >_{ADR1cr} . \end{aligned} \tag{5.47}$$

5.5.3 Numerical Results and Discussions

In this section, numerical results are presented to examine the effect of the cognitive radio features on the adaptive modulation performance when ADR scheme is applied. The system settings are the same as that of the ACR scheme discussed earlier.

Fig. 5.5 compares the BER performance for the conventional adaptive modulation applying the ADR scheme with the BER performance for the adaptive modulation in cognitive radio. In this figure, $K = 7$ and $m = 2$. Several observations can be made. First, the BER performance of the ADR scheme is degraded when applied

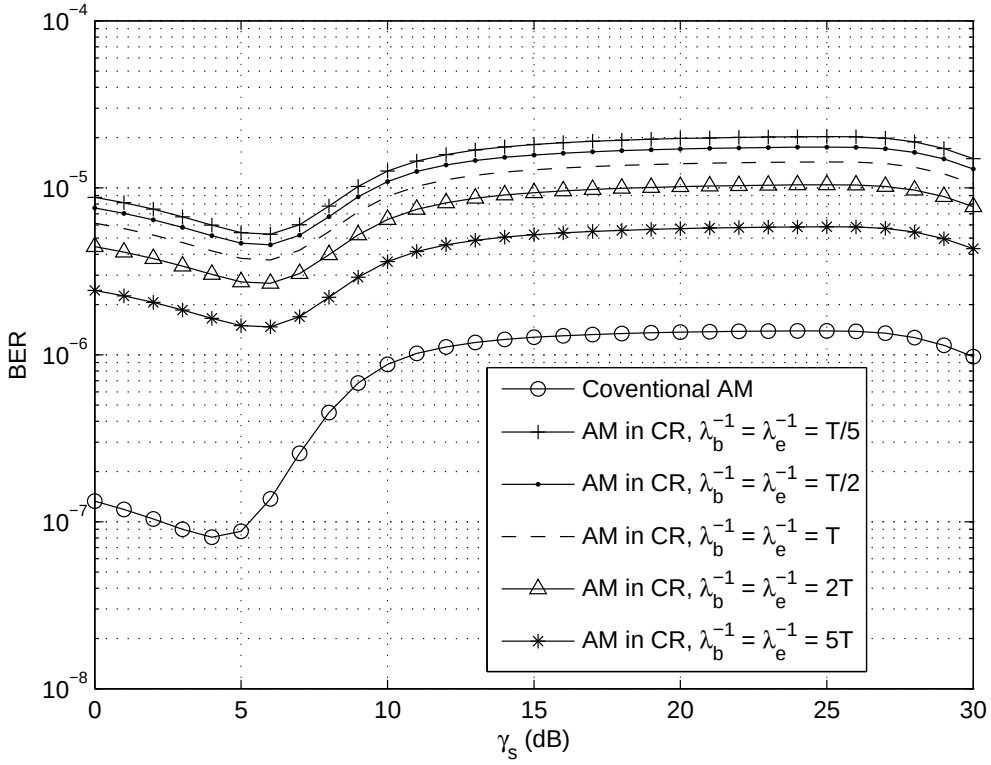

Figure 5.5: Comparison of the BER performance for the conventional adaptive modulation with the BER performance for the adaptive modulation in cognitive radio with ADR scheme and different channel holding times, with $\gamma_p = 0$ dB.

in the cognitive radio. This performance degradation increases as the decrease of the primary user busy and idle channel holding times, λ_b^{-1} and λ_e^{-1}, as expected. Second, the BER curves for adaptive modulation in cognitive radio are closer to the target BER value than the BER curves for the conventional adaptive modulation. This implies that the ADR scheme in cognitive radio has less room for improvement than the conventional ADR scheme. Note that the BER is not decreasing monotonically as the increase of γ_s in this case. This is caused by the uneven division of regions for γ_k to γ_{k+1} and the approximation error in the BER equations.

Fig. 5.6 examines the BER performance for the conventional ADR scheme and

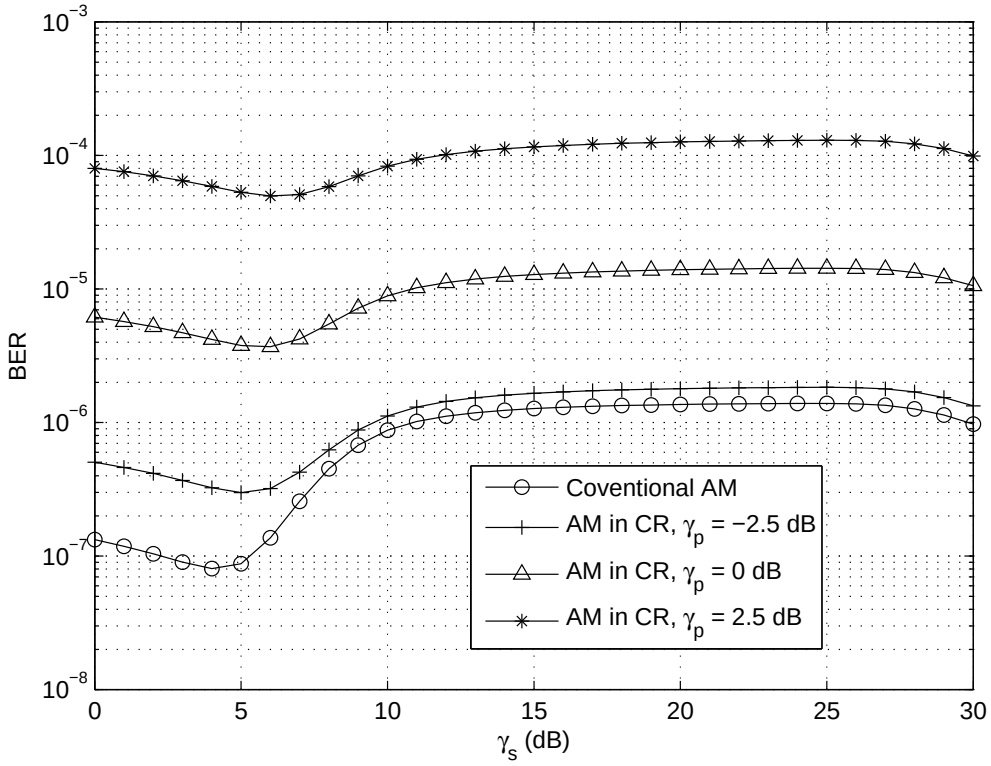

Figure 5.6: Comparison of the BER performance for the conventional adaptive modulation with the BER performance for the adaptive modulation in cognitive radio with ADR scheme and different values of γ_p, with $\lambda_b^{-1} = \lambda_e^{-1} = T$.

the ADR scheme in cognitive radio for different values of γ_p. When γ_p increases, the effect of the cognitive radio distinctive features on the adaptive modulation performance increase comparing with the conventional adaptive modulation, as was explained in the discussions of the ACR scheme in the last section. Hence, as can be seen from Fig. 5.6, the degradation of the BER performance of adaptive modulation in cognitive radio increases significantly as the increase of γ_p.

Fig. 5.7 presents the BER performance for the conventional adaptive modulation and the adaptive modulation in cognitive radio with the ADR scheme and different values of K. In this figure, $m = 2$, $\gamma_p = 0$ dB and $\lambda_b^{-1} = \lambda_e^{-1} = T$. As aforemen-

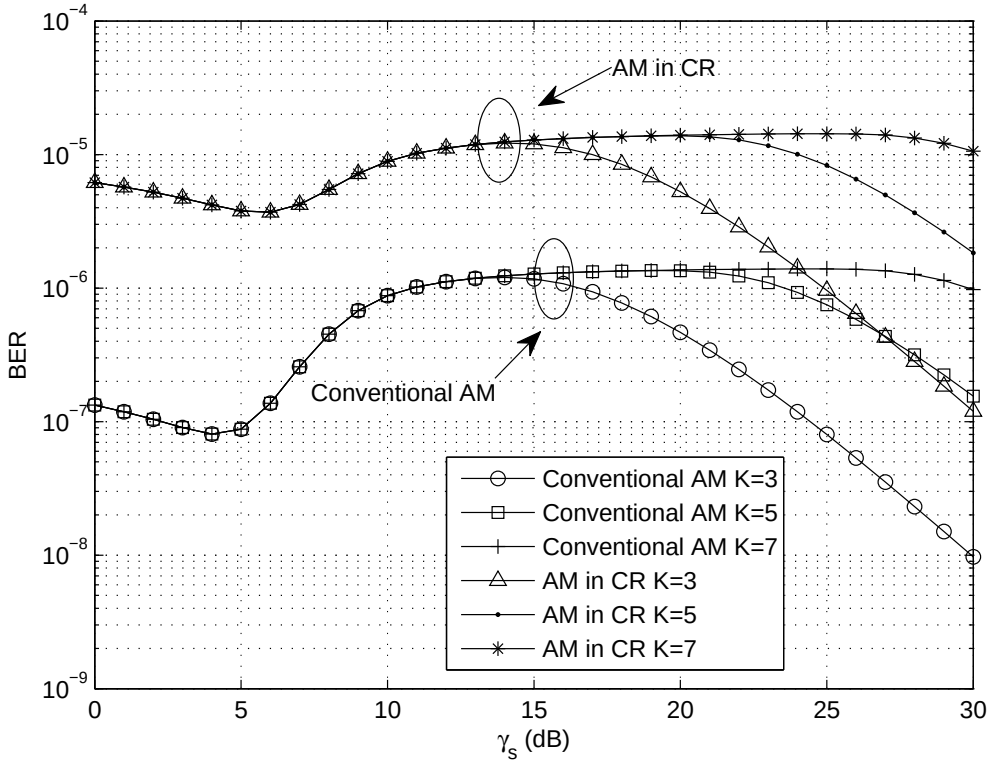

Figure 5.7: Comparison of the BER performance for the conventional ADR scheme with the BER performance for the ADR scheme in cognitive radio for different values of K, with $\gamma_p = 0$ dB, $\lambda_b^{-1} = \lambda_e^{-1} = T$ and $m = 2$.

tioned, in the ADR scheme, the value of the constellation size is an integer that is a power of 2. The channel SNR are therefore quantized to different regions with each region corresponding to and integer value of M. Hence, as can be seen from Fig. 5.7, as the increase of K, the BER performance improves for both the conventional ADR scheme and the ADR scheme in cognitive radio. Moreover, while the BER performance is always degraded when the adaptive modulation is applied in cognitive radio, the gaps between the BER curves for the conventional ADR scheme and the BER curves for the ADR scheme in cognitive radio are approximately the same for different values of K.

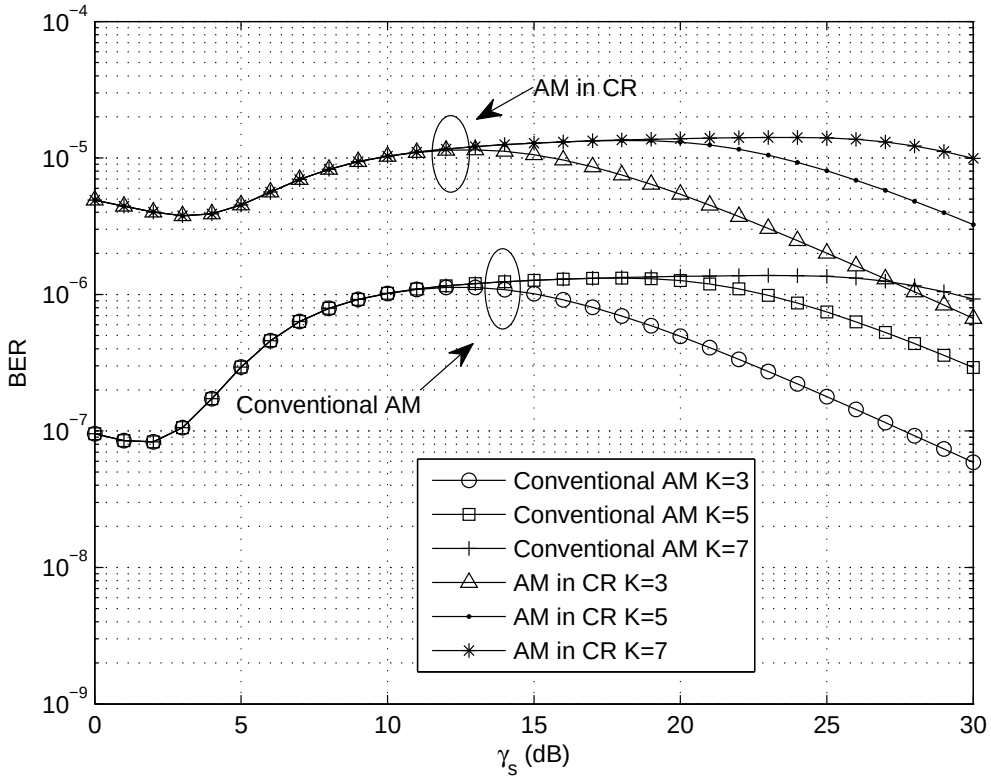

Figure 5.8: Comparison of the BER performance for the conventional ADR scheme with the BER performance for the ADR scheme in cognitive radio for different values of K, with $\gamma_p = 0$ dB, $\lambda_b^{-1} = \lambda_e^{-1} = T$ and $m = 1$.

Fig. 5.8 has the same system settings as Fig. 5.7 while the fading parameter is decreased from $m = 2$ to $m = 1$. Comparing with Fig. 5.7, it can be seen that for a given value of γ_s, the BER increases when m is decreased. This is true for both the conventional adaptive modulation and the adaptive modulation in cognitive radio. Moreover, the gaps between the BER curves for the conventional ADR scheme and the BER curves for the ADR scheme in cognitive radio are also increased when m decreases. This suggests that the harsh channel condition further degrades the BER performance regardless of the system models, which agrees with intuition.

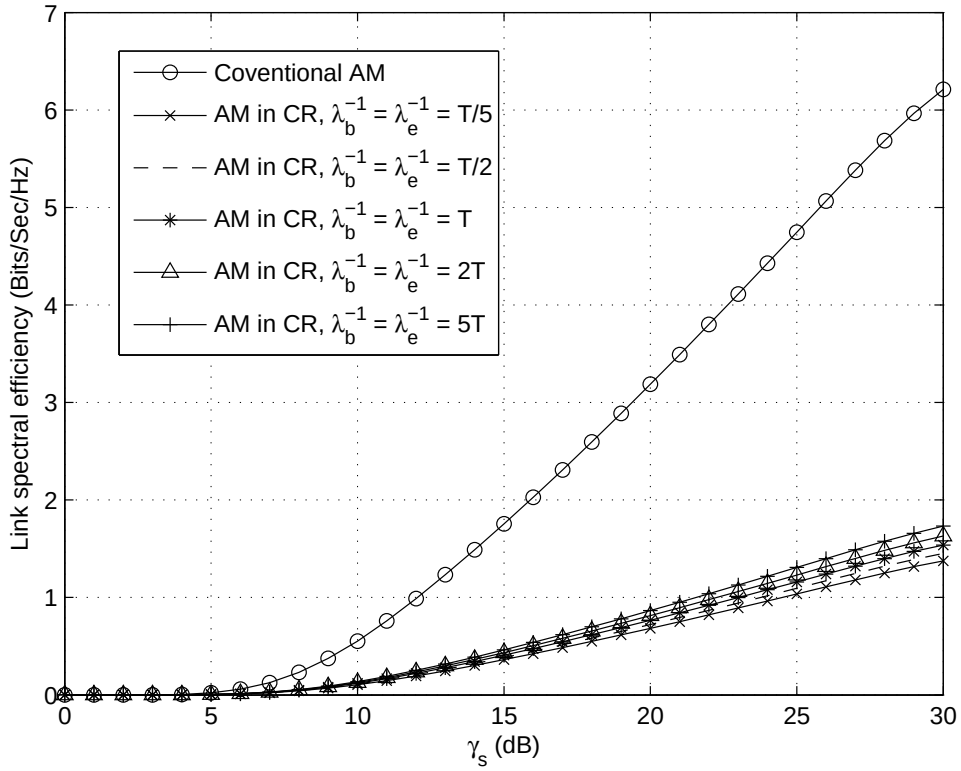

Figure 5.9: Comparison of the BER performance for the conventional ADR scheme with the BER performance for the ADR scheme in cognitive radio for different values of K, with $\gamma_p = 0$ dB, $\lambda_b^{-1} = \lambda_e^{-1} = T$ and $m = 1$.

Fig. 5.9 compares the link SE performance for the conventional adaptive modulation and the link SE performance for the adaptive modulation in cognitive radio applying the ADR scheme with different values of busy and idle channel holding times. As expected, the link SE performance is significantly degraded when the adaptive modulation is applied in cognitive radio. As the busy and idle channel holding time λ_b^{-1} and λ_b^{-1} increases, the primary user traffic intensity is reduced, hence the performance degradation of the link SE is decreased. This proves that although the link SE is not affected by the dynamic primary user traffic during the

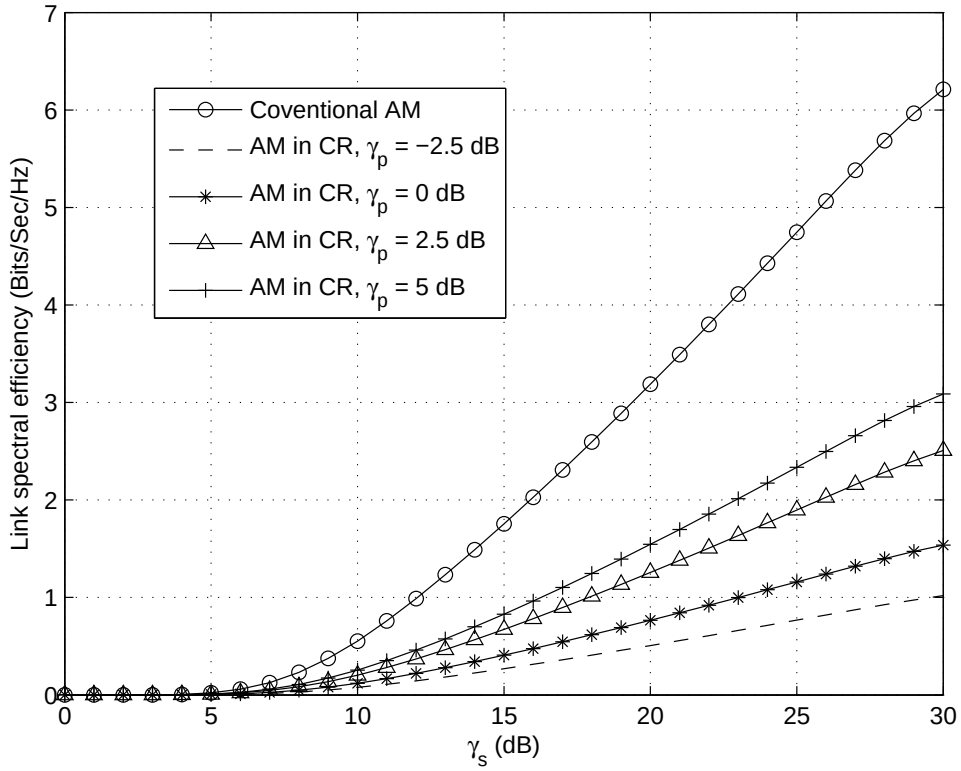

Figure 5.10: Comparison of the link SE performance for the conventional adaptive modulation with the link SE performance for the adaptive modulation in cognitive radio with ADR scheme and different primary user different channel holding times.

secondary user transmission, it is still affected by the primary user traffic during the spectrum sensing process, and the spectrum sensing quality itself.

Fig. 5.10 compares the link SE performance for the conventional adaptive modulation and the link SE performance for the adaptive modulation in cognitive radio applying the ADR scheme with different values of γ_p. As expected, while the link SE performance is always degraded when the ADR scheme is applied in the cognitive radio, it improves with the increase of γ_p. This agrees with the findings of the ACR scheme in Fig. 5.4.

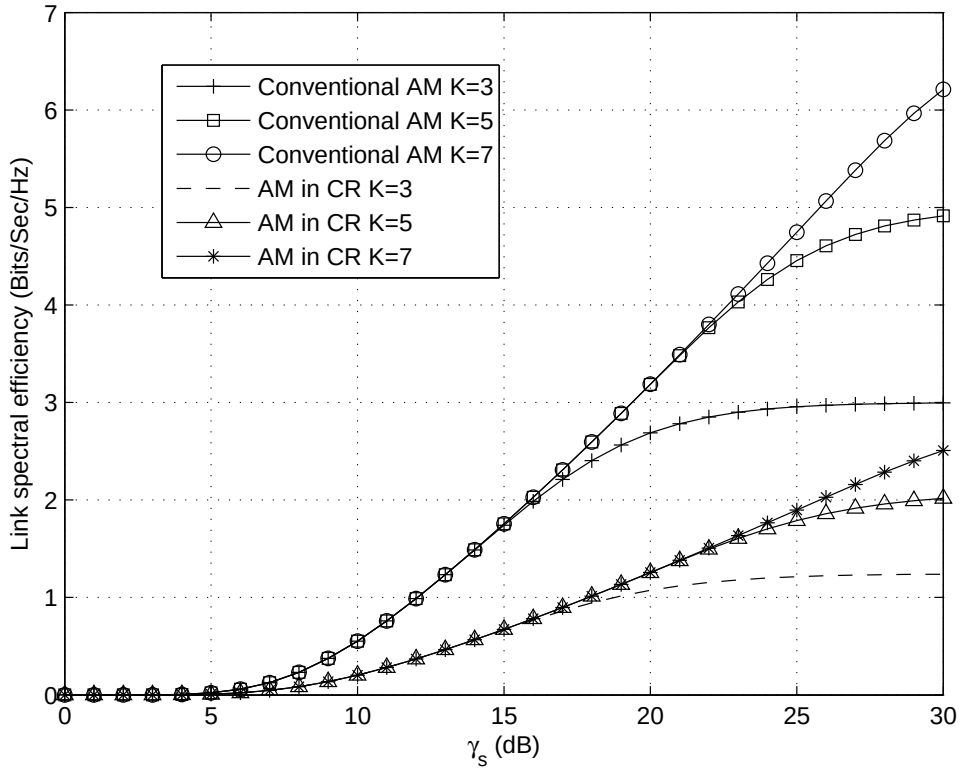

Figure 5.11: Comparison of the link SE performance for the conventional adaptive modulation with the link SE performance for the adaptive modulation in cognitive radio with ADR scheme and different values of K, with $\lambda_b^{-1} = \lambda_e^{-1} = T$.

Fig. 5.11 examines the link SE performance for the conventional adaptive modulation and the link SE performance for the adaptive modulation in cognitive radio applying the ADR scheme with different values of K. As can be seen, when the value of K increases, the link SE performance improves for both the conventional adaptive modulation and the adaptive modulation in cognitive radio. In this case, the improvement in the link SE performance for the conventional adaptive modulation as the increase of K is more significant than that of the adaptive modulation in cognitive radio.

5.6 Conclusions

In this chapter, the performance of the adaptive modulation in cognitive radio system has been analyzed. Both the ACR scheme and the ADR scheme of the adaptive modulation have been investigated, where the BER performance and the link SE performance have been examined for both schemes. The system performance has been compared to the performance of the conventional adaptive modulation where the primary user has the exclusive rights to the licensed channel. Numerical results have shown that the spectrum sensing and the primary user traffic of the cognitive radio cause considerable degradation for both the BER performance and the link SE performance. Higher primary user traffic intensity leads to larger gaps between the conventional adaptive modulation and the adaptive modulation in cognitive radio system. However, while the BER performance degraded further with the increase of the received primary user SNR, the performance of the link SE improves. It was also shown that both the BER performance and the link SE performance of the ADR scheme for adaptive modulation in cognitive radio improved as the increase of number of SDR regions.

Chapter 6

Spectrum Sensing Using Recovered Secondary Frames

6.1 Introduction

In the previous chapters, the analyses of the cognitive radios were based on systems which adopt the MAC frame structure proposed by the IEEE 802.22 WRAN standard. In this structure, the entire secondary link time is divided into superframes, where each superframe consists of multiple consecutive MAC frames. As illustrated by Fig. 1.7, the MAC frame is then sub-divided into the dedicated sensing slot and the secondary transmission slot. To make the discussion easier, this structure will be referred to as the traditional structure for the rest of this chapter. From the secondary user's point of view, this dedicated spectrum sensing slot is a "quiet" period where all secondary transmissions are forbidden so that spectrum sensing in the licensed channel can be performed. However, this "quiet" period will always lead to compromises in the secondary transmission time.

To solve this problem and aim at increasing the achievable throughput further, a novel frame structure for the cognitive radio was proposed in [112]. In this structure, after an initial spectrum sensing is performed to acquire the idle status of the licensed channel, the whole secondary frame is devoted for data transmission without any dedicated sensing or "quiet" period in the following secondary frames. The following sensing is only performed by using the recovered received secondary frames after the secondary user signal is decoded and removed from the received secondary frame at the secondary user receiver.

In [112], it was simply assumed that the secondary user signal can always be correctly decoded and be completely removed from the received secondary frame. Therefore, this structure always benefit from the longer operating duration and has several advantages over the traditional structure. First, by using the recovered secondary frame with duration of T for spectrum sensing to track the status of the licensed channel, the spectrum sensing time increases and therefore, the sensing accuracy improves. This is especially important for those detection algorithms that requires a long sensing time. Second, by using the whole secondary frame duration for secondary transmission, the achievable throughput of the secondary user is maximized. Third, the calculation of the optimal sensing time for each frame presented in the Chapter 3 is no longer required, as the secondary frame does not have any dedicated sensing period and only the recovered secondary frame is used for sensing.

However, in reality, decoding errors may occur such that the secondary user signal will not be completely removed. The recovered secondary frame used in the following spectrum sensing is therefore corrupted by the un-removed secondary user signal. In this case, the sensing accuracy based on the recovered received secondary frame will be reduced by the interference caused by the corruption. The reduced

sensing accuracy will consequently degrade the secondary user data transmission in the next frame due to possible interferences from the primary user as a results of the spectrum sensing error. This causes even larger decoding error. Eventually, the afore-mentioned advantage of the novel structure may be compromised by the accumulated errors. Hence, in reality, the results in [112] only provided an ideal upper bound of the system performance.

Furthermore, the system performance in [112] was analyzed for only one single secondary frame. However, in reality the data transmission suffers from the sensing error based on the previous frame even when there is no decoding error. This effect does not occur when only a single secondary frame is considered. Moreover, the primary user may change its occupancy status throughout the multiple secondary frames, which was also not considered in [112]. A more comprehensive investigation that considers the decoding error and multiple consecutive frames with primary user traffic is crucial in deploying the novel structure. It is therefore of great interest to investigate whether this novel structure can outperform the traditional structure or when the disadvantages will outplay the advantages in more realistic situations, where all the aforementioned practical conditions are taken into consideration.

In this chapter, the performance of the novel structure proposed in [112] is further developed to contain one complete superframe with multiple consecutive secondary MAC frames and is analyzed by taking into account the decoding errors as well as primary user traffic to give a more comprehensive comparison between the traditional structure and the novel structure. In order to fully examine the novel structure, the effects of different modulation schemes and different sensing algorithms are also studied. To take the investigation further, the effects of fading channels and error correction codes (ECC) are also considered.

The rest of this chapter is organized as follows. In Section 6.2, the performance of the traditional structure with multiple consecutive secondary frames is analyzed. The primary user traffic model used in this chapter is also introduced. The performance for traditional structure with both energy detection and covariance-matrix-based detection are presented. In Section 6.3, the details of the novel structure model is presented. Its ideal upper bound performance is analyzed, while the analysis in [112] is extended to include multiple consecutive secondary frames. A realistic analysis of the novel structure is then provided in Section 6.4, where the decoding errors, spectrum sensing performance and the secondary transmission performance will be discussed. In Section 6.5, the effect of fading channel is added into the analysis. The effect of the ECC is then evaluated in Section 6.6. Finally, Section 6.7 provides the conclusion for this chapter.

6.2 Traditional Frame Structure

Consider the conventional model presented in Chapter 3 in a complete superframe instead of one MAC frame, where the superframe consists of U consecutive secondary MAC frames. Assume that throughout the U consecutive frames, the occupancy status of the primary user changes depending on the primary user traffic, which adopts the primary user traffic model presented in Chapter 4. To reduce the complexity of the analysis, assume that the primary user occupancy status changes only occur between the secondary frames, similar to the assumption in [54, 68, 113]. In other words, it is assumed that when the primary user changes its occupancy status during the secondary frame, its effect on the system performance is not shown until the next frame. This is assumed for both the traditional structure and the novel structure to provide a fair comparison between these two models. The case when

the primary user changes its occupancy status during each secondary MAC frame can be analyzed by adopting the method used in the Chapter 3, as it is not the main focus of the discussion in this chapter, it is omitted here and can be treated as a future extension to the work in this chapter.

Throughout the U frames, the primary user changes its occupancy status multiple times, and the probability that the primary user arrives or departs from the licensed channel at the end of the X^{th} frame is expressed using the PMF of the busy and idle channel holding times, similar to (4.9) and (4.10) in Chapter 4, expressed as

$$f_{X\alpha}(X) = F_{\alpha}(XT) - F_{\alpha}\big((X-1)T\big), \tag{6.1}$$

and

$$f_{X\beta}(X) = F_{\beta}(XT) - F_{\beta}\big((X-1)T\big), \tag{6.2}$$

respectively, where $X = 1, 2, ...U$ is the frame index. The busy and idle channel holding times are assumed to follow any reasonable distributions, where (6.1) and (6.2) can be calculated by using (4.1) to (4.8) from Chapter 4.

6.2.1 Energy Detection

In the traditional frame structure, the spectrum sensing and transmission performance within each secondary frame is independent to that of the other frames. When energy detection is applied during the spectrum sensing, the system performance of each frame has been analyzed as the conventional model in the Chapter 3. As has been discussed, there are two scenarios where the secondary user can start its transmission at the end of the sensing period: the sensing correctly identifies the absence of the primary user, or the sensing mis-detects the presence of the primary

user. In this chapter, the analysis is extended to the entire superframe. Hence, in this case, the occurring probability of these two scenarios in the X^{th} frame can be expressed as $P_{H_0X}\left(1-\overline{P_{faG}}\left(\Psi_H,I\right)\right)$ and $P_{H_1X}\left(1-\overline{P_{dG}}\left(\Psi_H,I,\right)\right)$, respectively, where P_{H_0X} is the probability that the primary user is absent at the beginning of the X^{th} frame, and can be derived as

$$P_{H_0X}=P_{H_0X-1}\big(1-f_{X\alpha}\left(X\right)\big)+P_{H_1X-1}f_{X\beta}\left(X\right), \tag{6.3}$$

and P_{H_1X} is the probability that the primary user is present at the beginning of the X^{th} frame, and can be derived as

$$P_{H_1X}=P_{H_0X-1}f_{X\alpha}\left(X\right)+P_{H_1X-1}\big(1-f_{X\beta}\left(X\right)\big). \tag{6.4}$$

Note that in (6.3) and (6.4), when $X=0$, the equations becomes P_{H_0} and P_{H_1}, which are the *a priori* probabilities of the licensed channel being idle and busy, respectively.

The total achievable throughput of the secondary transmission in the U consecutive frames using the traditional structure can therefore be obtained as

$$\begin{aligned}R_{_{ED}}(I)=\sum_{X=1}^{U}\Big(&P_{H_0X}\big(1-\overline{P_{faG}}\left(\Psi_H,I\right)\big)C_{H_0}\\&+P_{H_1X}\big(1-\overline{P_{dG}}\left(\Psi_H,I\right)\big)C_{H_1}\Big)\frac{T-\tau}{T},\end{aligned} \tag{6.5}$$

where C_{H_0} and C_{H_1} are channel capacities defined as before. The term $\dfrac{T-\tau}{T}$ reflects the penalty on the secondary user data transmission due to the "quiet" period used for the spectrum sensing in each frame of the traditional structure.

6.2.2 Covariance-Matrix-Based Detection

The above analysis applies to energy detection. The performance can also be derived using other detection methods introduced in Chapter 2. In this section, performance of the maximum-eigenvalue detection and covariance-based detection are evaluated for the traditional structure.

Assume that the received primary user samples are Gaussian with zero mean and correlation $\rho^{|i-j|}$, where ρ is a constant and $|i-j|$ is the sample time difference. Define the sample auto-correlation of the received signal in the traditional structure model as

$$\Theta(l) = \frac{1}{I}\sum_{i=0}^{I-l} y_i y_{i-1}, \qquad l = 1, ..., L-1, \tag{6.6}$$

where y_i is the i^{th} received sample and L is the smoothing factor.

The sample correlation matrix of the received signal is then expressed as [114]

$$\Lambda_y = \begin{pmatrix} \Theta(0) & \Theta(1) & \dots & \Theta(L-1) \\ \Theta(1) & \Theta(0) & \dots & \Theta(L-2) \\ \vdots & \vdots & \vdots & \vdots \\ \Theta(L-1) & \Theta(L-2) & \dots & \Theta(0) \end{pmatrix}. \tag{6.7}$$

When the maximum-eigenvalue detector is applied during the spectrum sensing in the traditional structure model, the probability of false alarm can be derived as [115]

$$P_{faME}\left(\Psi_{ME} I\right) = 1 - TW_1\left(\frac{\Psi_{ME} I - \mu_{ME}}{\upsilon_{ME}}\right), \tag{6.8}$$

where $TW_1(\cdot)$ is the Tracy-Widom distribution of order 1, Ψ_{ME} is the decision threshold of the maximum-eigenvalue detector for the traditional model, μ_{ME} =

$\left(\sqrt{I-1}+\sqrt{L}\right)^2$ and $\upsilon_{ME} = \left(\sqrt{I-1}+\sqrt{L}\right)\left(\frac{1}{\sqrt{I-1}}+\frac{1}{\sqrt{L}}\right)$.

The probability of detection can be derived as

$$P_{dME}\left(\Psi_{ME}, I\right) = 1 - TW_1\left(\frac{\Psi_{ME} I - \frac{I\vartheta_{max}}{\sigma_w^2} - \mu_{ME}}{\upsilon_{ME}}\right), \tag{6.9}$$

where ϑ_{max} is the maximum eigenvalue of the statistical correlation matrix of the primary user signal and σ_w^2 is the noise variance.

Hence, using the maximum-eigenvalue detection in the traditional structure, for a pair of target probabilities $P_{faME}\left(\Psi_{ME}, I\right) = \widehat{P_{fa}}$ and $P_{dME}\left(\Psi_{ME}, I\right) = \widehat{P_d}$, the minimum number of samples required at spectrum sensing can be derived from (6.8) and (6.9) as

$$\Delta_{ME} = \frac{\upsilon_{ME}\sigma_w^2}{\vartheta_{ME}}\Big(TW^{-1}(1-\widehat{P_{fa}}) - TW^{-1}(1-\widehat{P_d})\Big). \tag{6.10}$$

When the covariance-based detector is applied in the traditional structure model during the spectrum sensing, the probability of false alarm can be derived as [116]

$$P_{faCOV}\left(\Psi_{COV}, I\right) = 1 - Q\left(\frac{\frac{1}{\Psi_{COV}}\left(1+(L-1)\sqrt{\frac{2}{I\pi}}\right)-1}{\sqrt{\frac{2}{I}}}\right), \tag{6.11}$$

where $Q(\cdot)$ is the Q-function given by $Q(t) = \frac{1}{\sqrt{2\pi}}\int_t^\infty e^{-u^2/2}du$ [91] and Ψ_{COV} is the decision threshold for the covariance-based detector in the traditional structure.

The probability of detection can be derived as

$$P_{dCOV}\left(\Psi_{COV}, I\right) = 1 - Q\left(\frac{\frac{1}{\Psi_{COV}} + \frac{G_L\gamma_p}{\Psi_{COV}(\gamma_p+1)} - 1}{\sqrt{\frac{2}{I}}}\right), \tag{6.12}$$

where $G_L = \frac{2}{L}\sum_{l=1}^{L-1}(L-l)|E\left[S_{p,i}S_{p,i-l}\right]/E\left[S_p^2\right]|$ with $E\left[S_p^2\right]$ being the primary user signal energy.

Hence, using the covariance-based detector in the traditional structure, for a pair of target probabilities $P_{faCOV}(\Psi_{COV}, I) = \widehat{P_{fa}}$ and $P_{dCOV}(\Psi_{COV}, I) = \widehat{P_d}$, the minimum number of samples required to achieve these targets can be derived from (6.11) and (6.12) as

$$\begin{aligned}\Delta_{COV} =& 2\Bigg(\frac{\gamma_p+1}{G_L\gamma_p}\Big(Q^{-1}(1-\widehat{P_d})(1+\frac{L-1}{\sqrt{\pi}}) \\ &- Q^{-1}(1-\widehat{P_{fa}})(1+\frac{G_L\gamma_p}{\gamma_p+1})+\frac{L-1}{\sqrt{\pi}}\Big)\Bigg)^2.\end{aligned} \tag{6.13}$$

The achievable throughput of the traditional structure model using the covariance matrix based detection can also be derived similar to that of (6.5) by replacing the probability of false alarm and the probability of detection with (6.8) and (6.9) for the maximum-eigenvalue detection and with (6.11) and (6.12) for the covariance-based detection.

6.2.3 Numerical Results and Discussions

Fig. 6.1 and Fig. 6.2 show the secondary transmission performance of the traditional structure in multiple consecutive secondary frames. In the examination, the smoothing factor L is set at $L = 5$, $\rho = 0.5$, $\gamma_p = -5$ dB and $\gamma_s = 5$ dB. In both figures, ED denotes the energy detection, ME denotes the maximum-eigenvalue detection and COVA denote the covariance-based detection. As can be seen from Fig. 6.1, when different spectrum sensing algorithms are applied, the individual secondary throughput are different for each algorithm, as a result of the difference in the sensing performance. Due to the better sensing performance of the

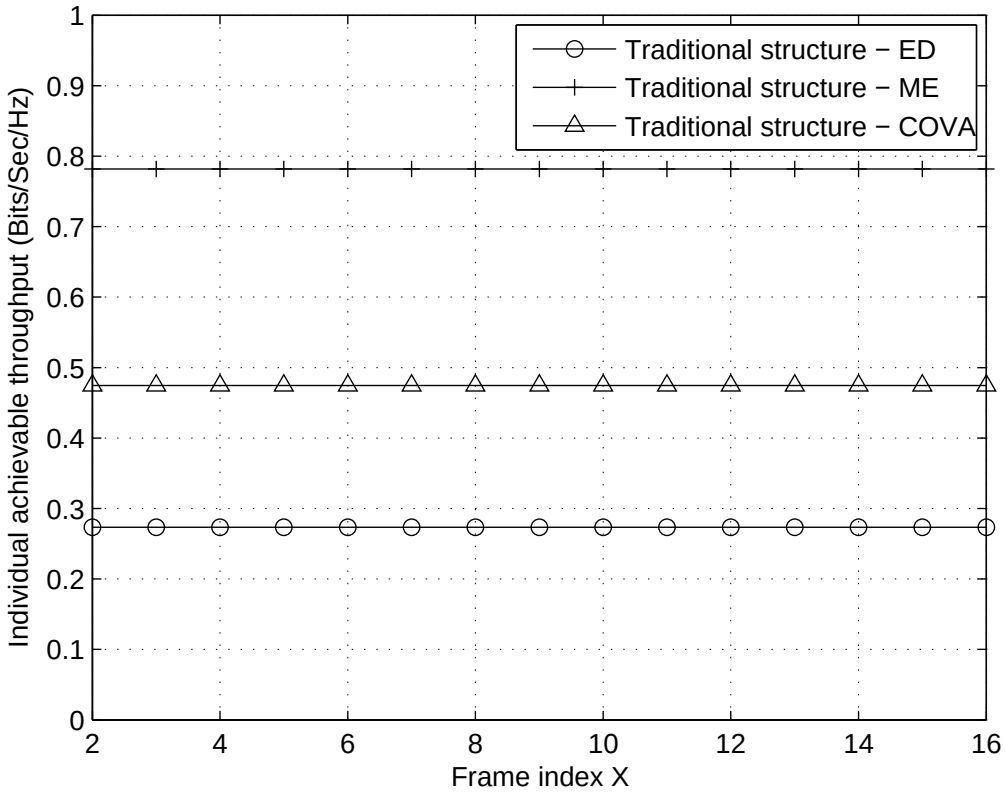

Figure 6.1: The individual achievable throughput of the X^{th} frame in the traditional structure model, with $\gamma_s = 5$ dB.

maximum-eigenvalue based detection, the traditional structure using this detection has the highest individual achievable throughput, while the energy detection has the smallest individual achievable throughput. However, for all sensing algorithms, the individual achievable throughput is always the same for different MAC frames in the traditional structure. This is because the performance of each secondary MAC frame is independent of the other frames in the traditional structure. Consequently, as can be see from Fig. 6.2, the total achievable throughput increases linearly as the increase of the total number of the secondary frames U.

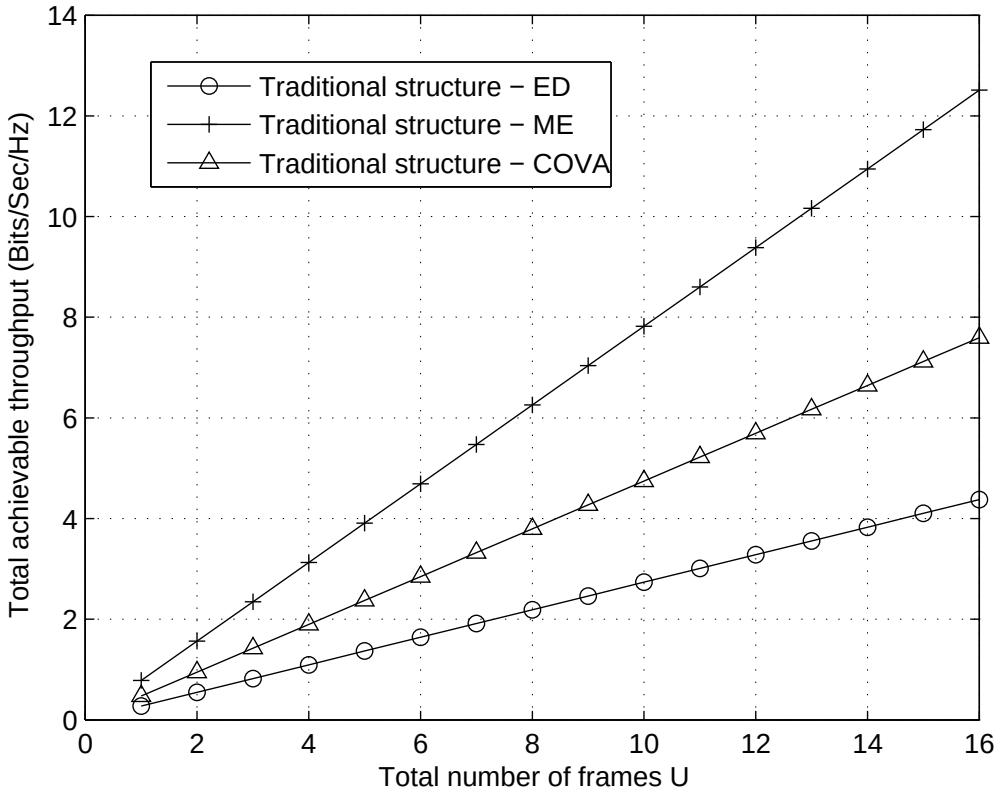

Figure 6.2: The total achievable throughput of U consecutive frames in the traditional structure model, with $\gamma_s = 5$ dB.

6.3 Ideal Upper Bound Performance of the Novel Structure

6.3.1 Novel Structure Model

In the novel structure, as illustrated by Fig. 6.3, after an initial spectrum sensing that acquires the idle status of the licensed channel in the first frame, the secondary user carries out its data transmission simultaneously as the spectrum sensing for the entire duration of T in the following secondary frames. The received signal at the

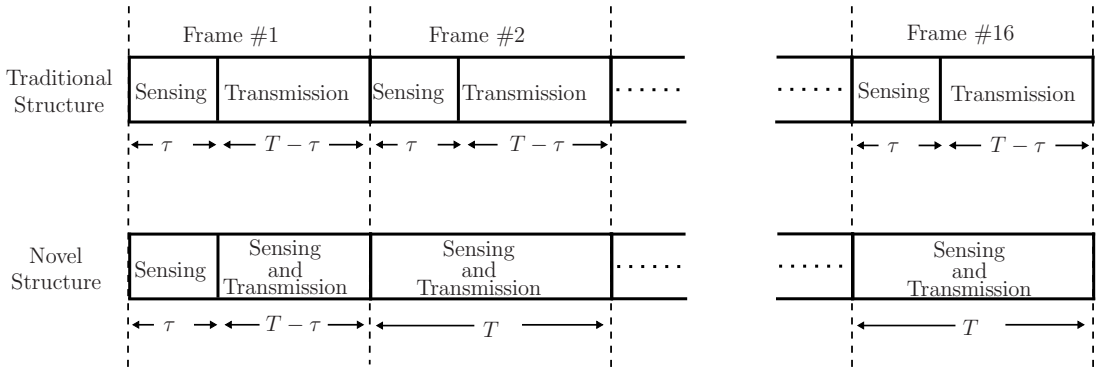

Figure 6.3: The novel structure.

secondary user receiver in the X^{th} frame can therefore be expressed as

$$y_{nov,j} = \begin{cases} s_{s,j} + w_j, & H_0, \\ s_j + s_{s,j} + w_j, & H_1, \end{cases} \tag{6.14}$$

where $j = 1, 2, \ldots\ldots J$, is the sample index, $s_{s,j}$ is the sample of the secondary user signal and all the other symbols are defined as before.

The following spectrum sensing is then performed at the secondary user receiver using the recovered received secondary frame, where the secondary user signal is decoded and deducted from the received secondary frame, as illustrated by Fig. 6.4. Ideally, as was assumed in [112], the decoding process for the received secondary frame is error free. The secondary user signal can hence be completely removed from the received signal in (6.14). The recovered received secondary frame used for the spectrum sensing can therefore be expressed as

$$y_{id,j} = \begin{cases} w_j, & H_0 \\ s_j + w_j, & H_1, \end{cases} \tag{6.15}$$

which becomes the same as the conventional spectrum sensing in (2.1), only with an increased number of samples due to the whole frame being used for sensing.

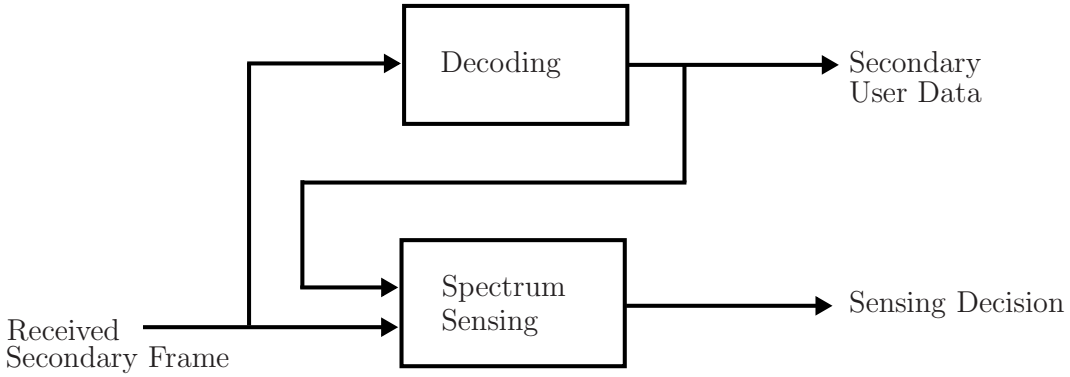

Figure 6.4: The spectrum sensing in the novel structure. Adapted from [112].

Thus, when energy detection is applied, the probability of false alarm in the X^{th} frame for the ideal case of the novel structure can be obtained as

$$P_{fa_{ED}id}\left(\Psi_{_{ED}id}, J\right) = \frac{1}{2} erfc\left(\frac{\Psi_{_{ED}id} - J}{2\sqrt{J}}\right), \tag{6.16}$$

where $\Psi_{_{ED}id}$ is the decision threshold in this case. The probability of detection can be derived as

$$P_{d_{ED}id}\left(\Psi_{_{ED}id}, J\right) = \frac{1}{2} erfc\left(\frac{\Psi_{_{ED}id} - J\gamma_p - J}{2\sqrt{2J\gamma_p + J}}\right). \tag{6.17}$$

It can be noted that the spectrum sensing in this case has a better performance with a larger probability of detection or a smaller probability of false alarm than those in the conventional model in (3.5) and (3.6), as the sensing duration in this case $T > \tau$.

At the end of the spectrum sensing, the secondary user stops data transmission

in the next frame if spectrum sensing considers the primary user to be present. Otherwise, the secondary user transmission continues in the next frame. In this case, the X^{th} frame can only be used for data transmission if spectrum sensing in the $(X-1)^{th}$ frame correctly identifies the primary user's absence or mis-detects the primary user's existence.

Therefore, the probability that the primary user is actually absent at the end of the $(X-1)^{th}$ frame and is correctly identified so that the X^{th} frame can be used for data transmission is derived as

$$\begin{aligned} P_{H_0idX} = P_{H_0idX-1}\left(1-P_{fa_{ED}id}\left(\Psi_{_{ED}id},J\right)\right)\left(1-f_{X\alpha}(X)\right) \\ +P_{H_1idX-1}\left(1-P_{d_{ED}id}\left(\Psi_{_{ED}id},J\right)\right)f_{X\beta}\left(X\right), \end{aligned} \tag{6.18}$$

and the probability that the primary user is present at the end of the $(X-1)^{th}$ frame and is mis-detected so that the X^{th} frame is used for data transmission is derived as

$$\begin{aligned} P_{H_1idX} =& P_{H_0idX-1}\left(1-P_{fa_{ED}id}\left(\Psi_{_{ED}id},J\right)\right)f_{X\alpha}(X) \\ &+P_{H_1idX-1}\left(1-P_{d_{ED}id}\left(\Psi_{_{ED}id},J\right)\right)\left(1-f_{X\beta}(X)\right). \end{aligned} \tag{6.19}$$

Since the secondary data transmission in the novel structure model is carried out for the entire frame duration of T, the transmission process does not suffer from the penalty caused by the "quiet" period, as in the traditional structure. Thus, the total achievable throughput of the U frames for the ideal upper bound performance of the novel structure model can be derived as

$$R_{_{ED}id} = \sum_{X=1}^{U}\left(P_{H_0idX}C_{H_0}+P_{H_1idX}C_{H_1}\right). \tag{6.20}$$

When the covariance matrix based detection is applied for the spectrum sensing, the probability of false alarm and the probability of detection can be obtained by replacing I with J in (6.8) and (6.9) for the maximum-eigenvalue detection, and in (6.11) and (6.12) for the covariance-based detection. The achievable throughput of the secondary transmission can then be derived by using (6.18) to (6.20) with the new probabilities of false alarm and the new probabilities of detection, respectively. Note that [112] only gives the results of the X^{th} frame based on (6.16) and (6.17), which ignores the fact that the sensing performance from the $(X-1)^{th}$ frame will affect the performance in the X^{th} frame, whereas the analysis in this section considers this fact in (6.18) and (6.19).

6.3.2 Numerical Results and Discussions

In this section, the analysis of the ideal upper bound performance of the novel structure is examined by presenting some numerical results. In the examination, the smoothing factor L is set at 5 and ρ is set at 0.5.

Fig. 6.5 compares the ROC curves of the spectrum sensing performance in the traditional structure with the ideal case of the novel structure model. As can be seen, the novel structure takes advantage of the longer sensing period and thus, has a better sensing performance. This is true for the energy detection, the maximum-eigenvalue detection and the covariance-based detection examined. For the same target probability of detection, the novel structure achieves a much lower probability of false alarm. Moreover, for the three different types of sensing algorithms examined in the ideal case of the novel structure, the covariance-base detection has worse performance than the maximum-eigenvalue detection but better performance than the energy detection. This agrees with the sensing performances in the traditional

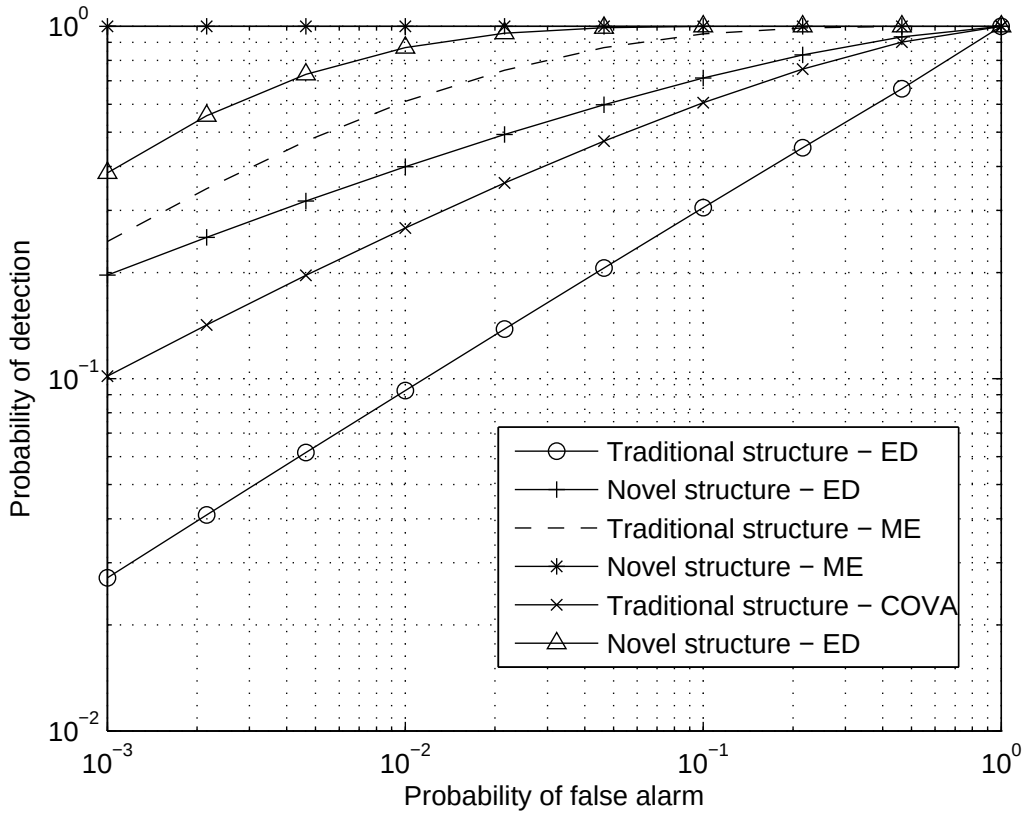

Figure 6.5: Comparison of the ROC curves of the spectrum sensing performance for the traditional structure and the ideal case of the novel structure.

structure.

Fig. 6.6 compares the individual achievable throughput for the traditional structure with the ideal case of the novel structure. In this figure, energy detection is applied for the spectrum sensing with $\gamma_p = -5$ dB and $\gamma_s = 5$ dB. As can be seen, the individual achievable throughput become larger than that of the traditional structure to begin with. This is due to the improvement in the sensing performance as demonstrated in Fig. 6.5 and the longer secondary transmission time in the novel structure. However, as the frame index X increases, the individual achievable throughput of the novel structure decreases and approaches zero. This is because af-

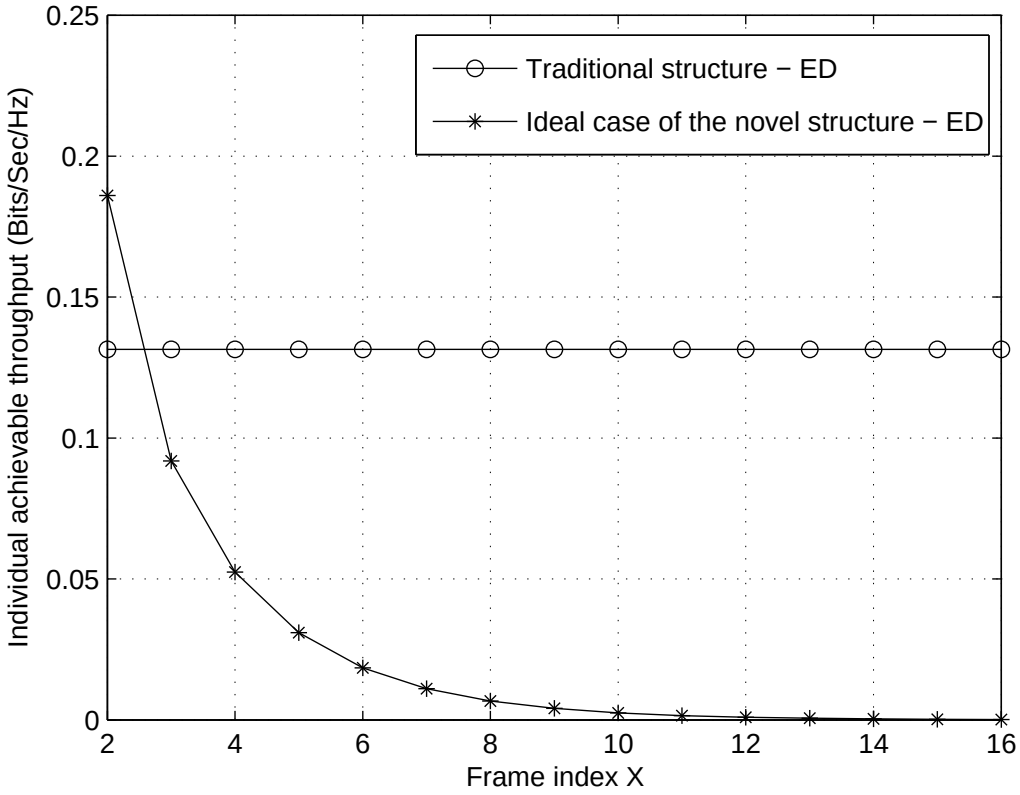

Figure 6.6: The individual achievable throughput of the X^{th} frame for the traditional structure and the ideal case of the novel structure when the energy detection is applied.

ter the initial idle status of the licensed channel is acquired, the probability that the X^{th} frame can be used for the secondary data transmission depends on the sensing results of the previous $X-1$ frames in the novel structure model. Since the probability that all the previous $X-1$ frames have mis-detection or not have false alarm decreases when X increases, the secondary transmission opportunity also decreases leading to smaller achievable throughput.

Similar observations can also be made for the novel structure applying the maximum-eigenvalue based detection and the covariance-based detection, as shown

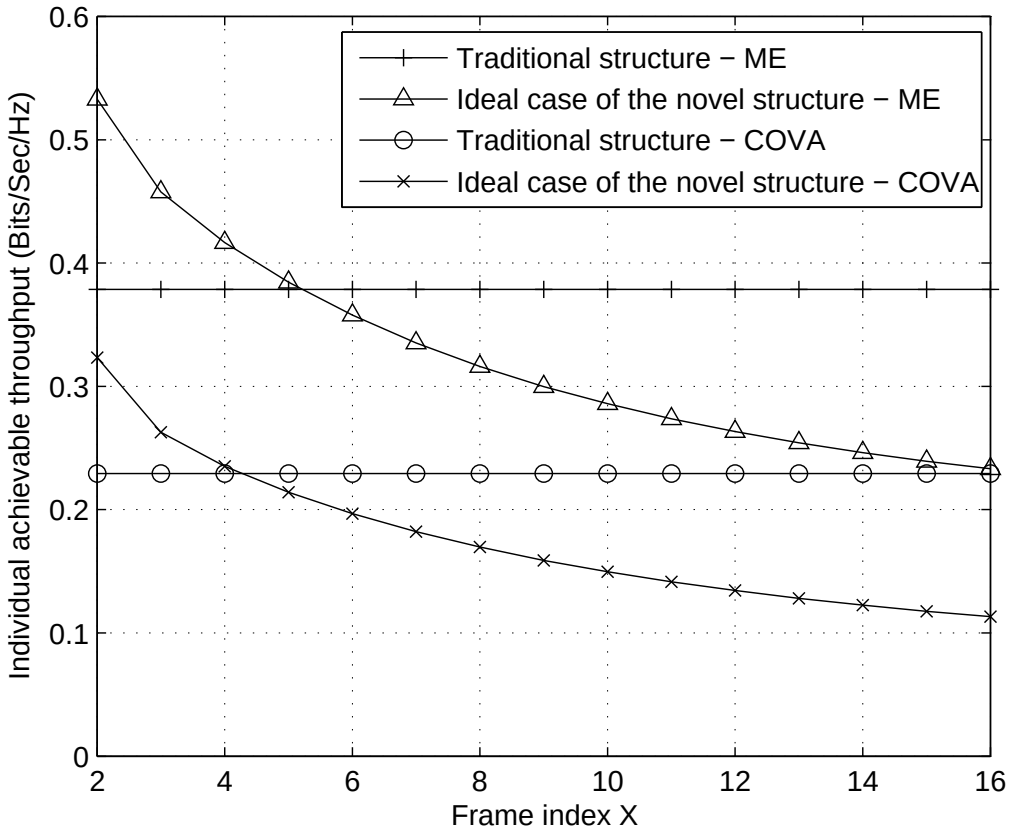

Figure 6.7: The individual achievable throughput of the X^{th} frame for the traditional structure and the ideal case of the novel structure when the maximum-eigenvalue detection and the covariance-based detection are applied.

in Fig. 6.7. Again, the individual achievable throughput decreases as the frame index X increases. However, the speed of decrease in this case is smaller than that of the energy detection in Fig. 6.6. Moreover, as can be seen, when the maximum-eigenvalue based detection is applied, the novel structure has a larger individual achievable throughput than that of the traditional structure for the first five secondary frames, whereas the achievable throughput is only larger for the first four secondary frames when the covariance-based detection is applied.

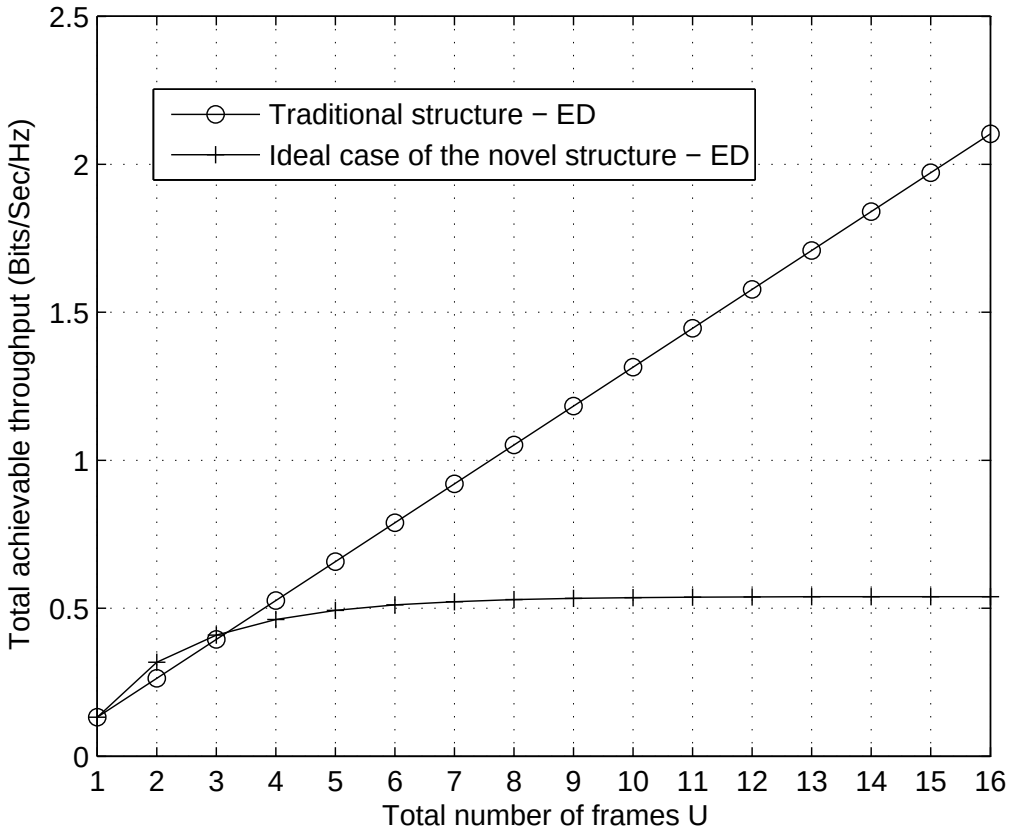

Figure 6.8: Total achievable throughput of U consecutive frames for the traditional structure and the ideal case of the novel structure when the energy detection is applied.

Fig. 6.8 examines the total achievable throughput of the U consecutive frames for the traditional structure and the ideal case of the novel structure. As can be seen, the total achievable throughput in both structures increase with the number of frames U. However, the total achievable throughput of the novel structure approaches an upper limit, whereas the total achievable throughput increases linearly in the traditional structure. Define the number of frames during which the ideal case of the novel structure has larger achievable throughput than the traditional structure

as the saturation threshold of the ideal case of the novel structure. When the total number of frames in the system is beyond this saturation threshold, the novel structure loses its throughput advantage even when the whole frame is used for data transmission. The existence of this saturation threshold is caused by the dependence of the secondary transmission opportunity on the sensing results of the previous frames. In this case, the saturation threshold is three frames.

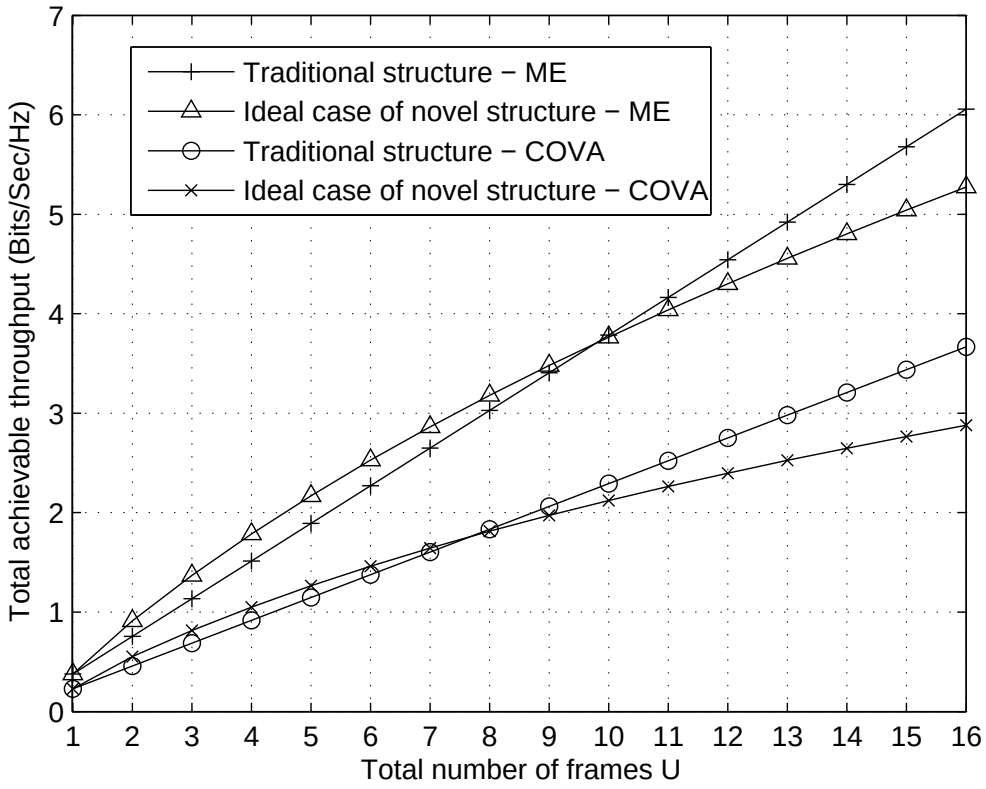

Figure 6.9: Total achievable throughput of U consecutive frames for the traditional structure and the ideal case of the novel structure when the maximum-eigenvalue detection and the covariance-based detection are applied.

Fig. 6.9 examines the total achievable throughput for the traditional structure and the ideal case of the novel structure when the maximum-eigenvalue detection

and the covariance-based detection are applied. Again, in the traditional structure, the total achievable throughput increases linearly as the total number of frames increases, whereas in the novel structure, the speed of increase of the total achievable throughput decrease as the increase of U. This agrees with the findings in Fig. 6.8 where energy detection is applied during the spectrum sensing. However, it can be noted that the rate of increase for the novel structure model in this case is much higher than that in Fig. 6.8. In other words, the saturation threshold value of the novel structure using maximum-eigenvalue detection and the covariance-based detection are much larger than that of energy detection. This is due to the improvement in the sensing performance by using the maximum-eigenvalue detection and the covariance-based detection. In this case, the saturation threshold is ten frames for the ideal case of the novel structure with the maximum-eigenvalue detection, and eight frames for the ideal case of the novel structure with the covariance-based detection.

6.4 Realistic Analysis of the Novel Structure

The analysis of the novel structure in the last section is based on the assumption that the secondary user signal in the received secondary frames can be correctly decoded and completely removed. It is therefore an ideal case of the novel structure, which provides an upper bound performance.

In reality, the decoding process for the received secondary frame in the novel structure is not ideal. Consequently, the secondary user signal may not always be correctly decoded and be completely removed from the received secondary frame. The sensing accuracy will therefore be adversely affected when the recovered received secondary frame is used for spectrum sensing. This further degrades the performance

of the novel structure. Moreover, neighbouring frames will affect each other and all the frames will be affected by the primary user traffic. The following analysis starts with the decoding process. Based on the imperfect decoding, the probability of false alarm and the probability of detection for the spectrum sensing are derived for the realistic case of the novel structure while considering multiple frames with primary user traffic.

6.4.1 Decoding

Consider binary phase shift keying (BPSK) for the secondary user signal. The received secondary frame at the secondary user receiver in the X^{th} frame can therefore be expressed as (6.14) with the secondary user signal $s_{s,j} = -\sqrt{\epsilon_b}$ or $s_{s,j} = +\sqrt{\epsilon_b}$, where ϵ_b is the bit energy of the secondary user signal. Note that the secondary user is assumed to be corrupted by AWGN only and there is only one bit per symbol in BPSK.

The received secondary frame at the secondary user receiver is then decoded. Denote the total number of transmitted secondary user symbols as ζ. The symbol duration of each secondary user signal symbol is therefore $t_\zeta = \dfrac{T}{\zeta}$. Denote the *a priori* probabilities of a $-\sqrt{\epsilon_b}$ and a $+\sqrt{\epsilon_b}$ being transmitted as $P_{(-\sqrt{\epsilon_b})}$ and $P_{(+\sqrt{\epsilon_b})}$, respectively.

When the primary user is absent from the licensed channel, the received secondary frame contains only the secondary user signal and the noise, as can be seen in (6.14). In this case, the symbol error rate of each secondary user symbol given

that a $-\sqrt{\epsilon_b}$ or a $+\sqrt{\epsilon_b}$ is transmitted can be expressed as

$$\begin{aligned} P_{serH_0} &= P_{serH_0(-\sqrt{\epsilon_b})} = P_{serH_0(+\sqrt{\epsilon_b})} \\ &= P\left(-\sqrt{\epsilon_b}|H_0\right) = P\left(+\sqrt{\epsilon_b}|H_0\right) \\ &= Q\left(\sqrt{2\gamma_s}\right). \end{aligned} \tag{6.21}$$

Assume that out of the ζ transmitted symbols, δ_0 symbols are $-\sqrt{\epsilon_b}$ and η_0 of the δ_0 symbols are incorrectly decoded as $+\sqrt{\epsilon_b}$. Similarly, assume that ϕ_0 symbols out of the $\zeta - \delta_0$ transmitted $+\sqrt{\epsilon_b}$ are incorrectly decoded as $-\sqrt{\epsilon_b}$. Thus, for a duration of $(\eta_0 + \phi_0)t_\zeta$, the secondary user signal is not removed from the received secondary frame, whilst for a duration of $(\zeta - \eta_0 - \phi_0)t_\zeta$, the secondary user signal is correctly decoded and completely removed. When the primary user is absent, the conditional probability of occurring for this case can be derived as

$$\begin{aligned} p(\zeta, \delta_0, \eta_0, \phi_0|H_0) =& \left(P_{(-\sqrt{\epsilon_b})}P_{serH_0}\right)^{\eta_0}\left(P_{(-\sqrt{\epsilon_b})}\left(1 - P_{serH_0}\right)\right)^{\delta_0-\eta_0} \\ &\cdot \left(P_{(+\sqrt{\epsilon_b})}P_{serH_0}\right)^{\phi_0}\left(P_{(+\sqrt{\epsilon_b})}\left(1 - P_{serH_0}\right)\right)^{\zeta-\delta_0-\phi_0} \end{aligned} \tag{6.22}$$

where independent symbols are assumed.

On the other hand, when the primary user is present in the licensed channel but is mis-detected by the secondary user in the $(X-1)^{th}$ frame, the data transmission is still carried out in the X^{th} frame. In this case, the received secondary frame contains the primary user signal, the secondary user signal and the noise. During the decoding process, the primary user acts as an interference to the secondary user signal, and the symbol error rate of each secondary user symbol given that a $-\sqrt{\epsilon_b}$

or a $+\sqrt{\epsilon_b}$ is transmitted can be derived as

$$\begin{aligned} P_{serH_1} &= P_{serH_1(-\sqrt{\epsilon_b})} = P_{serH_1(+\sqrt{\epsilon_b})} \\ &= P\left(-\sqrt{\epsilon_b}|H_1\right) = P\left(+\sqrt{\epsilon_b}|H_1\right) \\ &= Q\left(\sqrt{\frac{2\gamma_s}{1+\gamma_p}}\right). \end{aligned} \tag{6.23}$$

Similarly, assume that out of the ζ transmitted symbols, δ_1 symbols are $-\sqrt{\epsilon_b}$ and η_1 out of the δ_1 symbols are incorrectly decoded as $+\sqrt{\epsilon_b}$, whereas ϕ_1 symbols out of the $\zeta - \delta_1$ transmitted $+\sqrt{\epsilon_b}$ are incorrectly decoded as $-\sqrt{\epsilon_b}$. Thus, for a duration of $(\eta_1 + \phi_1)t_\zeta$, the secondary signal is not removed from the received secondary frame, whilst for a duration of $(\zeta - \eta_1 - \phi_1)t_\zeta$, the secondary signal is correctly decoded and completely removed. Thus, when the primary user is present, one has the conditional probability of occurring for this case as

$$\begin{aligned} p(\zeta, \delta_1, \eta_1, \phi_1|H_1) =& \left(P_{(-\sqrt{\epsilon_b})}P_{serH_1}\right)^{\eta_1}\left(P_{(-\sqrt{\epsilon_b})}\left(1-P_{serH_1}\right)\right)^{\delta_1-\eta_1} \\ &\cdot\left(P_{(+\sqrt{\epsilon_b})}P_{serH_1}\right)^{\phi_1}\left(P_{(+\sqrt{\epsilon_b})}\left(1-P_{serH_1}\right)\right)^{\zeta-\delta_1-\phi_1}. \end{aligned} \tag{6.24}$$

6.4.2 Spectrum Sensing Performance

After the secondary user signal is decoded and deducted from the received secondary frame, the recovered signal is used for the spectrum sensing. When the decoding error occurs such that the secondary user signal is not completely removed from the received secondary frame, the signal used for the spectrum sensing is different from those of the traditional structure model and the ideal case of the novel structure. In this case, when energy detection is applied, the spectrum sensing in the X^{th} frame

becomes a binary hypothesis test expressed as

$$Y_{re} = \begin{cases} \sum_{j=1}^{\eta_0 J/\zeta} (-2\sqrt{\epsilon_b} + w_j)^2 + \sum_{j=\eta_0 J/\zeta+1}^{\phi_0 J/\zeta+\eta_0 J/\zeta} (+2\sqrt{\epsilon_b} + w_j)^2 \\ \quad + \sum_{j=\eta_0 J/\zeta+\phi_0 J/\zeta+1}^{J} w_j^2, & H_0, \\ \sum_{j=1}^{\eta_1 J/\zeta} (s_j - 2\sqrt{\epsilon_b} + w_j)^2 + \sum_{j=\eta_1 J/\zeta+1}^{\phi_1 J/\zeta+\eta_1 J/\zeta} (s_j + 2\sqrt{\epsilon_b} + w_j)^2 \\ \quad + \sum_{j=\eta_1 J/\zeta+\phi_1 J/\zeta+1}^{J} (s_j + w_j)^2, & H_1. \end{cases} \tag{6.25}$$

Using the Gaussian approximation based on the central limit theorem, similar to the method presented in the Chapter 4, the mean and variance of Y_{re} under hypothesis H_0 and H_1 can be derived as

$$\begin{cases} \mu_{_{H_0}re} = J + \dfrac{4\gamma_s}{\zeta}(\eta_0 + \phi_0)J, \\ \sigma^2_{_{H_0}re} = 2J + \dfrac{16\gamma_s}{\zeta}(\eta_0 + \phi_0)J, \end{cases} \tag{6.26}$$

and

$$\begin{cases} \mu_{_{H_1}re} = J(1+\gamma_p) + \dfrac{4\gamma_s}{\zeta}(\eta_1 + \phi_1)J \\ \sigma^2_{_{H_1}re} = 2J + 4\gamma_p J + \dfrac{16\gamma_s}{\zeta}(\eta_1 + \phi_1)J \end{cases} \tag{6.27}$$

respectively. The conditional probabilities of false alarm, conditioned on the value of δ_0, η_0 and ϕ_0, can therefore be derived as

$$P_{fa_{ED}re}(\Psi_{_{ED}re}, J, \delta_0, \eta_0, \phi_0) = \frac{1}{2} erfc\left(\frac{\Psi_{_{ED}re} - \mu_{_{H_0}re}}{\sqrt{2\sigma^2_{_{H_0}re}}}\right), \tag{6.28}$$

where $\Psi_{_{ED}re}$ is the energy detection decision threshold for the novel structure model

with realistic decoding errors. The conditional probabilities of detection can be derived as

$$P_{d_{EDre}}(\Psi_{_{EDre}}, J, \delta_{_0}, \eta_{_1}, \phi_{_1}) = \frac{1}{2} erfc\left(\frac{\Psi_{_{EDre}} - \mu_{_{H_1 re}}}{\sqrt{2\sigma^2_{_{H_1 re}}}}\right). \tag{6.29}$$

By averaging the conditional probability of false alarm over the probability of occurring in (6.22), the unconditional probability of false alarm can be derived as

$$\begin{aligned}\overline{P_{fa_{EDre}}}(\Psi_{_{EDre}}, J) = &\sum_{\delta_{_0}=0}^{\zeta}\sum_{\eta_{_0}=0}^{\delta_{_0}}\sum_{\phi_{_0}=0}^{\zeta-\delta_{_0}}\binom{\zeta}{\delta_{_0}}\binom{\delta_{_0}}{\eta_{_0}}\binom{\zeta-\delta_{_0}}{\phi_{_0}} \\ &\cdot\frac{\left(p\left(\zeta,\delta_{_0},\eta_{_0},\phi_{_0}|H_0\right)P_{fa_{EDre}}(\Psi_{_{EDre}}, J, \delta_{_0}, \eta_{_0}, \phi_{_0})\right)}{\sum_{\delta_{_0}=0}^{\zeta}\sum_{\eta_{_0}=0}^{\delta_{_0}}\sum_{\phi_{_0}=0}^{\zeta-\delta_{_0}}\binom{\zeta}{\delta_{_0}}\binom{\delta_{_0}}{\eta_{_0}}\binom{\zeta-\delta_{_0}}{\phi_{_0}}p(\zeta,\delta_{_0},\eta_{_0},\phi_{_0}|H_0)}.\end{aligned} \tag{6.30}$$

The unconditional probability of detection can be derived by averaging the conditional probability of detection over the probability of occurring in (6.24) as

$$\begin{aligned}\overline{P_{d_{EDre}}}(\Psi_{_{EDre}}, J) = &\sum_{\delta_{_1}=0}^{\zeta}\sum_{\eta_{_1}=0}^{\delta_{_1}}\sum_{\phi_{_1}=0}^{\zeta-\delta_{_1}}\binom{\zeta}{\delta_{_1}}\binom{\delta_{_1}}{\eta_{_1}}\binom{\zeta-\delta_{_1}}{\phi_{_1}} \\ &\cdot\frac{\left(p\left(\zeta,\delta_{_1},\eta_{_1},\phi_{_1}|H_1\right)P_{d_{EDre}}(\Psi_{_{EDre}}, J, \delta_{_1}, \eta_{_1}, \phi_{_1})\right)}{\sum_{\delta_{_1}=0}^{\zeta}\sum_{\eta_{_1}=0}^{\delta_{_1}}\sum_{\phi_{_1}=0}^{\zeta-\delta_{_1}}\binom{\zeta}{\delta_{_1}}\binom{\delta_{_1}}{\eta_{_1}}\binom{\zeta-\delta_{_1}}{\phi_{_1}}p(\zeta,\delta_{_1},\eta_{_1},\phi_{_1}|H_1)}\end{aligned} \tag{6.31}$$

In this derivation, (6.31) is used in the Neyman-Pearson rule to determine the decision threshold for the spectrum sensing without the knowledge of the values of $\delta_{_1}$, $\eta_{_1}$ and $\phi_{_1}$ so that the primary user is protected by guaranteeing the average detection probability. Because in practice the values of $\delta_{_1}$, $\eta_{_1}$ and $\phi_{_1}$ are usually unknown and thus, the conditional probability of detection in (6.29) is averaged over (6.24) to

remove them, and the primary user can not be protected against the instantaneous detection probability that requires δ_1, η_1 and ϕ_1. The unconditional results obtained after averaging are independent of δ_1, η_1 and ϕ_1. Moreover, obtaining threshold by using average and instantaneous probabilities give almost identical performances.

6.4.3 Secondary User Transmission

After the spectrum sensing, the whole following frame can be used for the secondary data transmission if the sensing result favors the absence of the primary user. The probability that the X^{th} frame is idle and is used for the secondary user data transmission as a result of the correct spectrum sensing of the $(X-1)^{th}$ frame can be derived as

$$\begin{aligned} P_{H_0 reX} = {} & P_{H_0 reX-1}\big(1 - f_{X\alpha}(X)\big) \sum_{\delta_0=0}^{\zeta} \sum_{\eta_0=0}^{\delta_0} \sum_{\phi_0=0}^{\zeta-\delta_0} \binom{\zeta}{\delta_0} \binom{\delta_0}{\eta_0} \binom{\zeta-\delta_0}{\phi_0} \\ & \cdot \Big(\Big(p(\zeta, \delta_0, \eta_0, \phi_0 | H_0) \Big(1 - P_{fa_{ED}re}(\Psi_{_{ED}re}, J, \delta_0, \eta_0, \phi_0) \Big) \Big) \\ & + P_{H_1 reX-1} f_{X\beta}(X) \sum_{\delta_1=0}^{\zeta} \sum_{\eta_1=0}^{\delta_1} \sum_{\phi_1=0}^{\zeta-\delta_1} \binom{\zeta}{\delta_1} \binom{\delta_1}{\eta_1} \binom{\zeta-\delta_1}{\phi_1} \\ & \cdot \Big(\Big(p(\zeta, \delta_1, \eta_1, \phi_1 | H_1) \Big(1 - P_{d_{ED}re}(\Psi_{_{ED}re}, J, \delta_1, \eta_1, \phi_1) \Big) \Big) \end{aligned} \tag{6.32}$$

The probability that the X^{th} frame is busy but is still used for data transmission

due to mis-detection at spectrum sensing of the $(X-1)^{th}$ frame can be derived as

$$\begin{aligned} P_{H_1reX} =& P_{H_0reX-1} f_{X\alpha}(X) \sum_{\delta_0=0}^{\zeta} \sum_{\eta_0=0}^{\delta_0} \sum_{\phi_0=0}^{\zeta-\delta_0} \binom{\zeta}{\delta_0} \binom{\delta_0}{\eta_0} \binom{\zeta-\delta_0}{\phi_0} \\ & \cdot \Big(p(\zeta, \delta_0, \eta_0, \phi_0 | H_0) \Big(1 - P_{fa_{ED}re}(\Psi_{_{ED}re}, J, \delta_0, \eta_0, \phi_0) \Big) \Big) \\ & + P_{H_1reX-1} \big(1 - f_{X\beta}(X) \big) \sum_{\delta_1=0}^{\zeta} \sum_{\eta_1=0}^{\delta_1} \sum_{\phi_1=0}^{\zeta-\delta_1} \binom{\zeta}{\delta_1} \binom{\delta_1}{\eta_1} \binom{\zeta-\delta_1}{\phi_1} \\ & \cdot \Big(p(\zeta, \delta_1, \eta_1, \phi_1 | H_1) \Big(1 - P_{d_{ED}re}(\Psi_{_{ED}re}, J, \delta_1, \eta_1, \phi_1) \Big) \Big). \end{aligned} \tag{6.33}$$

Using (6.32) and (6.33), the total achievable throughput of the U frames when energy detection is used in the realistic case of the novel structure can be derived as

$$R_{_{ED}re} = \sum_{X=1}^{U} \left(P_{H_0reX} C_{H_0} + P_{H_1reX} C_{H_1} \right). \tag{6.34}$$

6.4.4 Covariance-Matrix-Based Detection

The system performance can also be derived for the novel structure considering the decoding errors when the covariance-matrix-based detection is applied. When the secondary user symbols are independent, the covariance matrix of the secondary user signal is diagonal. Hence, when the maximum-eigenvalue detection is applied, the conditional probability of false alarm can be derived as

$$P_{fa_{ME}re}(\Psi_{_{ME}re}, J) = 1 - TW_1 \left(\frac{\Psi_{_{ME}re} J - \mu_{_{ME}re}}{\upsilon_{_{ME}re}} \right) \tag{6.35}$$

where $\Psi_{_{ME}re}$ is the decision threshold for the realistic case of the novel structure when maximum-eigenvalue detection is applied, $\mu_{_{ME}re} = (\sqrt{J-1}+\sqrt{L})^2$ and $\upsilon_{_{ME}} = (\sqrt{J-1}+\sqrt{L})(\frac{1}{\sqrt{J-1}}+\frac{1}{\sqrt{L}})$,

The conditional probability of detection can be derived as

$$P_{d_{ME}re}(\Psi_{_{ME}re}, J) = 1 - TW_1\left(\frac{\Psi_{_{ME}re}J - \frac{J\vartheta_{max}}{\sigma_w^2+\sigma_{s_s}^2} - \mu_{_{ME}}re}{\upsilon_{_{ME}re}}\right), \tag{6.36}$$

where $\sigma_{s_s}^2 = \epsilon_b$ and ϵ_b is the secondary bit energy defined as before.

The unconditional probability of false alarm and unconditional probability of detection for the maximum-eigenvalue detection in the realistic case of the novel structure can then be derived by averaging (6.35) and (6.36) over (6.22) and (6.24), respectively. Similar to the method used for (6.30) and (6.31).

When the covariance-based detection is applied, the probability of false alarm can be derived as

$$P_{fa_{COV}re}(\Psi_{_{COV}re}, J) = 1 - Q\left(\frac{\frac{1}{\Psi_{_{COV}re}}\left(1 + (L-1)\sqrt{\frac{2}{J\pi}}\right) - 1}{\sqrt{\frac{2}{J}}}\right), \tag{6.37}$$

where $\Psi_{_{COV}re}$ is the decision threshold in this case.

The conditional probability of detection can therefore be derived as

$$P_{d_{COV}re}(\Psi_{_{COV}re}, J) = 1 - Q\left(\frac{\frac{1}{\Psi_{_{COV}re}} + \frac{G_L\gamma_p}{\Psi_{_{COV}re}\left(\gamma_p + \frac{\phi_1+\eta_1}{\varsigma}4\gamma_s+1\right)} - 1}{\sqrt{\frac{2}{J}}}\right). \tag{6.38}$$

The unconditional probability of false alarm and unconditional probability of detection for the covariance-based detection in the realistic case of the novel structure can then be derived by averaging (6.37) and (6.38) over (6.22) and (6.24), respectively.

The achievable throughput of the novel structure when the maximum-eigenvalue detection or the covariance-based detection is used for the spectrum sensing can then

be derived by using the same method as that of (6.32) - (6.34), through replacing the probability of false alarm and the probability of detection with (6.35) and (6.36) for the maximum-eigenvalue detection or (6.37) and (6.38) for the covariance-based detection.

When other types of modulation schemes are used for the secondary signal, such as quadrature phase shift keying (QPSK), the probability of error will be different. However, the performance of the novel structure model with decoding errors can be analyzed in a similar way to that in (6.21) to (6.38).

6.4.5 Numerical Results and Discussions

In this section, the performance of the novel structure with the realistic decoding errors is examined and compared with that of the traditional structure and the ideal case of the novel structure. Neyman-Pearson rule is applied to obtain the decision threshold for spectrum sensing by setting the target probability of detection to 0.9.

Fig. 6.10 shows the ROC curves of the spectrum sensing performance for different structures when the energy detection is applied in the X^{th} frame with $\gamma_p = -5$ dB and $\gamma_s = 0$ dB. Several observations can be made. First, benefiting from the longer spectrum sensing time, the novel structure always has a better sensing performance than the traditional structure. Second, compare the performance of the realistic case of the novel structure to that of the ideal case, it can be seen that the sensing performance degrades when the realistic decoding error is considered, while the ideal case only provides an upper bound of the sensing performance. Moreover, as the QPSK has a larger probability of decoding error which leads to more interfering secondary user signal in the processed secondary frame samples, the sensing performance is therefore worse for the QPSK, comparing with the BPSK.

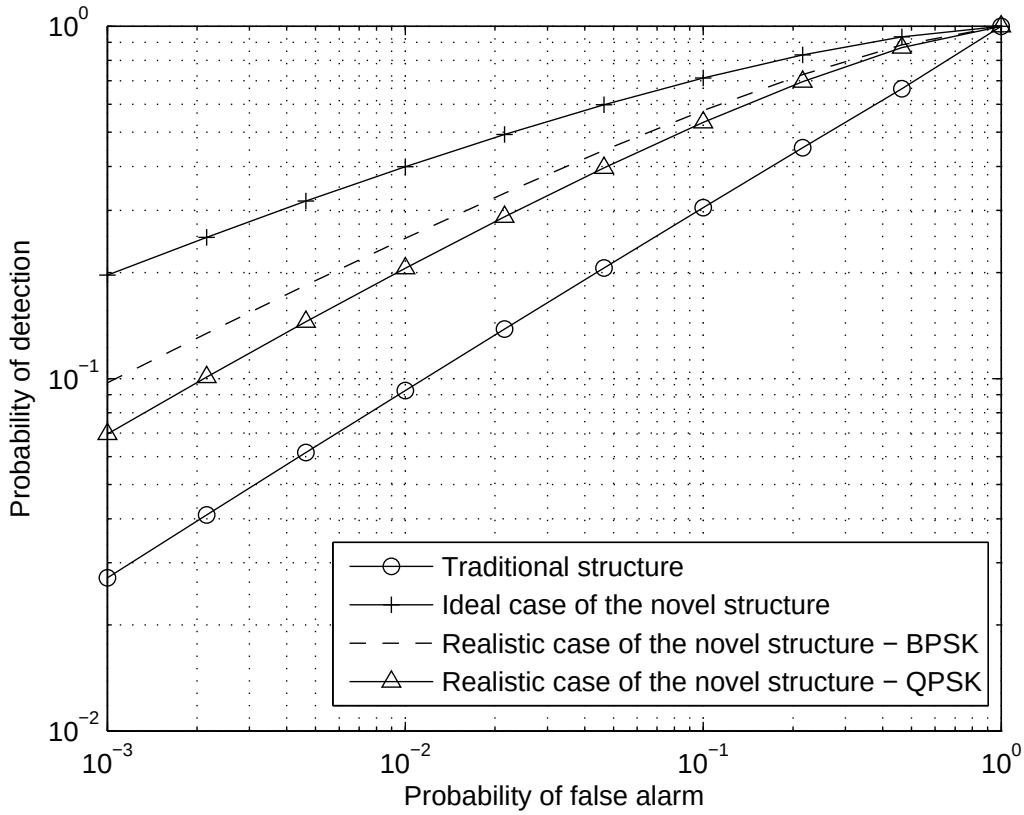

Figure 6.10: The ROC curves of spectrum sensing performance for the traditional structure and the novel structure when the energy detection is applied, with $\gamma_s = 0$ dB.

Fig. 6.11 has the same settings as Fig. 6.10 but for a different value of γ_s. It can be seen that, when γ_s is increased from 0 dB to 5 dB, the sensing performance of the realistic case of the novel structure improves, whilst the performances of the traditional structure and the ideal case do not change. This is explained as follows. In the traditional structure, the secondary transmission is stopped during the sensing. Therefore, the sensing process is not affected by the secondary user SNR. In the ideal case of the novel structure, the secondary user signal is assumed to be completely removed from the received secondary frame. Thus, the sensing

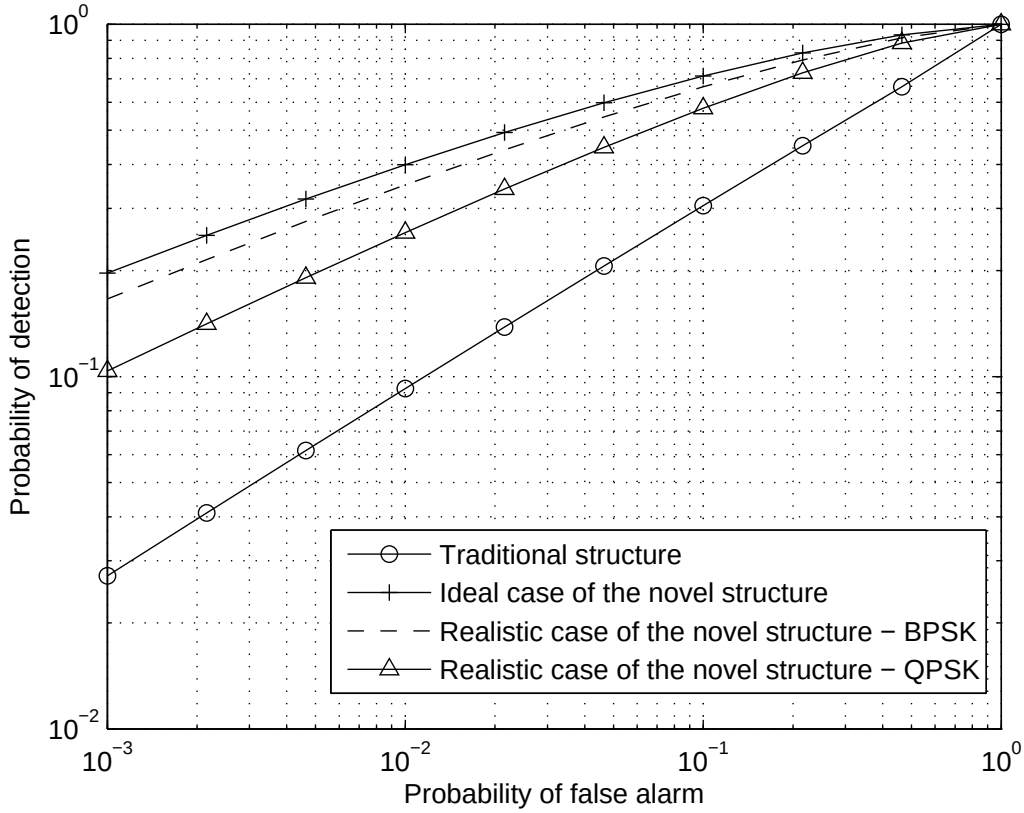

Figure 6.11: The ROC curves of spectrum sensing performance for the traditional structure and the novel structure when the energy detection is applied, with $\gamma_s = 5$ dB.

performance is not affected by the secondary user SNR either. In the realistic case of the novel structure with decoding errors, the increase of γ_s leads to the decrease of the probability of the decoding error, such that the sensing performance improves.

Fig. 6.12 examines the individual achievable throughput for the traditional structure and the novel structure when the energy detection is applied. Several observations can be made. First, as the frame index X increases, the individual throughput of the novel structure decreases and approaches zero, whereas the individual throughput of the traditional structure remains the same for all values of

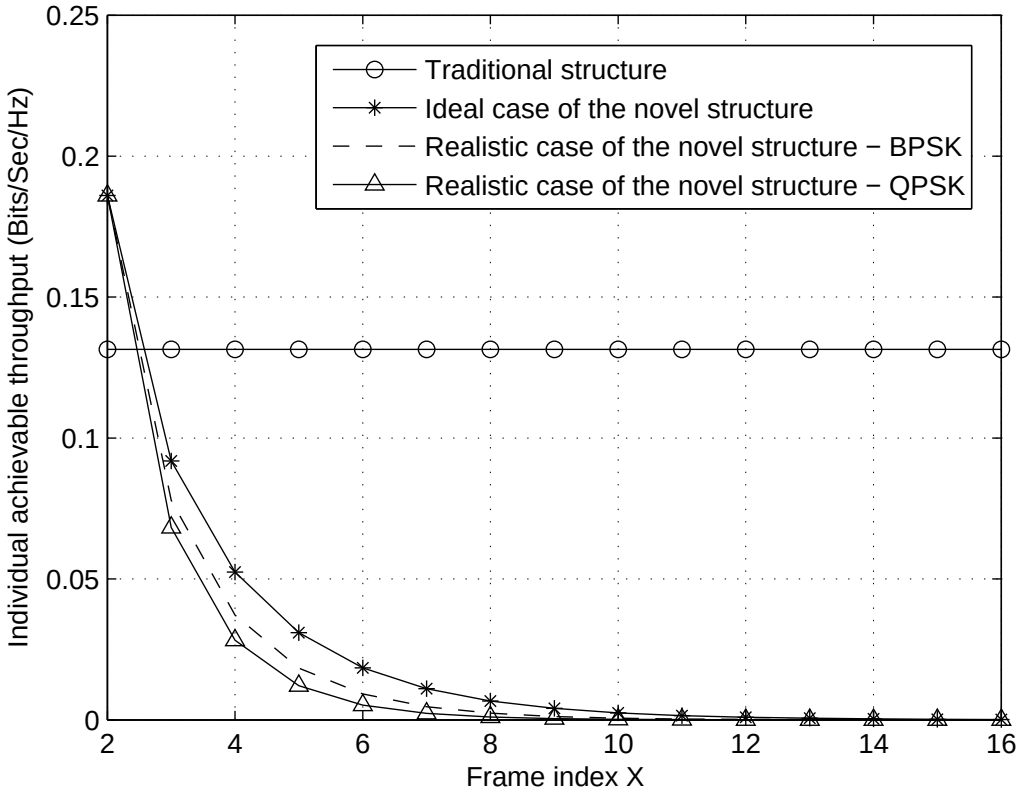

Figure 6.12: Individual achievable throughput of X^{th} frame for the traditional structure and the novel structure model when the energy detection is applied, with $\lambda_b^{-1} = \lambda_e^{-1} = 10T$.

X, as expected. Second, comparing the individual achievable throughput of the realistic case of the novel structure to that of the ideal case, it can be seen that the decrease of the achievable throughput is faster in the realistic case where the decoding error is considered. This is because the spectrum sensing performance is degraded when decoding errors occurs in the realistic case of the novel structure, as was examined in Fig. 6.10, such that the secondary transmission opportunity for the following secondary frame is reduced comparing with the idle case. Hence, the individual achievable throughput reduces faster. Moreover, for QPSK with a

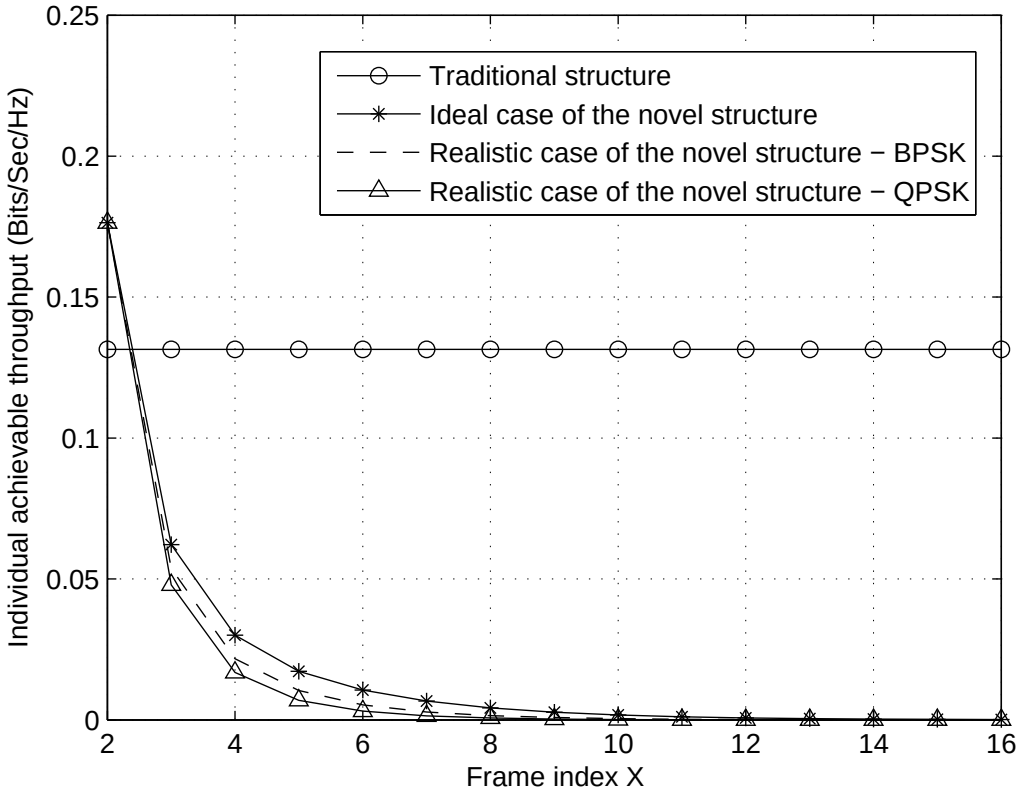

Figure 6.13: Individual achievable throughput of X^{th} frame for the traditional structure and the novel structure when the energy detection is applied, with $\lambda_b^{-1} = \lambda_e^{-1} = T$.

larger probability of decoding error, the decrease in the achievable throughput is more significant than that of the BPSK.

Fig. 6.13 has the same settings as Fig. 6.12 but with the busy and idle channel holding times decreased from $\lambda_b^{-1} = \lambda_b^{-1} = 10T$ to T. As can be observed, comparing with Fig. 6.12, the achievable throughput is further reduced when λ_b^{-1} and λ_e^{-1} are decreased, since shorter channel holding times indicate higher primary user traffic intensities, and hence higher probability of the primary user occupancy status occurs. This agrees with the findings in Chapter 3, Chapter 4 and Chapter 5, that

the primary user traffic degrades the performance of cognitive radio systems.

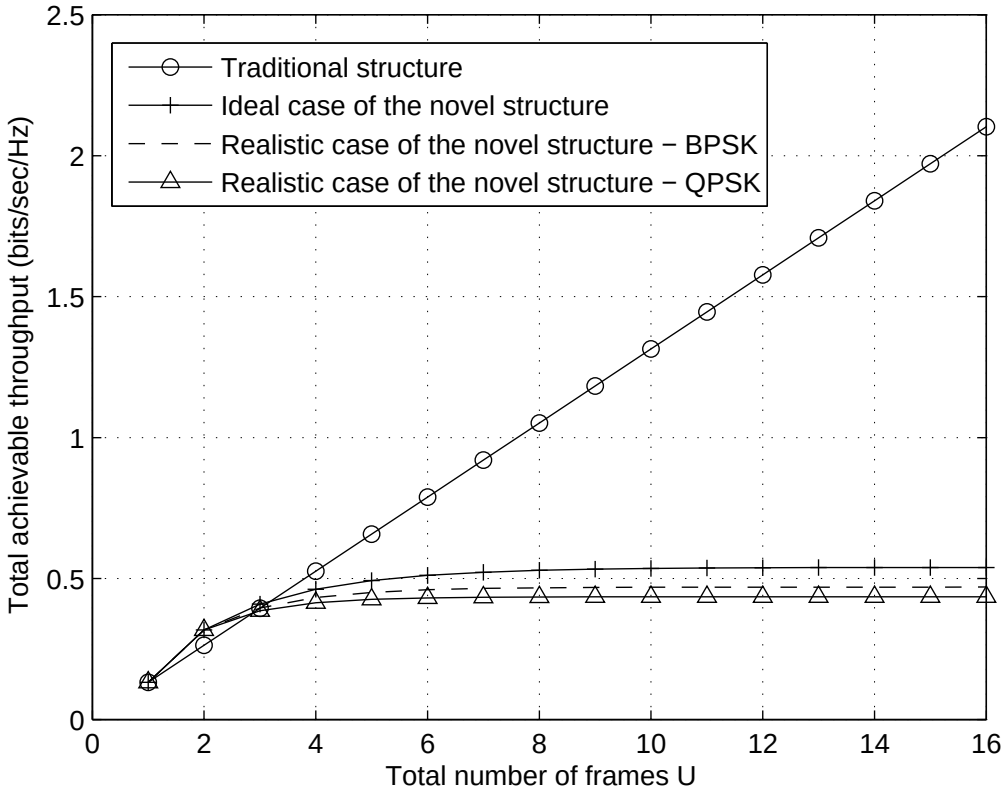

Figure 6.14: Total achievable throughput of U consecutive frames for the traditional structure and the novel structure model when the energy detection is applied.

Fig. 6.14 compares the total achievable throughput of the U consecutive frames for the traditional structure and the novel structure when the energy detection is applied. As can be seen, when the decoding errors are taken into consideration in the realistic case of the novel structure, the total achievable throughput is reduced comparing with that of the ideal case, as a result of the accumulated decoding errors. Moreover, the saturation threshold is also smaller for the realistic case of the novel structure, as the total achievable throughput enters the saturation region faster than that of the ideal case. However, in this case, the saturation threshold for both the

ideal case and the realistic case of the novel structure are three frames, since the saturation threshold can only be integer number of frames.

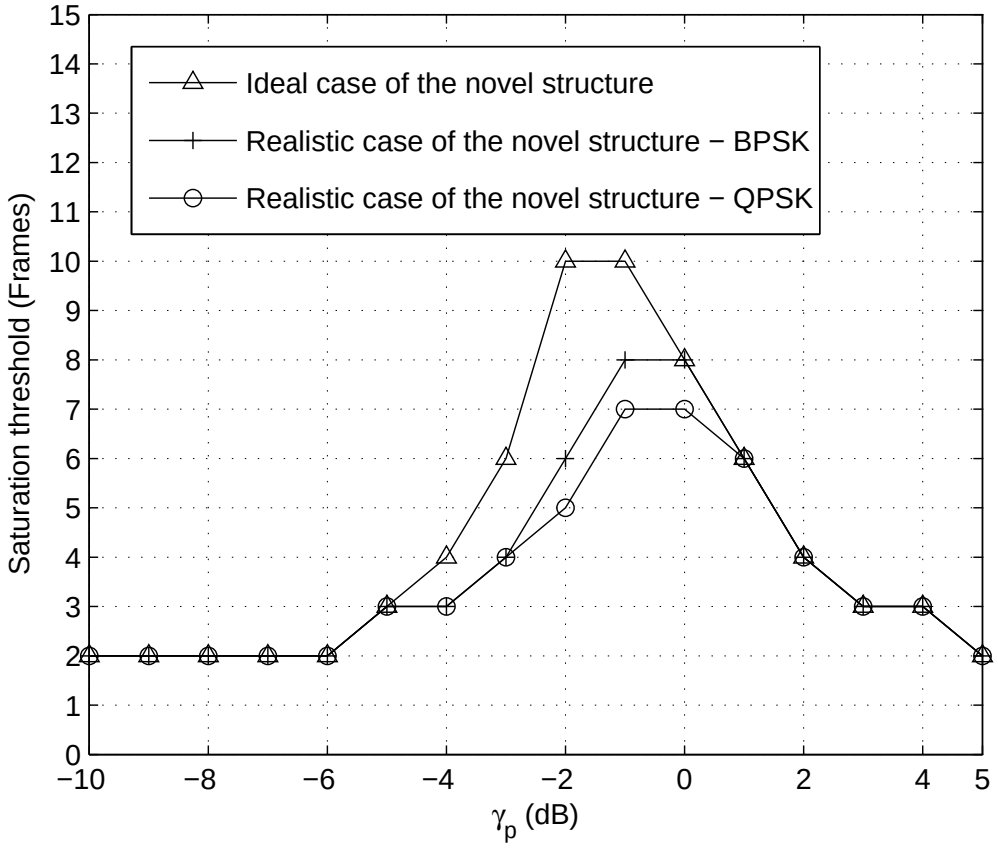

Figure 6.15: The saturation threshold of the novel structure for different values of γ_p.

Fig. 6.15 investigates the effect of the received primary user SNR on the saturation threshold of the novel structure, measured in the unit of number of frames. As can be seen, when γ_p increases at small values, the novel structure takes advantage of the improved sensing quality to capture more secondary transmission opportunities and hence, the saturation threshold of the novel structure increases. After γ_p reaches certain values, about -1 dB in this case, the improvement in the sens-

ing result become much less significant such that the novel structure suffers more from the primary user interference. Therefore the saturation threshold decreases as a result of the increased primary user interference. Moreover, when decoding errors are taken into consideration, the saturation threshold of the novel structure decreases further in the realistic case, which agrees with the findings in Fig. 6.14. When QPSK is used for the secondary user signal, the saturation threshold is further reduced comparing with that of the BPSK.

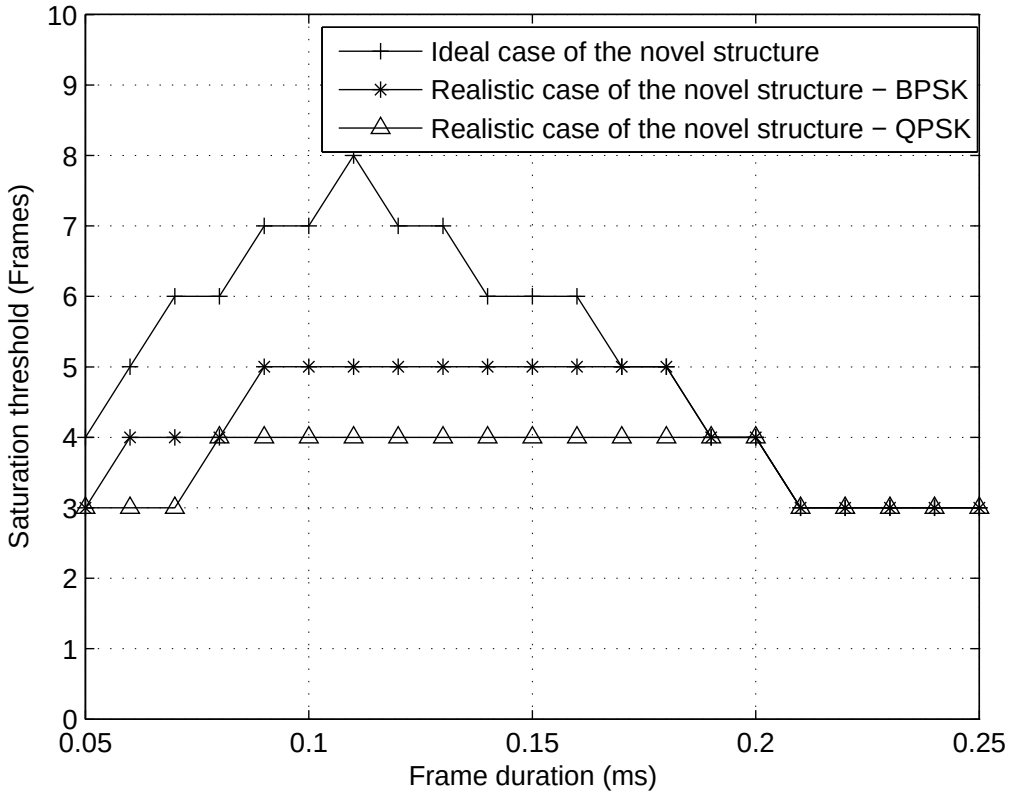

Figure 6.16: The saturation threshold of the novel structure for different values of T.

Fig. 6.16 investigates the effect of the frame duration T on the saturation threshold of the novel structure. As can be seen from Fig. 6.16, there exists an optimal

value of T where the saturation threshold of the novel structure or the advantage of the novel structure is maximized. This can be explained as follows. At small values of T, the advantage of the novel structure in the spectrum sensing increases as T increases. The saturation threshold of the novel structure therefore increases due to the increased secondary transmission opportunity. When the value of T increases further, as shown in the Chapter 3, the fraction of the frame used for the secondary transmission becomes larger for the traditional structure, and the sensing slot in the traditional structure is significantly smaller than the transmission slot. In this case, the traditional structure becomes similar to the novel structure from the secondary transmission's point of view. As well, since the channel holding time λ_b^{-1} and λ_e^{-1} are fixed, the increase of the frame duration leads to more status changes of the primary user. This increases the probability of decoding error and hence, further degrades the performance. Note that in the realistic case of the novel structure, the saturation threshold becomes constant values when the frame duration is between 0.1 ms and 0.2 ms. This is because the saturation threshold is measured in the number of frames, and in reality the number of frames can only be integer. Hence, although the actual crossing points of the total achievable throughput for the traditional structure and the novel structure are changing continuously with the frame duration, they are always approximated to the next smallest integer.

Fig. 6.17 compares the ROC curves of the spectrum sensing performance in different structures when the maximum-eigenvalue detection is applied for spectrum sensing. In this figure, the smoothing factor is set at 5 and ρ is set at 0.5. As can be seen, the spectrum sensing performance using the maximum-eigenvalue detection is much better than that of the energy detection in Fig. 6.10. When the decoding errors of the secondary user signal is taken into consideration in the realistic case of

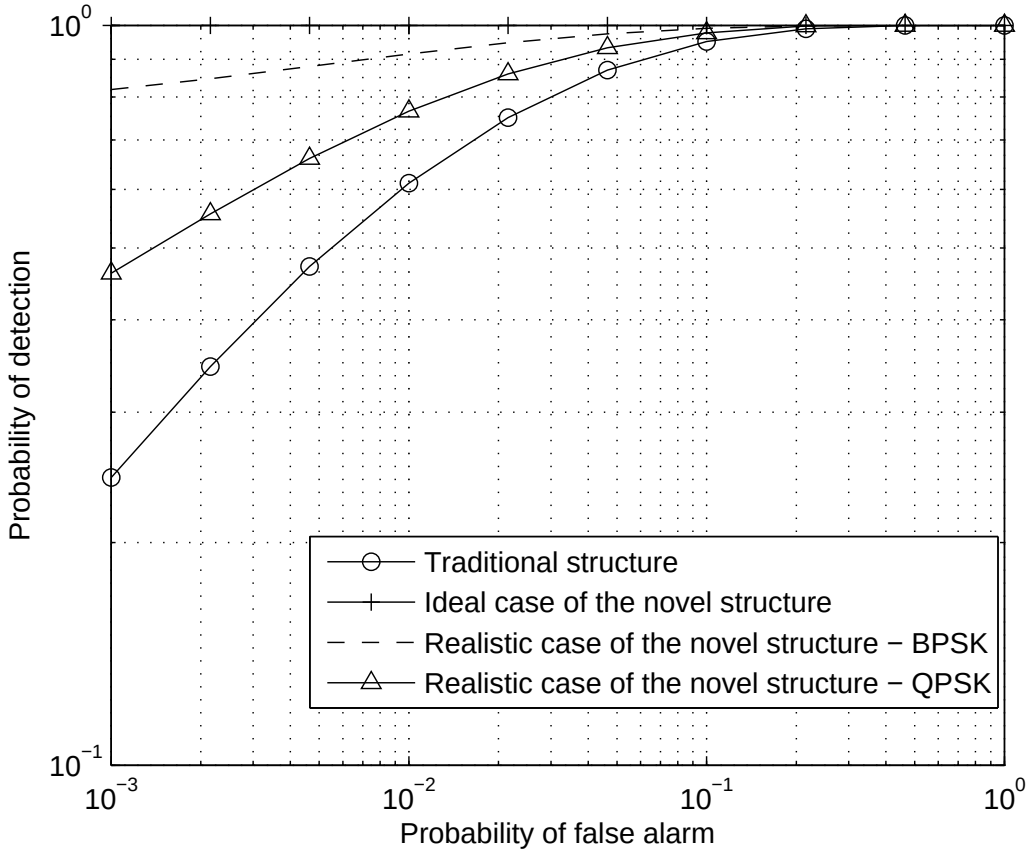

Figure 6.17: The ROC curves of spectrum sensing performance for the traditional structure and the novel structure when the maximum-eigenvalue detection is applied.

the novel structure, the sensing performance is degraded comparing with the ideal case of the novel structure. However, the sensing performance in this case is still better than that of the traditional structure as a result of the longer sensing duration of the novel structure, agrees with earlier findings.

Fig. 6.18 investigates the individual achievable throughput of the X^{th} frame for different models when the maximum-eigenvalue detection is applied for spectrum sensing. As can be seen, due to the improvement in the sensing performance, the individual achievable throughput for both the traditional structure and the novel

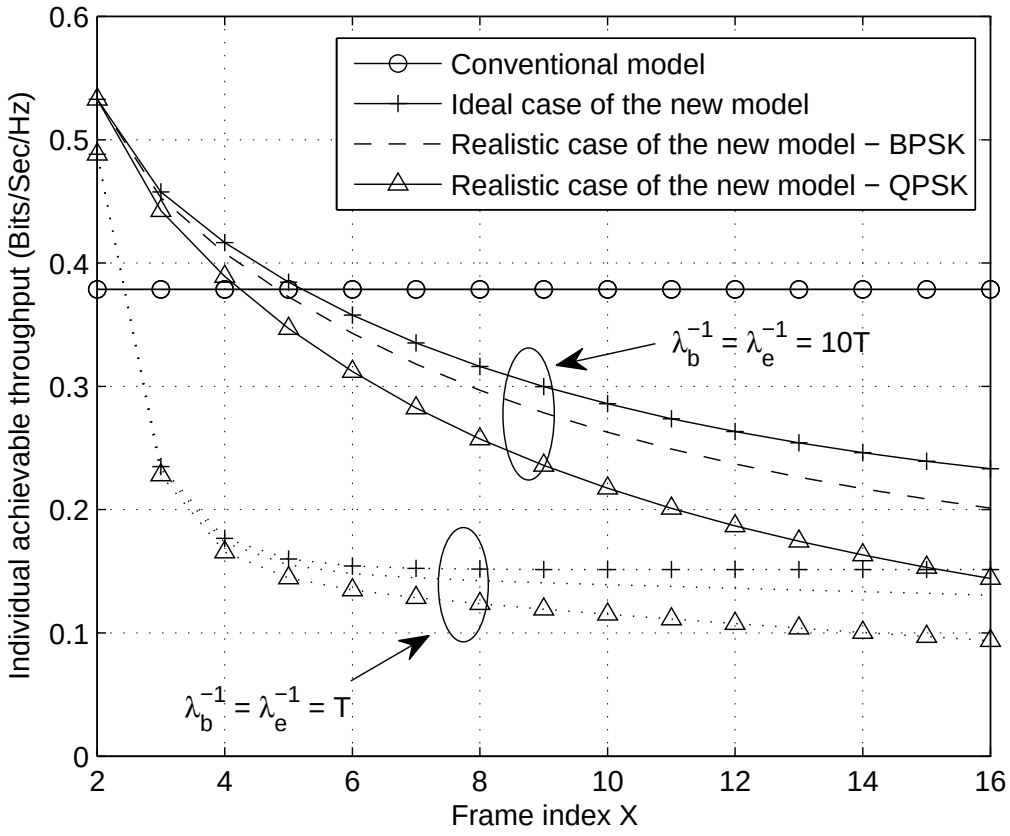

Figure 6.18: Individual achievable throughput of X^{th} frame for the traditional structure and the novel structure when the maximum-eigenvalue detection is applied.

structure become larger compared with that of the energy detection in Fig. 6.12. Again, the individual achievable throughput decreases as the frame index X increases. However, the speed of decrease is smaller than that of the energy detection. Fig. 6.18 has also presented the individual achievable throughput for the novel structure with an increased primary user traffic intensity. As can be seen, when the busy and idle channel holding times are decreased from $10T$ to T, the individual achievable throughput is significantly reduced, as expected. Nevertheless, the throughput performance with the higher primary user traffic intensity still shows

the same trend.

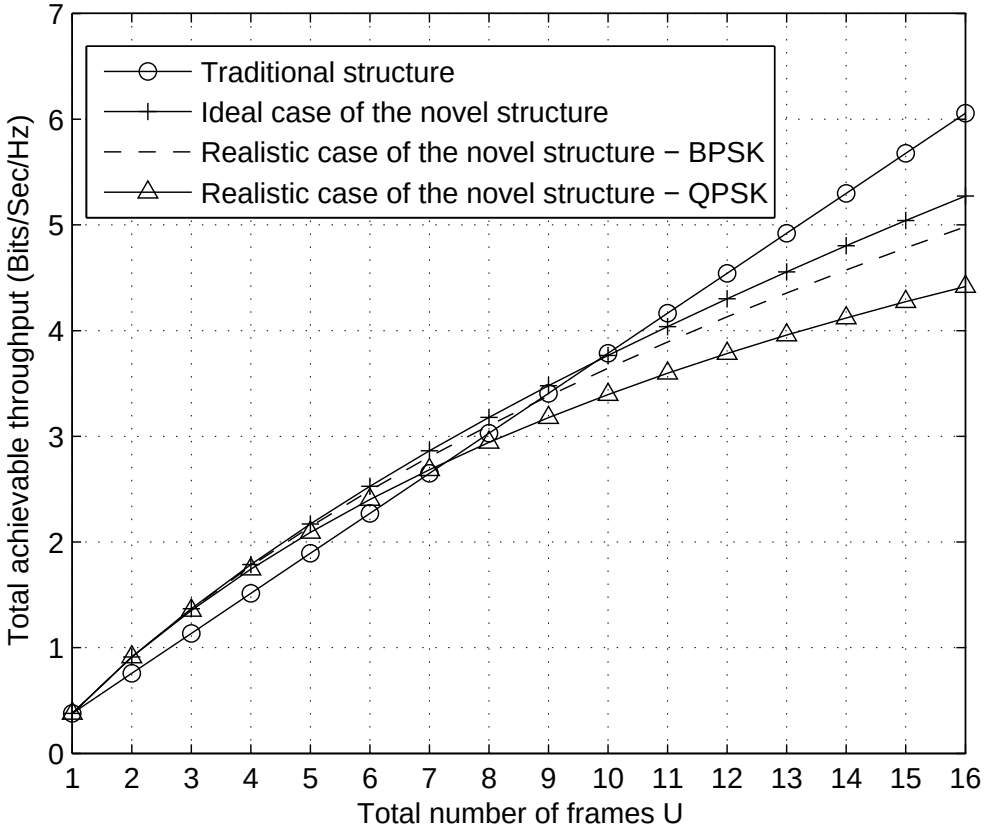

Figure 6.19: Total achievable throughput of U consecutive frames for the traditional structure and the novel structure when the maximum-eigenvalue detection is applied.

Fig. 6.19 examines the total achievable throughput of the U consecutive frames for different structures when the maximum-eigenvalue detection is applied for spectrum sensing. As can be seen, the total achievable throughput of the novel structure increases with the increase of U and a saturation threshold exists after which the novel structure loss its advantage. This agrees with the previous findings. However, it can also be noted that the rate of increase for the novel structure in this case is much higher than that of the novel structure with energy detection, and the satura-

tion threshold value of the novel structure using the maximum-eigenvalue detection is much larger than that of the energy detection. This is due to the improvement in the sensing performance by using the maximum-eigenvalue detection. Moreover, when the decoding error is taken into consideration in the realistic case of the novel structure, again, the achievable throughput is reduced comparing with the ideal case, as expected. Fig. 6.20 compares the ROC curves of spectrum sensing per-

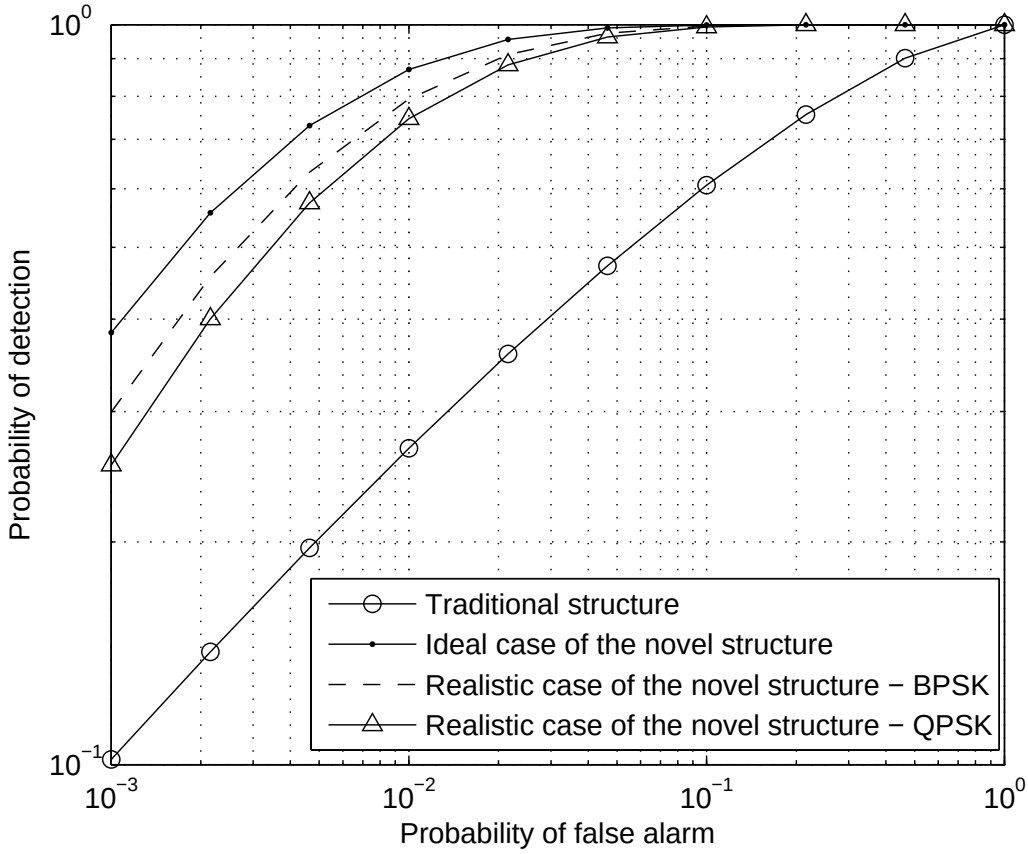

Figure 6.20: The ROC curves of spectrum sensing performance for the traditional structure and the novel structure when the covariance-based detection is applied.

formance for different structures when the covariance-based detection is applied for spectrum sensing. As can be seen, when the covariance-based detection is applied,

the performance of spectrum sensing is better than energy detection presented in Fig. 6.10, while it is worse than that of maximum-eigenvalue detection presented in Fig. 6.17. This agrees with the findings in Fig. 6.5 for the ideal case. The realistic case of the novel structure takes the advantage of the longer sensing period and has a better performance than the traditional structure, but is still worse than the performance of the ideal case where the decoding process is assumed to be error free.

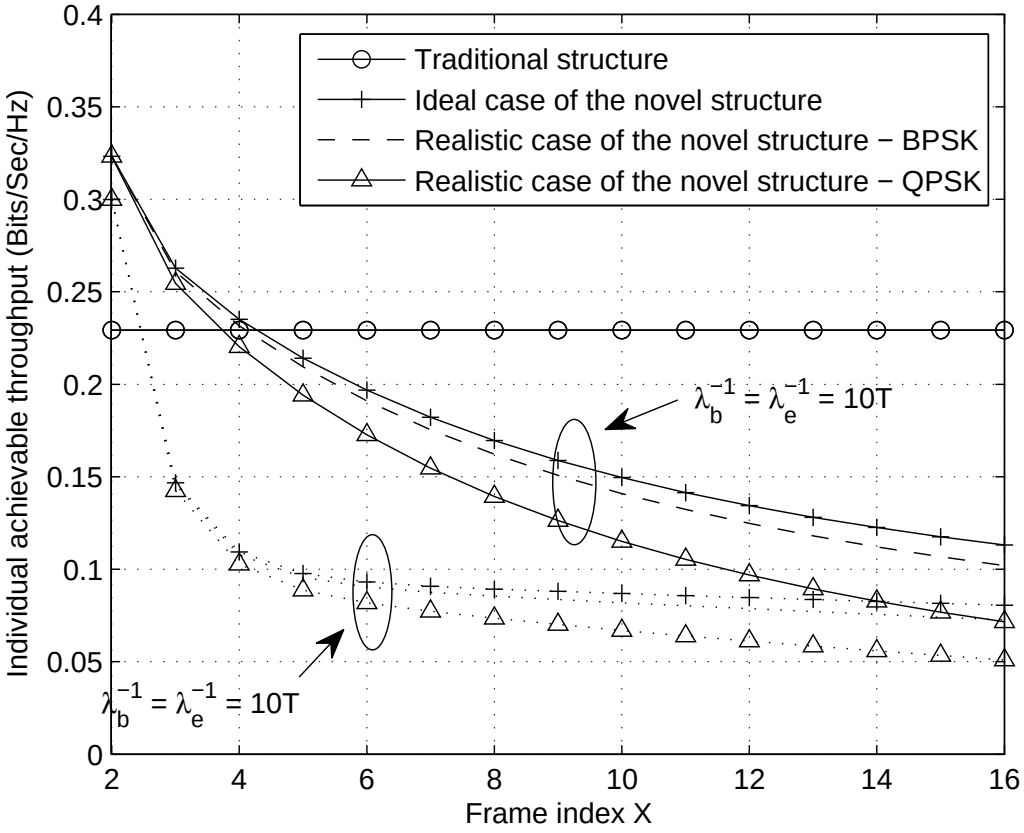

Figure 6.21: Individual achievable throughput of X^{th} frame for the traditional structure and the novel structure when the covariance-based detection is applied.

Fig. 6.21 compares the individual achievable throughput for different structures

when the covariance-based detection is used for spectrum sensing. First, similar relationship between the traditional structure and the novel structure can be observed. Similar to when the energy detection and the maximum-eigenvalue detection are applied, the advantage of the novel structure disappears as the increase of X, and the achievable throughput approaches a fixed value, while the upper bound performance is obtained in the ideal case. Compared with Fig. 6.12 and Fig. 6.17, it can be noticed that, the individual achievable throughput performance using the covariance-based detection in the novel structure with decoding errors falls between those for the energy detection and the maximum-eigenvalue detection. This also agrees with the findings from Fig. 6.20. When the channel holding time decreases from $10T$ to T , the performance of the novel structure degrades, as a result of the increased primary user traffic, as expected.

Fig. 6.22 provides the total achievable throughput of U consecutive frames for different structures when the covariance-based detection is applied for spectrum sensing. In this case, the saturation threshold of the novel structure is seven frames for the ideal case, seven frames for the realistic case of the novel structure with BPSK and six frames for the realistic case of the novel structure with QPSK. These figures are larger than those of energy detection but smaller than those of maximum-eigenvalue detection, as expected.

6.5 Effect of Fading Channels

In the above analysis of the novel structure for cognitive radio, it is assumed that the secondary user is only corrupted by AWGN. In practice, wireless signals may experience fading and consequently affects the system performance. In this section, the effect of fading is analyzed.

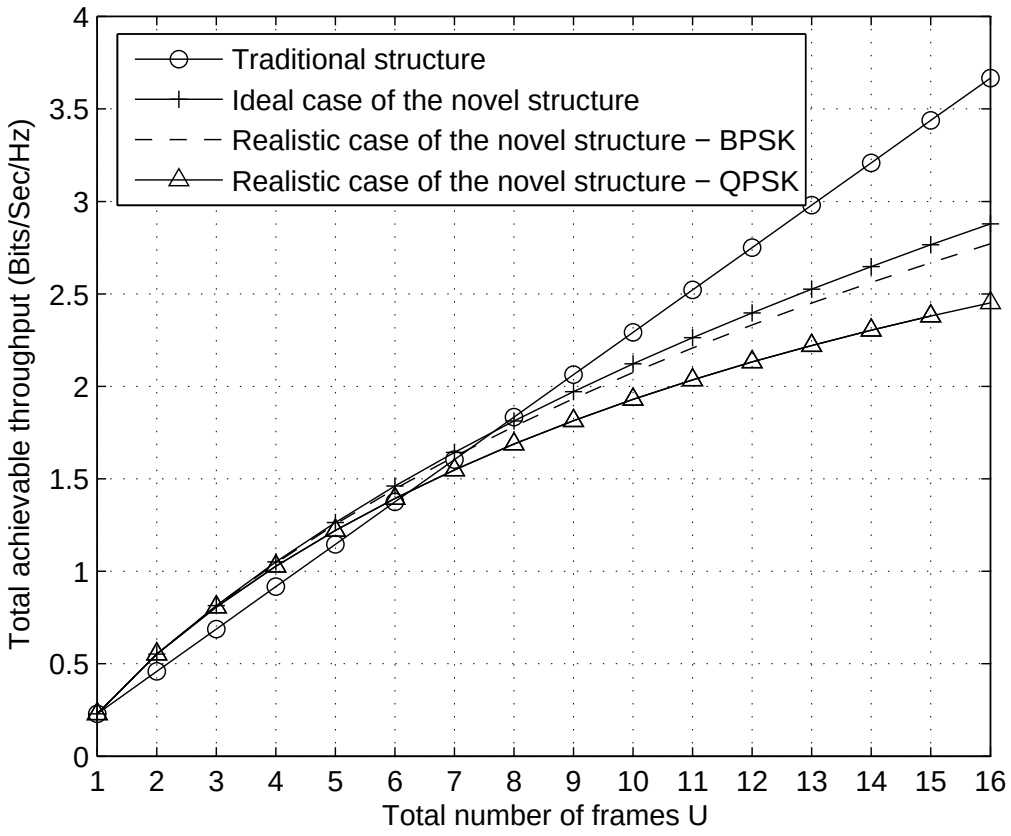

Figure 6.22: Total achievable throughput of U consecutive frames for the traditional structure and the novel structure when the covariance-based detection is applied.

As illustrated in Fig. 6.23, assume that the channel from the primary user transmitter to the secondary user receiver suffers from Rayleigh fading such that the fading coefficient h_p is Rayleigh distributed and the received primary user SNR is chi-square distributed with parameter $\overline{\gamma_{pu}}$. This is a reasonable assumption as the primary user is normally far away from the secondary user receiver without line-of-sight. Further, assume that the secondary signal also suffers from Rayleigh fading with fading coefficient h_s and parameter $\overline{\gamma_{su}}$. The received signal at the secondary

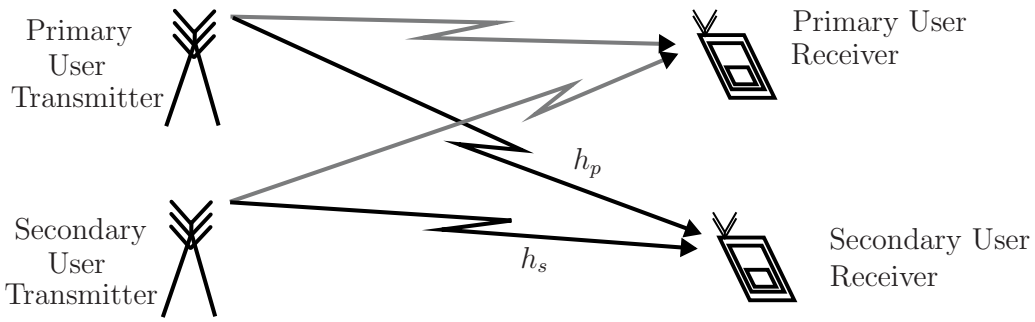

Figure 6.23: Primary user and secondary user fading channels.

receiver in (6.14) can be rewritten as

$$Y_{novF,j} = \begin{cases} h_s s_{s,j} + w_j, & H_0, \\ h_p s_j + h_s s_{s,j} + w_j, & H_1, \end{cases} \tag{6.39}$$

where the notations are defined as before.

When the primary user is absent, the received signal in (6.39) contains only the corrupted secondary user signal and noise. As h_s is random, the symbol error rate in (6.21) is averaged to give [117]

$$P_{serH_0F} = \int_0^\infty P_{serH_0} \frac{1}{\overline{\gamma_{su}}} e^{\frac{-\gamma_{su}}{\overline{\gamma_{su}}}} d\gamma_{su}, \tag{6.40}$$

where $\gamma_{su} = h_s^2 \gamma_s$, $\overline{\gamma_{su}} = E(h_s^2)\gamma_s$, and $E(h_s^2)$ is the average fading power of the secondary user.

When the primary user is present, taking into consideration the effect of fading experienced by both the primary user signal and the secondary user signal, the

symbol error rate in (6.23) is averaged to give

$$P_{serH_1F} = \int_0^\infty \int_0^\infty P_{serH_1} \frac{1}{\overline{\gamma_{su}}} e^{\frac{-\gamma_{su}}{\overline{\gamma_{su}}}} \frac{1}{\overline{\gamma_{pu}}} e^{\frac{-\gamma_{pu}}{\overline{\gamma_{pu}}}} d\gamma_{su}\gamma_{pu}, \tag{6.41}$$

where $\gamma_{pu} = h_p^2\gamma_p$, $\overline{\gamma_{pu}} = E(h_p^2)\gamma_p$, and $E(h_p^2)$ is the average fading power of primary user. The probability of occurring in (6.22) and (6.24) can then be re-derived by using the new symbol error rates in (6.40) and (6.41).

The conditional probability of false alarm in (6.28) can also be re-derived as

$$\begin{aligned} P_{fa_{EDreF}}\left(\Psi_{_{EDre}}, J, \delta_{_0}, \eta_0, \phi_{_0}\right) = \int_0^\infty & P_{fa_{EDre}}\left(\Psi_{_{EDre}}, J, \delta_{_0}, \eta_0, \phi_{_0}\right) \\ & \cdot \frac{1}{\overline{\gamma_{su}}} e^{\frac{-\gamma_{su}}{\overline{\gamma_{su}}}} d\gamma_{su}. \end{aligned} \tag{6.42}$$

The unconditional probability of false alarm is then obtained by averaging (6.42) over the new probability of occurring to remove the dependency on the values of $\delta_{_0}$, η_0 and $\phi_{_0}$.

The conditional probability of detection in (6.29) can be re-derived as

$$\begin{aligned} P_{d_{EDreF}}\left(\Psi_{_{EDre}}, J, \delta_{_1}, \eta_1, \phi_{_1}\right) = \int_0^\infty \int_0^\infty & \frac{1}{\overline{\gamma_{su}}} e^{\frac{-\gamma_{su}}{\overline{\gamma_{su}}}} \\ & \cdot \frac{1}{\overline{\gamma_{pu}}} e^{\frac{-\gamma_{pu}}{\overline{\gamma_{pu}}}} P_{d_{EDre}}\left(\Psi_{_{EDre}}, J, \delta_{_1}, \eta_1, \phi_{_1}\right) d\gamma_{su} d\gamma_{pu}. \end{aligned} \tag{6.43}$$

The unconditional probability of detection can then be obtained by averaging (6.43) over the new probability of occurring to remove the dependency on the values of $\delta_{_1}$, η_1 and $\phi_{_1}$.

When the effect of fading channel is considered, the achievable throughput of the secondary user transmission is also affected. When the primary user is absent,

the average channel capacity C_{H_0} becomes

$$C_{H_0F} = \int_0^\infty C_{H_0} \frac{1}{\overline{\gamma_{su}}} e^{\frac{-\gamma_{su}}{\overline{\gamma_{su}}}} \, d\gamma_{su} \tag{6.44}$$

and when the primary user is present, the average channel capacity C_{H_1} becomes

$$C_{H_1F} = \int_0^\infty \int_0^\infty C_{H_1} \frac{1}{\overline{\gamma_{su}}} e^{\frac{-\gamma_{su}}{\overline{\gamma_{su}}}} \frac{1}{\overline{\gamma_{pu}}} e^{\frac{-\gamma_{pu}}{\overline{\gamma_{pu}}}} d\gamma_{su} d\gamma_{pu}. \tag{6.45}$$

The total achievable throughput can then be derived by using (6.44) and (6.45).

Fig. 6.24 and Fig. 6.25 compare the ROC curves of the spectrum sensing for scenarios of with and without fading. In Fig. 6.24, $\gamma_p = \overline{\gamma_{pu}} = 0$ dB. As can be seen, when fading is taken into consideration in the analysis, at large values of probability of detection, the spectrum sensing performance is worse than that of the scenario when the AWGN channel is assumed, for both the traditional structure and the ideal case of the novel structure. When the probability of detection decreases, the sensing performance with fading outperforms that of the AWGN. Moreover, when the primary user SNR is decreased to $\gamma_p = \overline{\gamma_{pu}} = -5$ dB as in Fig. 6.25, the cross between the two scenarios appears at much higher values of probability of detection. This is explained as follows. When the primary user signal is assumed to be corrupted only by the AWGN. The analysis uses one instantaneous value of γ_p to calculate the sensing performance. When the fading channel is considered, the sensing performance is averaged over all possible instantaneous γ_p. So that if a large instantaneous γ_p is chosen for the result considering only AWGN, it will beat fading most of the time. On the other hand, if a small instantaneous γ_p is chosen for the result considering only AWGN, it might be inferior to fading in some cases because $erfc(\cdot)$ is a monotonical function of γ_p.

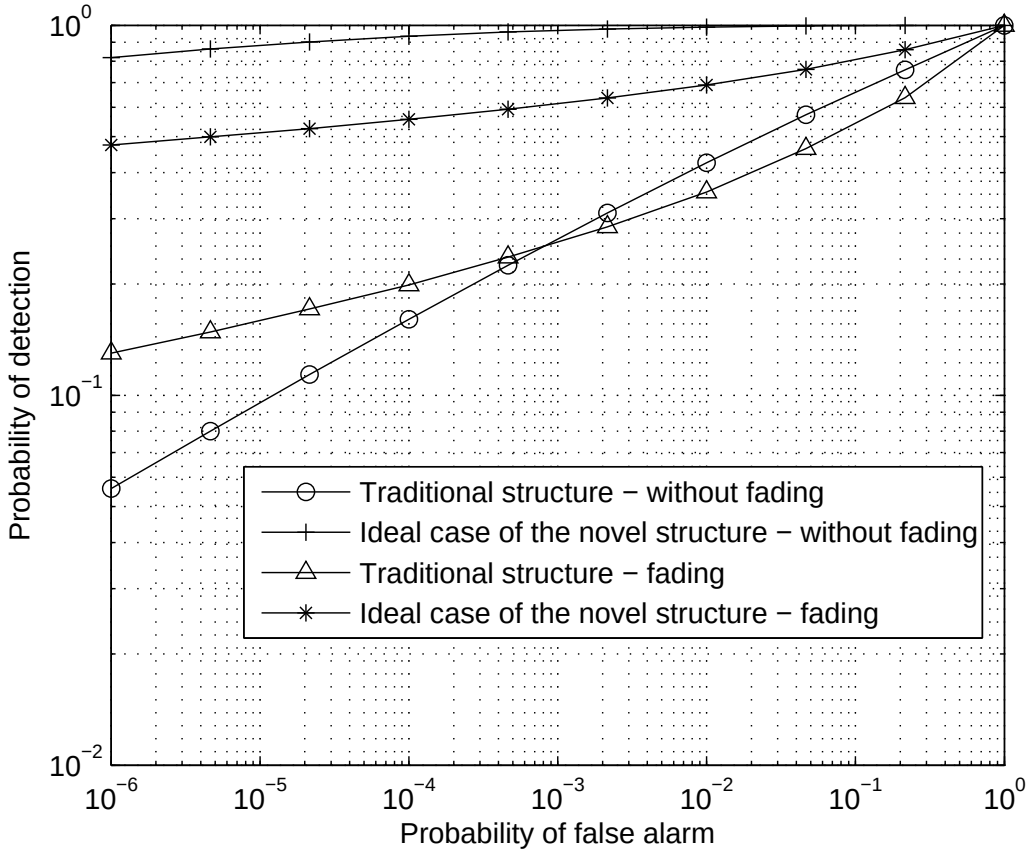

Figure 6.24: The effect of fading on the ROC curves of the spectrum sensing performance for the novel structure when the energy detection is applied, with $\gamma_p = 0$ dB and $\overline{\gamma_{pu}} = 0$ dB.

Fig. 6.26 examines the effect of fading on the ROC curves for different structures. One sees that, when the effect of fading is considered, similar observations to those of Fig. 6.10 can be made. The novel structure takes the advantage of longer sensing time and has better sensing performance than the traditional structure, while the upper bound performance is achieved when the decoding errors are not considered in the ideal case of the novel structure.

Fig. 6.27 and Fig. 6.28 examine the effect of fading on the achievable throughput

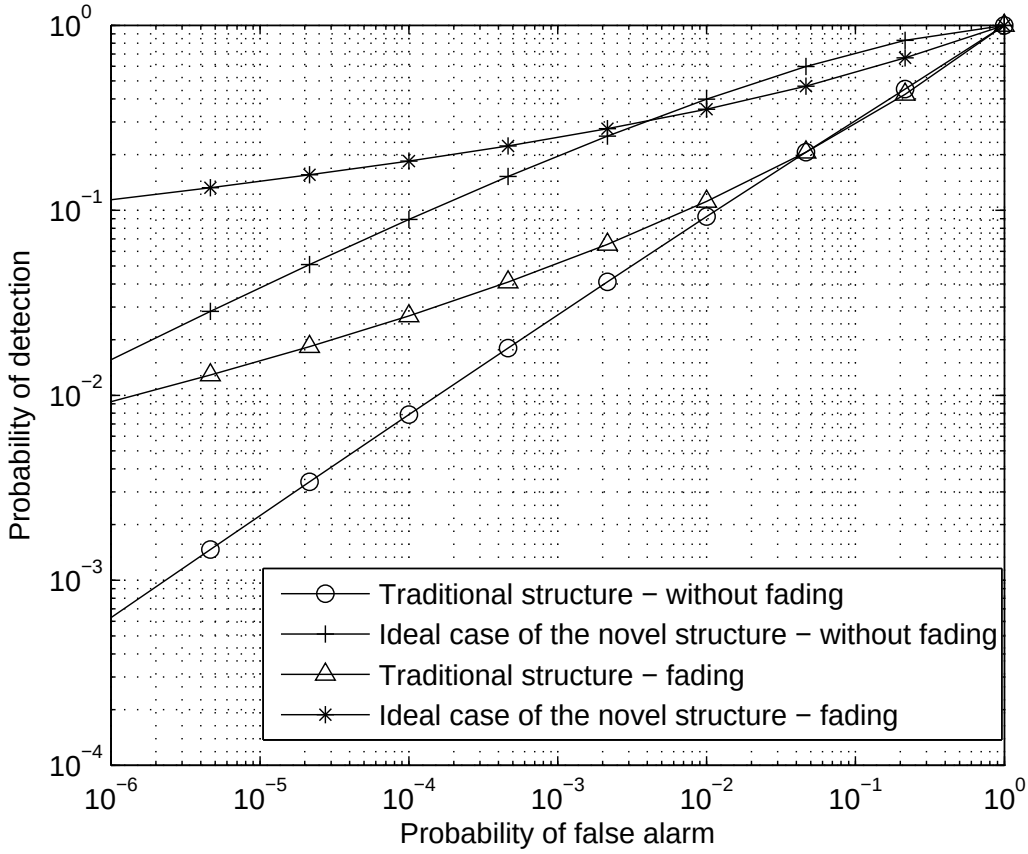

Figure 6.25: The effect of fading on the ROC curves of the spectrum sensing performance for the novel structure when the energy detection is applied, with $\gamma_p = -5$ dB and $\overline{\gamma_{pu}} = -5$ dB.

of the realistic case of the novel structure. In both figures, BPSK is assumed for the secondary user signal. As can be seen, in this case, both the individual throughput of the X^{th} frame and the total achievable throughput of U consecutive frames are reduced. Similar observations can also be made for the effects of fading on other detection algorithms and other secondary user signal modulation schemes.

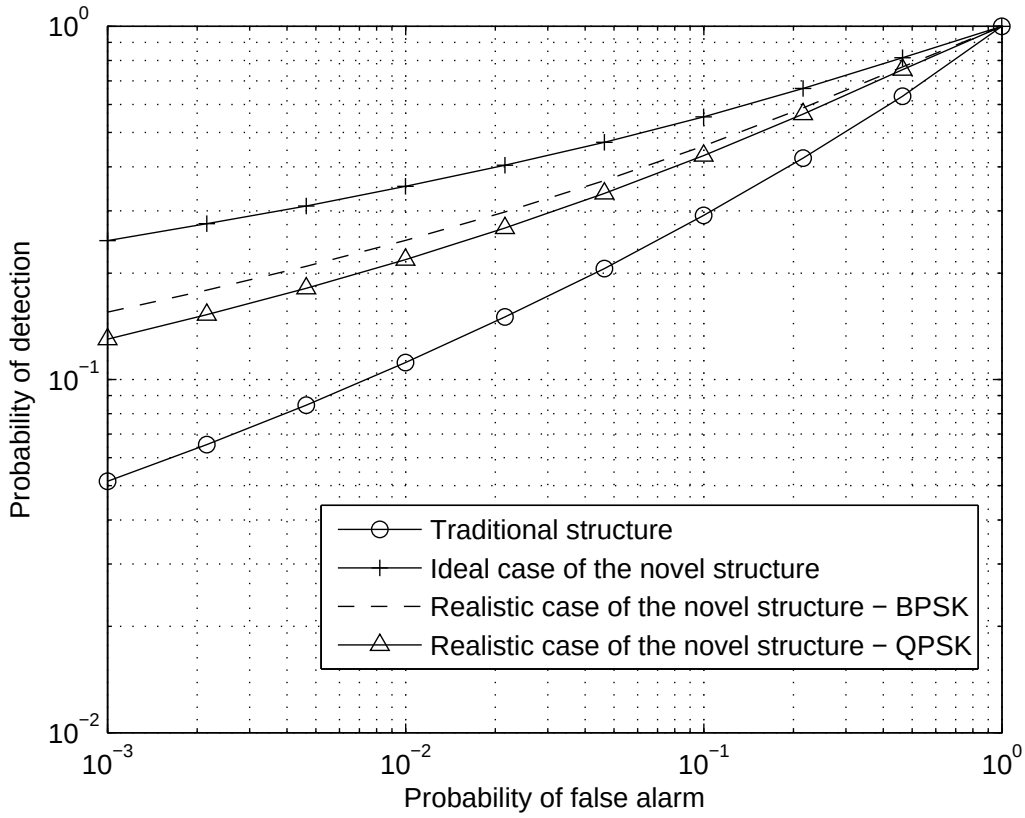

Figure 6.26: The effect of fading on the ROC curves of the spectrum sensing performance for different structure when the energy detection is applied.

6.6 Effect of Coded Signals

In the above analysis, the secondary user signal is also assumed to be uncoded. In practice, ECC can be applied to reduce errors at the receiver [117]. In this section, the ECC are applied to the analysis of the novel structure.

6.6.1 Golay(23,12)

Consider Golay (23, 12) coded BPSK signal for the secondary user signal. Golay (23, 12) is a binary linear code with minimum distance of $d_{min} = 7$ and can correct

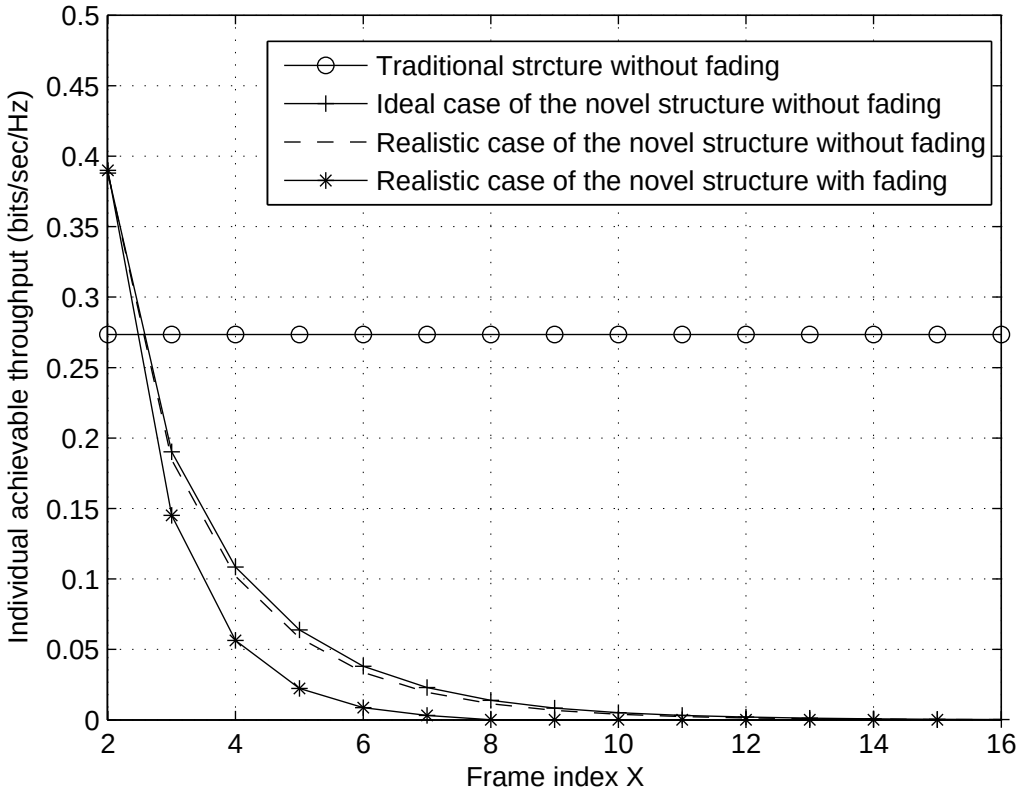

Figure 6.27: The effect of fading on the individual achievable throughput of the realistic case of the novel structure.

up to three errors in a block of 23 elements [117]. When hard decision decoding is applied at the secondary receiver, the probabilities of decoding error in (6.21) and (6.23) become

$$P_{serH_0Golay} = \sum_{v=4}^{23} \binom{23}{v} P_{serH_0}^{v} \left(1 - P_{serH_0}\right)^{23-v}, \tag{6.46}$$

and

$$P_{serH_1Golay} = \sum_{v=4}^{23} \binom{23}{v} P_{serH_1}^{v} \left(1 - P_{serH_1}\right)^{23-v} \tag{6.47}$$

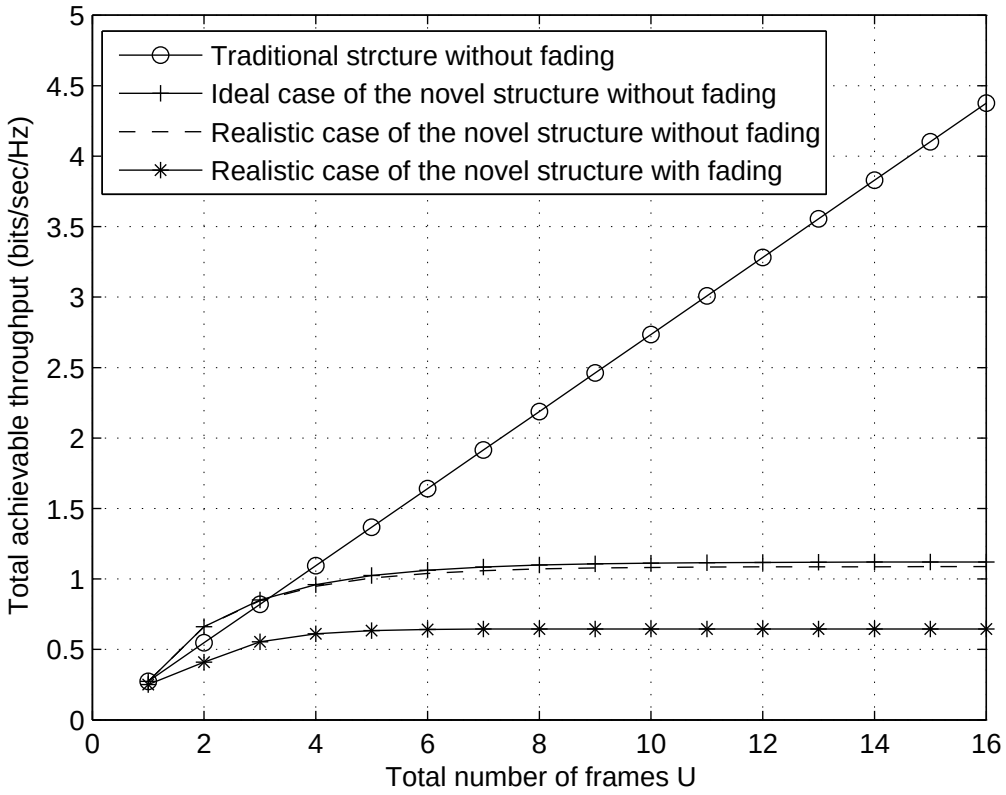

Figure 6.28: The effect of fading on the total achievable throughput of the realistic case of the novel structure.

respectively.

6.6.2 Hamming(7,4)

Alternatively, consider Hamming (7, 4) coded BPSK signal for the secondary user signal. Hamming (7, 4) is a linear block code with minimum distance of $d_{min} = 3$ and can correct only one error in a block of 7 elements [117]. The probabilities of

decoding error in (6.21) and (6.23) become

$$P_{serH_0Ham} = \sum_{v=2}^{7} \binom{7}{v} P_{serH_0}^{v} \left(1 - P_{serH_0}\right)^{7-v} \tag{6.48}$$

and

$$P_{serH_1Ham} = \sum_{v=2}^{7} \binom{7}{v} P_{serH_1}^{v} \left(1 - P_{serH_1}\right)^{7-v} \tag{6.49}$$

respectively.

Substituting (6.46) and (6.47) or (6.48) and (6.49) for (6.21) and (6.23) for the Golay (23, 12) coded secondary signal and the Hamming (7, 4) coded secondary signal, respectively, the performances of spectrum sensing and data transmission for realistic case of the novel structure implementing ECC can be analyzed in a similar way to before.

As has been previously discussed, when mis-detection occurs, the secondary user mistakenly considers the primary user to be absent from the licensed channel while it is actually present. In this case, the secondary user transmission is carried out with datarate equals to C_{H_0}. When such situation occurs in practice, the decoding of the received secondary user frame will have large errors due to the fact that the actual datarate is higher than the Shannon's channel capacity. One possible solution to such problem is that the secondary user always transmits at the lower datarate equals to C_{H_1}. However, in this case, very long block will be required at the decoding process and causing long time delay. Moreover, when ECC is applied, extra redundancy is introduced into the secondary transmission process. Consequently, the advantages of sensing without dedicated sensing slot in the novel structure become less significant. Hence, there exists a tradeoff between the performance of the traditional structure where dedicated sensing slot exists and the novel structure ap-

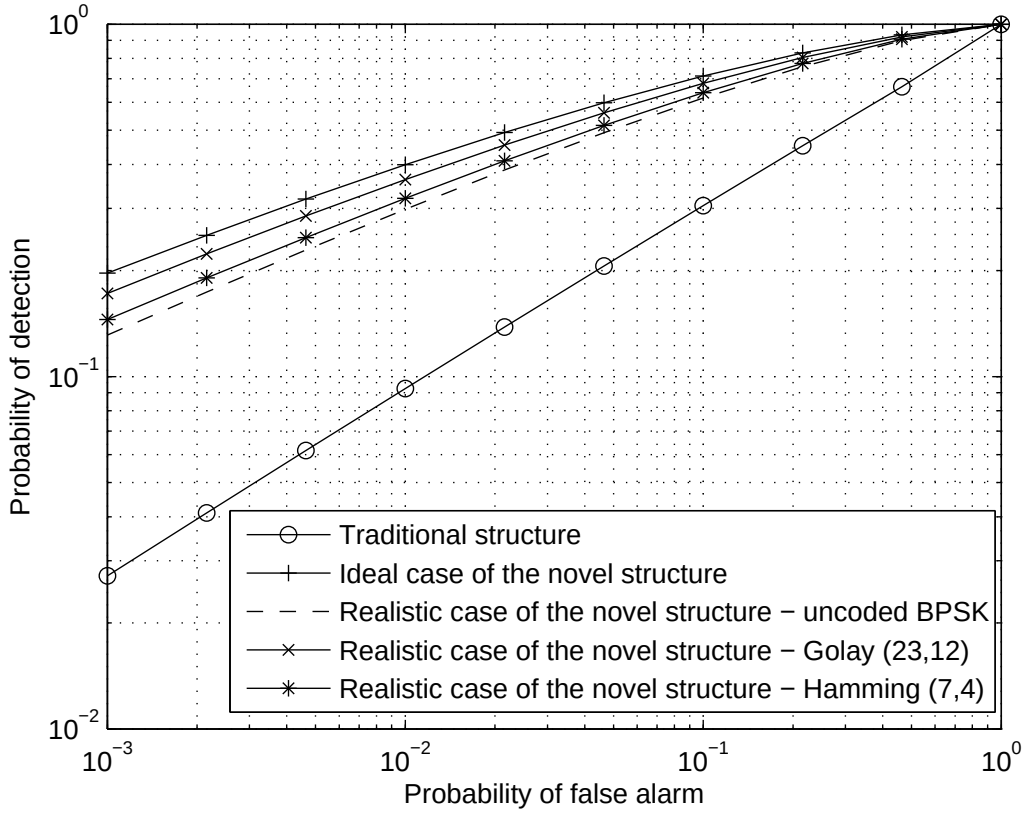

Figure 6.29: The effect of the ECC on the ROC curves of spectrum sensing performance for the novel structure.

plying ECC. That is to say when the redundancy bits introduced into the secondary transmission are over a certain limit, the novel structure will lose its advantage over the traditional structure completely.

Fig. 6.29 examines the effect of ECC on the spectrum sensing performance for the realistic case of the novel structures. In the figure, energy detection is used during the spectrum sensing and BPSK is used for the secondary user signal. When the ECC is applied, the decreased BER results in less residual secondary signal in the recovered secondary frame samples. Hence, the sensing performance is improved, as can be seen from Fig. 6.29. Moreover, when Golay (23,12) code is applied, the

sensing performance has larger improvement than that of the Hamming (7,4) code. Similar observations can also be made when other sensing algorithms are applied.

6.7 Conclusions

In this chapter, the realistic performance of the novel structure proposed in [112] has been analyzed and compared with that of the traditional structure and the ideal case performance. It has been shown that, while the novel structure benefits from the longer sensing period and the longer transmission period by using the whole secondary frame for data transmission and the whole recovered secondary frame for spectrum sensing in the tracking phase, respectively, as the number of transmitted secondary frames increases, the novel structure will lose its advantages and eventually underperform the traditional structure due to the accumulated errors from the spectrum sensing and the decoding process. There exists a saturation threshold below which the novel structure outperforms the traditional structure with multiple consecutive frames. This saturation threshold depends on the spectrum sensing algorithm and the secondary signal modulation scheme. The novel structure is more suitable for the covariance-matrix-based detection algorithm than for energy detection. The analysis in this chapter has also provided a guidelines to the choices of the parameters for best performance of cognitive radio in practice.

Chapter 7

Conclusions and Future Work

7.1 Introduction

The work presented at length in this thesis has focused on the performance analysis of cognitive radio. This chapter is intended to summarize the main contributions and findings of the work. To complete the content of the thesis, a section is also included to provide some potential ideals for future research.

The rest of this chapter is organized as follows. Section 7.2 summarize the main research findings. An executive conclusion regarding the impact of the research is also provided. Section 7.3 then discusses the potential directions for future research and initiatives for the reader to contemplate.

7.2 Conclusions and Contributions

Due to the nature of the radio frequency spectrum, traditional static spectrum allocation policies were struggling to cope with the ever increasing demand for wireless communication services. Cognitive radio therefore provided an efficient solution for

the conflict between spectrum scarcity and under-utilization. It enables the flexible secondary utilization of the licensed spectrum. In Chapter 1 of this thesis, an overview of cognitive radio was presented including an introduction to the IEEE 802.22 WRAN standard. A detailed review of cognitive radio enabling techniques was then provided in Chapter 2. Comprehensive discussions of the performance merits and limitations of these techniques were presented. After the background and the theoretical foundation of the research have been provided in the first two chapters, analytical evaluations of the cognitive radio systems performance with practical considerations has been presented in Chapter 3, Chapter 4, Chapter 5 and Chapter 6. The conducted research and contributions of this thesis can be summarized into several aspects as follows.

7.2.1 Dynamic Primary User Traffic and Primary User Multiple Changes Traffic

As was introduced in the motivation to this thesis, the random arrivals and departures of the primary user during the operation of the secondary user is a practical issue of cognitive radio that has not been previously considered in most literatures. In Chapter 3, by adopting a dynamic primary user traffic model, its effect on the sensing-throughput tradeoff of the cognitive radio was examined. The dynamic primary user traffic model takes one random arrival and departure of the primary user during the secondary frame into consideration while the channel holding times were assumed to be exponentially distributed. Through adopting this traffic model, a realistic analysis for the sensing-throughput tradeoff was derived.

The research on the effect of the primary user traffic was then taken further in Chapter 4, where a primary user multiple changes traffic model was established.

The traffic model takes into consideration of primary user multiple occupancy status changes and any reasonable channel holding time distributions. By establishing this multiple changes traffic model, a much more realistic and practical scenario was created for the cognitive radio system evaluations. In Chapter 4, its effect on the spectrum sensing performance was examined, where closed-form equations were derived for the probability of false alarm and the probability of detection. The effect of exponential, Gamma, Erlang and log-normal distributed channel holding times were also investigated.

Several findings regarding the dynamic primary user traffic and the primary user multiple changes traffic were concluded:

- First, it was found that when the random arrivals and departures of the primary user during the secondary frame was taken into account, a significant performance degradation can be observed in both the spectrum sensing performance and the secondary transmission achievable throughput.

- Second, the amount of the performance degradation was related to the primary user traffic intensity. As the primary user traffic intensity increased, the performance of cognitive radio further degraded as a result of the decreased channel holding times.

- Third, the amount of the performance degradation also depended on the received primary user SNR. The relationship between the sensing quality and γ_p given in Chapter 4 while considering the multiple changes traffic has shown that, the sensing performance improved as the increase of γ_p. However, the improvement of the spectrum sensing quality became much slower when the primary user occupancy status changes were taken into account, which further

indicated that the conventional performance evaluations of cognitive radio that did not consider the primary user traffic had been over optimistic.

- Fourth, the spectrum sensing performance further degraded as the number of the primary user occupancy status changes increased. However, the degree of degradation decreased and converged to a minimum performance due to the limited sensing duration and traffic intensity, suggesting a lower bound performance. This lower bound performance can potentially be adopted for future system performance predictions in realistic conditions.

- Fifth, it was also found that the optimal sensing time of the sensing-throughput tradeoff was affected by the primary user traffic. By analyzing the realistic performance of the system, it was concluded that the conventional performance analysis of the sensing-throughput tradeoff in previous literatures, where the randomness of the departure or arrival of the primary user was not included, no longer provide an accurate evaluation of the actual situation in this case. The heuristic relationship between the optimal sensing time and the primary user traffic intensity given in the thesis potentially provides a realistic guideline for choices of sensing times for future system designs.

- Finally, when examining the effects of different channel holding time distributions, it was found that the performance degradation of the cognitive radio due to the primary user traffic, has different sensitivities to different channel holding time distributions. This provides a potential insight for the future design of cognitive radio systems in different primary user networks with different channel conditions.

The investigation of the dynamic primary user traffic and primary user multiple

changes traffic was not limited to Chapter 3 and 4. Although it was not the only main research focus of the chapters, it was also examined in the Chapter 5 and 6, where performance degradations were also observed.

7.2.2 Transmission Enhancing Technique in Cognitive Radio System

Research was also carried out in the application of transmission enhancing technique in cognitive radio system, while taken into consideration of the cognitive radio distinctive characteristics. In Chapter 5, the performance of adaptive modulation in cognitive radio in a Nakagami-m fading channel has been analytically evaluated, where spectrum sensing performance, primary user interference and the dynamic primary user traffic have all been taken into consideration. The analysis was carried out for both the ACR scheme and the ADR scheme of adaptive modulation. In both cases, the BER performance and the link SE performance were derived. Comparison were provided between the performance of the conventional adaptive modulation and the adaptive modulation in cognitive radio system.

Several findings were concluded.

- First, the cognitive radio distinctive features degraded the BER performance for both the ACR scheme and the ADR scheme comparing with the conventional adaptive modulation.

- Second, when the received primary user SNR increased, further degradations of the BER performance can be observed for the adaptive modulation in cognitive radio.

- Third, the cognitive radio distinctive features also degraded the link SE perfor-

mance for both the ACR scheme and the ADR scheme of adaptive modulation.

- However, when the received primary user SNR increased, the link SE performance of the adaptive modulation in cognitive radio improved, due to the fact that link SE was determined before the secondary transmission.

- Fourth, both the BER performance and the link SE performance experienced further degradation when the primary user traffic intensity was increased. This agrees with the findings of Chapter 3 and Chapter 4 and is true for both the ACR scheme and the ADR scheme.

The evaluation of the adaptive modulation in cognitive radio presented in this thesis, has potentially provided a protocol for evaluations of similar systems. When other transmission enhancing techniques are applied in cognitive radio system, their performance can be examined by following the same method as presented in this thesis.

7.2.3 Analysis of the Novel Structure for Cognitive Radio

The performance of a novel structure for cognitive radio was investigated in Chapter 6, where the secondary transmission was performed for the entire frame duration T, while the spectrum sensing was performed using the recovered received secondary frame. Unlike previous works, in Chapter 6, the analysis has been extended to include multiple consecutive secondary frames, and taken into consideration of the realistic decoding errors for the secondary user signal, which was not previously considered. The spectrum sensing performance and the secondary transmission performance was examined for both the traditional structure proposed by the IEEE 802.22 WRAN standard and the novel structure, while both the ideal case and

the realistic case of the novel structure was included. In the analysis of the spectrum sensing performance, energy detection, maximum-eigenvalue detection and the covariance-based detection were all considered. Both BPSK and QPSK were examined for the secondary user signal modulation schemes. The effect of fading channel and ECC were also examined.

By comparing the performance of the novel structure to that of the traditional structure, several findings were concluded.

- First, due to the longer spectrum sensing duration, the novel structure always had a better sensing performance than the traditional structure. This was true for all three sensing algorithms examined.

- Second, the decoding error in the realistic case of the novel structure degraded the performance of the novel structure, while the upper bound performance can be obtained in the ideal case of the novel structure where the decoding error was not considered.

- Third, the sensing performance degradation in the realistic case of the novel structure with decoding errors was related to the secondary user SNR γ_s. When γ_s decreases, further degradations in the sensing performance was observed due to the increased decoding errors. Meanwhile, the sensing performance of the traditional structure and the ideal case of the novel structure was not affected by γ_s.

- Fourth, the sensing performance degradation in the realistic case of the novel structure was also found to be depending on the secondary user signal modulation schemes. When the QPSK was used instead of the BPSK, the sensing performance was further degraded due to the increased probability of decod-

ing errors. Again, the sensing performance of the traditional structure and the ideal case of the novel structure was not related to the modulation schemes.

- Fifth, as the increase of the secondary frame index X, the individual achievable throughput of the novel structure decreased and approached to zero, while the individual throughput of the traditional structure remained constant for all values of X.

- Sixth, it was found that the speed of increase of the total achievable throughput for the novel structure was reduced and converged to a fixed value as the increase of the total number of secondary frames U, whereas the total achievable throughput of the traditional structure increased linearly. An ideal upper bound performance of the total achievable throughput was provided in the ideal case of the novel structure.

- Seventh, by comparing the throughput performance of the novel structure to the traditional structure, it was found that a saturation threshold exist for the novel structure beyond which it lost its advantages over the traditional structure.

- This saturation threshold of the novel structure was related to the received primary user SNR and the secondary frame duration. The relationships between the saturation threshold and these two parameters given in the thesis, potentially provided a useful guideline for parameter decisions in future practical system designs for cognitive radio.

- It was also found that, the saturation threshold of the novel structure also depended on the decoding errors of the secondary user signal. When the realistic decoding error was taken into consideration in the novel structure,

the saturation threshold was reduced, as well as the individual and the total achievable throughput of the secondary transmission.

- Moreover, when the effect of fading channels was taken into consideration in the system evaluations, the performance of the cognitive radio was varied depending on the values of γ_p and $\overline{\gamma_{pu}}$. Nevertheless, the same performance patterns between the traditional structure and the novel structure can still be observed in fading channels.

- When the ECC was applied to the secondary user signal, the performance of the realistic case of the novel structure was improved since the ECC reduced the decoding errors.

- Similar performance patterns were also found when comparing the traditional structure and the novel structure applying different spectrum sensing algorithms, while the maximum-eigenvalue detection had the best performance out of the three considered.

- Last but not the least, when the primary user traffic was taken into consideration, degradations in the system performance of the novel structure were always observed. This agrees with the findings in the previous chapters.

The analysis of the novel structure performance presented in this thesis, has provided a realistic evaluation for the feasibility of the novel structure for practical cognitive radio systems, which has consequently opened up alternative views for future system designs.

7.2.4 Additional Observations

Some additional aspects which affects the performance of the cognitive radio system has also been observed in the thesis.

- In Chapter 3, the effect of the secondary user frame duration on the optimal sensing time of the MAC secondary frame was examined. It was found that the longer the secondary frame duration was, the smaller percentage of the frame time was used by the spectrum sensing to archive the optimal sensing-throughput tradeoff. This indicates that there is a potential tradeoff between the secondary frame duration and the primary user protection level, based on which parameters can be chosen when designing optimal cognitive radio systems.

- In Chapter 5, it was shown that both the BER performance and the link SE performance of the ADR scheme for adaptive modulation in cognitive radio improved with the increase in the value K, regardless of the dynamic primary user traffic.

- It was also noticed in Chapter 6 that regardless of the system structure employed, the covariance-based detection always had worse performance than the maximum-eigenvalue detection, whereas it was always better than that of the energy detection.

7.3 Future Research Directions

Bearing in mind the summary of the findings for the research works conducted in this thesis, the research on cognitive radio performance evaluations does not stop

here. Some of the results presented in this thesis provide both good foundation models for future performance evaluations and valuable guidelines for future system designs.

First of all, while it has not been considered in most previous literatures, the random departure and arrival of the primary user traffic is a realistic problem in all cognitive radio systems. The dynamic primary user traffic model established in this thesis, which takes the random departures and arrivals of the primary user into account, have potentially posed a practical problem that should be considered in all future performance evaluations of cognitive radio system. By adopting the primary user traffic model established in this thesis and following the same methodology presented, practical analysis of other cognitive radio system problems can be achieved. Meanwhile, optimizations of existing detectors and designs of new detectors with more practical performances could also be carried out. Or even new spectrum sensing algorithms which specifically tackle the primary user traffic problem in the cognitive radio systems could be developed. Moreover, research can also be carried out in studying the distributions of the number of the primary user occupancy status changes within the secondary frames.

Secondly, in this thesis, the analysis was focused on the performance of cognitive radio systems with individual non-cooperative secondary user. In practice, cooperation between secondary users are widely used to enhance the spectrum sensing performance. Therefore, the analysis for systems with individual secondary user presented in this thesis, can be used as a base model and incorporated into the analysis of system performances for cooperative cognitive radio systems.

Thirdly, most existing spectrum sensing algorithms and secondary data transmission methods considers the system design problem independently. Although

researches have been carried out on taking parameters such as the spectrum sensing errors into consideration in some transmission performance evaluations, or even as far as optimizing the spectrum sensing time to maximize the achievable throughput, there is still little work which considers the joint design of the spectrum sensing algorithm and the secondary data transmission method. The novel frame structure whose practical performance was evaluated in the Chapter 6, could be further developed to achieve such aims. A novel superframe structure similar to that of the IEEE 802.22 WRAN can be developed, with superframe preamble in place. A higher achievable throughput can be obtained by carefully choosing the number of novel frames according to the saturation threshold inside each superframe, while ensuring the spectrum sensing quality during the selection of transmission parameters. In return, an optimal spectrum sensing detector can be derived to maximize the secondary spectrum utilization efficiency in such system. Furthermore, by adopting similar designing concepts, other non-traditional sensing algorithms and transmission methods which does not follows the traditional periodically MAC frame structure may also be designed and evaluated.

Bibliography

[1] T. Yucek and H. Arslan, "A survey of spectrum sensing algorithm for cognitive radio applications," *IEEE Communications Surveys and Tutorials*, vol. 11, pp. 116 –130, First quarter 2009.

[2] "World mobile telecommunication market forecast," Tech. Rep. M. 2072, International Telecommunication Union Radiocommunication, 2006.

[3] D. Tse and P. Viswanath, *Fundamentals of wireless communications*. Cambridge University Press, 2005.

[4] "The UK frequency allocations," tech. rep., Roke Manor Research, 2007.

[5] "Table of frequency allocations used by the FCC and NTIA," tech. rep., National Telecommunications and Information Administration Office of Spectrum Management, U. S. Department of Commerce, August 2011.

[6] M. Matinmikko, M. Mustonen, H. Sarvanko, M. Hoyhtya, A. Hekkala, A. Mammela, M. Katz, and M. Kiviranta, "A motivating overview of cognitive radio: foundations, regulatory issues and key concepts," in *1st International Workshop on Cognitive Radio and Advanced Spectrum Management (CogART 2008)*, pp. 1 –5, 2008.

[7] I. F. Akyildiz, W. Y. Lee, M. C. Vuran, and S. Mohanty, "Next generation /dynamic spectrum access /cognitive radio wireless networks: a survey," *Computer Networks*, vol. 50, pp. 2127 –2159, September 2006.

[8] "United Kingdom frequency allocation table 2010," Tech. Rep. 16, National Frequency Planning Group, 2010.

[9] Q. Zhao and B. M. Sadler, "A survey of dynamic spectrum access: signal processing, networking, and regulatory policy," *IEEE Signal Processing Magazine: Special Issue on Resource-Constrained Signal Processing, Communications, and Networking*, vol. 24, pp. 79 –89, May 2007.

[10] D. Cabric, S. M. Mishra, D. Willkomm, R. Brodersen, and A. Wolisz, "A cognitive radio approach for usage of virtual unlicensed spectrum," in *14th IST Mobile Wireless Communication Summit*, June 2005.

[11] A. Ghasemi and E. S. Sousa, "Spectrum sensing in cognitive radio networks, requirements, challenges and design tradeoffs," *IEEE Communications Magazine*, vol. 46, pp. 32 –39, April 2008.

[12] "Report of the spectrum efficiency working group," tech. rep., Federal Communications Commission Spectrum Policy Task Force, 2002.

[13] M. A. McHenry and K. Steadman, "NSF spectrum occupancy measurements project summary," tech. rep., Shared Spectrum Company, August 2005.

[14] M. H. Islam, C. L. Koh, S. W. Oh, X. Qing, Y. Y. Lai, C. Wang, Y.-C. Liang, B. E. Toh, F. Chin, G. L. Tan, and W. Toh, "Spectrum survey in singapore: occupancy measurements and analyses," in *3rd International Conference on*

Cognitive Radio Oriented Wireless Networks and Communications (CROWNCOM 2008), pp. 1 –7, May 2008.

[15] S. D. Jones, E. Jung, X. Liu, N. Merheb, and I. J. Wang, "Characterization of spectrum activities in the u.s. public safety band for opportunistic spectrum access," in *IEEE International Symposium on New Frontiers in Dynamic Spectrum Access Networks (DySPAN 2007)*, pp. 137 –146, April 2007.

[16] R. I. C. Chiang, G. B. Rowe, and K. W. Sowerby, "A quantitative analysis of spectral occupancy measurements for cognitive radio," in *65th IEEE Vehicular Technology Conference (VTC2007)*, pp. 3016 –3020, April 2007.

[17] Y. Han, Y. Wen, W. Tang, and S. Li, "Spectrum occupancy measurement: focus on the TV frequency," in *2nd International Conference on Signal Processing Systems (ICSPS 2010)*, vol. 2, pp. 490 –494, July 2010.

[18] V. Blaschke, H. Jaekel, T. Renk, C. Kloeck, and F. K. Jondral, "Occupation measurements supporting dynamic spectrum allocation for cognitive radio design," in *2nd International Conference on Cognitive Radio Oriented Wireless Networks and Communications (CrownCom 2007)*, pp. 50 –57, August 2007.

[19] J. Bradford, T. Cook, D. Ramsbottom, and S. Jones, "Optimising usage of spectrum below 15GHz used for defence in the uk," in *IET Seminar on Cognitive Radio and Software Defined Radios: Technologies and Techniques*, pp. 1 –5, September 2008.

[20] M. Cave, "Independent audit of spectrum holdings final report," tech. rep., http://www.spectrumaudit.org.uk/index.htm, 2005.

[21] H. Arslan, *Cognitive radio, software defined radio, and adaptive wireless systems*. Springer, 2007.

[22] L. Berlemann and S. Mangold, *Cognitive radio for dynamic spectrum access*. Wiley, 2009.

[23] Y. Zeng, Y.-C. Liang, A. Hoang, and R. Zhang, "A review on spectrum sensing for cognitive radio: challenges and solutions," *EURASIP Journal on Advances in Signal Processing*, p. 2010:381465, 2010.

[24] M. Nekovee, "Cognitive radio access to TV white spaces: spectrum opportunities, commercial applications and remaining technology challenges," in *IEEE International Symposium on New Frontiers in Dynamic Spectrum Access Networks (DySPAN 2010)*, pp. 1 –10, April 2010.

[25] B. A. Fette, *Cognitive radio technology*. Elsevier Inc., 2006.

[26] J. Mitola, "Cognitive radio for flexible mobile multimedia communications," in *IEEE International Workshop on Mobile Multimedia Communications (MoMuC 1999)*, pp. 3 –10, 1999.

[27] J. Mitola and G. Q. Maguire, "Cognitive radio: making software radios more personal," *IEEE Personal Communications*, vol. 6, pp. 13 –18, August 1999.

[28] S. Haykin, "Cognitive radio: brain-empowered wireless communications," *IEEE Journal on Selected Areas in Communications*, vol. 23, pp. 201 –220, Feburary 2005.

[29] "Notice of proposed rulemaking and order: facilitation opportunities for flexible, efficient, and reliable spectrum use employing cognitive radio technologies," Tech. Rep. 03-322, Federal Communications Commission, 2005.

[30] M. Nekovee, "A survey of cognitive radio access to TV white spaces," *International Journal of Digital Multimedia Broadcasting*, vol. 2010, no. Article ID 236568, p. 11, 2010.

[31] "Cognitive radio technology: a study for Ofcom summary report," tech. rep., QinetiQ Ltd., 2007.

[32] B. Wang and K. J. R. Liu, "Advances in cognitive radio networks: a survey," *IEEE Journal of Selected Topics in Signal Processing*, vol. 5, pp. 5 –23, Feburary 2011.

[33] W. Lehr and J. Crowcroft, "Managing shared access to a spectrum commons," in *1st IEEE International Symposium on New Frontiers in Dynamic Spectrum Access Networks (DySPAN 2005)*, pp. 420 –444, November 2005.

[34] Y.-C. Liang, K.-C. Chen, G. Li, and P. Mahonen, "Cognitive radio networking and communications: an overview," *IEEE Transactions on Vehicular Technology*, vol. 60, pp. 3386 –3407, September 2011.

[35] D. B. Rawat and G. Yan, "Spectrum senisng methods and dynamic spectrum sharing in cognitive radio network: a survey," *International Journal of Research in Wireless Sensor Networks*, vol. 1, pp. 1 –13, March 2011.

[36] Q. Zhao and A. Swami, "A survey of dynamic spectrum access: signal processing and networking perspectives," in *IEEE International Conference on Acoustics, Speech and Signal Processing (ICASSP 2007)*, vol. 4, pp. 1349 – 1352, April 2007.

[37] Y. Xing, C. N. Mathur, M. Haleem, R. Chandramouli, and K. Subbalakshmi, "Dynamic spectrum access with QoS and interference temperature con-

straints," *IEEE Transactions on Mobile Computing*, vol. 6, no. 4, pp. 423 –433, 2007.

[38] J. Bater, H. P. Tan, K. Brown, and L. Doyle, "Modelling interference temperature constraints for spectrum access in cognitive radio networks," in *IEEE International Conference on Communications (ICC 2007)*, pp. 6493 –6498, June 2007.

[39] R. Zhang, Y. chang Liang, and S. Cui, "Dynamic resource allocation in cognitive radio networks," *IEEE Signal Processing Magazine*, vol. 27, pp. 102 –114, May 2010.

[40] G. R. Faulhaber, "Deploying cognitive radio: economic, legal and policy issues," *International Journal of Communication*, pp. 1114 –1124, August 2008.

[41] C. Cordeiro, K. Challapali, D. Birru, and N. S. Shankar, "IEEE 802.22: the first worldwide wireless standard based on cognitive radios," in *1st IEEE International Symposium on New Frontiers in Dynamic Spectrum Access Networks (DySPAN 2005)*, pp. 328 –337, November 2005.

[42] S. K. Jones, T. W. Phillips, H. L. V. Tuyl, and R. D. Weller, "Evaluation of the performance of prototype TV- band white space devices phase ii," tech. rep., Federal Communications Commission Office of Engineering and Technology, October 2008.

[43] M. Sherman, A. N. Mody, R. Martinez, C. Rodriguez, and R. Reddy, "IEEE standards supporting cognitive radio and networks, dynamic spectrum access, and coexistence," *IEEE Communications Magazine*, vol. 46, pp. 72 –79, July 2008.

[44] S. Yu, "IEEE 802.22 - 2011 standard for wireless regional area networks in TV whitespaces completed, http://www.businesswire.com/news/home/20110726007223/en/ieee-802.22tm-2011-standard-wireless-regional-area-networks, retrived on spetember 2012.," July.

[45] C. Cordeiro, K. Challapali, and D. Birru, "IEEE 802.22: An introduction to the first wireless standard based on cognitive radios," *Journal of Communications*, vol. 1, pp. 38 –47, April 2006.

[46] G. Ko, A. A. Franklin, S.-J. You, J.-S. Pak, M.-S. Song, and C.-J. Kim, "Channel management in IEEE 802.22 WRAN systems," *IEEE Communications Magazine*, vol. 48, pp. 88 –94, September 2010.

[47] W. Hu, D. Willkomm, M. Abusubaih, J. Gross, G. Vlantis, M. Gerla, and A. Wolisz, "Cognitive radios for dynamic spectrum access - dynamic frequency hopping communities for efficient IEEE 802.22 operation," *IEEE Communications Magazine*, vol. 45, pp. 80 –87, May 2007.

[48] C. Stevenson, G. Chouinard, Z. Lei, W. Hu, S. Shellhammer, and W. Caldwell, "IEEE 802.22: the first cognitive radio wireless regional area network standard," *IEEE Communications Magazine*, vol. 47, pp. 130 –138, January 2009.

[49] P. P. Hoseini and N. Beaulieu, "An optimal algorithm for wideband spectrum sensing in cognitive radio systems," in *IEEE International Conference on Communications (ICC 2010)*, pp. 1 –6, May 2010.

[50] Y. Chen and N. Beaulieu, "Performance of collaborative spectrum sensing for cognitive radio in the presence of gaussian channel estimation errors," *IEEE Transactions on Communications*, vol. 57, pp. 1944 –1947, July 2009.

[51] Y.-J. Choi, Y. Xin, and S. Rangarajan, "Overhead-throughput tradeoff in cooperative cognitive radio networks," in *IEEE Wireless Communications and Networking Conference (WCNC 2009)*, pp. 1 –6, April 2009.

[52] E. C. Y. Peh, Y.-C. Liang, Y. L. Guan, and Y. Zeng, "Optimization of cooperative sensing in cognitive radio networks: a sensing-throughput tradeoff view," *IEEE Transactions on Vehicular Technology*, vol. 58, pp. 5294 –5299, November 2009.

[53] Y. Pei, Y.-C. Liang, K. C. Teh, and K. H. Li, "Sensing-throughput tradeoff for cognitive radio networks: a multiple-channel scenario," in *20th IEEE International Symposium on Personal, Indoor and Mobile Radio Communications (PIMRC 2009)*, pp. 1257 –1261, September 2009.

[54] Y. Pei, A. T. Hoang, and Y.-C. Liang, "Sensing-throughput tradeoff in cognitive radio networks: how frequently should spectrum sensing be carried out?," in *18th IEEE International Symposium on Personal, Indoor and Mobile Radio Communications (PIMRC 2007)*, pp. 1 –5, September 2007.

[55] R. Murty, R. Chandra, T. Moscibroda, and P. Bahl, "Senseless: a database-driven white spaces network," *IEEE Transactions on Mobile Computing*, vol. 11, pp. 189 –203, Feburary 2012.

[56] J. Ojaniemi, J. Poikonen, and R. Wichman, "Effect of geolocation database update algorithms to the use of TV white spaces," in *7th International ICST*

Conference on Cognitive Radio Oriented Wireless Networks and Communications (CROWNCOM 2012), pp. 18 –23, June 2012.

[57] H. N. Tran, Y. D. Alemseged, C. Sun, and H. Harada, "On the effect of local sensing database to cognitive radio systems," in *14th International Symposium on Wireless Personal Multimedia Communications (WPMC 2011)*, pp. 1 –5, October 2011.

[58] D. Gurney, G. Buchwald, L. Ecklund, S. L. Kuffner, and J. Grosspietsch, "Geo-location database techniques for incumbent protection in the TV white space," in *3rd IEEE Symposium on New Frontiers in Dynamic Spectrum Access Networks (DySPAN 2008)*, pp. 1 –9, October 2008.

[59] D. Borth, R. Ekl, B. Oberlies, and S. Overby, "Considerations for successful cognitive radio systems in us TV white space," in *3rd IEEE Symposium on New Frontiers in Dynamic Spectrum Access Networks (DySPAN 2008)*, pp. 1 –5, October 2008.

[60] P. Pawelczak, K. Nolan, L. Doyle, S. W. Oh, and D. Cabric, "Cognitive radio: ten years of experimentation and development," *IEEE Communications Magazine*, vol. 49, pp. 90 –100, March 2011.

[61] H. R. Karimi, "Geolocation databases for white space devices in the uhf TV bands: specification of maximum permitted emission levels," in *IEEE Symposium on New Frontiers in Dynamic Spectrum Access Networks (DySPAN2011)*, pp. 443 –454, May 2011.

[62] V. Goncalves and S. Pollin, "The value of sensing for TV white spaces," in *IEEE Symposium on New Frontiers in Dynamic Spectrum Access Networks (DySPAN 2011)*, pp. 231 –241, May 2011.

[63] J. L. Burbank, "Security in cognitive radio networks: the required evolution in approaches to wireless network security," in *3rd International Conference on Cognitive Radio Oriented Wireless Networks and Communications (CROWNCOM 2008)*, pp. 1 –7, May 2008.

[64] M. J. Marcus, "Unlicensed cognitive sharing of TV spectrum: the controversy at the federal communications commission," *IEEE Communications Magazine*, vol. 43, pp. 24 – 25, May 2005.

[65] B. Wild and K. Ramchandran, "Detecting primary receivers for cognitive radio applications," in *1st IEEE International Symposium on New Frontiers in Dynamic Spectrum Access Networks (DySPAN 2005)*, pp. 124 –130, November 2005.

[66] I. F. Akyildiz, W. Y. Lee, M. C. Vuran, and S. Mohanty, "A survey on spectrum management in cognitive radio networks," *IEEE Communications Magazine*, vol. 46, pp. 40 –48, April 2008.

[67] W.-Y. Lee and I. F. Akyildiz, "Optimal spectrum sensing framework for cognitive radio networks," *IEEE Transactions on Wireless Communications*, vol. 7, pp. 3845 –3857, October 2008.

[68] A. Ghasemi and E. S. Sousa, "Optimization of spectrum sensing for opportunistic spectrum access in cognitive radio networks," in *4th IEEE Consumer*

Communications and Networking Conference (CCNC 2007), pp. 1022 –1026, January 2007.

[69] I. F. Akyildiz, B. F. Lo, and R. Balakrishnan, "Cooperative spectrum sensing in cognitive radio networks: a survey," *Physical Communication*, vol. 4, pp. 40 –62, 2011.

[70] D. Cabric, S. M. Mishra, and R. W. Brodersen, "Implementation issues in spectrum sensing for cognitive radios," in *38th Asilomar Conference on Signals, Systems and Computers*, vol. 1, pp. 772 –776, November 2004.

[71] D. Bhargavi and C. R. Murthy, "Performance comparison of energy, matched-filter and cyclostationarity-based spectrum sensing," in *IEEE Eleventh International Workshop on Signal Processing Advances in Wireless Communications (SPAWC 2010)*, pp. 1 –5, June 2010.

[72] H.-S. Chen, W. Gao, and D. G. Daut, "Signature based spectrum sensing algorithms for IEEE 802.22 wran," in *IEEE International Conference on Communications (ICC 2007)*, pp. 6487 –6492, June 2007.

[73] M. Subhedar and G. Birajdar, "Spectrum senisng thechniques in cognitive radio networks: a survey," *International Journal of Next-Generation Networks (IJNGN)*, vol. 3, pp. 37 –51, June 2011.

[74] R. Tandra and A. Sahai, "Fundamental limits on detection in low snr under noise uncertainty," in *International Conference on Wireless Networks, Communications and Mobile Computing (IWCMC 2005)*, vol. 1, pp. 464 – 469, June 2005.

[75] H. Urkowitz, "Energy detection of unknown deterministic signals," *Proceedings of the IEEE*, vol. 55, pp. 523 –531, April 1967.

[76] S. M. Kay, *Fundamentals of statistical signal processing, Volume 2: detection theory*. Prentice Hall PTR, 1998.

[77] F. F. Digham, M.-S. Alouini, and M. K. Simon, "On the energy detection of unknown signals over fading channels," *IEEE Transactions on Communications*, vol. 55, pp. 21 –24, January 2007.

[78] W. A. Gardner, "Exploitation of spectral redundancy in cyclostationary signals," *IEEE Signal Processing Magazine*, vol. 8, pp. 14 –36, April 1991.

[79] S. Wang, B. Zhang, H. Liu, and L. Xie, "Parallelized cyclostationary feature detection on a software defined radio processor," in *International Symposium on Signals Systems and Electronics (ISSSE 2010)*, vol. 1, pp. 1 –4, September 2010.

[80] R. F. Ustok and B. Ozbek, "Spectrum sensing based on cyclostationary feature detection for cognitive radios with multiple antennas," in *IEEE 19th Conference on Signal Processing and Communications Applications (SIU 2011)*, pp. 550 –553, April 2011.

[81] N. Han, S. Shon, J. H. Chung, and J. M. Kim, "Spectral correlation based signal detection method for spectrum sensing in IEEE 802.22 wran systems," in *8th International Conference on Advanced Communication Technology (ICACT 2006)*, vol. 3, pp. 1765 –1770, Feburary 2006.

[82] W. A. Gardner, "Signal interception: a unifying theoretical framework for feature detection," *IEEE Transactions on Communications*, vol. 36, pp. 897 –906, August 1988.

[83] Y. Zeng, C. L. Koh, and Y.-C. Liang, "Maximum eigenvalue detection: theory and application," in *IEEE International Conference on Communications (ICC 2008)*, pp. 4160 –4164, May 2008.

[84] Y. Zeng and Y.-C. Liang, "Maximum-minimum eigenvalue detection for cognitive radio," in *18th IEEE International Symposium on Personal, Indoor and Mobile Radio Communications (PIMRC 2007)*, pp. 1 –5, September 2007.

[85] Y. Zeng and Y. chang Liang, "Eigenvalue-based spectrum sensing algorithms for cognitive radio," *IEEE Transactions on Communications*, vol. 57, pp. 1784 –1793, June 2009.

[86] Y. Zeng and Y.-C. Liang, "Spectrum-sensing algorithms for cognitive radio based on statistical covariances," *IEEE Transactions on Vehicular Technology*, vol. 58, pp. 1804 –1815, May 2009.

[87] Y. Zeng and Y.-C. Liang, "Covariance based signal detections for cognitive radio," in *2nd IEEE International Symposium on New Frontiers in Dynamic Spectrum Access Networks (DySPAN 2007)*, pp. 202 –207, April 2007.

[88] Y.-C. Liang, Y. Zeng, E. Peh, and A. T. Hoang, "Sensing-throughput tradeoff for cognitive radio networks," in *IEEE International Conference on Communications (ICC 2007)*, pp. 5330 –5335, June 2007.

[89] Y. Zeng, Y. C. Liang, E. Peh, and A. T. Hoang, "Sensing-throughput tradeoff for cognitive radio networks," *IEEE Transactions on Wireless Communications*, vol. 7, pp. 1326 – 1337, April 2008.

[90] Y. C. L. A. Hoang and Y. Zeng, "Adaptive joint scheduling of spectrum sensing and data transmission in cognitive radio networks," *IEEE Transactions on Communications*, vol. 58, pp. 235 –246, January 2010.

[91] I. S. Gradshteyn and I. M. Ryzhik, *Table of integrals, series, and products*. San Diego, CA: Academic, sixth ed., 2000.

[92] A. Papoulis and S. U. Pillai, *Probability, random variables and stochastic processes*. McGraw Hill, fourth ed., 2002.

[93] J. C. Bellamy, *Digital telephony*. John Wiley & Sons. Inc., 2000.

[94] S. Geirhofer, L. Tong, and B. M. Sadler, "Cognitive radio for dynamic spectrum access - dynamic spectrum access in the time domain: modeling and exploiting white space," *IEEE Communications Magazine*, vol. 45, pp. 66 – 72, May 2007.

[95] Y. Chen and N. C. Beaulieu, "Performance of collaborative spectrum sensing for cognitive radio in the presence of gaussian channel estimation errors," *IEEE Transactions on Communications*, vol. 57, pp. 1944 – 1947, July 2009.

[96] N. Moayeri and H. Guo, "How often and how long should a cognitive radio sense the spectrum?," in *IEEE Symposium on New Frontiers in Dynamic Spectrum Access Networks (DySPAN 2010)*, pp. 1 –10, April 2010.

[97] H. Li and H. Fu, "An adaptive sensing period algorithm in cognitive radio networks," in *IEEE International Conference on Communications Technology and Applications (ICCT 2009)*, pp. 436 –439, October 2009.

[98] R. A. Guerin, "Channel occupancy time distribution in a cellular radio system," *IEEE Transactions on Vehicular Technology*, vol. 36, pp. 89 –99, August 1987.

[99] C. Jedrzycki and V. C. M. Leung, "Probability distribution of channel holding time in cellular telephony systems," in *46th IEEE Vehicular Technology Conference (VTC 1996)*, vol. 1, pp. 247 –251, April 1996.

[100] F. Barcelo and J. Jordan, "Channel holding time distribution in cellular telephony," *Electronics Letters*, vol. 34, pp. 146 –147, January 1998.

[101] X. Li and S. A. Zekavat, "Traffic pattern prediction and performance investigation for cognitive radio systems," in *IEEE Wireless Communications and Networking Conference (WCNC 2008)*, pp. 894 –899, 2008.

[102] M. Alwakeel, "Approximating handoff number and handoff rate in cellular networks with arbitrary call holding time and cell residence time distributions," in *IEEE International Conference on Computer Science and Information Technology (ICCSIT 2009)*, pp. 22 –26, August 2009.

[103] Y. Fang, I. Chlamtac, and Y. B. Lin, "Modeling PCS networks under general call holding time and cell residence time distributions," *IEEE/ACM Transactions on Networking*, vol. 5, pp. 893 –906, December 1997.

[104] S. Ross, *Probability and statistics for engineers and scientists*. Elsevier Inc., fourth ed., 2009.

[105] J. Ma, X. Zhou, and G. Y. Li, "Probability-based periodic spectrum sensing during secondary communication," *IEEE Transactions on Communications*, vol. 58, pp. 1291 –1301, April 2010.

[106] M. S. Alouini and A. J. Goldsmith, "Adaptive modulation over nakagami fading channels," *Kluwer Wireless Personal Communications*, vol. 13, pp. 119 – 143, November 2000.

[107] W. T. Webb and R. Steele, "Variable rate QAM for mobile radio," *IEEE Transactions on Communications*, vol. 43, pp. 2223 –2230, July 1995.

[108] K. Kuchi and V. Prabhu, "Performance evaluation for widely linear demodulation of pam/qam signals in the presence of rayleigh fading and co-channel interference," *IEEE Transactions on Communications*, vol. 57, pp. 183– 193, January 2009.

[109] Y. Kegen and I. Oppermann, "Performance of decorrelating receivers in multipath rician fading channels," *IEEE Transactions on Wireless Communications*, vol. 5, pp. 2009– 2016, August 2006.

[110] Y. Chen and N. C. Beaulieu, "Maximum likelihood estimation of snr using digitally modulated signals," *IEEE Transactions on Wireless Communications*, vol. 6, pp. 210 –219, January 2007.

[111] M. K. Simon and M.-S. Alouini, *Digital communication over fading channels*. John Wiley & Sons. Inc., second ed.

[112] S. Stotas and A. Nallanathan, "Overcoming the sensing-throughput tradeoff in cognitive radio networks," in *IEEE International Conference on Communications*, pp. 1 –5, May 2010.

[113] C.-L. Wang, H.-W. Chen, and Z.-Y. Tsai, "Throughput maximization for cognitive radio networks with wideband spectrum sensing," in *IEEE Wireless Communications and Networking Conference (WCNC 2012)*, pp. 1293 –1298, April 2012.

[114] Y. Zeng, C. L. Koh, and Y.-C. Liang, "Maximum eigenvalue detection: theory and application," in *IEEE International Conference on Communications (ICC 2008)*, pp. 4160 –4164, May 2008.

[115] Y. Chen, C. Wang, and B. Zhao, "Performance comparison of feature-based detectors for spectrum sensing in the presence of primary user traffic," *IEEE Signal Processing Letters*, vol. 18, pp. 291 –294, May 2011.

[116] Y. Chen, C. Wang, and B. Zhao, "Performance comparison of featurebased detectors for spectrum sensing in the presence of primary user traffic," *IEEE Signal Processing Letters*, vol. 18, pp. 291 –294, May 2011.

[117] J. G. Proakis, *Digital communications*. McGraw-Hill, Inc., third ed., 1995.